MAGED2: the gene associated with Bartter syndrome type 5 is a key regulator of Gαs signalling in the developing kidney

Inaugural-Dissertation

zur

Erlangung des Doktorgrades

der Mathematisch-Naturwissenschaftlichen Fakultät

der Universität zu Köln

vorgelegt von

Björn Michael Reusch

aus Werneck

Köln

2023

Die vorliegende Dissertation wurde am Institut für Humangenetik der Universität zu Köln unter der wissenschaftlichen Anleitung von Herrn Priv.-Doz. Dr. med. Bodo Beck und Frau Prof. Dr. rer. nat. Brunhilde Wirth angefertigt und von der Mathematisch-Naturwissenschaftlichen Fakultät der Universität zu Köln im Jahr 2023 als Inaugural-Dissertation zur Erlangung des Doktorgrades im Promotionsfach Biologie angenommen.

Table of contents

Table of figures

List of tables

List of abbreviations

A	adenosine
AMP	adenosine monophosphate
ANOVA	analysis of variance
ATP	adenosine triphosphate
AS	amino acids
a.u.	arbitrary unit
BCA	bicinchoninic acid
bp	base pairs
BS	Bartter syndrome
BSA	bovine serum albumin
C	cytosine
Ca	calcium
°C	degree Celsius
cAMP	cyclic AMP
cDNA	complementary DNA
dDAVP	1-Desamino-8-D-Arginin-Vasopressin
dNTP	deoxynucleoside triphosphate
dH2O	demineralized water
DMEM	Dulbecco's Modified Eagle Medium
DMSO	dimethyl sulfoxide
DNA	deoxyribonucleic acid
E. *coli*	Escherichia coli
EDTA	ethylenediaminetetraacetic acid
EtBr	ethidium bromide
EtOH	ethanol
FC	fold change
FCS	fetal calf serum
FDS	false discovery rate
fs	frameshift
G	guanosine
GO	gene ontology
h	hour

HEK293T	human embryonic kidney 293T cells
HRP	horseradish peroxidase
IF	immunofluorescent
kb	kilobases
kDa	kilodalton
log	logarithm
M	molar
MAGED2	melanoma-associated antigen Family D2
MeOH	methanol
Mg^{2+}	magnesium ion
mg	milligram
$MgCl_2$	magnesium chloride
$MgSO_4$	magnesium sulfate
min	minute
ml	milliliter
mM	millimolar
mpkCCD	mouse principal kidney collecting duct cells
mRNA	messenger RNA
MS	mass spectrometry
n	number of biological replicates
NaCl	sodium chloride
NaOH	sodium hydroxide
ng	nanogram
nm	nanometer
nM	nanomolar
ns	not significant
OMIM	Online Mendelian Inheritance in Man
PBS	phosphate-buffered saline
PCR	polymerase chain reaction
PFA	paraformaldehyde
PI	protease inhibitor
PMSF	phenylmethylsulfonyl fluoride
RNA	ribonucleic acid
RNase	RNA endonuclease

RT	room temperature
s	second
SD	standard deviation
SDS	sodium dodecyl sulfate
SDS-PAGE	sodium dodecyl sulfate polyacrylamide gel electrophoresis
ssODN	single-stranded oligodeoxynucleotide
T	thymidine
TEMED	N,N,N',N'-tetramethylethylenediamine
tracrRNA	Trans-activating crRNA
U	units
µg	microgram
µl	microliter
µM	micromolar
WB	western blot
WT	wildtype
%	percent

Gene, Protein and Peptide names

ACTB	Actin Beta
AMN	Amnionless
AQP2	Aquaporin 2
ADH	Antidiuretic hormone
AKT	Protein kinase B
AVPR2	Arginine Vasopressin Receptor 2
BSND	Barttin CLCNK Type Accessory Subunit Beta
CBP	CREB-binding protein
CDK	Cyclin-dependent kinase
CLCNKA	Chloride Voltage-Gated Channel Ka
CLCNKB	Chloride Voltage-Gated Channel Kb
CLK4	CDC Like Kinase 4
CREB	cAMP response element-binding protein
CTGF	Connective Tissue Growth Factor
DNAJB1	DnaJ Heat Shock Protein Family (Hsp40) Member B1
EDA	Ectodysplasin A
EIF4EBP2	Eukaryotic Translation Initiation Factor 4E Binding Protein 2
EnAC	Epithelial Na channel
EPO	Erythropoietin
ERK	extracellular-signal regulated kinase
Gαs	Gs alpha subunit
GLUT-1	Glucose transporter 1
GNAS	Guanine Nucleotide Binding Protein (G Protein), Alpha Stimulating
GPCR	G-protein coupled receptor
GRK	GPCR kinase
HIF	Hypoxia-inducible factor
HIF1A	Hypoxia-inducible factor 1A
JNK	c-Jun N-terminal kinase

KCNJ1	Potassium Inwardly Rectifying Channel Subfamily J Member 1
LRP2	Low Density Lipoprotein receptor-related Protein 2; Megalin
MAGED2	Melanoma-associated antigen D2
MED14	Mediator Complex Subunit 14
MYC	MYC Proto-Oncogene
MYL3	Myosin light chain 3
NABP2	Nucleic Acid Binding Protein 2
Na^+K^+ATPase	Sodium-potassium adenosine-triphosphate pump
NCC	Na+-Cl− cotransporter
NHE3	Na(+)/H(+) Exchanger 3
NKCC2	Na-K-2Cl-Cotransporter
ORC1	Origin Recognition Complex Subunit 1
ORC6	Origin Recognition Complex Subunit 6
NHE3	Na(+)/H(+) Exchanger 3
p53	Tumor protein 53
pCREB	phospho-CREB
pERK	phospho-ERK
RAB11FIP1	RAB11 Family Interacting Protein 1
RAB11FIP3	RAB11 Family Interacting Protein 3
PKA	Protein kinase A
PLK1	Polo like kinase A
PRPF18	Pre-MRNA Processing Factor 18
ROMK	Renal Outer Medullary Potassium channel
RPA	Replication protein A
SHH	Sonic hedgehog
SCNN1B	Sodium Channel Epithelial 1 Subunit Beta
SLC12A1	Solute Carrier Family 12 Member 1
SLC12A3	Solute Carrier Family 12 Member 3
SOSS	Sensor Of Single-stranded DNA
SULT1C2	Sulfotransferase Family 1C Member 2
SYNPO	Synaptopodin

TRAIL	TNF-related apoptosis-inducing ligand
TRAIL-R2	TNF-related apoptosis-inducing ligand receptor 2
TAZ	Tafazzin
TP53	Tumor protein 53
TSC22D3	TSC22 Domain Family Member 3
VEGF	Vascular endothelial growth factor
YAP	Yes-associated protein 1

Declaration of contributions

Parts of this thesis were published in the Journal of Proteomics:

2022:

Reusch B, Bartram MP, Dafinger C, Palacio-Escat N, Wenzel A, Fenton RA, Saez-Rodriguez J, Schermer B, Benzing T, Altmüller J, Beck BB, Rinschen MM. MAGED2 controls vasopressin-induced aquaporin-2 expression in collecting duct cells. J Proteomics. 2022 Feb 10;252:104424. doi: 10.1016/j.jprot.2021.104424. Epub 2021 Nov 12. PMID: 34775100.

Summary

Pathogenic variants in the Melanoma-Associated Antigen D2 (*MAGED2*) gene have been identified as the cause of the severe but transient antenatal Bartter syndrome type 5 (BS5) accounting for approximately 10% of all Bartter syndrome cases. The disorder is characterized by severe polyhydramnios leading to premature delivery and still birth as well as postnatal polyuria that declines after a few weeks or months followed by normal further development.

The underlying molecular mechanisms of BS5 and especially the function of MAGED2 in kidney physiology had been largely unknown so far.

In this study, we show that *Maged2* expression in mouse embryonic kidneys declines during development. As MAGED2 interacts with G-protein alpha subunit Gαs (*GNAS*), it was inferred to play a role in G-protein coupled receptor (GPCR) signalling. Accordingly, we showed that knockdown of *MAGED2* in HEK293T cells induces major changes in protein phosphorylation but not in protein abundance. In the murine collecting duct cell line mpkCCD, *Maged2* knockdown modulated vasopressin type 2 receptor (V2R)-induced phosphorylation-dependent signalling in terms of cAMP kinetics and weakened phosphorylation on downstream targets like cAMP response element-binding protein (CREB). Unexpectedly, *Maged2* knockdown resulted *in vitro* in a marked increase of the water channel aquaporin-2 (AQP2) abundance upon long-term V2R activation, which was mediated transcriptionally.

To further analyse *Maged2* function *in vivo*, we generated a knock-in mouse model of the human mutation p.R446C via CRISPR/Cas9. Mendelian ratio of *Maged2*$^{R446C/Y}$ mice was clearly skewed towards the wildtype genotype. Affected male mice also showed impaired embryonic development in form of general paleness as well as slightly decreased body and kidney weight. On the proteome level MAGED2 loss in P0 kidneys led to significant alterations of abundance of 307 proteins, with 112 proteins showing increased and 195 proteins showing decreased expression. Remarkably, Gαs was significantly upregulated, while the Thiazide-Sensitive Sodium-Chloride Cotransporter (NCC) was significantly downregulated.

Localization studies in kidneys from P0 *Maged2*$^{R446C/Y}$ mice could not show an aberrant localization of targets defective in other types of BS like the cotransporters Na-K-2Cl Cotransporter 2 (NKCC2), NCC and the Potassium Inwardly Rectifying Channel

Subfamily J Member 1 (ROMK), while the apical localization of AQP2 and also its phosphorylated form pAQP2 were clearly impaired. A similar diffuse instead of apical AQP2 distribution was observed in the only available kidney sections from a stillborn BS5 infant.

Taken together, MAGED2 modulates GPCR-signalling at a specific period of time and acts as a desensitizer of V2R *in vitro*. Moreover, we demonstrate that *Maged2* loss *in vivo* impairs the abundance and the targeting of numerous renal proteins which could explain the overall severe character of the disease in comparison to other forms of Bartter syndrome.

The studies presented here serve as a basis for further research on BS5, potentially allowing the development of targeted treatments for this disease. Especially the mouse model will help us to dissect the complex effects of MAGED2 in health and disease and integrate the discovery in the context of tubulopathies and general fluid homeostasis. Ultimately, backtracking the reductive cascade of MADED2 functions will yield a more precise understanding of fluid and electrolyte homeostasis during embryonic development and beyond.

Zusammenfassung

Pathogene Varianten des Gens Melanoma-Associated Antigen D2 (*MAGED2*) wurden als Ursache für das schwerwiegend aber transient verlaufende Bartter-Syndrom Typ 5 (BS5) identifiziert, das für schätzungsweise 10% aller Fälle des Bartter-Syndroms verantwortlich ist. Die Krankheit ist gekennzeichnet durch schwerwiegendes Polyhydramnion, das zu Früh- und Totgeburt führt, sowie durch postnatale Polyurie, die nach ein paar Wochen oder Monaten abnimmt und dem eine normale weitere Entwicklung folgt.

Der zugrunde liegende Mechanismus von BS5 und speziell die Funktion, die MAGED2 in der Nierenphysiologie ausführt, waren bisher größtenteils unbekannt.

In dieser Studie zeigen wir, dass die *Maged2* Expression in der Mausniere während der Entwicklung abnimmt. Da MAGED2 mit G-protein alpha subunit Gαs (*GNAS*) interagiert, wurde vermutet, dass es eine Rolle im G-Protein-gekoppelten Rezeptor (GPCR)-Signalweg spielt. Folgerichtig konnten wir zeigen, dass eine Verminderung der *MAGED2*-Expression in HEK293T-Zellen große Veränderungen in der Proteinphosphorylierung aber keine in der Proteinmenge verursacht. In der Sammelrohrzelllinie mpkCCD modulierte eine Verminderung der *Maged2*-Expression einen auf Phosphorylierung beruhenden Signalweg, der durch Aktivierung des Vasopressin Typ 2 Rezeptors (V2R) induziert wird, hinsichtlich cAMP-Kinetik und verminderter Phosphorylierung von nachgeschalteten Zielen wie cAMP response element-binding protein (CREB). Unerwarteterweise führte eine Verminderung der *Maged2*-Expression *in vitro* zu einem deutlichen Anstieg der Aquaporin-2 (AQP2)-Menge während der Langzeitaktivierung von V2R, die transkriptionell reguliert wurde.

Um die Funktion von *Maged2* auch *in vivo* zu analysieren, generierten wir ein Knock-In-Mausmodell der humanen, pathogenen Mutation p.R446C. Das Mendelsche Verhältnis hierbei war deutlich in Richtung des Wildtyps verschoben. Betroffene Mäuse zeigten eine beeinträchtigte Embryonalentwicklung in Form einer generellen Blässe sowie leicht reduziertem Körper- und Nierengewicht. Auf Proteomebene führte der Verlust von *Maged2* zu einem signifikant veränderten Vorkommen von 307 Proteinen, von denen 112 ein erhöhtes und 195 Proteine ein vermindertes Aufkommen zeigten. Bemerkenswerterweise war Gαs signifikant hochreguliert, während der Thiazid-sensitive Sodium-Chlorid Cotransporter (NCC) signifikant herunterreguliert war.

Lokalisationsstudien in P0-Nieren von *Maged2*$^{R446C/Y}$-Mäusen zeigten keine Fehllokalisierung der kritischen Cotransporter Na-K-2Cl Cotransporter 2 (NKCC2), NCC und des Renal Outer Medullary Potassium (K) channel (ROMK), während die apikale Lokalisierung von AQP2 sowie der phosphorylierten Form pAQP2 deutlich beeinträchtigt war. Eine ähnlich diffuse Verteilung anstatt einer apikalen Lokalisierung von AQP2 wurde auch in den einzig verfügbaren Nierenschnitten eines totgeborenen BS5-Patienten beobachtet.

Zusammengefasst kann man sagen, dass MAGED2 den GPCR-Signalweg während eines spezifischen Zeitraums moduliert und als Desensibilisierer von V2R *in vitro* wirkt. Darüber hinaus zeigen wir, dass der Verlust von *Maged2 in vivo* die Menge und Ziellokalisierung vieler renaler Proteine beeinträchtigt, was in Summe den schwerwiegenden Charakter der Krankheit im Vergleich zu anderen Formen des Bartter Syndroms erklären könnte.

Die hier präsentierten Versuche dienen als Grundlage für ein weiteres Erforschen von BS5, was möglicherweise die Entwicklung einer gezielten Behandlung der Erkrankung erlaubt. Insbesondere das Mausmodell wird uns helfen, die komplexen Auswirkungen von MAGED2 auf Gesundheit und Krankheit zu analysieren und diese Ergebnisse in den Kontext von Tubulopathien und allgemeiner Flüssigkeitshomöostase zu stellen. Letztendlich wird die Rückverfolgung der reduktiven Kaskade von MADED2-Funktionen zu einem genaueren Verständnis der Flüssigkeits- und Elektrolythomöostase während der Embryonalentwicklung und darüber hinausführen.

1 Introduction

A rare disease is characterized by its low number of affected individuals. In the European Union, a disease is defined as rare when its prevalence is not more than 50 per 100,000 ("Regulation (EC) N°141/2000 of the European Parliament and of the Council of 16 December 1999 on orphan medicinal products," 2000). Although individually rare, collectively, rare diseases have an approximate prevalence of 3.5 – 5.9% (Nguengang Wakap et al., 2020) making them a substantial cause of disease and death. Nevertheless, due to the low prevalence there is a general lack of knowledge and expertise in diagnosing and treating them. High costs for the development of novel treatments for small groups of patients have greatly hampered the development of targeted treatment options in the past, but progress in molecular diagnostics, biotechnology, and a transformed corporate attitude toward the neglect of rare disease are gradually improving the situation.

The majority of inherited kidney diseases is rare and to date more than 300 monogenic conditions have been identified that affect approximately two million Europeans including diseases of renal transport, development, metabolism and inflammation (Bassanese et al., 2021; Devuyst et al., 2014; Shayman, 2006; Soliman, 2012). The study of rare kidney disorders has provided novel and important insights not only relevant for the underlying cause of a specific disease, but has also been a major driver for our understanding of general molecular processes, which again has facilitated knowledge and treatment of common kidney diseases.

One example is the Bartter syndrome (BS) spectrum, which constitutes a group of rare diseases impairing the kidney's ability to reabsorb salts and water (Ohlsson et al., 1984; Seyberth et al., 1985). Investigations of this prototypic form of tubulopathy have substantially improved our understanding of renal salt and electrolyte handling and, hence, also of the basic principles underlying more common diseases like hypertension.

This work focussed on the most recently discovered form BS5, which results in severe polyhydramnios and perinatal polyuria (Laghmani et al., 2016).

1.1 Amniotic fluid as essential factor of embryonic development

1.1.1 Function and dynamics of amniotic fluid

Amniotic fluid (AF), which originates from maternal plasma, plays an important role in the proper embryonical development as it fulfils essential, mostly mechanical, functions (Underwood et al., 2005). Amount and composition changes regularly during pregnancy adapting to the needs at particular time points of development (Underwood et al., 2005). The aqueous environment protects the embryo from external trauma by extenuating the impact of blunt forces through its physical characteristics (Ostergard, 1970). Also, unhampered morphogenesis, especially of the extremities, can only take place in such an environment without physical barriers (Graham et al., 1980; Miller et al., 1981; Moh et al., 2012).

Containing many substances of the innate immune system like α-defensins, lactoferrin or lysozyme, the AF also plays an important role as barrier against pathogens (Akinbi et al., 2004). Besides, AF contains many nutritive factors like carbohydrates, proteins, lipids, enzymes and hormones that are essential for embryonic growth (Underwood et al., 2005).

During embryonic development the amount of AF depicts a curve with an initial increase until about 33 weeks of gestation and a subsequent decline until birth (Brace & Wolf, 1989; Moore & Cayle, 1990). The volume of AF increases from about 25 ml at 10 weeks to a plateau of 800 ml at 28 weeks to decrease to a volume of approximately 400 ml at birth (Brace & Wolf, 1989; Underwood et al., 2005).

After keratinization of the embryonic skin and the incipient kidney function in the 2nd trimester of pregnancy, the total amount of AF is determined by different factors (Figure 1) that contribute either to production or to consumption of the fluid (Underwood et al., 2005). The most important AF producing factors are fetal urine and lung fluid production opposed to fetal swallowing as well as transmembranous and intramembranous absorption as elimination processes (El-Haddad et al., 2004; Gilbert & Brace, 1993).

1.1.2 Imbalances in the volume of amniotic fluid (AF)

A relevant imbalance between the producing and consuming processes may lead to pathological changes of the amount of AF with potential severe impacts on the fetal development. These changes can be quantified by ultrasonic measurements of the amniotic fluid index (AFI) depending on the volume of AF. For this purpose, the uterus is divided in four quadrants from which the anteroposterior diameters of the largest empty fluid pockets not containing fetal parts are summated (Phelan et al., 1987). Another method is the measurement of the so-called single maximal vertical pocket (MVP), where only the largest empty fluid pocket is measured in the same way like with the AFI method (Manning et al., 1981).

A too low amount of AF, defined by an AFI < 5 cm or a MVP < 2 cm, is defined as oligohydramnios (Peipert & Donnenfeld, 1991). Oligohydramnios can occur during otherwise uncomplicated pregnancies, but may also contribute to a complicated pregnancy course resulting in an adverse outcome with meconium in the amniotic fluid, meconium aspiration syndrome (MAS), need for Caesarean delivery, low birth weight, respiratory distress syndrome, hypoplasia of the lung or arthrogryposis due to a lack of movement (Klaassen & Kemper, 2010; Magann et al., 2007). A severe oligohydramnios and the concomitant increase of fluid pressure becomes manifest in the so-called Potter sequence, which depicts a collection of physical abnormalities of the face, lung and the bones and often leads to stillbirth (Insoft & Todres, 2009; Potter, 1946). One main cause of oligohydramnios lies in an impaired fetal urine production due to renal congenital dysplasia, bilateral agenesis of the kidney or polycystic kidney disease (Insoft & Todres, 2009; Klaassen & Kemper, 2010).

A too high amount on the other hand, defined by an AFI of > 25 cm or single deepest pocket (SDP) > 8 cm, is called polyhydramnios (Magann et al., 2007) and can be observed in approximately 0.2 – 2% of all pregnancies (Alexander et al., 1982; Dashe et al., 2002; Hill et al., 1987; Hobbins et al., 1979; Pri-Paz et al., 2012). Causes of polyhydramnios can sometimes be traced back to maternal or acquired conditions like diabetes, infections *in utero*, drug abuse and abnormalities of the placenta or to fetal conditions like genetic anomalies, Rh iso-immunization, anomalies of the gastro intestinal duct like duodenal atresia or anomalies of the central nervous system that affect the ability to swallow or multiple pregnancy (Lallar et al., 2015; Pri-Paz et al., 2012; Sigmon et al., 2022).

Each of these conditions can have serious consequences resulting in perinatal morbidity and mortality (Hwang & Bordoni, 2021; Peipert & Donnenfeld, 1991). According to OMIM (McKusick, 2007) more than 198 genes had been associated with polyhydramnios. One of the most frequent recognized monogenic causes of polyhydramnios is the Bartter syndrome spectrum, which results from defective tubular salt transport (Cunha & Heilberg, 2018).

However, in about 50% of all pregnancies complicated by polyhydramnios no underlying condition can be found and the cause remains idiopathic (Abele et al., 2012; Dashe et al., 2002; Hamza et al., 2013).

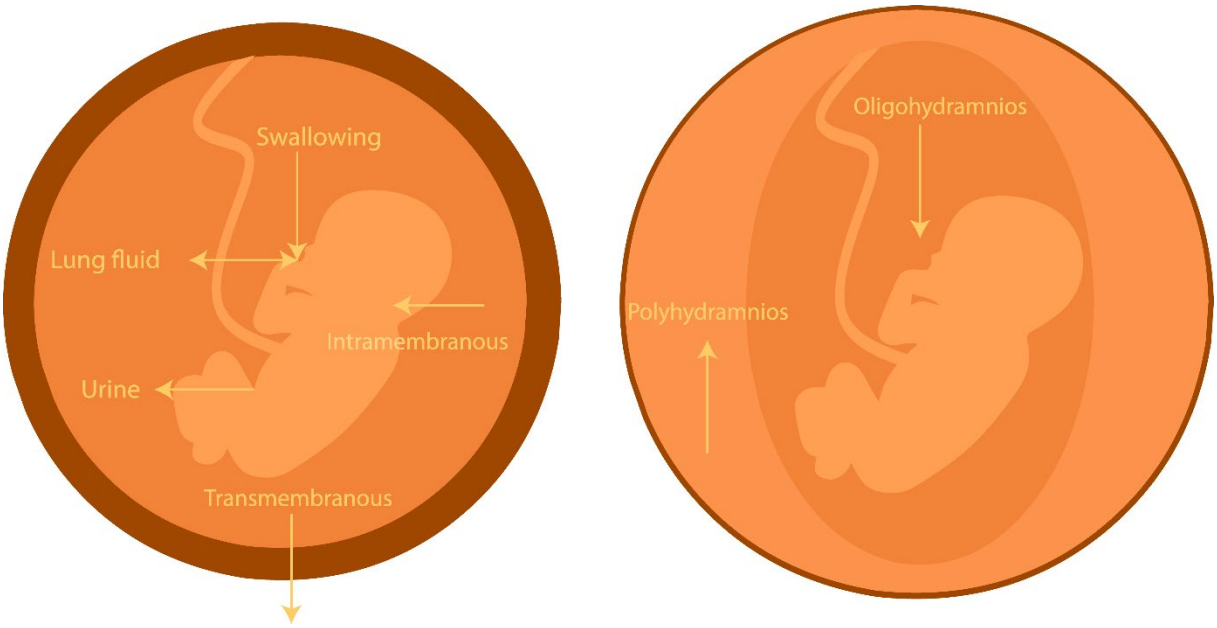

Figure 1: Amniotic fluid homeostasis is dependent on consuming and producing processes. *An imbalance in one of these processes leads either to polyhydramnios or to oligohydramnios.*

1.2 Kidney ion transport

The kidney is a bean-shaped organ which lies retroperitoneally between the 12th thoracic and the 3rd lumbar vertebrae and whose principal task is to keep the homeostasis of volume and composition of extracellular fluids by maintaining plasma osmolality, pH, plasma composition of electrolytes as well as the excretion of metabolism end products (Wallace, 1998). The work units of a kidney are the approximately 1.2 million nephrons which consist of the Bowman's capsule surrounding the glomerular capillary tuft, the proximal convoluted tubule, the loop of Henle as well as the distal convoluted tubule that flows into the collecting ducts

(Wallace, 1998). The process of forming urine starts by glomerular filtration of blood plasma, which is pressed in the glomerulus through capillary pressure via the efferent arteriole constraining fluid and small solutes through the pores while holding back proteins which are too large to pass (Wallace, 1998). Salts on the other hand can pass freely the glomerular filter making a reabsorption in the subsequent segments of the nephron necessary in order to maintain volume and composition of the internal milieu and prevent salt loss as well as volume depletion (Seyberth & Schlingmann, 2011).
The kidney usually filters approximately 180 litres of blood per day while the production of urine is limited to an average of 1 – 2 litres per day showing that a high percentage of the primary urine is reabsorbed to the blood (Wallace, 1998). The main factors of this reabsorption are water, electrolytes like sodium, calcium, potassium, magnesium, phosphate, bicarbonate and chloride as well as nonelectrolytes like glucose, amino acids, urea, uric acid and creatinine (Wallace, 1998). Reabsorption takes place in the tubules and is accomplished either by active transport mechanisms requiring energy to shift substances like sodium, potassium, calcium, phosphate and uric acid against an osmotic gradient or passive transport mechanisms requiring no energy to shift substances like urea, water and chloride down an osmotic gradient (Wallace, 1998). Water reabsorption is controlled by vasopressin (ADH) while sodium and potassium reabsorption as well as phosphate secretion is influenced by aldosterone and adrenal cortical hormone (Wallace, 1998). The main structure for sodium reabsorption (ca. 25%) while being impermeable for water depicts the thick ascending limb of the loop of Henle (TAL), whose main ion channel at the luminal membrane is the furosemide-sensitive sodium–potassium–chloride cotransporter (NKCC2) which is encoded by the *SLC12A1* gene (Cunha & Heilberg, 2018; Gamba et al., 1994; Seyberth & Schlingmann, 2011; Simon, Karet, Hamdan, et al., 1996). NKCC2 carries sodium coupled with potassium and chloride from the tubular lumen within the cell via an electrochemical gradient induced by the ATP-dependent basolateral sodium-potassium adenosine-triphosphate (Na^+K^+ATPase) pump (Cunha & Heilberg, 2018; Katz & Epstein, 1967). Ion transport inside the cell changes the intracellular ion balance resulting in the need for further transport processes. K^+ is eliminated actively from the inside of the cell to the lumen by the renal outer medullary K^+ (ROMK) channel encoded by the *KCNJ1* gene (Ho et al., 1993; Kleta & Bockenhauer, 2018). Chloride reabsorption to the basolateral side is conducted by ClC-Ka encoded by the gene *CLCNKA* and ClC-Kb encoded by the gene *CLCNKB* which, requires the subunit

barttin encoded by the *BSND* gene (Hennings et al., 2017; Kieferle et al., 1994; Matsumura et al., 1999; Simon et al., 1997). Mutations in one of these genes can lead to Bartter syndrome (BS), a collective term for a group of tubulopathies characterised by renal salt wasting, hypokalemia, metabolic alkalosis, hyperreninemia and a variable degree of antenatal manifestations like polyhydramnios (Unwin & Capasso, 2006). To date, BS is likely the best studied renal tubular disorder, although many questions remain unanswered.

1.3 The Bartter syndrome spectrum

BS was first described by Frederic Bartter in two African American patients with hypertrophy and hyperplasia of the juxtaglomerular apparatus of the kidneys as well as aldosteronism and impairment of urinary concentrating ability while having normal blood pressure (Bartter et al., 1962).

Three decades later, genetic studies could attribute mutations in the different ion transporter proteins involved in sodium and chloride transport in the TALH to different subtypes of the syndrome with similar symptoms (Figure 2).

All types have in common that salt reabsorption in the TALH is severely impaired leading to salt wasting and, hence, to polyuria (Chaimovitz et al., 1973; Cunha & Heilberg, 2018).

Defective sodium reabsorption is detected in the macula densa, a part of the juxtaglomerular apparatus (JGA) playing an important role in the homeostasis of body fluid, electrolyte composition as well as blood pressure (Peti-Peterdi, 2015). As a consequence, the expression of cyclooxygenase-2 and, hence, prostaglandin is induced leading to an increased activation of the renin-aldosterone system (Gasongo et al., 2019; Konrad et al., 2021; Tsujii et al., 1998). As a result, hypokalemic and hypochloremic metabolic alkalosis develops (Gasongo et al., 2019; Konrad et al., 2021).

The spectrum of BS is composed of five distinct BS types and in a broader sense also Gitelman syndrome (GS), which exhibit variable and type dependent symptoms and are caused by mutations in different ion transporters or related proteins (Knoers, 2006; Seyberth & Schlingmann, 2011).

1.3.1 Bartter syndrome

BS1 accounts for about 25% of Bartter syndrome cases and is caused by mutations in the *SLC12A1* gene encoding the cotransporter Na-K-2Cl-Cotransporter (NKCC2), which is located in the ascending limb of Henle's loop (Simon, Karet, Hamdan, et al., 1996; Stevenson et al., 2022). BS1 may already manifest during pregnancy with fetal polyuria resulting in polyhydramnios and premature delivery (Ohlsson et al., 1984). Postnatal, neonates experience polyuria, which can lead to a waste of sodium and potassium as well as to hypokalemic metabolic alkalosis (Starremans et al., 2003). Moreover, hypercalciuria in combination with high levels of prostaglandins in urine are associated with the development of nephrocalcinosis and also growth retardation can be observed in patients (Vergine et al., 2018). BS2, which accounts for approximately 10% of Bartter cases, has its cause in mutations of the *KCNJ1* gene (Simon, Karet, Rodriguez-Soriano, et al., 1996; Stevenson et al., 2022). This gene encodes the Potassium Inwardly Rectifying Channel Subfamily J Member 1 (ROMK), which recycles the potassium that has entered the cell via NKCC2 in order to keep a potassium homeostasis that is crucial for proper sodium reabsorption (Hebert, 1998). Consequently, except for transient hyperkalemia, symptoms of BS2 are very similar to the ones observed in BS1.

Bartter syndrome type 3 (BS3) once thought to represent the mildest form of Bartter syndrome is caused by homozygous mutations of the *CLCNKB* gene (Simon et al., 1997). Today it has become clear that BS3 has a more diverse phenotypic spectrum ranging from antenatal to classical BS (diagnosis during childhood) and a Gitelman-like phenotype (Seys et al., 2017). This form of BS accounts for approximately 20% - 30% of all BS cases and may be the most common type worldwide (Stevenson et al., 2022). The protein Chloride channel Kb (CLCNKB) can be abundantly found in the ascending limb of the loop of Henle, the distal tubule as well as the collecting duct and is responsible for the reabsorption of chloride (Cheng et al., 2017; Rodriguez-Soriano et al., 2005). This subtype is characterised by an onset in infancy or early childhood with hypokalaemic alkalosis, salt–wasting, low blood pressure and normal magnesium levels without nephrocalcinosis (Rodriguez-Soriano et al., 2005; Simon et al., 1997). As the disease cannot be healed, life-long treatment must be accomplished. Secondary increases of prostaglandin and aldosterone have to be decreased as well as losses of electrolytes have to be supplemented which is achieved by administration

of potassium chloride supplementation as well as non-steroidal anti-inflammatory drugs (Kleta & Bockenhauer, 2006).

BS4 can be subdivided in two types. Type 4a accounts for less than 10% of Bartter cases and has its cause in mutations of the *BSND* (Barttin) gene (Birkenhager et al., 2001; Stevenson et al., 2022). Barttin depicts a subunit of the Chloride channel Ka (CLCNKA) and CLCNKB essential for their proper function (Estevez et al., 2001). The digenic form on the other hand is caused by mutations in *CLCNKA* and *CLCNKB,* which accounts for less than 5% of Bartter cases (Schlingmann et al., 2004; Stevenson et al., 2022). Both forms of BS4 have exclusively deafness as symptom due to defects of the ClC-K-Barttin complex that also recycles chloride ions in the inner ear which, in turn, is important for maintaining the transcellular transport of potassium by NKCC1 essential for hearing (Birkenhager et al., 2001; Estevez et al., 2001).

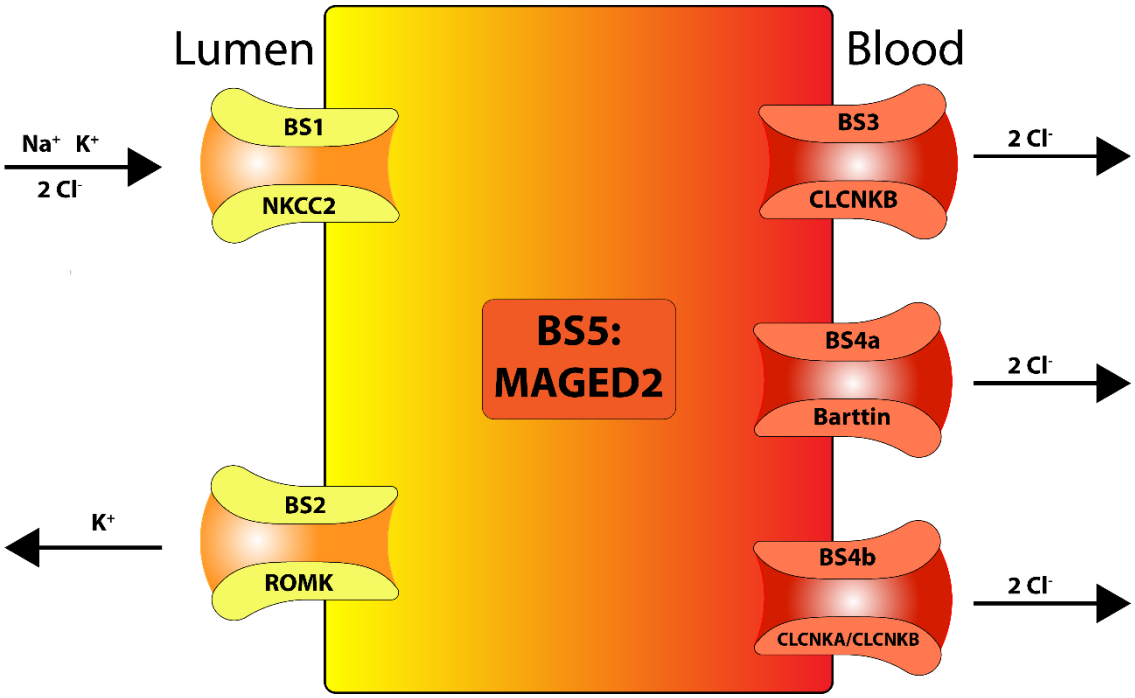

Figure 2: Subtypes of Bartter-syndrome and the function of the ion channels*. While BS1-4 is caused by pathogenic variants in cotransporters or ion channels, BS5 is caused by mutations in MAGED2, a protein not directly involved in tubular transport, but supposed to play a function in signalling processes. Modified from (Reusch et al., 2021).*

1.3.2 Gitelman Syndrome (GS)

While the general prevalence of BS is frequently estimated in the range of 1:500,000 to 1:1,000,000, the prevalence of GS is commonly estimated to be 1:40,000 making it the most common tubulopathy worldwide (Gladziwa et al., 1995; Ji et al., 2008). Onset of disease in most cases is above the age of six years and in a high number of cases a diagnosis is made not before adulthood (Knoers & Levtchenko, 2008). Due to biallelic pathogenic variants in the *SLC12A3* gene, which encodes for the renal thiazide-sensitive sodium-chloride co-transporter (NCC), salt transport in the distal nephron is highly impaired in GS comparable to BS (Knoers, 2006). GS is also characterized by hypokalemia and metabolic alkalosis as well as secondary aldosteronism, but frequent hypomagnesemia and hypocalciuria allow clinical differentiation to BS (Gitelman et al., 1966; Knoers & Levtchenko, 2008). Loss of NCC function leads to a reduced ability to reabsorb NaCl in the distal convoluted tubule (DCT) and to an increased amount of NaCl entering the collecting duct, which leads to salt loss and polyuria resulting in mild volume contraction and, thus, to an activation of renin and aldosterone (Knoers & Levtchenko, 2008). Sodium is then reabsorbed in the cortical collecting duct by the Epithelial Na(+) Channel Subunit Alpha (ENaC) channel at the expense of a loss of potassium and hydrogen ions, which causes the hypokalaemia and metabolic alkalosis (Knoers & Levtchenko, 2008).

Hypomagnesemia most likely arises from the renal downregulation of the epithelial magnesium channel transient receptor potential cation channel subfamily M member 6 (TRMP6) which is expressed at the apical membrane of the distal convoluted tubule as well as in the brush border of the duodenum (Blaine et al., 2015; Nijenhuis et al., 2005).

1.3.3 Transient antenatal Bartter syndrome

After more than a decade without the identification of a new BS gene, we could associate mutations of the Melanoma-associated antigen D2 (*MAGED2*) with an unusual type of antenatal BS (BS5) (Laghmani et al., 2016). In the index family (F1) three pregnancies with male fetuses were complicated by severe polyhydramnios leading to preterm delivery and a stillborn infant in one case (Figure 3). The course of

disease in the two other infants was characterized by severe polyuria with salt-loss as well as hypercalciuria leading to medullary nephrocalcinosis (Laghmani et al., 2016). Whole-exome sequencing revealed a hemizygous mutation in the X-chromosomal gene *MAGED2* (c.1038C→G, p.Y346*) in the affected male (Laghmani et al., 2016).

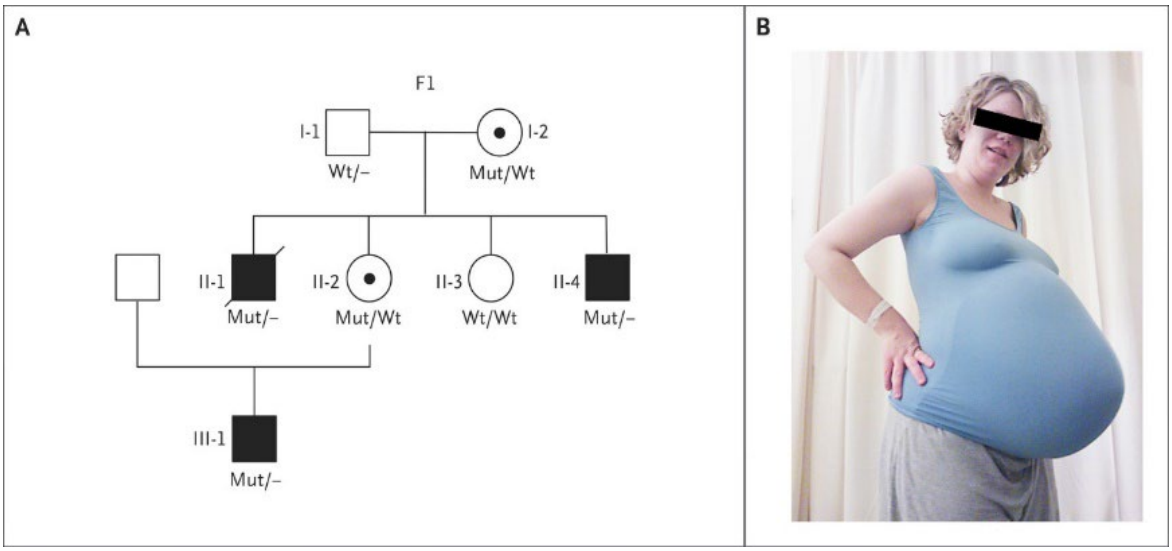

Figure 3: Genetic and clinical characteristics of the index family. *(A) Pedigree of the index family, in which pregnancies with three male siblings (black squares) were complicated by severe polyhydramnios while pregnancies with female fetuses (circles) were uneventful. (B) Clinical manifestion of the polyhydramnios of F1.II-2 during pregnancy with male fetus F1.III-1 (Laghmani et al., 2016).*

In eight further families with either antenatal Bartter syndrome or idiopathic polyhydramnios without mutations in the conventional Bartter syndrome genes, inherited *MAGED2* mutations could be found (Figure 4A and B). In two families, de-novo mutations could be detected (Figure 4A and B) (Laghmani et al., 2016).

In the meantime, studies from multiple groups could confirm the association of antenatal Bartter syndrome cases and mutations in *MAGED2*. In a French cohort, 17 antenatal Bartter syndrome cases from 16 families carried mutations in *MAGED2* (Legrand et al., 2018), studies of two several Chinese groups reported a novel complete deletion of *MAGED2* (Yang et al., 2019) as well as a frame-shift (X. Wu et al., 2021) and a missense mutation (Ma et al., 2021). Remarkably, *MAGED2* mutations accounted for 9% of all cases of antenatal Bartter syndrome in the French cohort as well as for 38% of patients without mutations in the genes causing BS1-4 and for 44% of male patients without mutations in the genes causing BS1-4 (Legrand et al., 2018). The disease is mainly characterised by severe polyhydramnios, premature birth, postnatal polyuria with salt-wasting, hypercalciuria, hyperreninemia and

hyperaldosteronism which all is concomitant with a high risk of premature death (Laghmani et al., 2016).

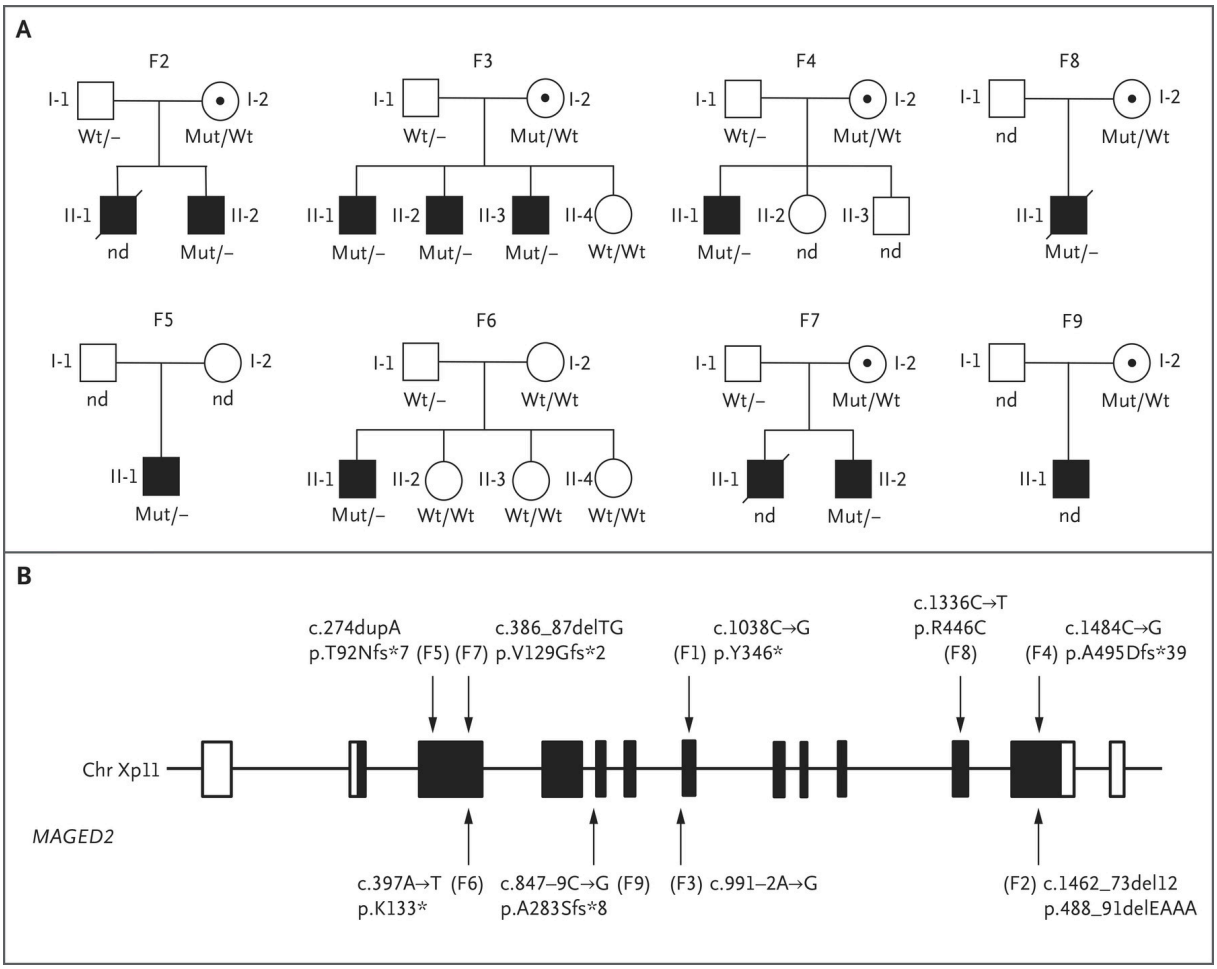

Figure 4: Pedigree of families with mutations in MAGED2 leading to BS5*. (A) illustrates the family trees of six additional families with transient antenatal Bartter's syndrome (F2-F7) and idiopathic polyhydramnios during pregnancies with male fetuses (F8 and F9). (B) shows the seven truncating mutations and two nontruncating mutations that were identified in MAGED2 in our initial study. Adopted by Laghmani et al., 2016*

The most striking clinical difference between BS5 and all other previously known forms of BS or GS is the transient character of tubular dysfunction (Figure 5). While patients affected with one of the autosomal recessive BS or GS have life-long fluid losses and require long-term treatment with electrolyte supplementation as well as medication with nonselective or COX2-selective inhibitors (Ma et al., 2021), patients with BS5 will have an excellent prognosis beyond the perinatal and neonatal period. In the follow-up of a patient from the index family at 2 years of age, tubular and glomerular function were in a normal range (Laghmani et al., 2016).

A further unique feature about BS5 in comparison to the other forms of BS is the fact that MAGED2 has no obvious role in renal ion or water transport.

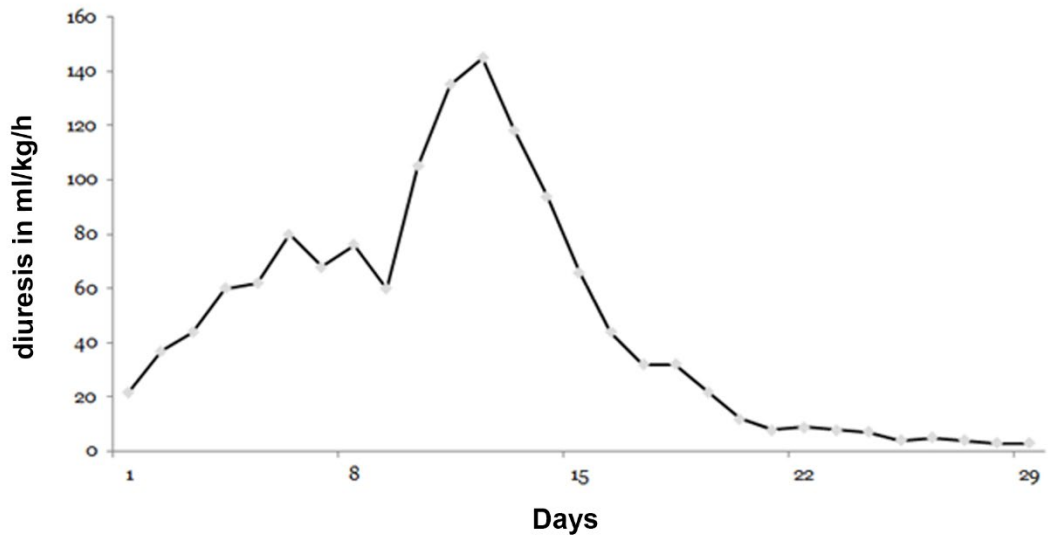

Figure 5: Exemplary postnatal course of transient polyuria in individual III-1 (F1). *Polyuria strongly increases after birth and declines after a few days (personal communication with Prof. Dr. Martin Kömhoff).*

1.4 MAGED2

MAGED2 belongs to the family of *MAGE* genes which is an ancient protein family that has its origin in a single gene in protozoa that just recently went through an expansion to a multigene family (Figure 6A and B) via retrotransposition, gene duplication and other gene modifications in placental mammals (Lee & Potts, 2017). The first described members of that gene family - *MAGEA*, *MAGEB* and *MAGEC* – are organized in three or four exons and are highly expressed in various kinds of cancer while being silent in normal tissue except for male germ cells (Dabovic et al., 1995; De Plaen et al., 1994; Lucas et al., 2000; Lucas et al., 1998; Lurquin et al., 1997; Muscatelli et al., 1995; Rogner et al., 1995; van der Bruggen et al., 1991).

Members of the subfamily *MAGED*, however, are organized in 11 exons and are expressed ubiquitously also in normal tissue (Lucas et al., 1999). Moreover, *MAGED2* was found to be highly expressed in mice during embryonic development especially in the brain while during adulthood no MAGED2 protein could be detected anymore at P60 in Western Blot analyses (Bertrand et al., 2004).

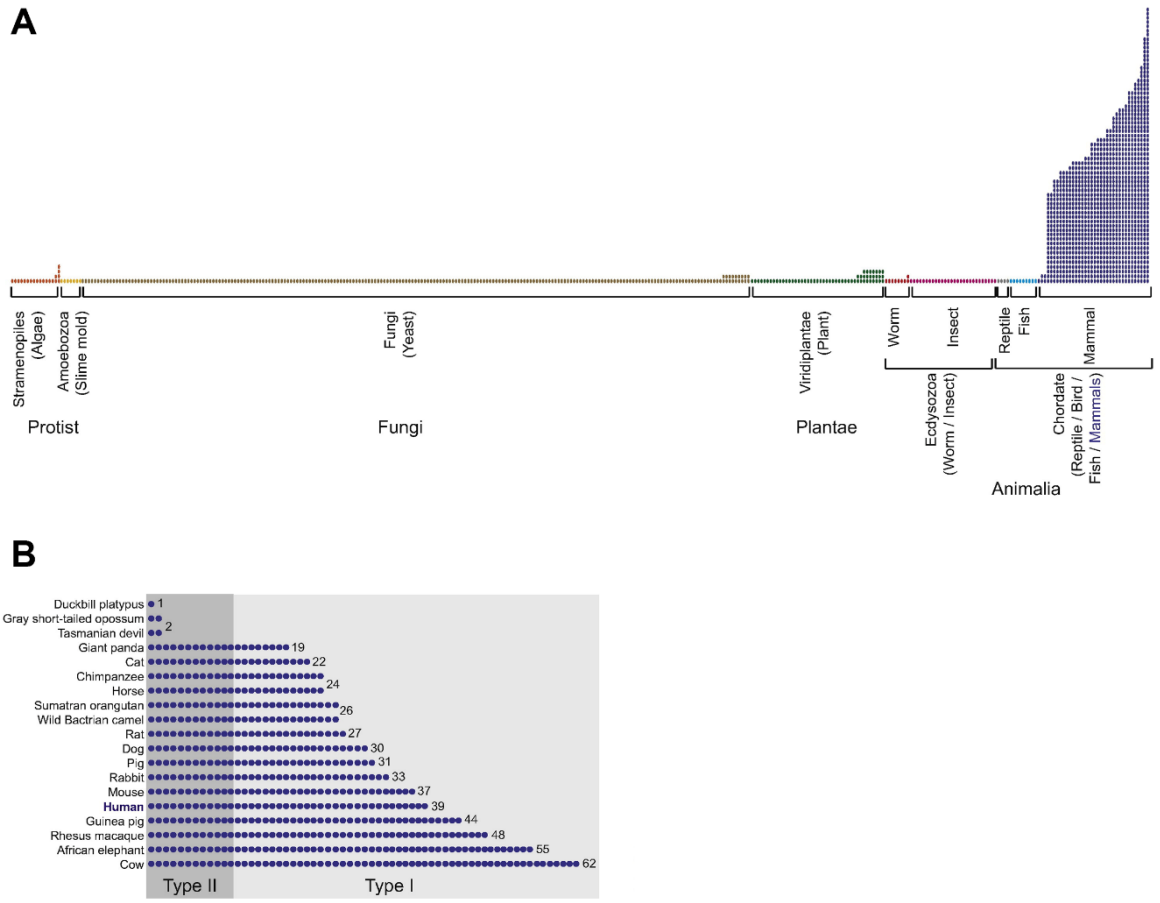

Figure 6: Evolution of the MAGE genes *(A) MAGE genes are highly conserved in all eukaryotes with a rapid expansion from a single MAGE to a multigene family in mammals. (B) Recent expansion of MAGE genes in mammals. Adopted by Lee et al., 2017.*

All *MAGE* genes have in common a structure called the MAGE homology domain (MHD), which has an approximate size of 170 aa and all human MHDs share approximately 46% of their protein sequence identity. There are many amino acids that are highly conserved among the different human MAGE isoforms (Barker & Salehi, 2002)

Structural studies could show that the MHD consists of two tandem winged-helix (WH) motifs from which every WH has a characteristic helix-turn-helix motif, which is packed against an antiparallel β-sheet (Doyle et al., 2010; Newman et al., 2016). Several interactions between the MHD and other proteins could have been shown before. Therefore, MAGE proteins seem to be interacting with E3 RING ubiquitin ligases via their MHD to form MAGE-RING ligases (MRLs) enhancing their activity and, thus, influence many cellular processes (Doyle et al., 2010). E3 ubiquitin ligases are the

enzymes that promote the final step in the transfer of ubiquitin to substrate proteins, which determines the fate of the modified proteins (Zheng & Shabek, 2017). Ubiquitination not only tags proteins for proteasomal degradation but is also involved in the regulation of protein endocytosis and trafficking (Foot et al., 2017; Glickman & Ciechanover, 2002; Haglund & Dikic, 2012).

The function of MAGED2 in the kidney is widely unknown. It has been shown to interact with the tumour suppressor protein p53 hypothesising a role in the regulation of the cell cycle (Papageorgio et al., 2007). Moreover, *MAGED2* is upregulated in several forms of cancer, which is why it can be used as diagnostic marker (Hashimoto et al., 2015; Li et al., 2020). In colorectal and gastric cancer MAGED2 was shown to be able to facilitate cell adhesion and, thus, metastasis of the cancer cells (Kanda et al., 2016). In breast cancer, increased MAGED2 expression is also correlated with cell invasion and metastasis as well as a poorer prognosis of patient survival (Jia et al., 2019; Thakur et al., 2022).

In the kidney, MAGED2 protein is present in fetal renal cortex primarily in interstitial but also tubular epithelial cells (Laghmani et al., 2016). In adult kidney MAGED2 is present in the entire distal tubule (Laghmani et al., 2016; Lee et al., 2015). Interactome analysis of HEK293T cells expressing wild-type MAGED2 or the R446C missense variant showed a loss of interaction of MAGED2^{R446C} with the chaperone DNAJB1 and the Gs alpha subunit Gαs (encoded by *GNAS*), which is part of the G Protein coupled receptor pathway (GPCR) (Laghmani et al., 2016). Loss of function of MAGED2 in kidney sections from the deceased individual II-1 (F1) showed reduced expression as well as virtual absence of NKCC2 and NCC from the apical cell membrane compared to wild-type kidney (Laghmani et al., 2016). Moreover, studies in HEK293T cells showed that MAGED2 overexpression leads to a higher amount of NKCC2 and NCC expression and maturation (Laghmani et al., 2016).

1.5 Aim of the study

The precise functions of MAGED2 in the kidney are still not well understood. Alongside *MAGED2*, only one other *MAGE* type II gene, *MAGEL2*, is known to be associated with a human disease. Pathogenic variants in this gene result in Schaaf-Yang syndrome, a disease resembling Prader-Willi Syndrome (PWS) in many clinical aspects, such as

autism spectrum disorder, intellectual disability and a wide range of further clinical and behavioural characteristics associated with PWS (Schaaf et al., 2013). *MAGED2* is highly homologous to *MAGEL2* (Boccaccio et al., 1999; Lucas et al., 1999) and is strongly expressed in several tissues during embryonic development but pathogenic variants exclusively result in a renal phenotype. What makes the kidney so susceptible for MAGED2 dysfunction and what molecular changes underlie the transient nature of the disease?

Consequently, our aim was to further analyse MAGED2 associated signalling processes, in particular its ability to modulate G-protein coupled receptor signalling based on its interaction with Gαs. A further aim was to dissect and characterize the effects of aberrant GPCR signalling on known target molecules like the cotransporters and ion channels associated with BS and tubular dysfunction.

These aims should be investigated using the following strategies:

1. In a first approach alterations of signalling processes due to *MAGED2* loss should be investigated in a cell model with endogenous MAGED2 expression. For this purpose, we will downregulate endogenous *MAGED2* in HEK293T cells with siRNA and analyse the consequences on the proteomic and phosphoproteomic level by mass spectrometry (MS)-based approaches.

2. In a next step, a bit closer to the renal context, *Maged2* loss will be investigated in mouse collecting duct cells (mpkCCD), a cell line derived from the distal tubule that responds to vasopressin and aldosterone without further manipulation (Bens et al., 1999; Yu et al., 2009). We choose this cell line because a thick-ascending limb cell-line with endogenous NKCC2 and NCC protein expression is currently not available (Hannemann et al., 2009; Kompatscher et al., 2018). Physiological response from mpkCCD cells to vasopressin induces expression and membranous transport of AQP2, making the apical membrane permeable for water (Nielsen et al., 1995). As the associated receptor vasopressin receptor 2 (V2R) represents a member of the GPCR family, induction of this signalling pathway seems to be an adequate mechanism to study the role of MAGED2 on Gαs and the further downstream signalling cascade. Alterations due to *Maged2* loss will be investigated after short-term vasopressin treatment, which induces changes of phosphorylation patterns, as well as after long-

term treatment, which affects transcriptional processes with phosphoproteomic and proteomics approaches, respectively as well as Western Blot and qPCR experiments of crucial targets.

3. As cell systems are of limited use to understand the complex spatiotemporal changes that result from loss of *Maged2* in the kidney, we decided to design knock-in mouse models of the missense mutation R446C and the stop mutation Y346X identified from the initial cohort. The R446C mutation was found in a severely affected patient and was used for interactome analysis demonstrating a loss of Gαs interaction (Laghmani et al., 2016). We will characterize the phenotype of the mouse model and examine the effects of *Maged2* loss in the kidney at developmental stage P0. Here, we will study GPCR signalling and localisation of crucial cotransporters and channel proteins associated with BS by immunofluorescence (IF) stainings. Whole mouse kidneys will be subjected to a proteomic approach to investigate alterations on protein level due to *Maged2* loss.
This will provide a deeper understanding of the molecular mechanism responsible for BS5, help to explain the transient nature of the disorder and reveal new insights into the functionality of the kidney with regard to fluid and electrolyte homeostasis.

2 Results

2.1 MAGED2 is expressed in the mouse kidney in early embryonic stages

As former studies had shown that *Maged2* expression in murine embryos and brains decreased during embryonic development (Bertrand et al., 2004), we wanted to check if this pattern can also be observed in the developing mouse kidney. For this purpose, we checked *Maged2* expression as well as the expression of important renal ion transport proteins and water channels at stage E14.5, E18.5 and P0 in wild-type embryonic mice (Figure 7). It can clearly be seen that also in the kidney the expression of *Maged2* mRNA as well as of MAGED2 protein decreases during embryonic development (Figure 7A and B). Contrary to the expression of *Maged2* mRNA, the expression of mRNA of the important renal ion co- transporter *Slc12a3* (NCC), *Slc12a1* (NKCC2) and the channel protein *Aqp2* increased during renal development (Figure 7C).

Although expressed on the X-chromosome, a significant difference in *Maged2* mRNA expression between male and female mice could not be observed although expression in male animals is slightly lower (Figure 7D).

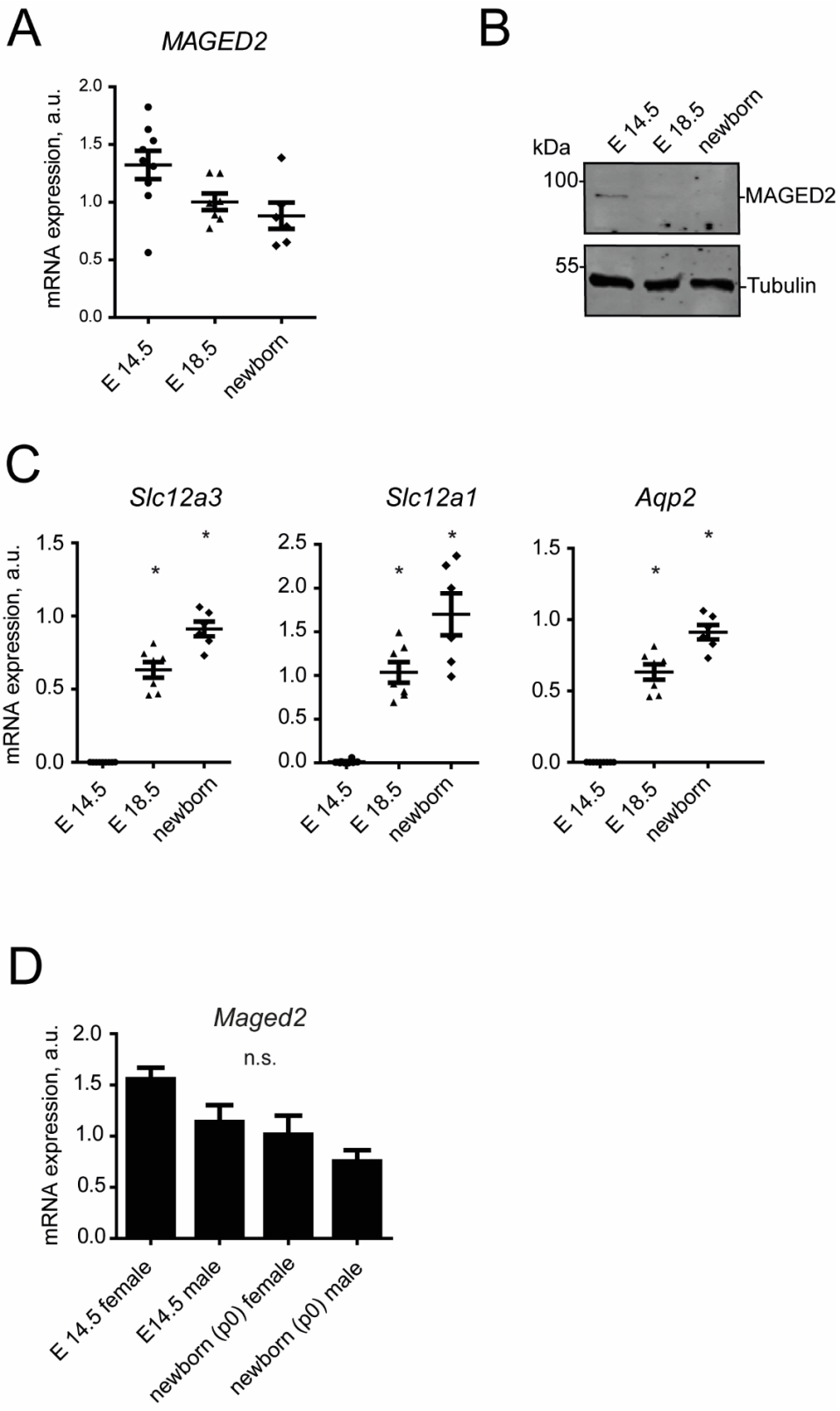

Figure 7: Maged2 is expressed in the mouse kidney during embryonic development*. (A) qPCR analysis of Maged2 mRNA expression in murine embryonic tissue at the indicated embryonic stages. (P<0.05 in one-way ANOVA followed by Tukey's post-test for E14. vs newborn. N=9 for E.14.5, N=7 for E18.5 and N=6 for newborn) (B) Western blot analysis of MAGED2 protein in murine embryonal tissue at the indicated embryonic stages. As loading control Tubulin was used. Representative blot of n=3 animals. (C) qPCR analyses of the mRNA expression of the transporters NCC, NKCC2 and AQP2 of mouse tissue at the indicated embryonic stages. (*P<0.05 in one-way ANOVA followed by Tukey's post-test. N=9 for E.14.5, N=7 for E18.5 and N=6 for newborn). (D) qPCR analysis of Maged2 mRNA in murine embryonal tissue at the indicated embryonic stages and discriminated between male and female.*

To examine the expression of *Maged2* also in other murine tissues, I mined transcriptome data from Wang et al. who performed transcriptome analysis of six tissues from embryonic and adult mice (Wang et al., 2021). The data shows that *Maged2* is ubiquitously expressed in kidney, brain, heart, liver, lung and retina tissue with a similar pattern of decrease throughout development from embryonic stage E15.5 to the adult stage P42 (Figure 8). The mRNA data of *Slc12a1*, *Slc12a3*, *Aqp2* and *Kcnj1* with expression confined to kidney show a similar pattern that could be seen in our murine tissue with increasing mRNA abundances from embryonic stage E15.5 to adult stage P42 (Figure 9). Moreover, the data shows that mRNA of these proteins is exclusively expressed in the kidney.

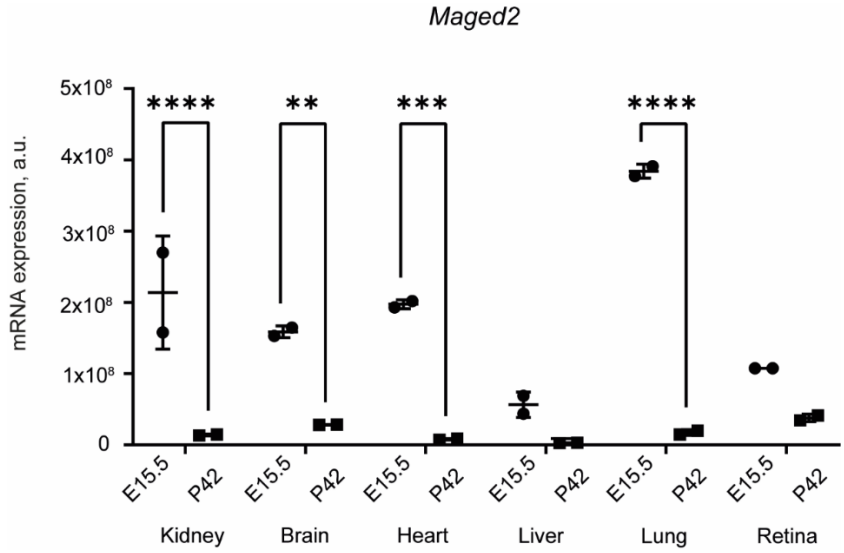

Figure 8: Maged2 is expressed in different organs during embryonic development*. Transcriptomic data was analysed from Wang et al., 2021 with Graphpad Prism software (N=2 for embryonic and adult mouse each. *P<0.05; **P<0.01; ***P<0.001 ****P<0.0001 in two-way ANOVA followed by Tukey's test).*

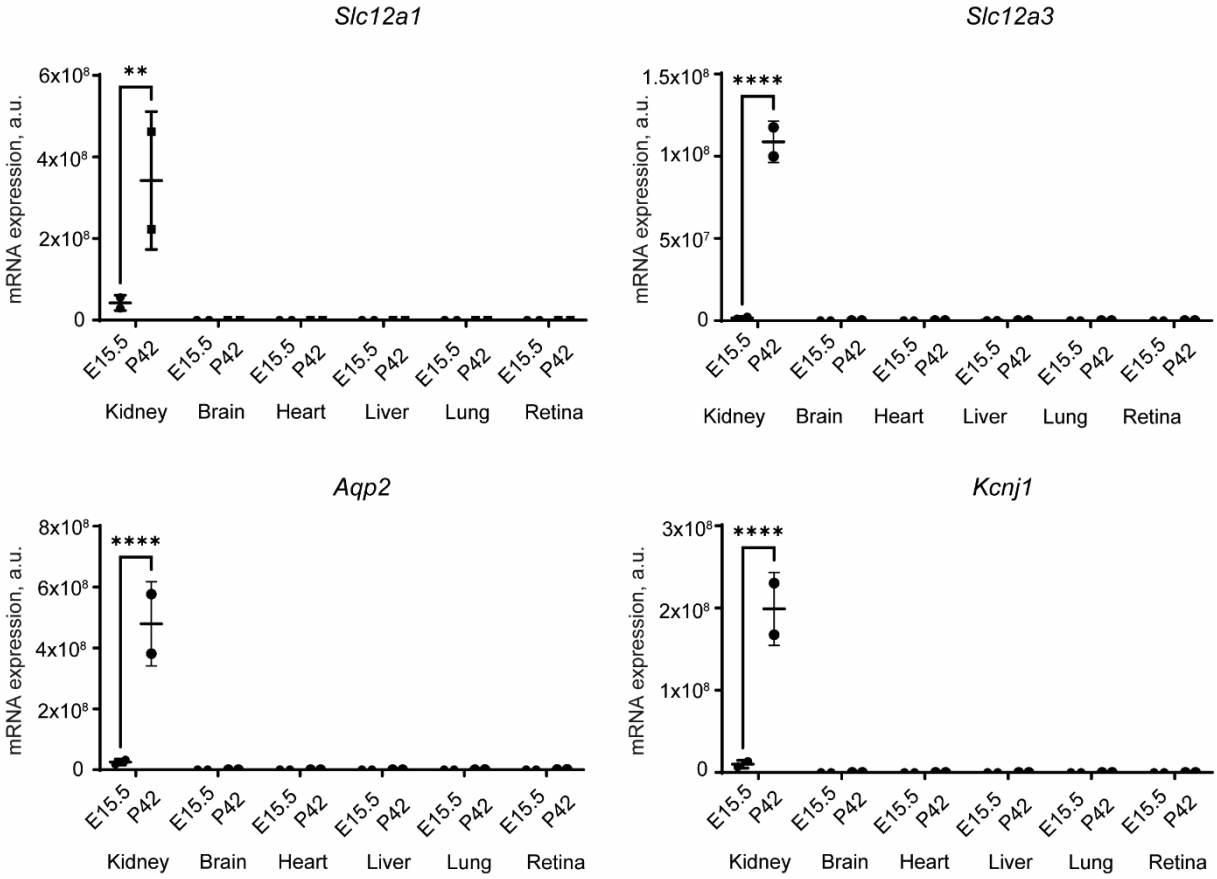

Figure 9: Crucial cotransporter and channel proteins are exclusively expressed in the kidney. *Transcriptomic data was analysed from Wang et al., 2021 with Graphpad Prism software. (N=2 for embryonic and adult mouse each. *P<0.05; **P<0.01; ***P<0.001 ****P<0.0001 in two-way ANOVA followed by Tukey's test).*

2.2 MAGED2 is a presumptive regulator of G-protein coupled receptor (GPCR) signalling

2.2.1 Proteomic analysis of HEK293T cells with *MAGED2* siRNA knockdown

HEK293T cells show a high endogenous MAGED2 expression (Figure 10A). For further understanding of the role of MAGED2 in these cells, proteomic analysis was performed with pellets of cells with and without *MAGED2* knockdown induced by siRNA treatment.

Successful siRNA knockdown could be confirmed by both Western Blot and proteomic analyses (Figure 10A and 10B). Western Blot quantification indicate a residual MAGED2 expression of approximately 11.6% (SD=2.4%) in the cells treated with *MAGED2* siRNA.

Proteome analysis showed that, despite MAGED2, no other proteins were differentially expressed in the cells treated with siRNA compared to the cells treated with non-specific siRNA (Figure 10B).

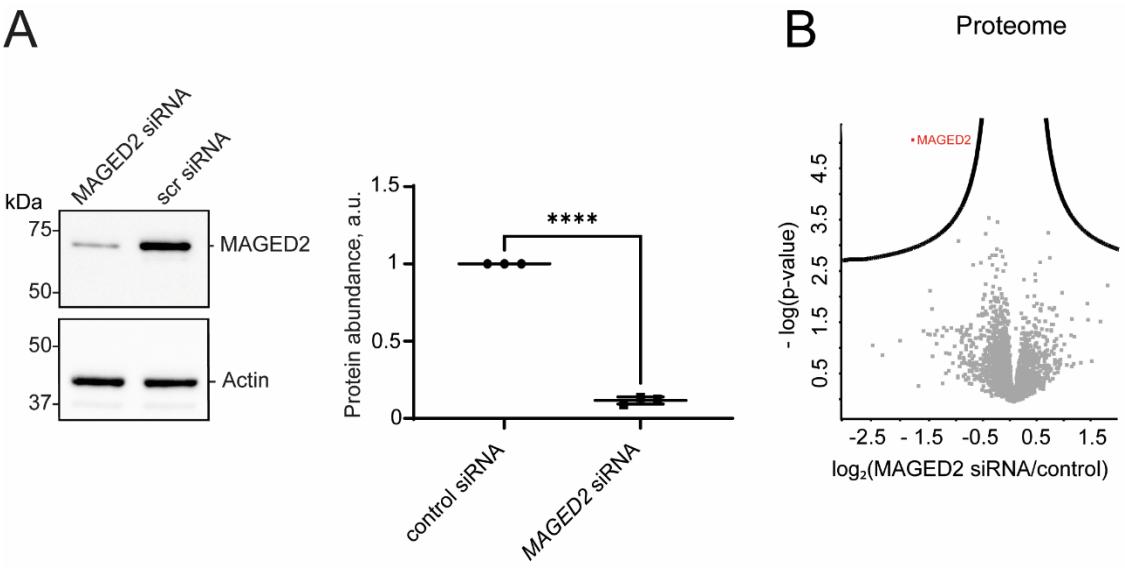

Figure 10: MAGED2 knockdown in HEK293T cells has no effect on the proteome. *(A) Western Blot analysis of MAGED2 in HEK293T cells treated with either MAGED2 siRNA or scrambled (scr) control siRNA. Beta Actin is used as loading control. Quantification was constituted with Image Lab software and statistic with GraphPad Prism (n=3, unpaired t-test, ****P<0.0001) (B) Proteome analysis of HEK293T cells after treatment with MAGED2 siRNA in comparison to scrambled siRNA treated control cells. Each dot represents a protein. Only the expression of MAGED2 was significantly altered (FDR = 0.05).*

2.2.2 Phosphoproteomic analysis of HEK293T cells with MAGED2 siRNA knockdown

As no additional altered protein expression in HEK293T cells after *MAGED2* siRNA treatment could be observed, a phosphoproteome analysis was performed with pellets of the same cells to check the impact of *MAGED2* knockdown on the post-transcriptional level as protein phosphorylation plays a major role in cell signalling and other cellular processes. In total, 1387 phospho-peptides were detected, from which 489 showed a significantly changed abundance in siRNA treated cells compared to control cells indicating strong alterations of the phosphorylation state (Figure 11).

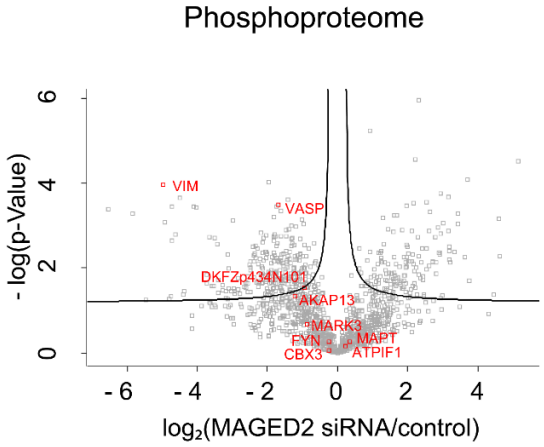

Figure 11: MAGED2 knockdown in HEK293T cells modulates phosphorylation processes. *Phosphoproteome analysis of HEK293T cells with MAGED2 siRNA versus control scrambled siRNA treatment. Each dot represents a phosphorylation site. Known targets of PKA phosphorylation are labelled with their protein symbol.*

Most remarkable, a modification of basophilic kinase associated phosphorylation motifs could be observed (Figure 12A and B).

Changes in the phosphoproteomic data, thus, were more pronounced than in the proteomic data suggesting a role of MAGED2 in signalling processes rather than as modulator of protein expression *in vitro* (Figure 12C).

We and also other groups could observe an interaction of MAGED2 with Gαs, which indicates a role of MAGED2 in signalling pathways related to GPCR (Huttlin et al., 2017; Laghmani et al., 2016). Data mining dynamic G-protein coupled receptor interactome datasets confirmed this hypothesis. Paek et al. used ascorbate peroxidase-catalysed proximity labelling (APEX) to track GPCR signalling in living cells (Paek et al., 2017).

Interestingly, MAGED2 was found as a protein associated with the GPCR angiotensin II type 1 receptor (Figure 12D) as well as the β2 adrenergic receptor (data not shown) in this dataset (Paek et al., 2017). These studies suggest a role of MAGED2 in GPCR-related signalling.

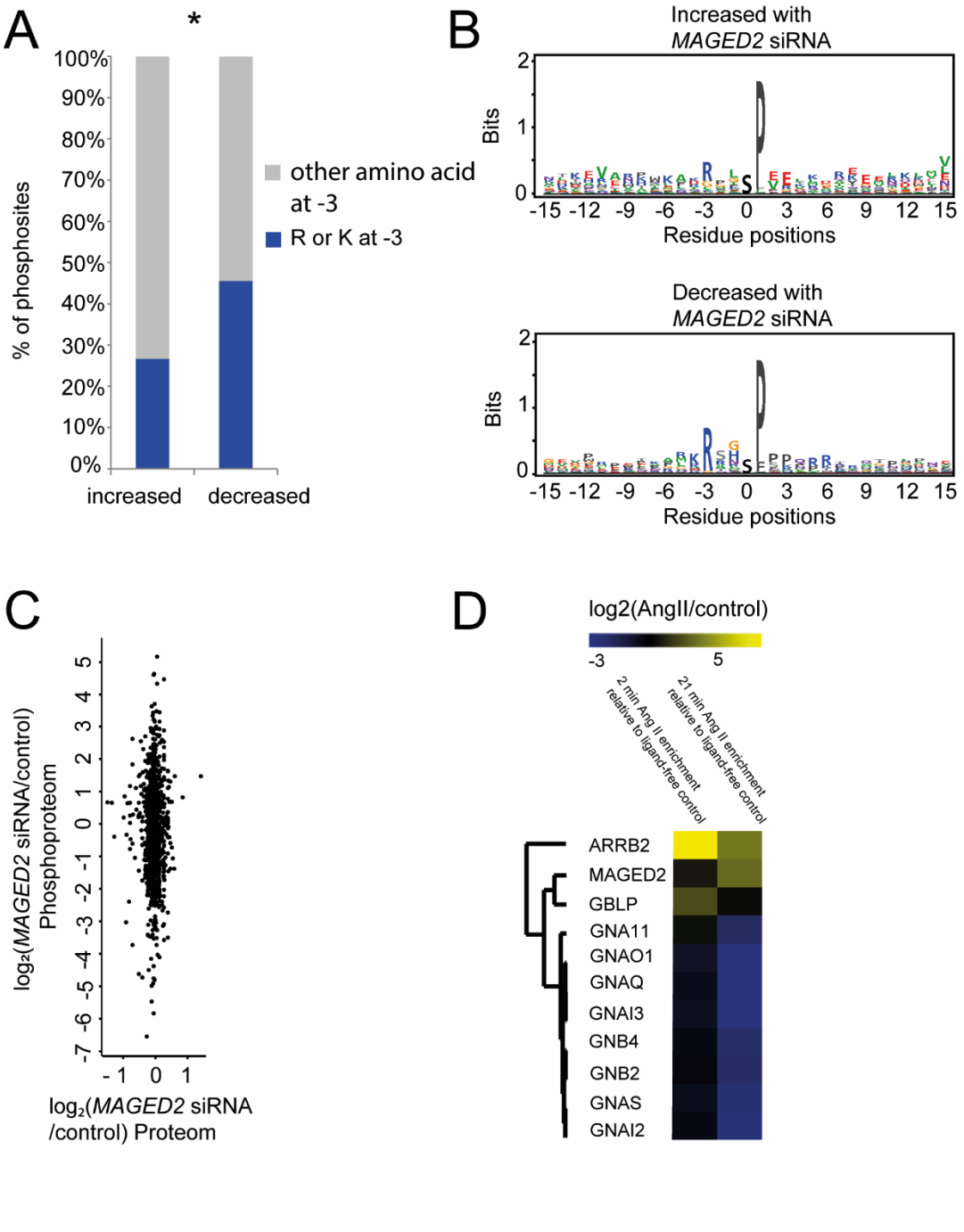

Figure 12: MAGED2 is a putative regulator of G-protein coupled receptor signalling. *(A) Characterization of the altered phosphorylation motifs by classifying motifs as basophilic or not (based on presence of R or K at the -3 position). Here was an overrepresentation of basophilic motifs in the phosphorylation sites decreased by MAGED2 knockdown. Fisher's exact test p<0.001. (B) Sequence logos showing overrepresented phosphorylation motifs increased and decreased in HEK293T cells after MAGED2 siRNA treatment. (C) Scatterplot indicating MAGED2 siRNA-induced changes in phosphoproteome (y axis) and proteome (x-axis) in HEK293T cells. Phosphorylation sites are more strongly affected by MAGED2 siRNA. (D) Reanalysis of published proteins in proximity to AT1R-APEX after angiotensin II treatment at two different time points (Paek et al., 2017). MAGED2 is recruited to AT1R after 21 minutes.*

2.3 MAGED2 as a modulator of vasopressin signalling in mpkCCD cells

Although HEK293T cells are of renal origin, they do not express any ion channel, cotransporter or water channel as they have more an epithelial character (Varghese et al., 2006). Thus, they are a cell model sufficient for many research applications but are no adequate model system for studying the effects of MAGED2 deficiency in the context of GPCR signalling. For this reason, we chose the murine cell-line mpkCCD for further studies. This cell-line is derived from murine cortical collecting duct of a transgenic mice carrying the SV40 large antigen under the control of the SV40 enhancer and the L-type pyruvate kinase promoter that show Cl^- and H_2O transport induced by vasopressin treatment (Bens et al., 1999; Chassin et al., 2007). The Arginine Vasopressin Receptor 2 (V2R) is the primary receptor of the collecting duct (CD) and once activated, this GCPR finally results in the insertion of AQP2 water channels in the apical membrane of the principal cells in the CD (Nielsen et al., 1995). Unlike the basolateral membrane which constitutively expresses AQP3/4 water channels, the apical membrane is dependent on V2R mediated APQ2 water transport (Ecelbarger et al., 1995; Terris et al., 1995). Not surprisingly, pathogenic variants of *AVPR2* or *AQP2* result in a condition known as nephrogenic diabetes insipidus (NDI), which is characterized by massive, inappropriately diluted urine volumes resulting in polyhydramnios, polyuria and hypernatraemic dehydration (Deen et al., 1994; Rosenthal et al., 1992; Weinberg et al., 2010). For the experiments, mpkCCD cells had to be grown on membrane supports until polarization and were then treated with a synthetical derivate of vasopressin (1-Desamino-8-D-Arginin-Vasopressin; dDAVP) on the basolateral side inducing endogenous AQP2 expression due to activation V2R (Hasler et al., 2002).

There are two ways for vasopressin-induced analysis. For the short-term analysis, mpkCCD cells are treated with dDAVP for 30 – 120 minutes, although it has to be mentioned that each short-term exposure follows a prefixed long-term exposure of 72 hours followed by dDAVP starvation of one hour to reach sufficient amounts of the proteins involved in the AQP2 pathway. Short-term dDAVP treatment activates the receptor AVPR2 which induces a cascade of processes involving an increase of intracellular cAMP and an activation of protein kinase A dependent phosphorylation processes which results in phosphorylation and trafficking of AQP2 to the apical

membrane (Yu et al., 2009). These processes strongly decrease in the course of 3 days while AQP2 expression and translation remains highly elevated leading to the assumption that long-term effects of dDAVP treatment are based on PKA-independent processes (Kortenoeven et al., 2012).

Maged2 was stably knocked down by using a PiggyBac transposase vector creating the two *Maged2* knock-down (kd) cell-lines hairpin 1 (hp1) and hairpin 2 (hp2). Efficiency of the knock down was checked by qPCR and Western Blot experiments. Significant reduction of *Maged2* mRNA as well as MAGED2 protein was demonstrated on mRNA and protein level, respectively (Figure 13).

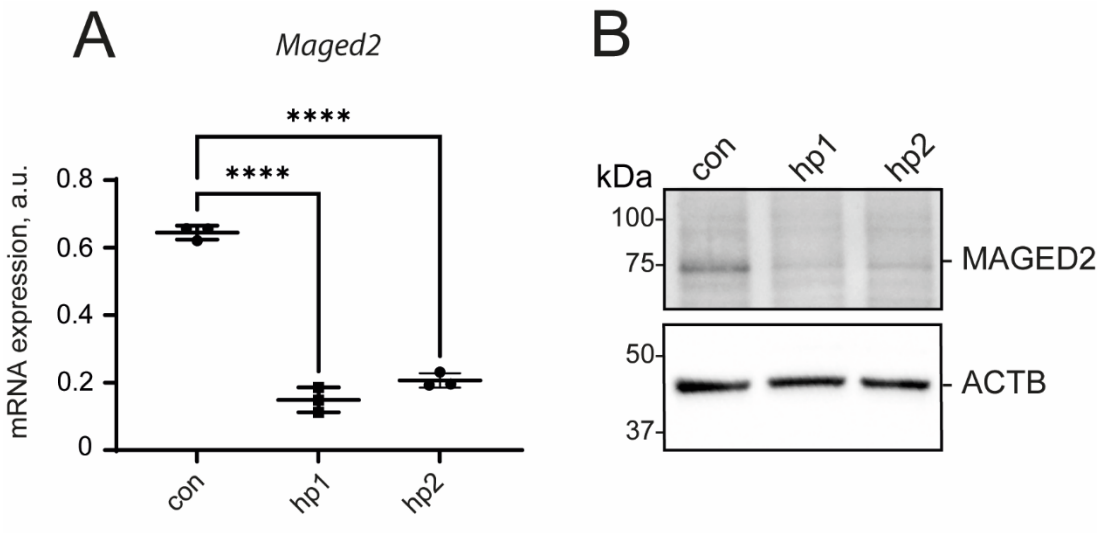

Figure 13: Maged2/MAGED2 is knocked down in mpkCCD cells. (A) *RT-qPCR of Maged2 in control mpkCCD as well as the knock-down cell lines hp1 and hp2 (n=3, unpaired t-test, ****P<0.0001). (B) Western Blot analysis of MAGED2 protein abundance in control mpkCCD as well as the knock-down cell lines hp1 hp2. ACTB was used as loading control (n=3).*

2.3.1 Short-term dDAVP signalling

Short-term dDAVP treatment leads to an activation of V2R and a GPCR downstream signalling cascade with increasing endogenous cAMP levels (Oksche & Rosenthal, 1998). To investigate if *Maged2* knock-down leads to changed cAMP kinetics, a cAMP assay was performed with measurements after 2 minutes, 30 minutes and 120 minutes. cAMP kinetics upon short-term dDAVP treatment of mpkCCD cells show a clear alteration in MAGED2 kd cells in comparison to wild-type cells. While there is a slight increase of cAMP in the wild-type cells followed by a soft decrease over time, the

change of cAMP kinetics in the kd cells is much steeper with a strong increase after 2 minutes and a strong decrease after 30 minutes. cAMP levels after 120 minutes decreased in all samples to a similar level (Figure 14).

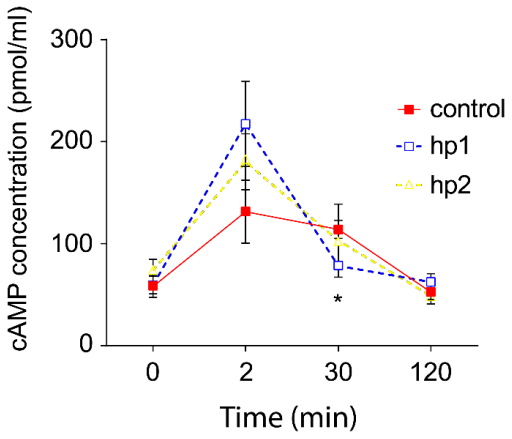

Figure 14: Maged2 depletion alters cAMP kinetics in mpkCCD cells. *Time course of cAMP levels in mpkCCD cells after treatment with 1 nM dDAVP at the indicated time points. *p<0.05 in a two-tailed t-test, n=3 (hairpins) or 4 (control).*

One target protein of the induced cAMP signalling cascade is the cAMP response element-binding protein (CREB) which is phosphorylated by several putative kinases like PKA and PKC on its serine 133 (S133) leading to an increased AQP2 expression as well as phosphorylation in order for proper AQP2 transport to the apical membrane (Gonzalez & Montminy, 1989; Hozawa et al., 1996; Matsumura et al., 1997).
After treatment of mpkCCD cells with dDAVP for 30 minutes, pCREB signalling shows a clear increase in the control cell-line while signalling kinetics seem to be altered in the *Maged2* knock-down cell lines. Here, we see only a weak or no pCREB response (Figure 15A), while pERK decrease due to vasopressin treatment is similar to those in the wild-type cells (Figure 15B) and according to the literature (Rinschen et al., 2010).

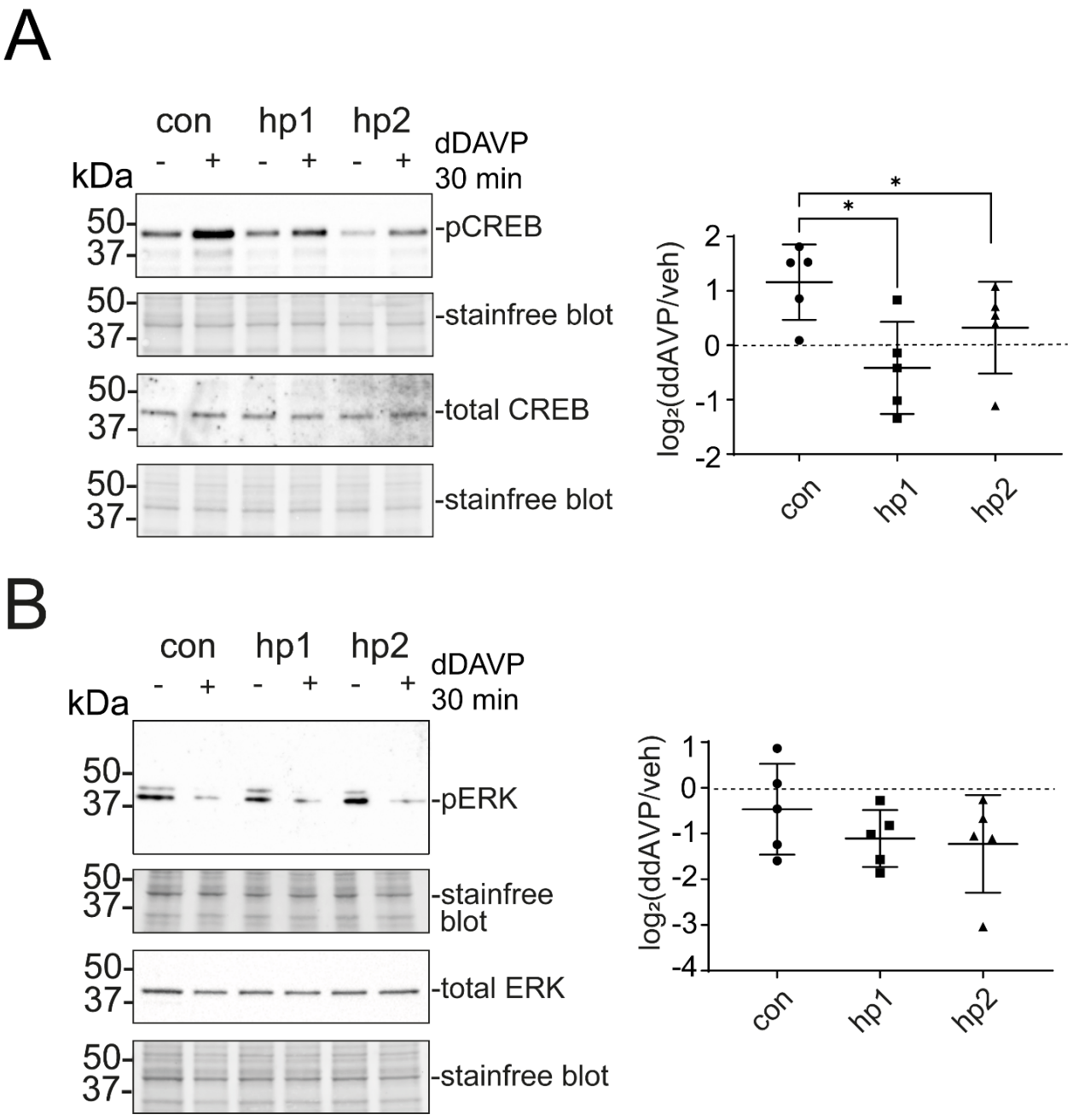

Figure 15: MAGED2 modulates short-term V2R dependent signalling in mpkCCD cells. *(A) Western Blot analysis of pCREB in mpkCCD cells after short-term treatment with 1 nM dDAVP for 30 minutes. The short-term exposure was preceded by a long-term exposure followed by a 6h dDAVP starvation. For the quantification, the pCREB level was normalized with the corresponding total CREB level signal and the logarithmic ratio of dDAVP treated to untreated sample was plotted (n=4; **P < 0.01, one-way ANOVA, Dunnett's multiple comparison test). (B) Western Blot analysis of pERK in mpkCCD cells after short-term treatment with 1 nM dDAVP for 30 minutes. The short-term exposure was preceded by a long-term exposure followed by a 6h dDAVP starvation. For the quantification, the pERK level was normalized with the corresponding total ERK level signal and the logarithmic ratio of dDAVP treated to untreated sample was plotted (n=4; one-way ANOVA, Dunnett's multiple comparison test). As negative control the stainfree blot was used.*

Cell pellets of short-term dDAVP treated mpkCCD cells were also investigated on a phosphoproteomic level by a mass spectrometry (MS) approach. Overall, no overt alterations between wild-type and kd cells were found (Figure 16A). However, the overall fraction of increased basophilic sites is decreased in the cells with depleted *Maged2* (Figure 16B and C).

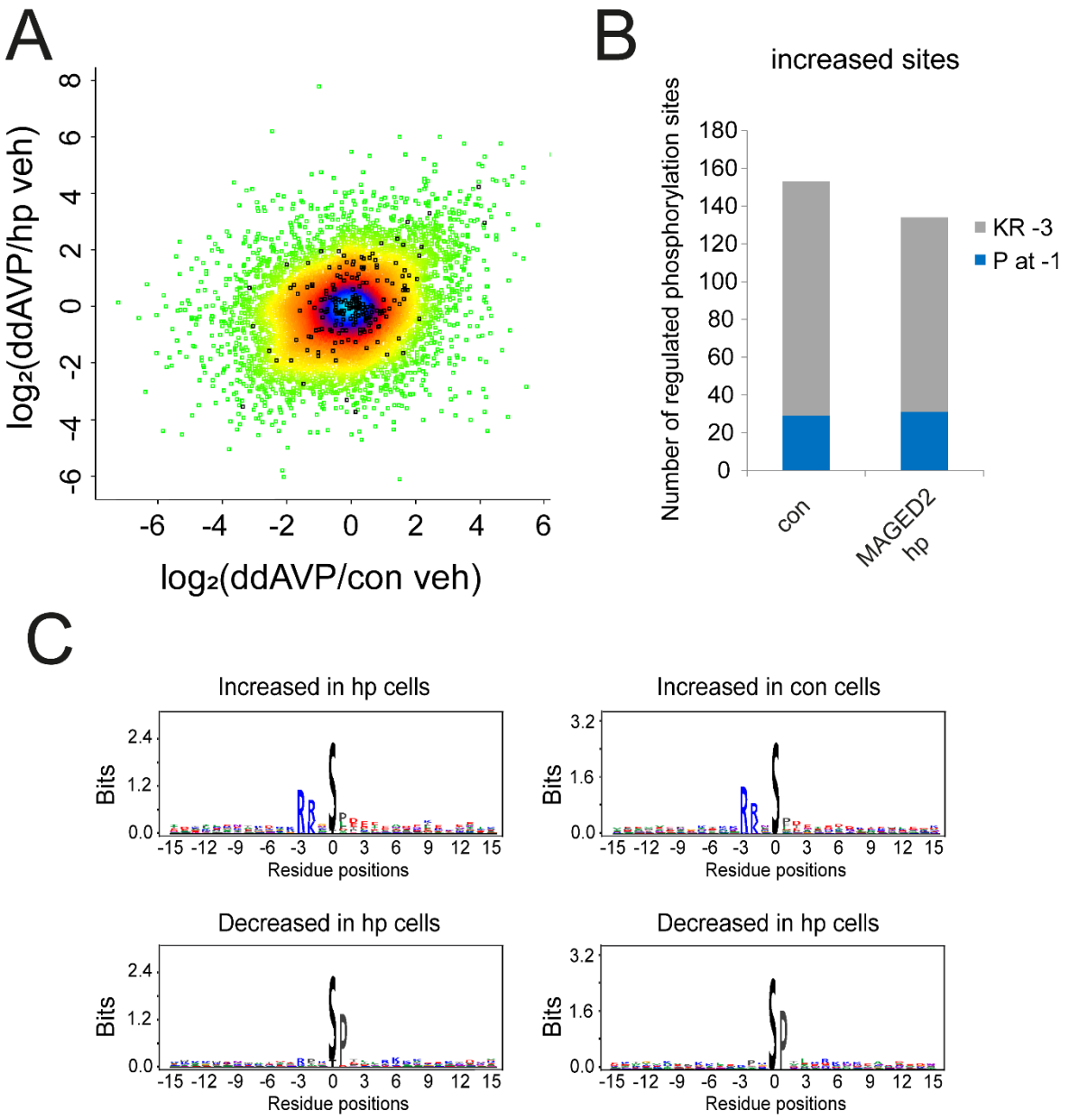

Figure 16: MAGED2 modulates the phosphoproteome of mpkCCD cells. *(A) Scatterplot of phosphorylation sites perturbed by dDAVP in MAGED2 hp versus control cell lines. Density is coded by colour. Overall, a moderate correlation of vasopressin induced phosphorylation in hp and control cells is observed (R=0.25). Black: known targets of PKA phosphorylation. (B) Characterization of the increased phosphorylation motifs by classifying motifs as basophilic or not (based on presence of R or K at the -3 position). Fraction of basophilic sites was reduced in MAGED2 hp cells (p=0.03 in Chi-Square test). (C) Sequence logos showing overrepresented phosphorylation motifs increased and decreased in MAGED2 hp and control mpkCCD cells after short-term dDAVP treatment.*

Phosphoproteomic data was also analysed using the PHONEMeS (PHOsphoproteomic NEtworks for Mass Spectrometry) tool, which computes changes of phospho-MS data due to perturbation within the framework of a network of potential kinase/phosphatase-substrate (K/P-S) interactions (Terfve et al., 2015).

As V2R is a GPCR, protein kinase A (PKA) was considered to be the most direct effector kinase of phosphorylation signalling when stimulated with dDAVP and, hence, was used as the source of the analysis (here the PKA subunit KAPCA). Some alterations in phosphorylation signalling could be detected suggesting slight alterations of non-canonical GPCR associated pathways. Namely, alterations could be detected in hippo, AKT, ERK, JNK and CDK-related pathways (Figure 17).

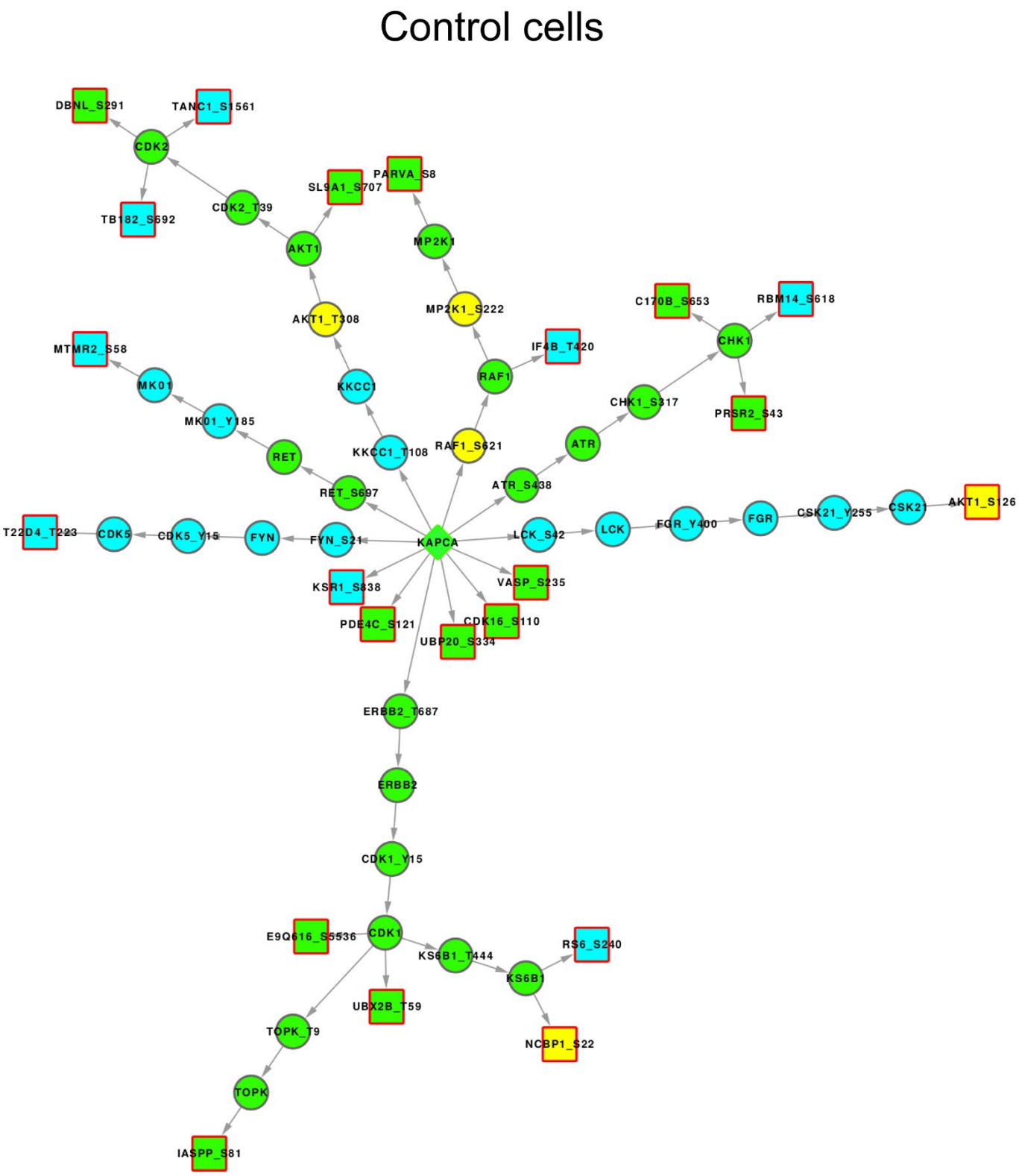

Figure 17: Maged2 modulates phosphorylation networks in mpkCCD cells. *Analysis of the phosphoproteomic data concerning differences in the phosphorylation networks between control and Maged2 depleted mpkCCD cells obtained from PHONEMeS (Terfve et al., 2015). The red-bordered square nodes represent significantly perturbed phospho-sites. Green-filled and yellow-filled nodes both represent proteins that are found in both networks, whereas the yellow-filled nodes have different phosphorylation sites. Considerable network rewiring can be observed.*

Maged2 depleted cells

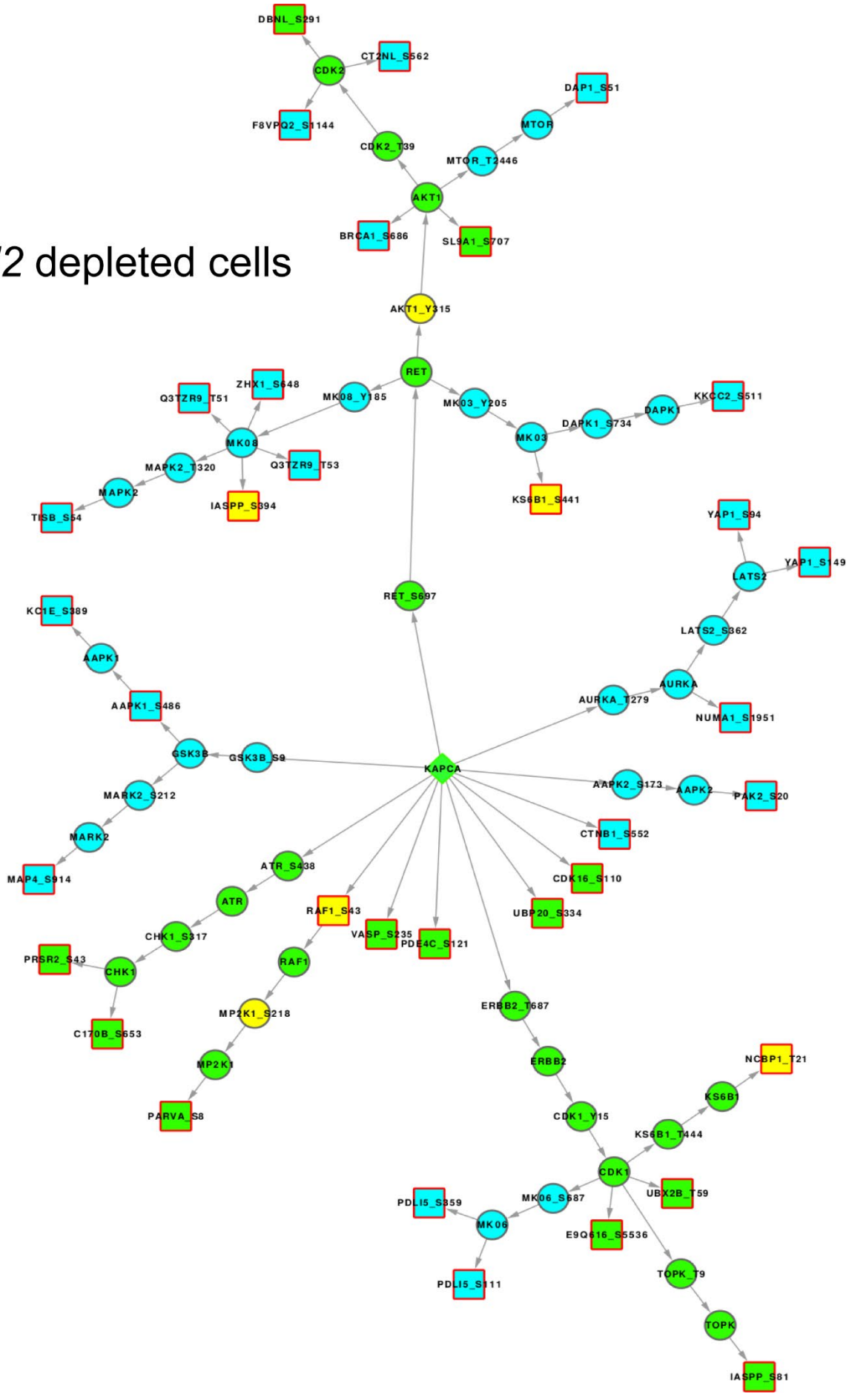

2.3.2 Signalling associated with long-term dDAVP treatment

While short-term dDAVP treatment induces changes in cAMP related phosphorylation processes, long-term treatment of dDAVP probably affects the PKA-independent transcriptional program. For this purpose, mpkCCD cells treated with dDAVP for 72 hours were analysed by Western Blot and qPCR.

As expected these experiments could clearly show an increase of AQP2 protein upon dDAVP treatment in all samples (Figure 18A). Nevertheless, the increase in AQP2 protein abundance was significantly higher in the *Maged2* depleted cells in comparison to the wild-type cells (Figure 18A). This significant higher increase could also be observed in the qPCR experiments confirming that these changes occur on the transcriptional level (Figure 18B).

Also proteomic analyses of pellets derived from long-term dDAVP treated cells showed an enrichment of AQP2 in the *Maged2* depleted cells confirming this finding (Figure 18C). Moreover, it could be shown that there is also an enrichment of the abundance of mediator complex subunit 14 (MED14) playing a role in transcriptional processes Figure 18C).

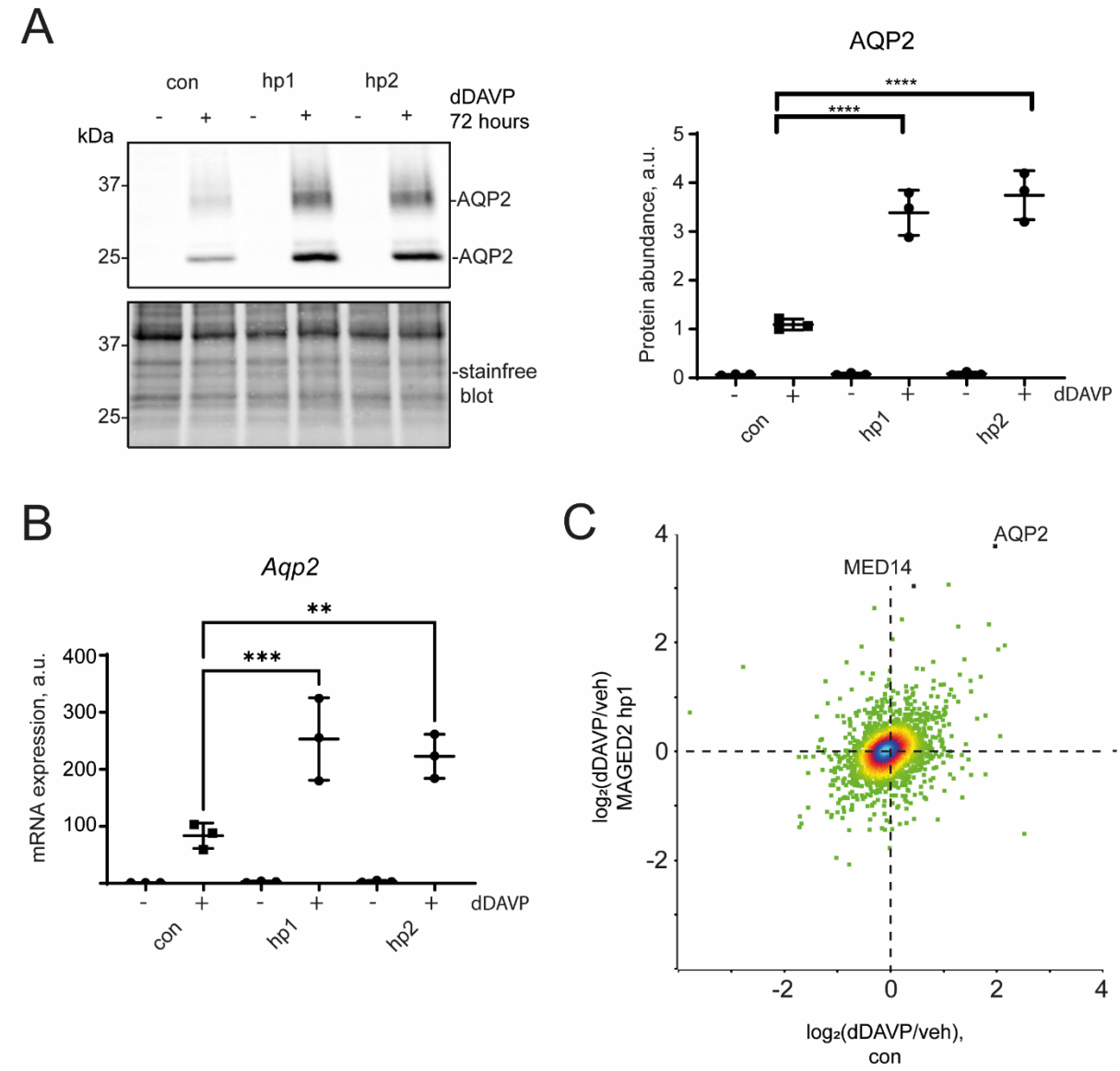

Figure 18: MAGED2 modulates long-term V2R dependent signalling in mpkCCD cells. *(A) Western Blot analysis of AQP2 protein in mpkCCD cells after 72 hours of dDAVP treatment (n=3; ****P<0.0001; one-way ANOVA, Dunnett's multiple comparison test). (B) Aqp2 mRNA expression in mpkCCD cells after 72 hours of dDAVP treatment (n=4; **P<0.01; ***P<0.001; one-way ANOVA, Dunnett's multiple comparison test). (C) Proteome analysis of mpkCCD hp and control cells after long-term (72h) dDAVP treatment. Each dot represents a protein and its ratio of dDAVP/vehicle in the respective cell lines. AQP2 and MED14 were significantly increased in MAGED2 hp cells after dDAVP treatment (n=3 replicates).*

Interestingly, vasopressin treatment resulted in lower *Maged2* mRNA levels in wildtype mpkCCD cells (Figure 19).

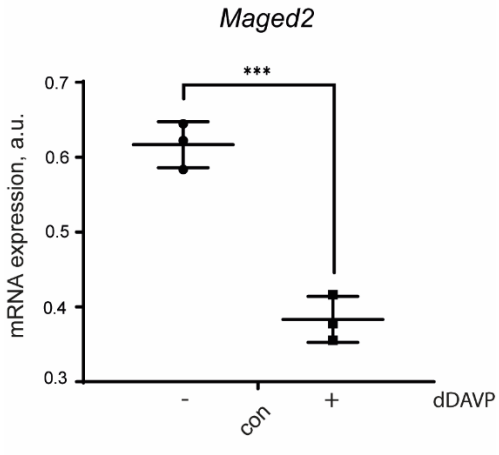

Figure 19: Maged2 expression decreases after long-term dDAVP treatment in control mpkCCD cells. *Maged2 mRNA expression in mpkCCD cells after 72 hours of dDAVP treatment (n=3; ***P<0.001; unpaired t-test)*

As *Aqp2* expression is correlated with an increased expression of *Avpr2* encoding V2R, the mRNA abundance was checked by qPCR. The *Avpr2* expression increased upon long-term vasopressin treatment but without significant changes between wild-type and *Maged2* depleted cells (Figure 20A). AQP2 is not the only protein, whose expression is controlled by vasopressin binding to the V2R. The amiloride-sensitive epithelial sodium channel (ENaC) plays an important role in NaCl reabsorption in the distal nephron and is not only controlled by the hormone aldosterone but also by vasopressin (Ecelbarger et al., 2000; Masilamani et al., 1999). The qPCR data clearly shows an increase of ENaC upon vasopressin treatment without significant changes between wild-type and the *Maged2* depleted cells (Figure 20B).

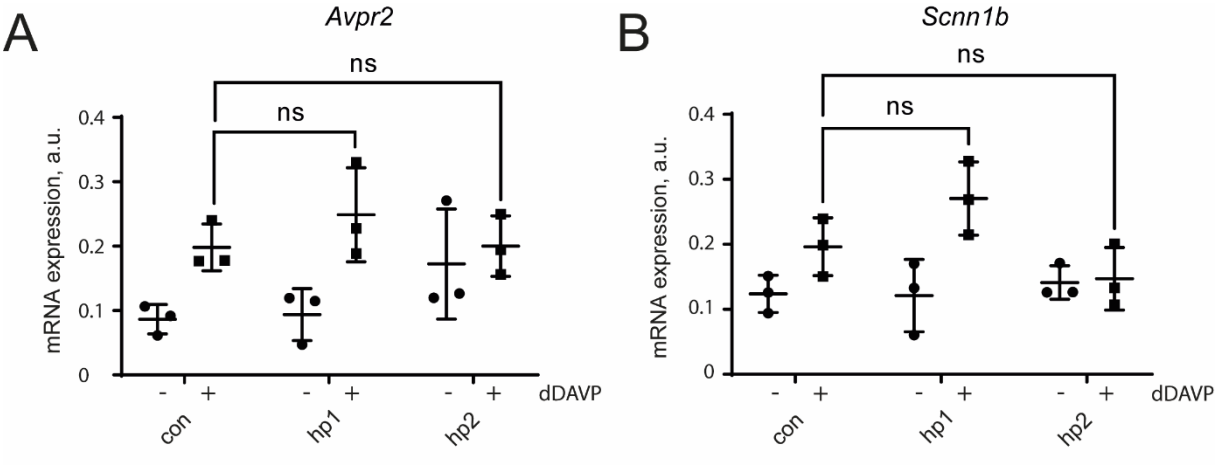

Figure 20: Maged2 does not modify Avpr2 and Scnn1b mRNA expression in mpkCCD cells after long-term dDAVP treatment*. (A) Avpr2 mRNA expression in mpkCCD cells after 72 hours of dDAVP treatment (n=3; not significant; one-way ANOVA, Dunnett's multiple comparison test).*

The Phonemes analysis in the short-term treated mpkCCD cells (Figure 17) showed alterations in different phosphorylation pathways. One of these altered pathways is the hippo signalling pathway. To investigate if these changes also occurred on the transcriptional level, qPCR analyses were performed. Nevertheless, no changes in the hippo pathway components *Yap*, *Taz*, *Ctgf* and *Myc* could be observed on the transcriptional level (Figure 21).

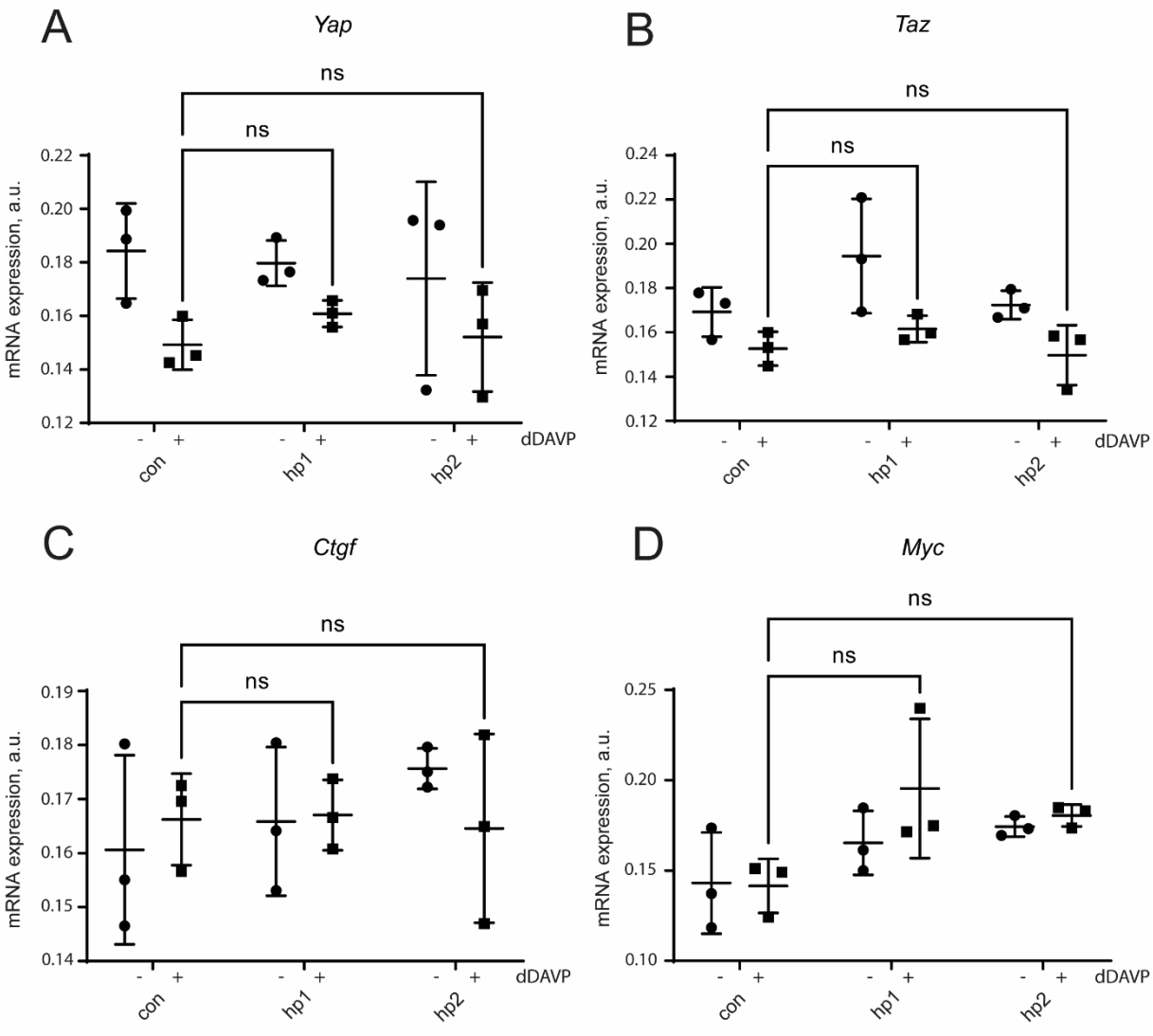

Figure 21: MAGED2 does not modulate the expression of targets of the hippo pathway. *(A) Yap, (B) Taz, (C) Ctgf and (D) Myc mRNA expression in mpkCCD cells after 72 hours of dDAVP treatment (n=3; one - way ANOVA, Dunnett's multiple comparison test).*

2.3.3 AQP2 localization in patient tissue

Based on the *in vitro* findings from mpkCCD cells, we checked AQP2 abundance and localization in available paraffinized kidney sections of the deceased BS5 patient F1.II-1 (Figure 22). As controls adult human kidney as well as kidney tissue from age-matched abortion tissue was used.

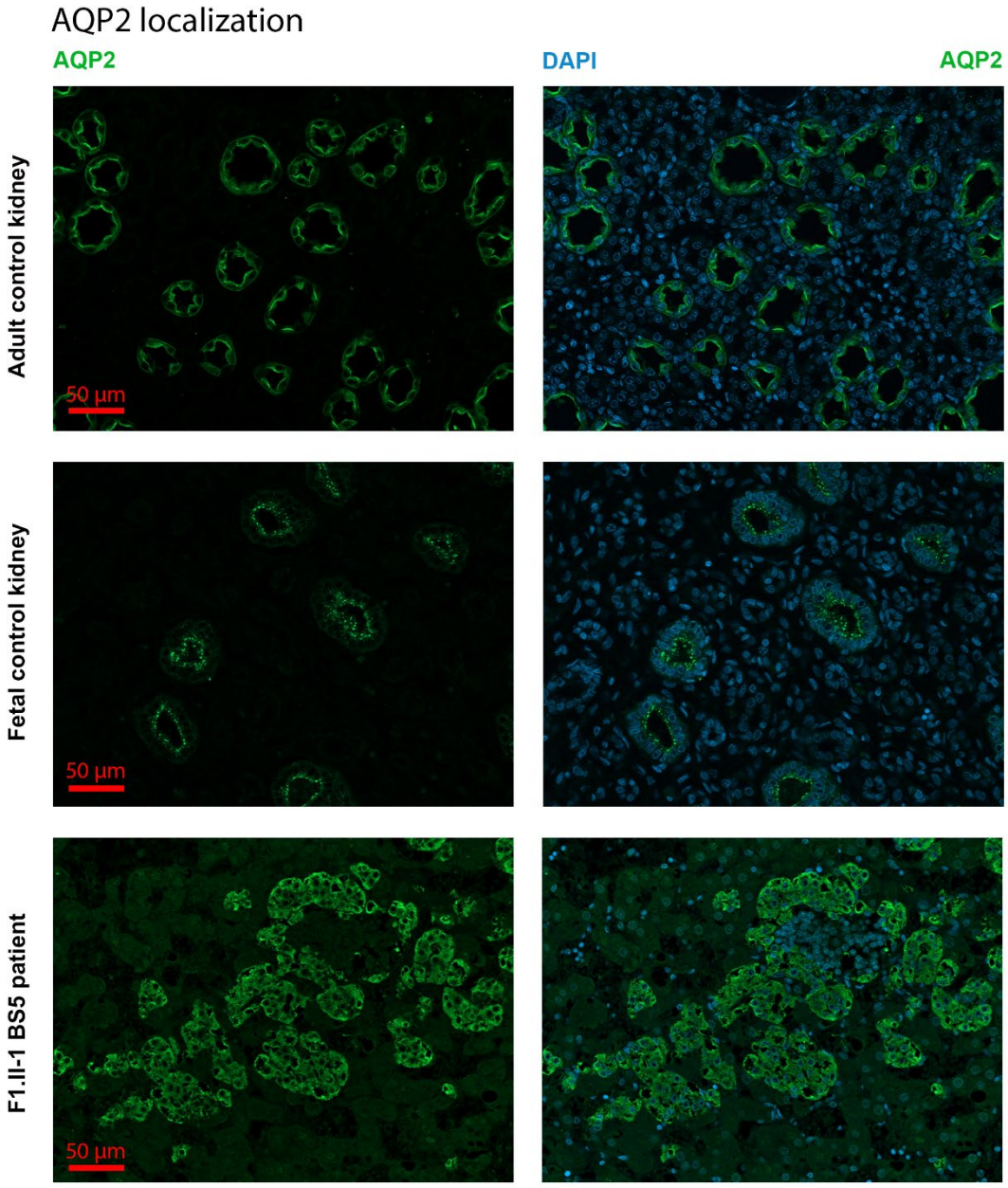

Figure 22: AQP2 localization of AQP2 in human healthy and BS5 kidney. *Immunofluorescence staining of AQP2 as well as nucelar staining (DAPI) in adult and control fetal kidney as well as a fetal kidney from a deceaced BS5 patient. Adult and fetal control kidney show apical AQP2 localization, while F1.II-1 exhibits diffuse intracellular distribution. Scale bars: 50 µm.*

The collecting ducts in the control adult kidney tissue show a distinct staining pattern on the apical membrane, which can also be seen in a less pronounced form in the control fetal tissue obtained from a stillbirth. In the BS5 patient tissue, on the other hand, no clear apical localization of AQP2 was observed. AQP2 staining showed a diffuse distribution within the cells. It should be noted that the patient tissue used in this study was derived from a single patient and the quality of the tissue obtained from stillbirths or abortions is limited.

2.4 The MAGED2 variant R446C as model for *in vitro* and *in vivo* studies of BS5

Almost all pathogenic mutations found in MAGED2 to date are truncating mutations (X. Wu et al., 2021). In our initial study we could also detect one missense mutation of arginine 446 (R446C) in one family, in which pregnancy was complicated by severe polyhydramnios and the foetus died at gestational week 22 (Laghmani et al., 2016). The same missense mutation as well as another mutation at the same position with another amino acid substitution to histidine (R446H) has also been detected in the French cohort (Legrand et al., 2018). A third missense mutation (A533V) has been detected in a Chinese patient (Ma et al., 2021). MAGED2 missense mutations result in a similar BS5 phenotype and do not differ in severity from truncating mutations. In our initial study we could demonstrate that the R446C mutation resulted in a loss of interaction with Gαs and DNAJB1 (Laghmani et al., 2016).

2.4.1 Altered localization of FLAG-MAGED2^{R446C} in Cos7 cells

Immunofluorescence stainings of MAGED2 wild-type and R446C cDNA constructs in Cos-7 cells show an altered localization of MAGED2. While wild-type MAGED2 is localized in the cytoplasm and the nucleus, the R446C mutant is only localized in the cytoplasm (Figure 23).

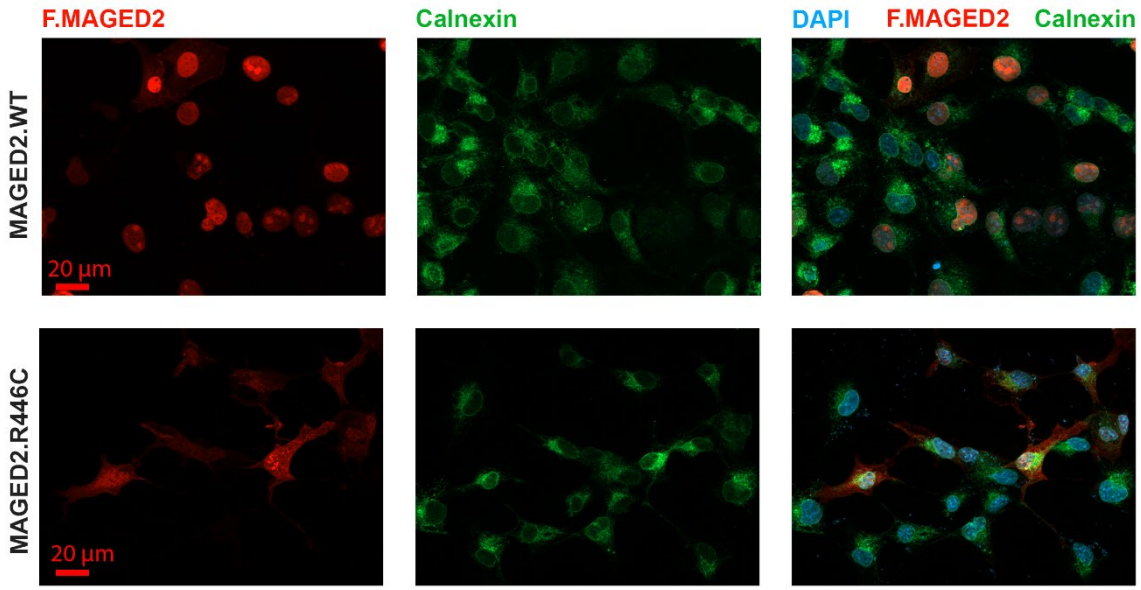

Figure 23: MAGED2^{R446C} loses its nuclear localization. *Immunofluorescence staining of Flag-tagged wildtype and MAGED2.R446C cDNA constructs. As marker the endoplasmatic reticulum protein Calnexin was used. Wildtype F.MAGED2 is localized in the cytoplasm as well as in the nucleus while F.R446C MAGED2 is restricted to the cytoplasm. Scale bars: 20 µm.*

2.4.2 Generation of MAGED2^{R446C} in an *in vivo* mouse model

MAGED2 cDNA in human and in mice is highly conserved. Especially the so-called MAGE homology domain (aa 286-456), in which the R446C mutation is located, shows a very high homology (Figure 24).

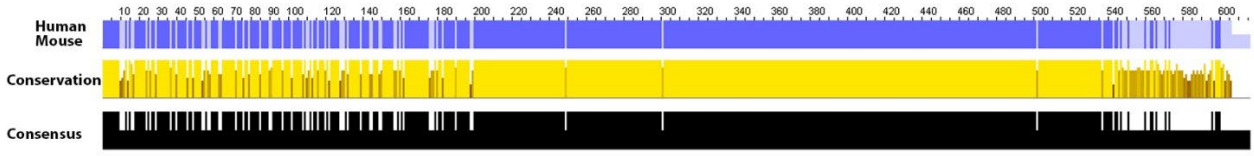

Figure 24: Human and mouse MAGED2 protein is highly conserved. *Alignment of human and murine MAGED2 protein sequence in order to highlight the conservation by using the MEGA genetic analysis tool. The alignment shows the high homology of the MHD, in which also the R446C mutation occurs (Tamura et al., 2021).*

Knock-in mice were created in cooperation with the CECAD by using a CRISPR/Cas9 electroporation technology. Beside the c.1336C>T nucleotide change to create the R446C mutation, the silent mutation c.1029C>T was inserted to avoid recutting and allow better genotyping. The sequencing of the F0 generation delivered unclear results. As in four litters with a male breeder only wildtype pups were born, the electroporation was repeated, which resulted in 29 pups in the F0 generation. Here, the mutation was heterozygously present in three pups and hemizygously in one pup. The male hemizygous pup was then used in the backcrossing with a female breeder resulting in two wildtype animals and two heterozygous females. For the further experiments, heterozygous females were mated with breeder male animals.

A total of 195 pups were born from matings between *Maged2*$^{R446C/WT}$ female mice and wildtype male mice from a sample of 12 different mice. Although the litter were slightly smaller in these matings, the difference was not statistically significant compared to randomly selected wildtype matings from the Mausoleum database (Figure 25A). From the 195 pups, 45% (88) were female, 45% (88) were male and from 10% (19) the sex could not be determined as they died before genotyping was possible. So, no sex bias was observed (Figure 25B).

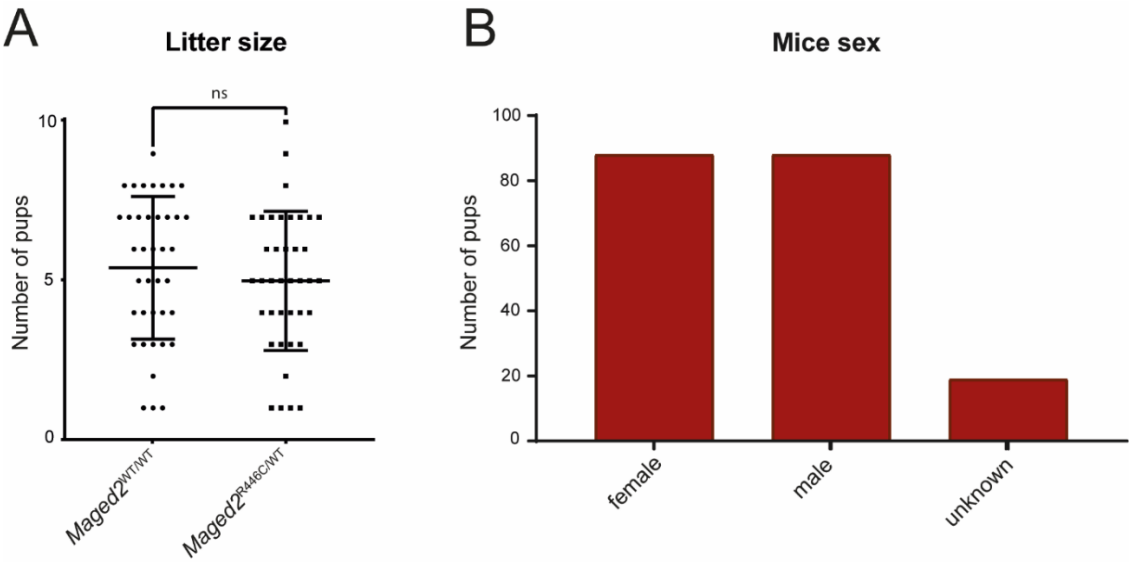

Figure 25: Average litter size of matings and sex ratio of the pups. *(A) Average litter size of randomly chosen matings of wildtype male mice with female wildtype or Maged2$^{R446C/Wt}$ mice (N=45 for wildtype and N=39 for R446C, P-value=0.54 in a two-tailed unpaired t-test). (B) Total number of pups and their sex, N=195. Analysis was performed with GraphPad prism 9.4.1.*

Genotyping was performed from ear tags or from tail tips in the case of pups used in experiments or dead pups that were collected from the litter. According to Mendelian rules 25% of each genotype and sex was expected.

21% of all mice were wildtype females, 18.5% females heterozygous for R446C, 26.7% wild-type males, 10% males hemizygous for R446C, and 3% of male pups could not be genotyped. Mendelian ratios, thus, are preserved in female gestations, while there is a clear trend to a wild-type genotype in male mice (Figure 26A).

20 of the pups that were stillborn or died at P0 could be genotyped. Here we see an increased number of dead pups with either female heterozygous or male hemizygous R446C genotype (Figure 26B).

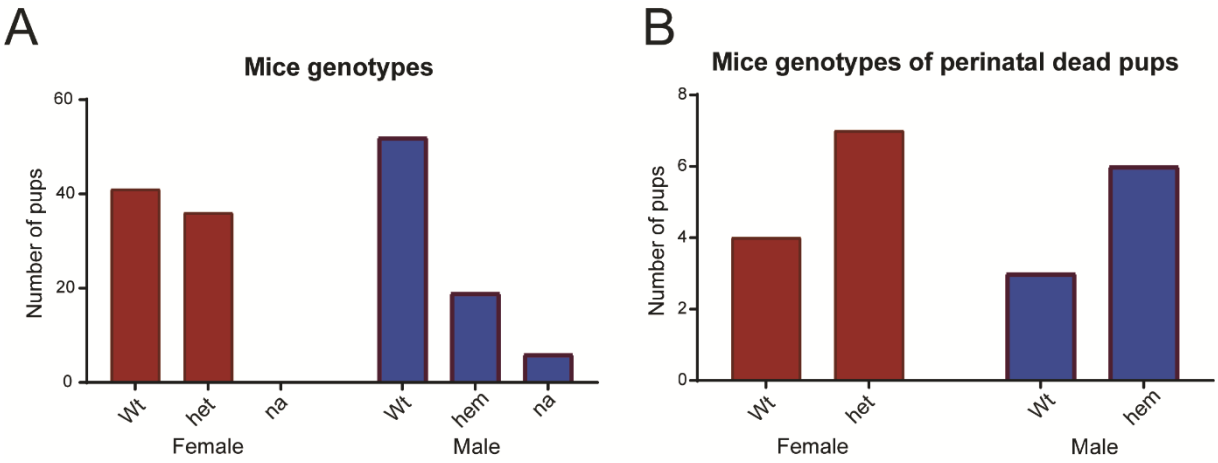

Figure 26: Genotype distribution of surviving and perinatal dead pups. *(A) Genotype distribution of mice that have survived the perinatal stage or were euthanized at P0. Female mice show a Mendelian ratio of wildtype and MAGED2$^{R446C/Wt}$, while in male animals the genotype is skewed to wildtype. (B) Genotype distribution of pups found dead at P0. Both heterozygous and hemizygous genotypes are increased towards the wildtype phenotype. Analysis was performed with GraphPad prism 9.4.1.*

For the following experiments 17 male P0 mice were euthanized. 7 of these mice were genotyped as hemizygous for R446C, while 11 of these mice were genotyped as wildtype.

Body weight of the *Maged2*$^{R446C/Y}$ mice was slightly lighter than that of wild-type mice without reaching significance (Figure 27). Also, the kidney weight *Maged2*$^{R446C/Y}$ mice was slightly lighter than that of wild-type mice without reaching significance (Figure 27).

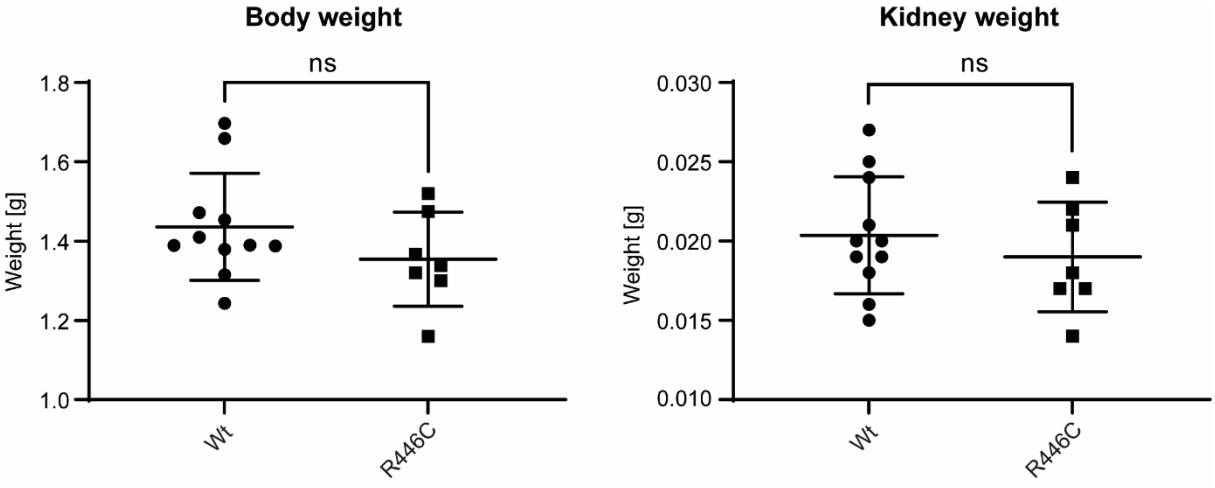

Figure 27: Body and kidney weight of the P0 pups depending on their genotype. *(A) Body weight of wildtype and Maged2$^{R446C/Y}$ male mice (N=11 for wildtype and N=7 for R446C, 2-tailed unpaired t-test p=0.21). (B) Kidney weight of wildtype and Maged2$^{R446C/Y}$ male mice (N=11 for wildtype and N=7 for R446C, 2-tailed unpaired t-test p=0.45). Analysis was performed with GraphPad prism 9.4.1.*

57% (4) of the males hemizygous for R446C showed a phenotype characterized by pale skin colour, an absence of urine in the bladder and no milk in the stomach. 28,5% (2) pups showed malformations of the intestine.

As *Maged2*$^{R446C/Y}$ mice often had no or just a low amount of urine, available urine samples were pooled and analysed for sodium, potassium and calcium concentrations by a blood gas analyser. The measurements show that in comparison to wildtype mice, *Maged2*$^{R446C/Y}$ mice had increased excretions of sodium and calcium, while the potassium excretion was decreased (Table 1).

Urinal electrolytes	*Maged2*$^{WT/Y}$	*Maged2*$^{R446C/Y}$
Na^+	74 mM	126 mM
K^+	46,7 mM	19,8 mM
$Ca2^+$	0,54 mM	0,9 mM

Table 1: Increased sodium and calcium excretion in* Maged2$^{R446C/Y}$ *mice. *Due to too low amounts of urine from individual mice, urines from three animals each were pooled and analysed on a radiometer.*

For general histomorphology of kidney sections, HE stainings were performed with paraffinized kidneys from male wildtype and *Maged2*$^{R446C/Y}$ mice, which yielded unremarkable results (Figure 28A). For a more detailed view of the proximal tubules, a PAS reaction was performed. This reaction highlights structures that are rich in glycogens like the brush border of proximal tubule cells which are lined by microvilli (Banning, 1959). PAS reactions of *Maged2*$^{R446C/Y}$ kidneys seem to have a weaker staining and, thus, may have a deficient composition of the brush border (Figure 28B).

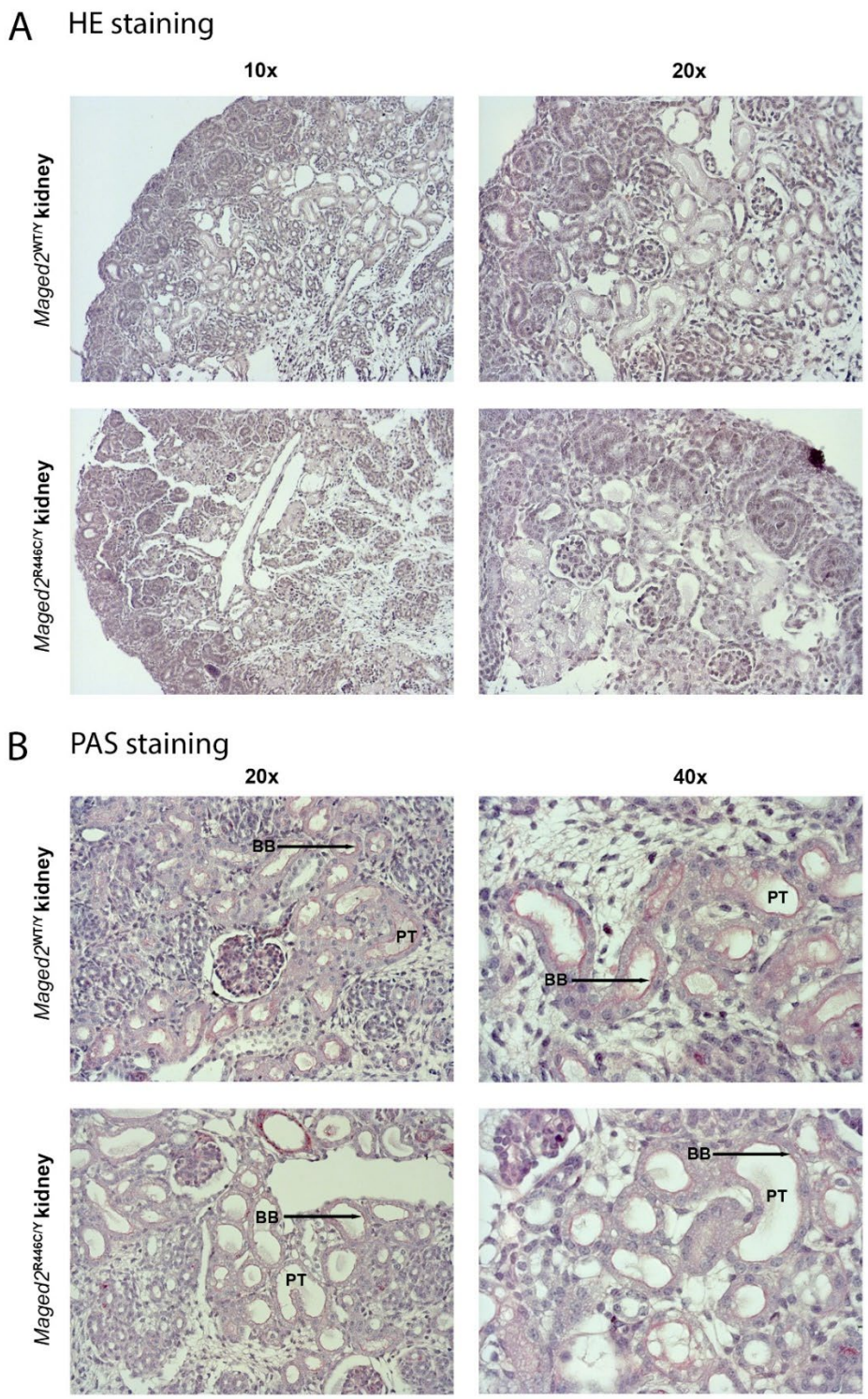

Figure 28: Maged2 depletion alters renal brush border appearance. *(A) HE staining of Maged2R446C/Y kidneys do not show alterations in kidney architecture (n=5 for wildtype and n=4 for Maged2$^{R446C/Y}$). (B) PAS-stainings of show a less developed brush border Maged2$^{R446C/Y}$ kidneys in comparison to WT kidneys (PT=proximal tubule, BB = brush border). Representative pictures (n=5 for wildtype and n=4 for Maged2$^{R446C/Y}$).*

2.4.2.1 Localization of renal cotransporters and channels in kidneys from WT and *Maged2*$^{R446C/Y}$ mice

Paraffin-embedded mouse kidneys were sectioned and stained using immunofluorescence for BS-relevant renal cotransporters and channels.

For NKCC2 both abundance as well as localization seem to be unaltered in wildtype and mutant animals with a signal at the apical membrane that pointed to a correct localization of NKCC2 (Figure 29A).

Also NCC seems to have a similar expression and apical localization in both wildtype and mutant samples (Figure 29B).

For AQP2, an altered localization was observed. AQP2 is localized at the apical membrane and required for luminal water permeability in the collecting duct (Eto et al., 2010). While in wildtype kidney tissue correct apical localization was observed, kidneys from pups bearing the R446C mutation showed a diffuse AQP2 distribution within the cell (Figure 30A). This was also reconfirmed in stainings of the phosphorylated form of AQP2 (Ser256; Figure 30B). Phosphorylation is necessary for proper AQP2 trafficking (Eto et al., 2010).

For the renal potassium channel ROMK, again no differences in abundance and localization were observed between wildtype and mutant kidney tissue (Figure 31).

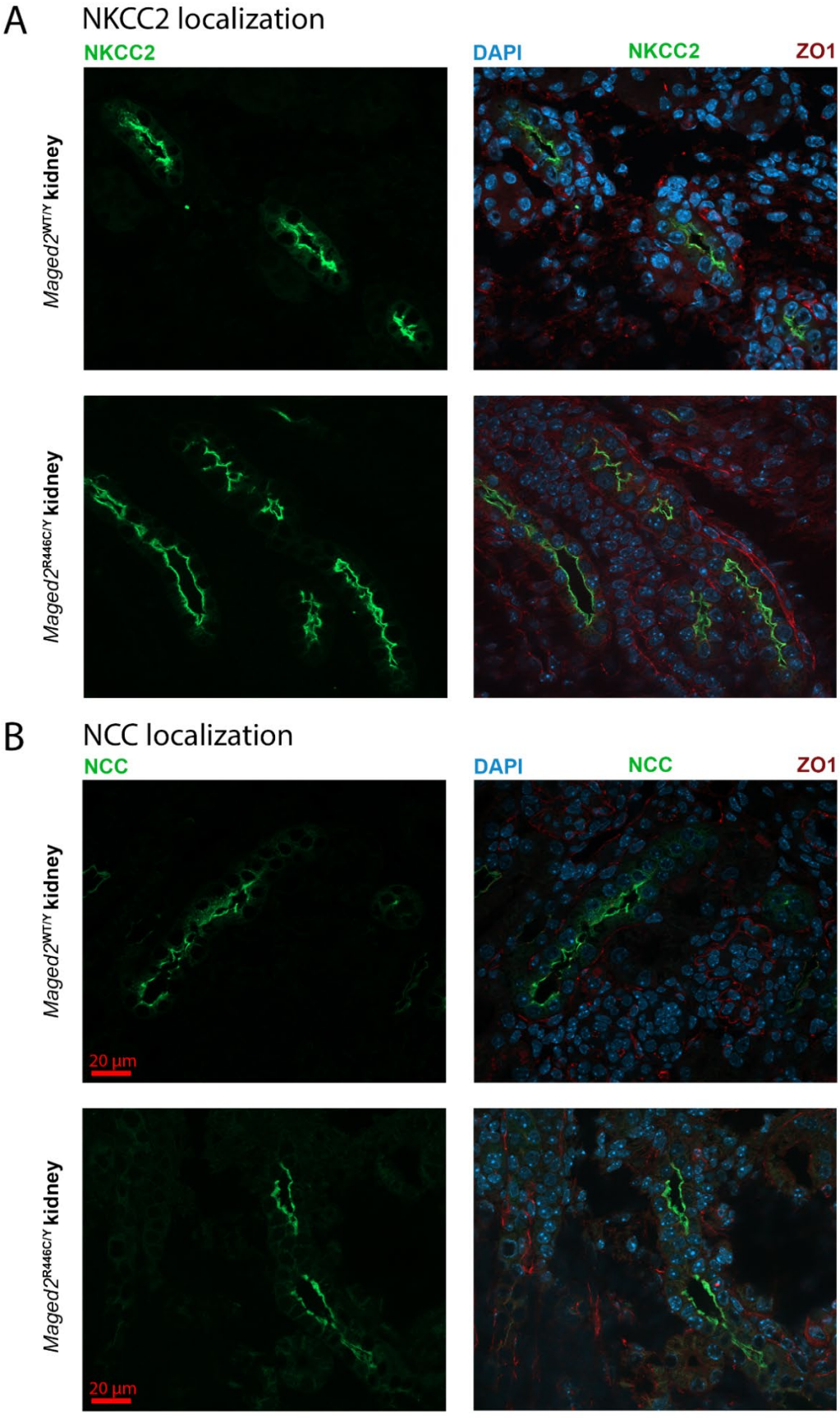

Figure 29: Correct localization of NKCC2 and NCC in kidneys from Maged2$^{R446C/Y}$ mice. *Representative IF stainings of NKCC2 and NCC within murine embryonic renal tissue at P0. Both WT and mutant kidneys show a similar apical distribution of the protein. As marker the tight junction protein ZO1 and for the nuclear staining DAPI was used. Scale bars: 20 µm.*

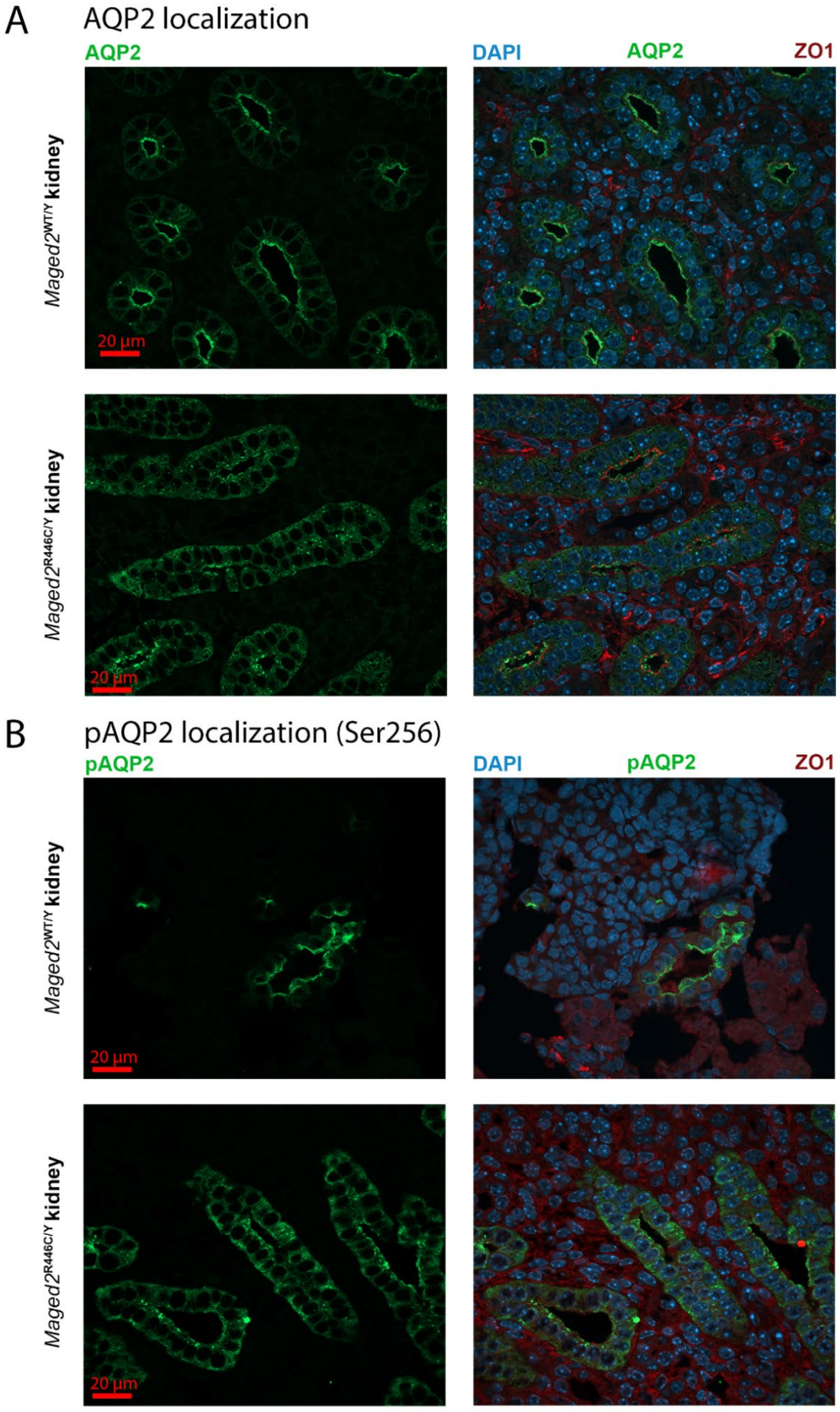

Figure 30: Aberrant localization of AQP2 and its phosphorylated form in kidneys from Maged2$^{R446C/Y}$ mice. *Representative IF stainings of AQP2 and pAQP2(Ser256) within murine embryonic renal tissue at P0. Both WT and mutant kidneys show a similar apical distribution of the protein. As marker the tight junction protein ZO1 was used and DAPI for the nuclear staining. Scale bars: 20 µm.*

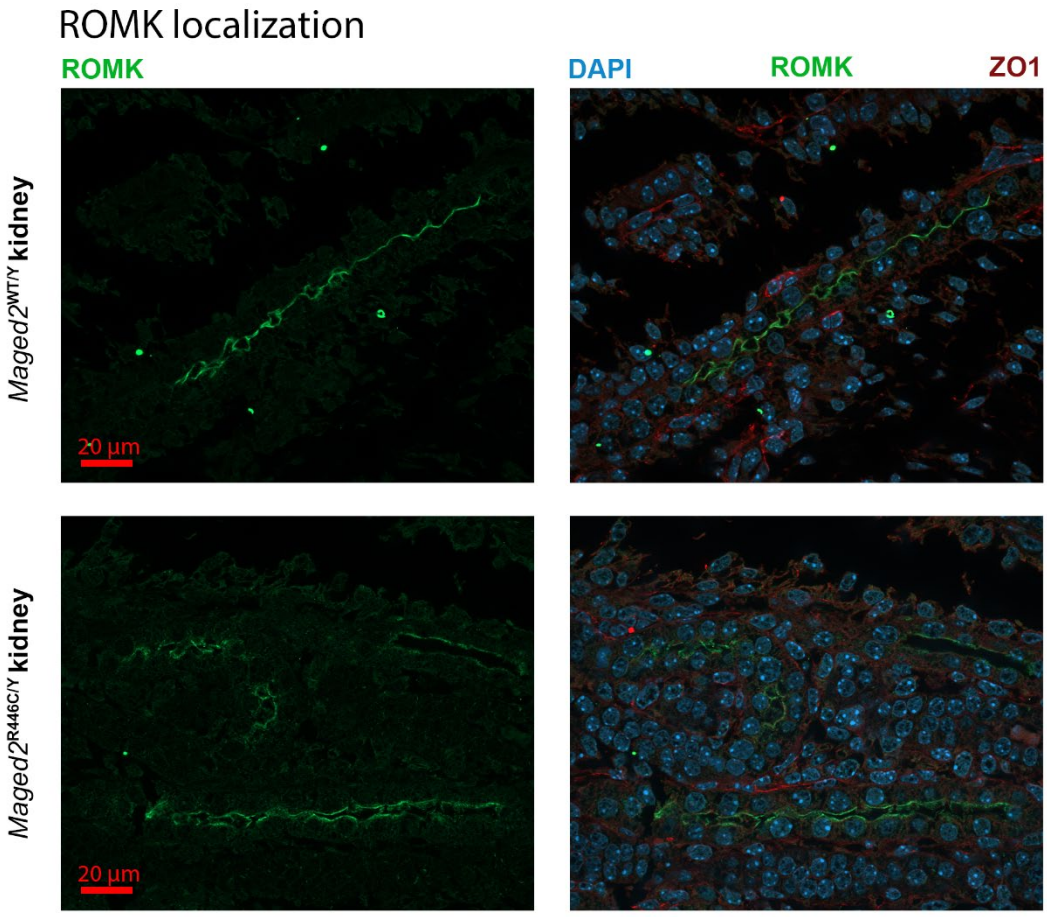

Figure 31: Correct localization of ROMK in kidneys from Maged2$^{R446C/Y}$ mice. *Representative IF stainings of ROMK within murine embryonic renal tissue at P0. Both WT and mutant kidneys show a similar apical distribution of the protein. As marker the tight junction protein ZO1 was used and DAPI for the nuclear staining. Scale bars: 20 µm.*

2.4.2.2 Proteome analysis of mouse kidneys

Proteome abundance was measured in whole kidneys from five *Maged2*$^{R446C/Y}$ versus five wild-type males and the abundance compared between the two groups. In total, 9846 proteins were detected. The analysis revealed a significant shift in the abundance of 307 proteins, with 112 proteins showing increased and 195 proteins showing decreased expression. The volcano plot in Figure 32 shows the 20 most significantly upregulated (in red) and the 20 most significantly downregulated proteins (in blue). Our results show that MAGED2.R446C protein was significantly decreased. As BS5-relevant cotransporter NCC is among the 195 proteins that are significantly downregulated, while no significant change of abundance of NKCC2 and AQP2 was detected. The proteins which are downregulated most significantly are SULT1C2, FABP7, HIBADH, CP, GM2A, GGT1, NAA80, ALB, BDH1, TTR, SORD and KNG1.
Interestingly, Gαs is the 2nd most significant upregulated protein in the kidneys of Maged2$^{R446C/Y}$ animals. Other proteins that are upregulated significantly are NABP2, MYL3, TSC22D3, ORC6, EIF4EBP2, CLK4 and PRPF18.
Each protein can be associated with so-called gene ontology (GO) terms representing the current knowledge of that particular gene or its corresponding product. These associations were divided in the three categories biological processes (GOBP), molecular function (GOMF), and cellular component (GOCC).
Biological processes that are upregulated are mostly part of the SOSS complex that assesses the G2 checkpoint and, hence, the further mitotic cycle as well as the regulation of developmental processes (Figure 33). Biological processes that are downregulated involve several metabolic and catabolic processes (Figure 33).
Molecular functions that are upregulated involve catalytic activity acting on DNA (Figure 34). Molecular functions that are downregulated involve oxidoreductase activity, hydrolase activity, exopeptidase activity, NAD binding and vitamin binding (Figure 34).
Protein clusters significantly upregulated can be found in apical part of cells, serine/threonine protein kinase complexes and sarcomeres (Figure 35). Cell compartments with downregulated clusters are mitochondrial structures and brush border compartments in the proximal tubule (Figure 35).

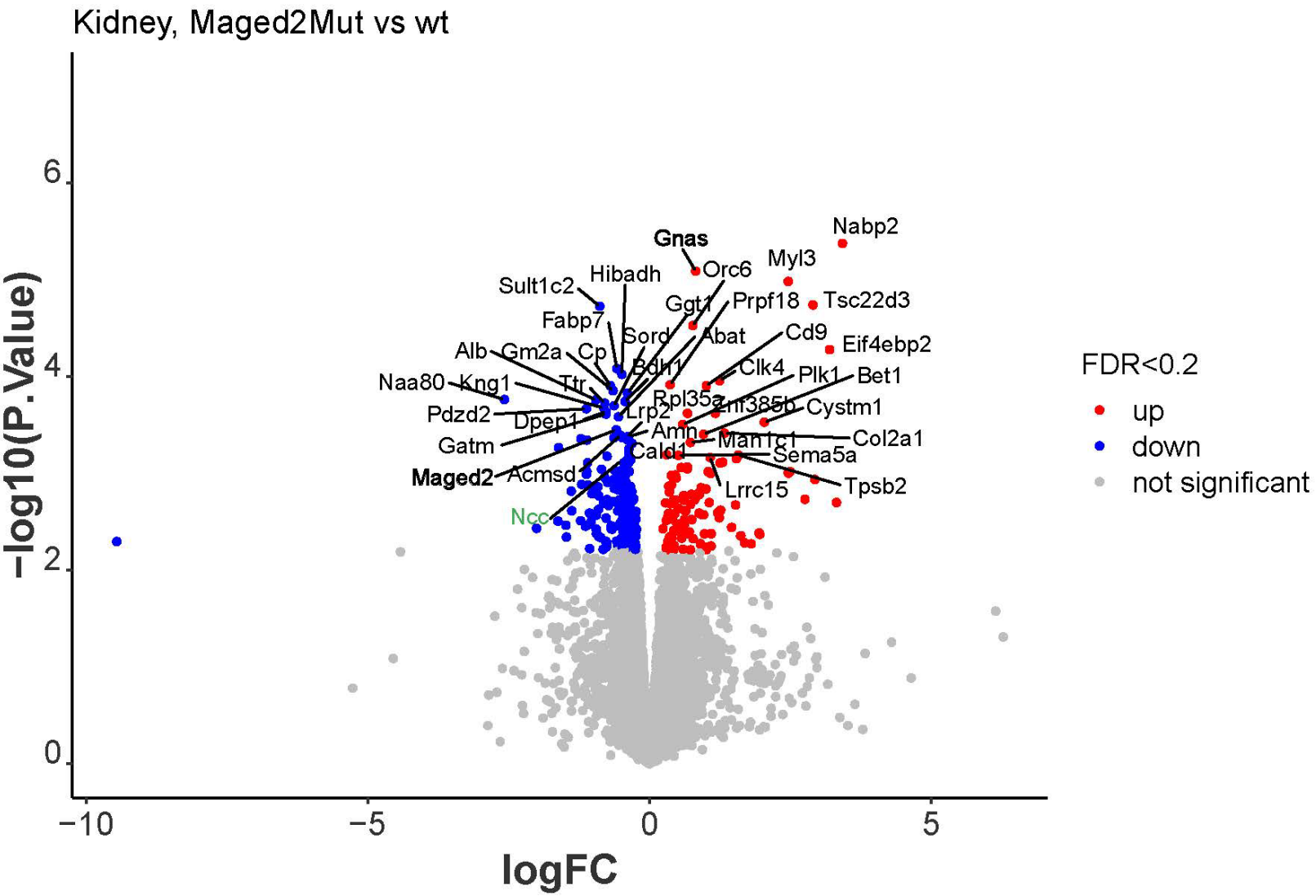

Figure 32: MAGED2 loss leads to changes of the proteome in kidneys from Maged2$^{R446C/Y}$ mice. *Volcano plot of the proteome analysis of kidneys from male wildtype and hemizygous R446C mice. Each dot represents a protein and its log fold change. The top 20 upregulated and the top 20 down-regulated proteins are mentioned (n=5 replicates; *FDR<0.2). Gnas and Maged2 as BS5-relevant proteins are marked in bold. Ncc as BS5-relevant protein on rank 69 of the significantly downregulated proteins is marked in green.*

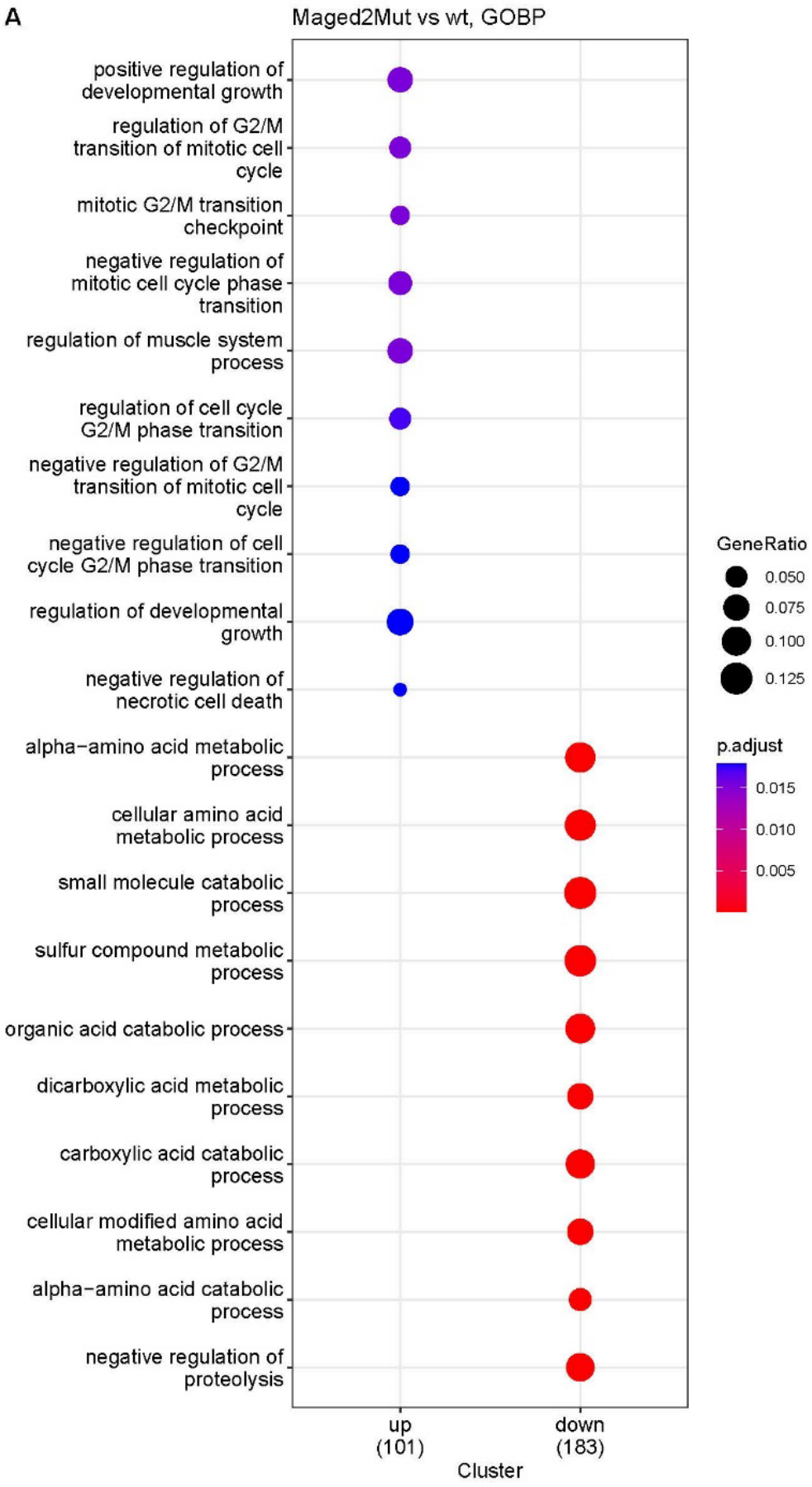

Figure 33: MAGED2 loss leads to alterations in biological processes*. GO-term enrichment analysis for biological process (GOBP) of the 10 most upregulated and downregulated clusters sorted by mean –log10 p values.*

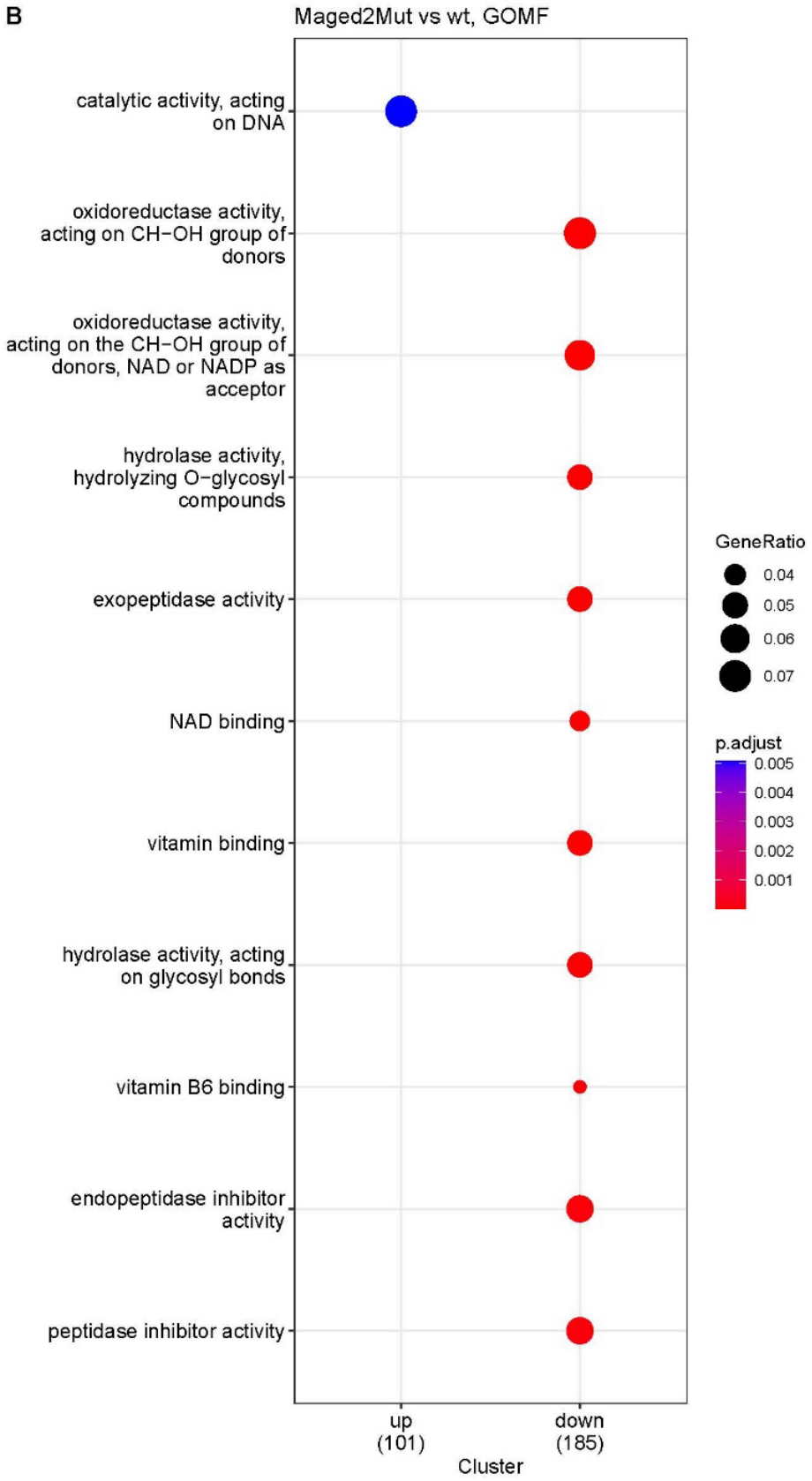

Figure 34: MAGED2 loss leads to alterations in molecular functions*. GO-term enrichment analysis for molecular function (GOMF) of the upregulated and the 10 most downregulated clusters sorted by mean –log10 p values.*

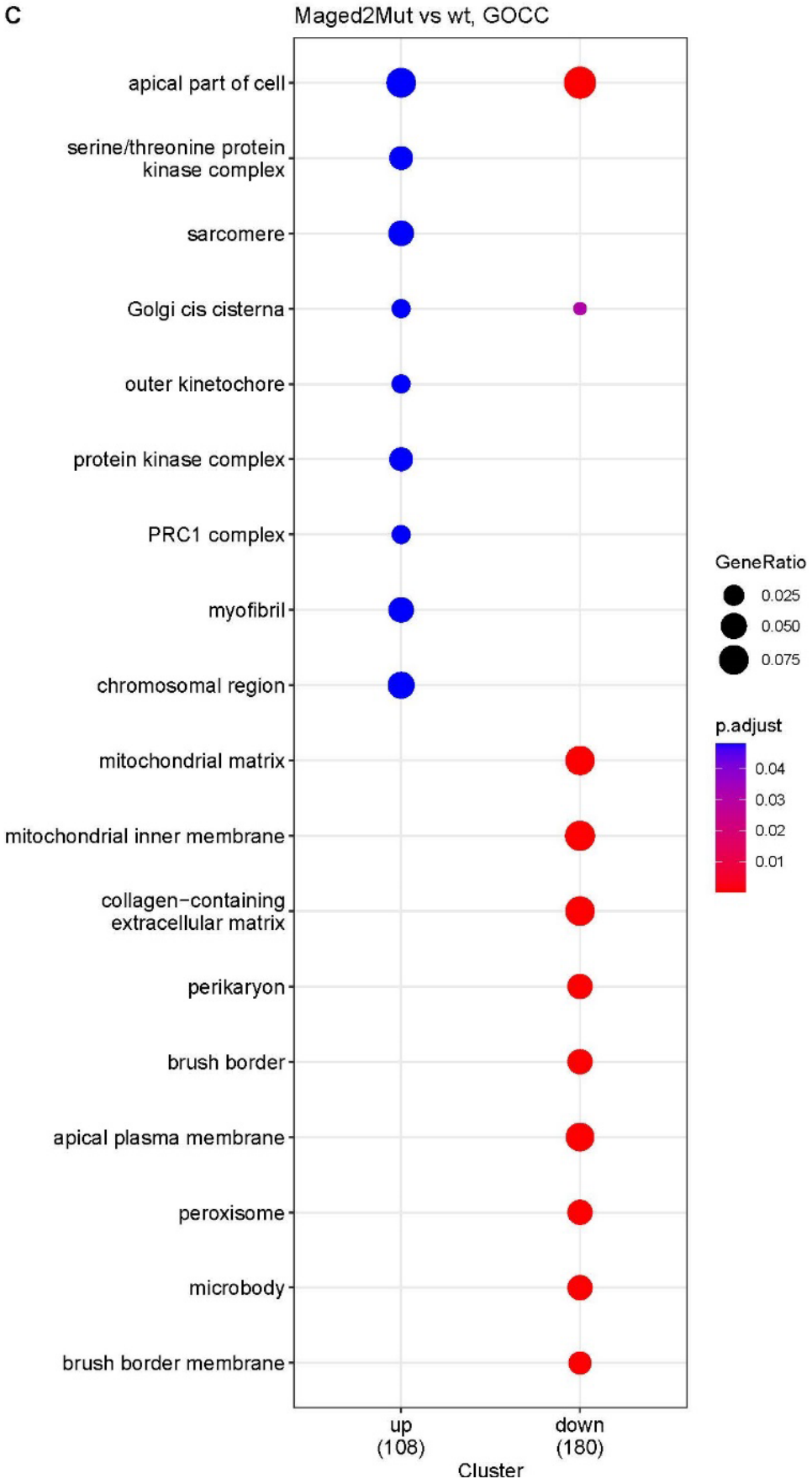

Figure 35: MAGED2 loss leads to alterations in cellular compartments. *GO-term enrichment analysis for cellular compartment (GOCC) of the 10 most upregulated and downregulated clusters sorted by mean –log10 p values.*

3 Discussion

MAGED2 belongs to the highly conserved *MAGE* family of genes, which is characterized by its MAGE homology domain that all members of this gene family share (Lee & Potts, 2017). While the expression of type 1 *MAGE* genes is restricted to testis and other reproductive tissues, type 2 *MAGE* genes like *MAGED2* are ubiquitously expressed (Lee & Potts, 2017). The *MAGED2* gene is located in a gene cluster that had been associated with X-mental retardation (XMR) on Xp11.2 (Langnaese et al., 2001), which led to a first association of *MAGED2* with neurological disease. However, further larger screening studies in XMR did not confirm an involvement of *MAGED2* in the disease (Tarpey et al., 2009). Other studies have revealed then a correlation between elevated levels of *MAGED2* expression and various types of cancer (Hashimoto et al., 2015; Kanda et al., 2016; Shen et al., 2021). In particular, its ability to inhibit the tumour necrosis factor-related apoptosis-inducing ligand (TRAIL) death receptor 2 (TRAIL-R2) probably leads to a greater survival rate for cancer cells, as they are less susceptible to apoptosis induced by TRAIL (Tseng et al., 2012; Yamamoto et al., 2020).

Accordingly, identifying *MAGED2* as a monogenic cause for a novel type of BS, a disease spectrum almost exclusively affecting the kidney, was quite surprising (Laghmani et al., 2016). Also confusing was the transient character of the disease, which allows the infant to develop normally once the critical time period with prenatal polyhydramnios and postnatal polyuria had passed leading to the assumption that *MAGED2* executes a crucial but limited spatiotemporal function for proper fetal fluid and electrolyte homeostasis (Laghmani et al., 2016). Meanwhile, over 30 pathogenic variants of the *MAGED2* gene are known that result in BS5 (Table 2).

Nucleotide (cDNA)	Protein	Onset of PH (wk)	Gestational age at delivery (weeks)	Outcome	Polyuria	Reference
c.384_385TG	p.V129Gfs*2	20	28	S	Yes	(Laghmani et al., 2016; Reinalter et al., 1998)
c.1038C>G	p.Y346*	19	27;31	2S, 1D	Yes	(Laghmani et al., 2016)
c.1462_73del12	p.488_491delEAAA	20	28	1S, 1D	Yes	"
c.991-2A>G	p.?	19	34;33;31	3S	No; na; na	"
c.1484C>G	p.A495Dfs*39	20	24	1S	Yes	"
c.274dupA	p.T92Nfs*7	20	26	1S	Yes	"
c.397A>T	p. K133*	19	27	1S	Yes	"
c.386_87delTG	p.V129G fs*2	na	30;29	1S, 1D	Yes	"
c.1336 C>T	**p.R446C**	**19**	**22**	**1D**	**No**	**"**
c.847- 9C>G	p. A283Sfs*8	19	29	1S	No	"
c.1426C>T	p.R476*		29	2S, 1D	Yes	unpublished
c.607C.T	p. R203*		-	1S	Yes	(Legrand et al., 2018)
c.842_843dup	p. R282Gfs*7	yes	-	1S	Yes	"
c.967C.T	p. R323*		-	1S	Yes	"
c.967dup	p. R323Pfs*18		-	1S	Yes	"
c.10851 + G>A	p.?		-	1S	Yes	"
c.12711 + G>A	p.?		-	1S	Yes	"
c.1336C>T	**p. R446C**	**no**	**33**	**1S**	**Yes**	**"**
c.1337G>A	p. R446H		-	1S	Yes	"
c.1366G>T	p. V456F	no	-	1S	Yes	"
c.1384_13864 + del	p.?	yes	-	1S	Yes	"
c.1420C>T	p. Q474*		-	1S	Yes	"
c.1458_1466del	p. E488_A490del		-	1S	Yes	"
c.1464_1475del	p. A490_A493del		-	1S	Yes	"
c.1515_1516dup	p. G506Vfs*71		-	1S	Yes	"
Complete deletion	p.?		-	1S	Yes	"
-	-	21	29	1S	Yes	(Meyer et al., 2018)
c.823delG	p. D275Mfs*13	19	36	1S	No	(Arthuis et al., 2019)
Complete deletion	-	20	nd	3D, 1na		(Yang et al., 2019)

Table 2: Genotypical and clinical features of known MAGED2 variants. *Review from literature. S=number of survivors, D=number of dead infants and nd=no data. Modified from (X. Wu et al., 2021).*

The precise and multifaceted functions of MAGED2 in the developing kidney are still unclear. By using cell models as well as a mouse model, we discovered:

1. *MAGED2* knockdown via siRNA in HEK293T cells induced numerous changes in phosphorylation patterns.
2. *Maged2* knockdown via shRNA in the renal collecting duct cell-line mpkCCD also showed alterations in phosphorylation patterns after short-term dDAVP treatment as well as changed abundance of the proteins AQP2 and MED14 after long-term dDAVP treatment, providing further confirmation that MAGED2 is involved in GPCR signalling.
3. P0 *Maged2*$^{R446C/Y}$ mice showed an increased lethality and a renal phenotype. IF analysis of the kidneys revealed an impaired AQP2 localization to the apical membrane, while other target transporters like NKCC2, NCC and ROMK showed normal distribution. Preliminary data on urinary excretion indicate sodium and calcium wasting in line with the human phenotype. Furthermore, numerous changes in the abundance of more than 300 proteins were detected by proteome analysis in kidneys from P0 *Maged2*$^{R446C/Y}$.

All in all, our results indicate that *MAGED2* deficiency leads to numerous alterations on the transcriptional and post-transcriptional level contributing to the severe phenotype of BS5.

3.1 MAGED2 adds a new layer of complexity to fetal and early postnatal fluid homeostasis

Mouse mRNA data show that *Maged2* expression is highest during embryonic kidney development and decreases as the mouse approaches birth, while the specific ion cotransporter and channel proteins associated with BS show an opposite spatiotemporal expression. A similar mRNA expression pattern has been detected in other organs like liver, heart and retina by datamining (Wang et al., 2021). In line with these findings is the similar expression pattern of MAGED2 protein that has been observed in brain tissue during different embryonic stages (Bertrand et al., 2004). All in all, this points to an important general role of *MAGED2* in development, but little is known about the context of kidney disease.

MAGED2 role in embryonic development is also reflected by its upregulation in several kinds of cancer. Research has demonstrated that embryonic development and tumour growth share many similarities, particularly in terms of genomic homeostasis, which is likely controlled by the regulation of embryonic factors (Huilgol et al., 2019; Manzo, 1989, 2019). Embryonic development is in need of stem cells that form - via morphogen gradients and transcription factors - differentiated cell types terminated in their pluripotency (Huilgol et al., 2019). The development of cancer reflects this process in an opposite way. Here, a differentiated cell re-develops to a cell with stem-cell character via cellular and molecular mechanisms caused by activation of actual repressed genes (Huilgol et al., 2019; Roy & Hebrok, 2015). Exemplary factors are Octamer binding transcription factor 4 (*OCT4*), which is upregulated in pluripotent stem cells keeping their pluripotency during gastrulation (Nichols et al., 1998) but also attributes to cancer initiation and progression (Liu et al., 2013) or *MYC*, which is overexpressed in embryonic liver inducing proliferation but also promotes tumorigenesis (Beer et al., 2004). Also, GPCR dependent pathways and *GNAS* as one element have been shown to play an important role in cancer progression. Especially activating mutations contribute to unregulated growth of some endocrine tumours and constitutively active GPCRs have been detected in cancer driving DNA-viruses (Dorsam & Gutkind, 2007; Turan & Bastepe, 2015). Malignant cells also often abuse normal GPCR signalling for autonomous proliferation, avoided immune detection and also the metastatic character (Dorsam & Gutkind, 2007). Association of *MAGED2* overexpression in tumours with a poorer prognosis for the patient have been shown for hepatic cancer (Hashimoto et al., 2015), gastric cancer (Kanda et al., 2016) and lymphoma (Shen et al., 2021). MAGED2 physically interacts with the tumour suppressor protein p53 and inhibits its function promoting cancerous characteristics of the cells (Papageorgio et al., 2007). Also, it could be shown that GPCR signalling was able to inhibit p53 protein accumulation by increasing p53 ubiquitination and subsequent degradation (Steffen et al., 2020).

3.2 MAGED2 alters phosphorylation patterns

In this work, a first set of proteomic studies was performed to understand the function of *MAGED2* in two cell systems. Due to a lack of patient tissue and the ethical dilemma

to ask for tissue of stillborn children, conducting experiments on patient material proved to be largely impossible. As alternative, we decided to use the cell line HEK293T as it has proven to be useful in our initial study in terms of MAGED2 interaction partners (Laghmani et al., 2016). As all pathogenic *MAGED2* variants most likely lead to a loss of function, we knocked *MAGED2* down via siRNA. On the proteomic level, no significantly altered protein patterns were detected in HEK293T cells with siRNA induced MAGED2 knock-down for 48 hours. On the other hand, downregulation of MAGED2 led to dramatic changes of the phosphoproteome, as about 35% of all detected phospho-peptides (489 of 1387) had a differential abundance. Especially a modification of basophilic kinase associated phosphorylation motifs were detected. These kinases are characterized by the basic amino acids arginine (R) and lysine (K) at position -3 and -2 of the phospho-site, respectively, and also PKA belongs to this class of kinases (Limbutara et al., 2019). These results show that MAGED2 plays an important role in post-transcriptional processes.

HEK293T cells are an immortalized cell-line derived from human embryonic kidney cells that were exposed to DNA of human adenovirus type 5 (Graham et al., 1977). Although they are of renal origin, they do not express relevant cotransporter and channel proteins as they have more an epithelial character (Varghese et al., 2006) and are, thus, a limited model for studying complex biological processes that occur in specialized tubular cells.

For this reason, we next chose the mouse cell-line mpkCCD for further studies. This cell-line is an immortalized cell-line that has its origin in cells of the cortical collecting duct and still possesses its original features (Duong Van Huyen et al., 1998). Importantly, these highly polarized cells show typical characteristics of tight epithelial cells while showing Cl^- and AQP2 transport induced by vasopressin treatment (Figure 36) (Chassin et al., 2007). Commercially available kidney cell lines, on the other hand, as well as even cultures of primary kidney cells are not capable of expressing AQP2 and, thus, of responding to vasopressin (Furuno et al., 1996; Kuo et al., 2018). The hormone vasopressin is synthesized in the hypothalamus and secreted from the posterior pituitary gland in response to changes of water homeostasis that are sensed by vascular volume and baroreceptors (Boone & Deen, 2008; Bourque et al., 1994). Vasopressin reaches then the kidney over the blood stream, where it binds to V2R situated on the basolateral membrane of principal collecting duct cells, which induces a signalling cascade over Gαs and adenylate cyclase (AC) leading to increased

intracellular cAMP levels, an activation of PKA and finally to phosphorylation of vesicular AQP2 protein which is then incorporated in the apical membrane making it permeable for water (Figure 42)(Nielsen et al., 1995). As our previous studies had shown that MAGED2 is expressed also in tubular cells outside the TALH (Laghmani et al., 2016), mpkCCD cells seemed to be a more adequate system to study some aspects of MAGED2-dependent GPCR signalling due to activation of V2R *in vitro* by desmopressin (dDAVP). dDAVP is a synthetic derivate of vasopressin synthesized by deamination of hemicysteine at position 1 and a substitution of the D-arginine at position 8 for L-arginine and possesses an even higher and prolonged antidiuretic activity than vasopressin (Lethagen, 1994; Zaoral et al., 1967). It is widely used as therapeutic treatment of diabetes insipidus centralis (with impaired or missing ADH production) and enuresis (Lethagen, 1994).

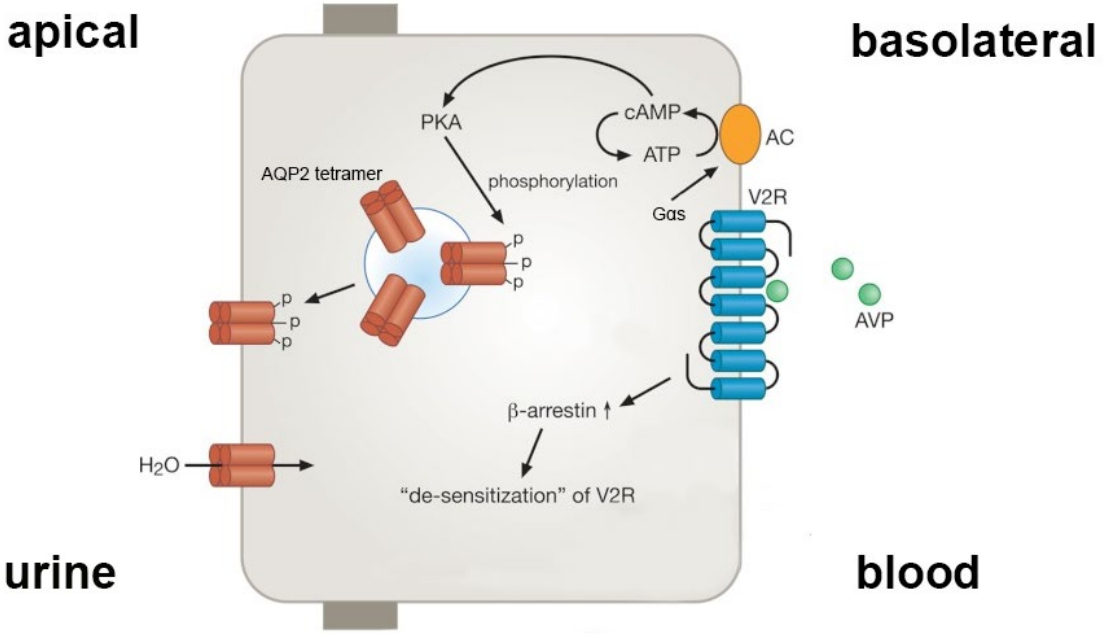

Figure 36: AVP-mediated AQP2 trafficking in principal cells of the renal collecting duct. *In principal cells of the kidney collecting duct, arginin-vasopressin (AVP) binds to the basolateral G protein-coupled vasopressin receptor AVP2R (V2R) which then activates adenylate cyclase (AC) via Gαs. This leads to an increase in intracellular cAMP, activation of PKA, phosphorylation of AQP2 and its insertion and accumulation in the apical plasma membrane, making the luminal side of the cell permeable for water through AQP2 channels. Modified from (Moeller et al., 2013).*

Short-term treatment of the mpkCCD cells with dDAVP showed that a knockdown of *Maged2* alters cAMP level kinetics and makes the response to the stimulus more variable. Changes of phosphorylation patterns were also observed in the Western Blot experiments with phosphorylated CREB. This transcription factor is directly

phosphorylated at its Ser133 site by PKA as response to increasing cAMP levels in the kidney (Montminy & Bilezikjian, 1987). Upon activation CREB recruits CREB-binding protein (CBP) and induces the transcription of more than 4,000 target genes (Dyson & Wright, 2016; Zhang et al., 2005). In our cell model, the pCREB response to the stimulus turned out to be significantly weaker in the *Maged2* depleted cell-lines leading to the assumption that the GPCR signalling response to vasopressin treatment is impaired. The phosphoproteomic data of the mpkCCD cells show a reduction of increased basophilic sites in the *Maged2* depleted cells, which could similarly be observed in HEK293T cells with siRNA-induced *MAGED2* knockdown. Subsequent PHONEMEs analysis revealed a multitude of altered signalling pathways. PHONEMEs is an informatic tool that combines phosphoproteome data with a so-called Prior Knowledge Network (PKN), which is built from already known relations between kinases or phosphatases to their substrates with regard to a perturbation factor (Gjerga et al., 2021; Terfve et al., 2015). As our studies suggested an effect of MAGED2 especially on basophilic signalling processes, PKA was chosen as perturbation factor. Interestingly, some perturbations of β-Arrestin mediated signalling pathways such as protein kinase B (AKT) or ERK were observed. β-Arrestins are modulator proteins of a large fraction of GPCR dependent processes and especially play an important role in the termination of GPCR signalling (Xiao et al., 2010). This termination is achieved by binding of G protein-coupled receptor kinases (GRKs) to ligand-activated GPCRs thereby phosphorylating them and inducing the binding of β-arrestins (Krupnick & Benovic, 1998). β-arrestins, in turn, induce clathrin-mediated endocytosis of the GPCRs which leads either to recycling or degradation (Zhai et al., 2022). Nevertheless, former studies had shown that internalized Gαs and β-Arrestin complexes also mediate long-term sustained GPCR signalling (Thomsen et al., 2016). Further differentially phosphorylated targets are found in hippo and cyclin-dependent kinases (CDK)-related pathways. While CDK pathways play an important role in control of the mitotic cell cycle (Gitig & Koff, 2001), the hippo pathway is a regulator of the common embryonic development as well as of the development of the kidney regarding the control of organ size, cell proliferation and apoptosis (Wong et al., 2016). On the mRNA level, however, only an upregulation of hippo targets after vasopressin treatment could be detected in both wildtype and *Maged2* depleted mpkCCD cells without significant changes between the cell-lines. It will be of interest to re-examine the interplay between these signalling relays in a tissue context in the future experiments.

A recent study has shown that the MAGE homology domain (MHD) of MAGED2 is the structure interacting with the Gαs α-helical domain (AHD) of Gαs (Ahn et al., 2022). This structure together with the Ras-like GTPase domain (RD) forms a nucleotide-binding pocket that binds guanosine diphosphate (GDP) in the inactive state, in which Gαs is forming a complex with Gβγ (Milligan & Kostenis, 2006; Preininger et al., 2013). Activation of the GPCR leads to a conformational change of the complex leading to an opening of the pocket and a substitution of GDP to guanosine triphosphate (GTP) forming an intermediate state that is slowly closed until the complex is in its active state and dissociates from the GPCR activating a downstream signalling cascade (Ahn et al., 2022; Ritter & Hall, 2009). Surprisingly, the authors have shown that binding of GTP and a fast dissociation from the receptor was followed by a relative long intermediate state during which the AHD is closing. Moreover, they were able to show by using Tryptophan-Induced Quenching (TrIQ) - a fluorescent approach using the quenching effect of intrinsic tryptophans on labelled fluorophores for measuring distances within proteins (Mansoor et al., 2010) - that MAGED2 not only interacts with the AHD, but also controls AHD kinetics by accelerating its closing, thus, probably regulating the GPCR activation cascade (Figure 37) (Ahn et al., 2022). Consequently, a loss of MAGED2 rewires GPCR kinetics probably by decelerating the activation-inactivation cycle of Gαs. As this process is relatively upstream of the GPCR signalling cascade this could explain the extensive changes on the phosphoproteomic level that we were able to observe in HEK293T and mpkCCD cells.

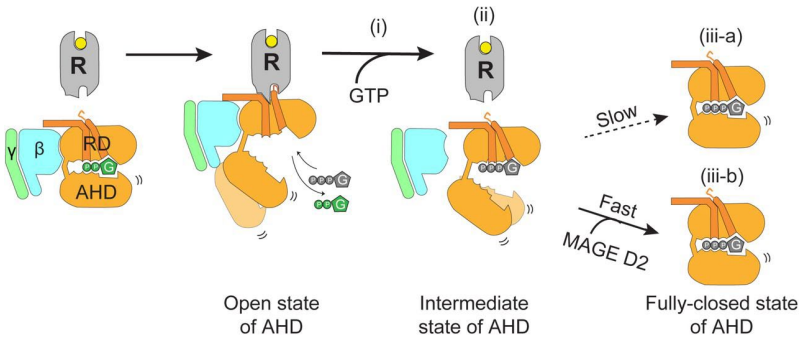

Figure 37: Cartoon illustrating the proposed course of GPCR activation after GTP binding depending on MAGED2. *An activated receptor (R) is inducing GDP release and subsequent binding of GTP to the empty nucleotide-binding pocket (i). Gαs then dissociates from the receptor and the other subunits Gβγ (ii) and goes through a long-lasting intermediate state until it is closed. MAGED2 accelerates AHD closing. Adopted from Ahn et al., 2022.*

3.3 Change of proteome composition in long-term DDAVP treated mpkCCD cells

While the proteome composition was not altered by *MAGED2* knockdown in HEK293T cells, protein expression patterns were clearly changed in the *Maged2* depleted mpkCCD cell-line in response to long-term vasopressin treatment. While short-term treatment induces changes of phosphorylation patterns leading to AQP2 trafficking to the membrane, long-term treatment leads to increased AQP2 protein and mRNA levels (Hasler et al., 2002; Hayashi et al., 1996). These elevated AQP2 levels have been shown to be induced by increased binding of RNA polymerase II to the *AQP2* gene and, thus, an increased expression of the gene with the help of CREB and putative other transcription factors (Sandoval et al., 2016). Remarkably, this vasopressin-dependent process seems to be highly selective for AQP2 as it is the by far most upregulated protein in ligand-activated mpkCCD cells (Sandoval et al., 2016). On the transcriptional level we could now observe a significantly stronger increase of *Aqp2* mRNA levels in the *Maged2* depleted cells, which was then confirmed also on the protein level via Western Blot experiments. mRNA levels of *Scnn1b* coding for EnAC, another vasopressin-dependent sodium channel, showed no difference between *Maged2* depleted and wildtype cells. Also, *Avpr2* expression in the *Maged2* depleted cells was not altered. The proteomic data also confirmed a significant higher abundance of AQP2 protein. In addition, MED14 was identified as another protein with significant higher protein abundance. This protein is a subunit of the mediator complex which plays a major role as mediator of transcription factors and RNA polymerase II (Allen & Taatjes, 2015). In mammals the mediator complex is built of 26 subunits that bind to transcription factors at their activation domains in order to transmit regulatory signals from transcription factors that are bound to DNA in their promoter or enhancer locus to the RNA polymerase II, which results in the formation of the preinitiation complex inducing transcription (Allen & Taatjes, 2015; Richter et al., 2022; Soutourina, 2018). Depletion of 10 of the 25 Mediator complex subunits in yeast as well as a knockout of various mammalian Mediator subunits led to embryonic lethality which shows the vital role of the single subunits (Ito et al., 2002; Soutourina et al., 2011; Stevens et al., 2002; Tudor et al., 1999; Westerling et al., 2007). MED14, at this juncture, plays a major role as module that connects the head, middle and tail structures (Robinson et al., 2015). Interestingly, regulation of the mediator complex

has also been shown to be driven by vasopressin and leads to a translocation to the nucleus in mpkCCD cells after long-term dDAVP treatment (Schenk et al., 2012). Hence, in the *Maged2* depleted mpkCCD cells an increased MED14 abundance could lead to a rise of vasopressin induced AQP2 levels. This is also consistent with the finding that each mediator subunit regulates the expression of a determined gene subset and not the entire transcription process (Allen & Taatjes, 2015).

An upregulation of AQP2 *in vivo* would result in an increased reabsorption of water leading to consequences similar to that of the syndrome of inappropriate secretion of antidiuretic hormone (SIADH) or the nephrogenic syndrome of inappropriate antidiuresis (NSIAD)(Bartter & Schwartz, 1967; Feldman et al., 2005). NSIAD is caused by gain-of-function mutations of *AVPR2* leading to a constitutively active V2R and, hence, increased water reabsorption characterised by hyponatremia, hypo-osmolality and natriuresis (Feldman et al., 2005). The disease can be treated by blocking the V2R with the receptor antagonist tolvaptan (Ghali et al., 2009). Although hyponatremia was observed in BS5 patients from the initial cohort (Laghmani et al., 2016) as well as in individual BS and Gitelman cases (Schepkens et al., 2001; Verma et al., 2020) an effect of fluid resuscitation apparently counters the observed polyhydramnios and postnatal transient polyuria in BS5. The IF stainings of the *Maged2*$^{R446C/Y}$ mice lead to the assumption that AQP2 trafficking to the apical membrane may be defective, which would explain why an increased abundance of AQP2 would not necessarily result in increased water reabsorption. Still, it has to be emphasized that increased AQP2 upregulation after dDAVP treatment occurred in a stylised *in vitro* cell model.

Another protein that was significantly upregulated in *Maged2* depleted mpkCCD cells was synaptopodin. This protein is dispensable for proper kidney function but has been found to play a protective role for podocytes after induced injury via its involvement in the reorganization of the actin filament (Ning et al., 2020). If this protein also plays a protective role in conjunction with *Maged2* depletion has to be further assessed.

All in all, it can be said that *Maged2* depletion of mpkCCD cells lead to changes of phosphorylation patterns after dDAVP short-term treatment and to changes on AQP2 and MED14 abundance on the proteome and mRNA level which clearly shows that MAGED2 is a modulator of GPCR signalling (Figure 38).

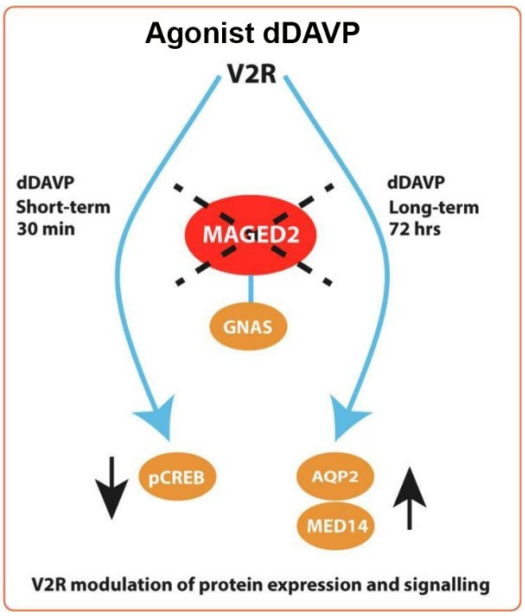

***Figure 38: MAGED2 modulates dDAVP signalling in mpkCCD cells**. Cartoon illustrating consequences of short-term and long-term dDAVP exposure. Short-term exposure induced changes of phosphorylation patterns (as investigated target pCREB), long-term dDAVP treatment increased the abundance and transcription of Aqp2 and Med14. Modified from (Reusch et al., 2021).*

3.4 *Maged2*$^{R446C/Y}$ mice show pathological phenotypes

3.4.1 Phenotypical characterization of the *Maged2*$^{R446C/Y}$ mice

Most of the pathogenic variants that have been found to date in *MAGED2* lead to a total loss of MAGED2 protein in male individuals. In our initial study we detected in family F8 a true missense mutation at position R446C in the MAGE homology domain leading to a loss of interaction with Gαs and DNAJB1 (Laghmani et al., 2016). The mother of this patient suffered from severe polyhydramnios and the foetus died at 22 weeks of gestation (Laghmani et al., 2016). Beside the loss of interaction with Gαs, IF stainings of wild-type and R446C cells in Cos7 cells show that while the wild-type MAGED2 is present in the cytosol and in the nucleus, the MAGED2^{R446C} mutant is only present in the cytoplasm and loses its ability to reach the nucleus. Also, other studies have demonstrated that MAGED2 localization is highly variable and changes during the cell cycle leading to the assumption that it plays an important role in the cell cycle (Pirlot et al., 2016). Furthermore, in this study MAGED2 deletion mutants of putative nuclear localization signal sequences (NLSs) have been created, from which one mutant (Δ203-254) lost its ability for nuclear localization (Pirlot et al., 2016) similar to what we have seen in Cos7 cells.

Given that our studies using HEK293T cells are useful to uncover interaction partners and even mpkCCD cells are limited in their ability to fully replicate the complexities of biological processes at the tissue level, we chose to generate a mouse model bearing the human pathogenic R446C variant for further investigation. Due to the high conservation of human and murine *MAGED2* the position of the mutation is identical in both species. Via CRISPR/Cas9 the mutation as well as a silent mutation 3 positions upstream were inserted into zygotes via electroporation and implanted in C57BL/6N mice. For the experiments heterozygous female mice were mated with wildtype male mice. At birth the male mice were used for the experiments while the female mice were used for the further breeding. In total, the sex ratio of the mice reached nearly 50%, which shows that no sex was deprived during gestation.

When looking at the genotypes female mice showed an almost mendelian ratio of wildtype and heterozygous genotype, while in male mice the genotype ratios were markedly reduced. Analysis of the already dead pups at P0 showed an increased number of male pups hemizygous for the R446C mutation indicating that the perinatal stage seems to be critical. Still, the genotyping results of the dead pups have to be interpreted with caution as dead newborn pups often are eaten by the mother (Weber et al., 2016), which could impact the ratio. Interestingly, in mouse models of the BS1 gene *Slc12a1* as well as the BS3 gene *Clcnkb*, pups were born in mendelian ratios and mortality in *Slc12a1*$^{-/-}$ mice commences in the postnatal stage while the *Clcnkb*$^{-/-}$ phenotype is much milder (Grill et al., 2016; Takahashi et al., 2000). Given that symptoms in human BS5 patients typically begin around weeks 19-21 of gestation and most patients who died, died during pregnancy, it is likely that the critical stage of BS5 occurs earlier. Consequently, genotype distribution in mice should be determined at different stages of development in further studies to precisely determine the most critical stage.

Severe polyhydramnios, one of the most prominent symptoms of BS5, is also expected to be present in pregnant mice. But as males hemizygous for the R446C mutation only constituted a small percentage of the litter an appearance as in humans could not be detected. Determination of amniotic fluid volumes in mice, thus, requires euthanizing of pregnant mice to remove the individual gestation sacs and analyse them. These studies need to be conducted in future experiments. As BS1 is characterized by severe polyhydramnios in humans, the absence of this condition in *Slc12a1*$^{-/-}$ mice suggests that the regulation of amniotic fluid in mice functions differently (Takahashi et al., 2000).

The bulk of the male *Maged2*$^{R446C/Y}$ pups showed several symptoms. For instance, it was conspicuous that the bladder of many affected animals was empty. This could be traced back to problems in urine production due to volume depletion and prerenal failure. Other frequent symptoms were a pale skin, an empty and blood-filled stomach or malformations of the intestine. Also, body and kidney weight were slightly decreased in *Maged2*$^{R446C/Y}$ pups without reaching significance. In BS5 patients no decreased body weight could be detected (Legrand et al., 2018). Likewise, in other mouse models of the Bartter-associated genes *Slc12a1* and *Clcnkb* no differences in weight at birth have been, but body weight decreased over time in untreated mice as water and salt loss progressed (Grill et al., 2016; Kemter et al., 2014; Takahashi et al., 2000). Normal growth and development of male *Maged2*$^{R446C/Y}$ mice after the critical prenatal and perinatal phases resembles the human phenotype, as four male *Maged2*$^{R446C/Y}$ mice survived this phase with ages between 200 and 600 days before they were sacrificed. Urine parameters indicate salt wasting of sodium and calcium, although it has to be mentioned that these values usually are analysed from urine samples collected from 24 hours. Due to the low amount of urines from individual mice, we had to pool the samples and dilute them with water. In further studies these measurements have to be repeated and also compared to blood electrolyte levels.

HE stainings of P0 paraffin kidney sections did not reveal gross morphological changes of the kidney. However, the PAS staining showed that the brush border of proximal tubule cells was less prominent developed in *Maged2*$^{R446C/Y}$ mice than in wildtype kidneys. Interestingly, our proteomic approach revealed the downregulation of a cluster of proteins predominantly located in the brush border. This lower abundance were traced back to impaired development of this structure. As BS has not been linked with disturbances of the proximal tubule yet, this discovery is interesting and will be discussed later. To evaluate potential alterations of further brush border structures, PAS staining of the intestine of *Maged2*$^{R446C/Y}$ mice should be performed, as the apical surface of enterocytes also forms a brush border.

IF stainings of NKCC2, NCC and ROMK showed an apical distribution in wildtype as well as in *Maged2*$^{R446C/Y}$ animals indicating normal distributed cotransporters in the *Maged2*$^{R446C/Y}$ animals. Still, IF stainings were just conducted with the kidneys of P0 animals. Further experimentation is necessary to evaluate the localization of cotransporters at different prenatal time points in order to determine if alterations in localization contribute to the BS5 phenotype during gestation.

AQP2 distribution, on the other hand, was markedly different in the kidneys of *Maged2*$^{R446C/Y}$ mice. While wildtype animals show AQP2 accumulations at the apical membrane of the collecting duct cells, AQP2 in kidneys of *Maged2*$^{R446C/Y}$ mice showed a diffuse localization in the cells. This was seen even more clearly when looking at the pAQP2 staining. Also, the kidney of the deceased foetus F1.II-1 lacked apical localization of AQP2, while the kidney of an age-matched control foetus clearly showed a normal AQP2 distribution. In the inactivated state AQP2 is mainly localized in intracellular vesicles (Takata et al., 2008). Upon activation by ADH, AQP2 is phosphorylated by PKA and translocated to the apical plasma membrane by exocytosis of the vesicles increasing the water permeability of the membrane and, hence, water reabsorption and concentration of the urine (Katsura et al., 1997; Takata et al., 2008). The most important phosphorylation site of AQP2 is Ser256. AQP2 with mutated Ser256 is also not able to translocate to the apical membrane (Katsura et al., 1997), which leads to the assumption that there are alterations of phosphorylation processes existent. Further phosphoproteomic studies of *Maged2*$^{R446C/Y}$ kidney material could reveal alterations in phosphorylation patterns. Also, localization studies of AQP2 must be conducted at further time points. As BS5 is characterized by a transient phenotype, normal AQP2 localization at an older age would indicate that perinatally mislocated AQP2 strongly contributes to polyhydramnios and polyuria.

Interestingly, our proteomic approach also shows significant downregulation of the proteins RAB11 Family-Interacting Protein 1 (RAB11FIP1) and RAB11 Family-Interacting Protein 3 (RAB11FIP3). Former studies have shown that AQP2 trafficking to the plasma membrane is dependent on F-actin and the motor protein myosin Vb (Nedvetsky et al., 2007). This transport process also needs the involvement of specific proteins of the Rab family of GTPases, which induce the coupling of motor proteins to the vesicles (Bock et al., 2001). There are also intermediate proteins that are able to bind both RAB and motor proteins, which might play a role in the regulation of recycling processes (Nedvetsky et al., 2007). For AQP2 especially the intermediate protein RAB11 Family-Interacting Protein 2 (RAB11FIP2) plays an important role in the shuttling to the apical membrane, as it is able to bind RAB11 and myosin Vb (Nedvetsky et al., 2007). RAB11FIP1 and RAB11FIP3 also bind to RAB11 but do not bind to myosin Vb and so an influence of these two proteins on the AQP2 shuttling was not detected yet but is worth to be further analysed.

3.4.2 Kidneys of *Maged2*$^{R446C/Y}$ mice show a highly altered proteome

Proteome analyses of murine kidneys show a multitude of proteins that are differentially expressed in kidneys of *Maged2*$^{R446C/Y}$ animals in comparison to wildtype kidneys. In total, 112 proteins showed an increased and 195 proteins a decreased abundance while being involved in a multitude of different cellular processes. It has to be mentioned that proteome analyses were conducted with whole kidneys from P0 mice. Further proteomic analyses of distinct renal tubular segments could give an even more precise picture of *Maged2*-dependent protein abundance alterations.

3.4.2.1 MAGED2 plays an important role in cell-cycle control

The protein that was upregulated the most is NABP2. This protein is a subunit of the Sensor of Single-stranded DNA (SOSS) complex which plays an important role in the repair of double-strand breaks (DSB) via homologous recombination (HR) (Huang et al., 2009). DSB are cytotoxic lesions of the DNA that can lead to genomic instability or even induce tumorigenesis if they are not repaired properly (Friedberg, 2003). One of the first steps in the process of HR is the resection of the DSB, which produces single-stranded DNA (ssDNA) that is recognized and bound by so-called Single-stranded-DNA-binding proteins like replication protein A (RPA) or NABP2 (Richard et al., 2008; Wold, 1997). Mutated NABP2 leads to defective checkpoint activation, increased sensitivity for radiation and enhanced genomic instability (Richard et al., 2008). Mouse NABP2 also has been shown to protect newly replicated telomeres and to be lethal in combination with developmental abnormalities when knocked out (Gu et al., 2013). Interestingly, in humans, NABP2 also regulates the stability and transcriptional activity of p53 by protecting it from ubiquitin-mediated degradation (Xu et al., 2013). In human cancer cells MAGED2 physically interacts with p53 and impairs its transcriptional ability (Papageorgio et al., 2007). *MAGED2* knockdown even increased the transcription of *p53* itself (Tseng et al., 2012) although this was not observed in our proteomics data. Furthermore, it is striking that GO enrichment analysis also reveals an upregulation of further gene clusters being involved in cell cycle regulation, especially in the regulation of the G2/M checkpoint. This important cellular security measure ought to prevent the cell from entering mitosis with DNA damage (Reinhardt & Yaffe, 2009). Polo Like

Kinase 1 (PLK1) is a protein with significant higher abundance in kidneys of *Maged2*$^{R446C/Y}$ mice. This kinase is a major regulator of the initiation of mitosis as it controls the activity of the CDK1/Cyclin B complex which induces mitosis as well as regulates the separation of the cytoplasm and membrane formation by activation of the mitotic kinesin-like protein 1 (MKPL1) (Gavet & Pines, 2010; Liu et al., 2004). Further upregulated proteins (ORC1, ORC6, HMGA2, CCNB1) underline the estimated role of MAGED2 in these processes. It could already be shown that MAGED2 changes its localization during cell cycle and after cellular stress also indicating a role in cell cycle regulation (Pirlot et al., 2016). Other studies even could associate MAGED2 with DNA damage response (DDR) activities due to its phosphorylation by the protein kinases ataxia telangiectasia mutated (ATM) and ATM and RAD3-related (ATR) as a consequence of ionizing radiation (Matsuoka et al., 2007). ATM and ATR are the most important kinases of the DDR response and transduce signals to molecules which control cell cycle arrest, DNA repair, transcription factors and apoptosis to maintain genome stability (Cimprich & Cortez, 2008). ATR activation is triggered by ssDNA stretches bound by RPA (Cimprich & Cortez, 2008), while ATM activation also requires NABP2 (Paquet et al., 2015), which is increased in the kidneys of *Maged2*$^{R446C/Y}$ mice according to our proteome data. In the following downstream cascade CHK1 and CHK2 kinases are activated by ATR and ATM, respectively, which induce inhibition of cyclin-dependent kinases (CDK), which leads to a regulation of cell cycle checkpoints (Matsuoka et al., 2000; Zhao & Piwnica-Worms, 2001). In former studies MAGED2 has been shown to play an important role in cell cycle regulation by acting on the ATM/CHK2 and ATR/CHK1 elements of the DDR as well as the E3 ubiquitin ligase complexes SCF and APC/C (Trussart et al., 2018). It also negatively regulates the expression of tumour necrosis factor-related apoptosis-inducing ligand (TRAIL) death receptor 2 (TRAIL-R2) and saves cancer cells from TRAIL-induced apoptosis (Allen & Taatjes, 2015).

These results are also in line with the perturbations of CDK-related pathways that was observed in the PHONEMEs analysis of mpkCCD phosphoproteome data.

However, the impact of MAGED2-associated alterations on cell cycle regulation to the renal phenotype remains unclear and was not further investigated, especially as *Maged2*$^{R446C/Y}$ mice show morphological normal kidneys.

3.4.2.2 Upregulation of Gαs abundance in the kidneys of MAGED2$^{R446C/Y}$ mice

Most remarkably, Gαs is the protein with the second most significant increase of abundance in kidneys from *Maged2*$^{R446C/Y}$ mice compared to wildtype mice. The abundance is more than six times higher than in wildtype mice. As already discussed in 3.2, we have shown that MAGED2 interacts with Gαs and modifies downstream cAMP-dependent signalling pathways. As MAGED2 accelerates Gαs AHD closing and, thus, is supposed to control its activity, an upregulation of Gαs expression in mouse kidney could be a futile compensatory mechanism to counterbalance deficient MAGED2 and cAMP signalling.

Interestingly, a recent study was able to associate MAGED2 function with the hypoxia-inducible factor (HIF) signalling pathway during hypoxia, thus, linking MAGED2 to a further signalling pathway in HEK293T cells (Seaayfan, Nasrah, Quell, Kleim, et al., 2022). During pregnancy blood supply to the kidney is approximately only one fifth of the levels that are achieved postnatally resulting in relative hypoxic conditions of several tissues like the renal medulla, where NKCC2 is expressed (Brezis & Rosen, 1995). While hypoxia usually is characterized as pathological condition, it plays also a crucial role during embryonic development (Simon & Keith, 2008). One of the factors that is upregulated during hypoxia is the transcription factor HIF. Under normoxic conditions HIF1A has a very short half-life of just 5 minutes as it is quickly hydroxylated at conserved proline sites by proline hydroxylase (PHD) and factor inhibiting HIF-1 (FIH) followed by binding of Hippel–Lindau E3 ligase that targets the protein for proteasomal degradation (Gunaratnam & Bonventre, 2009; Ikeda & Kakeya, 2021; Maxwell et al., 1999; Rezvani et al., 2011). Under hypoxic conditions HIF1A is stabilized and translocates to the nucleus, where it forms a dimer with HIF-1β and regulates in a complex with hypoxia response element (HRE) and p300/CBP specific genes targeting hypoxic disturbances (Figure 39) (Choi et al., 2008; Ikeda & Kakeya, 2021). These genes encode proteins important for the homeostasis of cell function under hypoxic conditions like erythropoietin (EPO), vascular endothelial growth factor (VEGF),

glucose transporter-1 (GLUT1) as well as other proteins that enhance anaerobic energy metabolism, erythropoiesis as well as protective pathways (Haase, 2006).

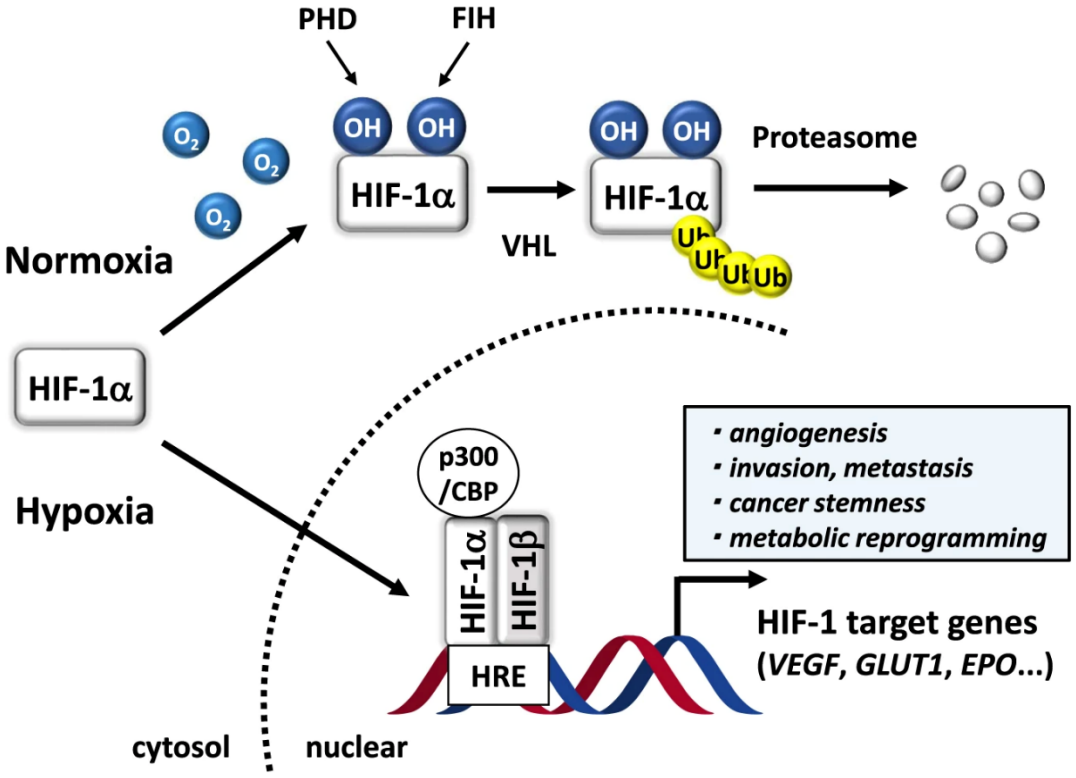

Figure 39: The molecular mechanism of HIF signalling. *HIF signalling is a process in which HIF-1α is hydroxylated by PHD and factor inhibiting HIF-1 (FIH) under normoxia, and then interacts with von Hippel-Lindau (VHL) for degradation by the proteasome. In contrast, under hypoxia, HIF-1α accumulates and translocates to the nucleus, leading to the formation of a heterodimer with HIF-1β. These complexes then bind to the hypoxia response element (HRE) with p300/CBP, activating the expression of numerous genes, including VEGF, GLUT1, and EPO. Adapted from (Ikeda & Kakeya, 2021).*

A total knock-out of *Hif1a* leads to embryonic lethality and abnormal vascularization, especially of capillary networks (Ryan et al., 1998).

Murine *Hif1a* expression in kidney tissue during embryonic development is similar to that of *Maged2* with gradual decline of mRNA (Figure 40) (Wang et al., 2021).

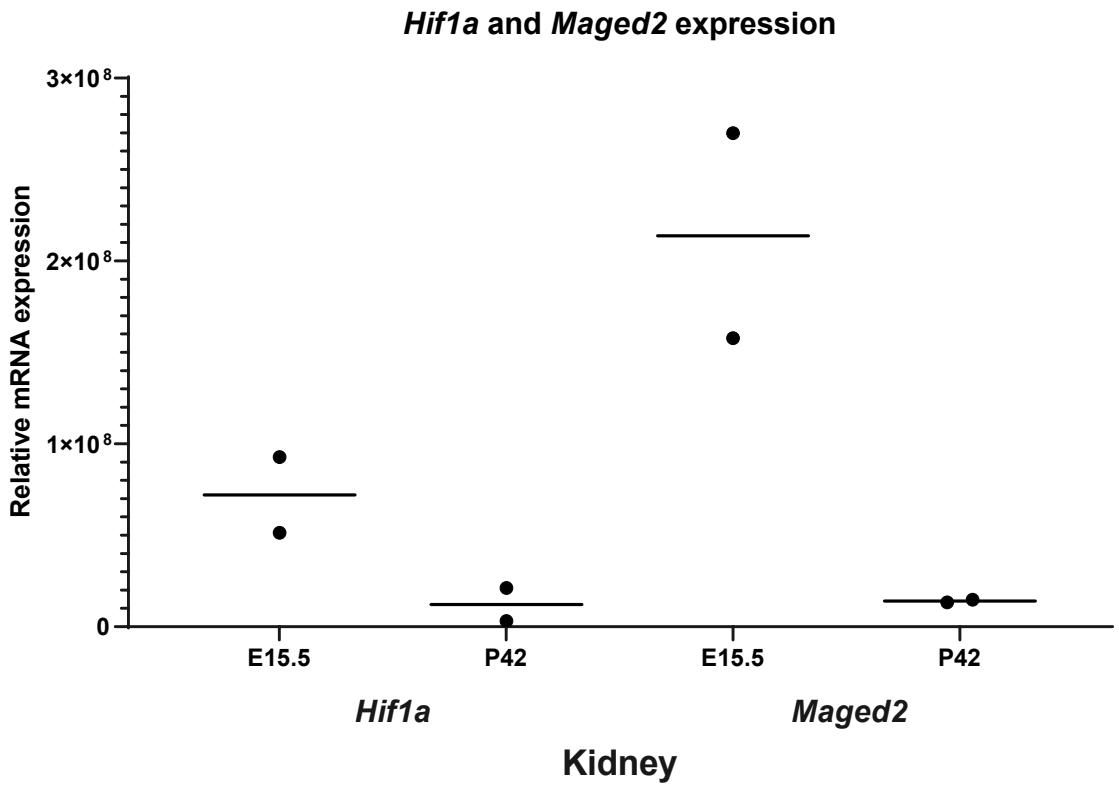

Figure 40: Hif1a and Maged2 expression in embryonic and postnatal development. *Transcriptomic data was analysed from Wang et al., 2021 with Graphpad Prism software. N=2 for embryonic and adult mouse each (error bars = SD).*

Seeayfan et al. have shown that under normoxic conditions *MAGED2* depletion had no effect of the Gαs localization at the cell membrane. Under hypoxic conditions, on the other hand, membranous localization of Gαs was lost and changed to an intracellular localization with a vesicular and diffused pattern due to increased Mouse double minute 2 homolog (MDM2)-dependent ubiquitination leading to Gαs endocytosis from the plasma membrane (Seaayfan, Nasrah, Quell, Kleim, et al., 2022). Aberrant Gαs localization, in turn, *in vivo* impairs correct AQP2 localization to the apical membrane, which is a highly cAMP and PKA-dependent process in the perinatal period (Baum et al., 1998) pointing to an essential role of MAGED2 during hypoxia in embryonic development (Figure 41).

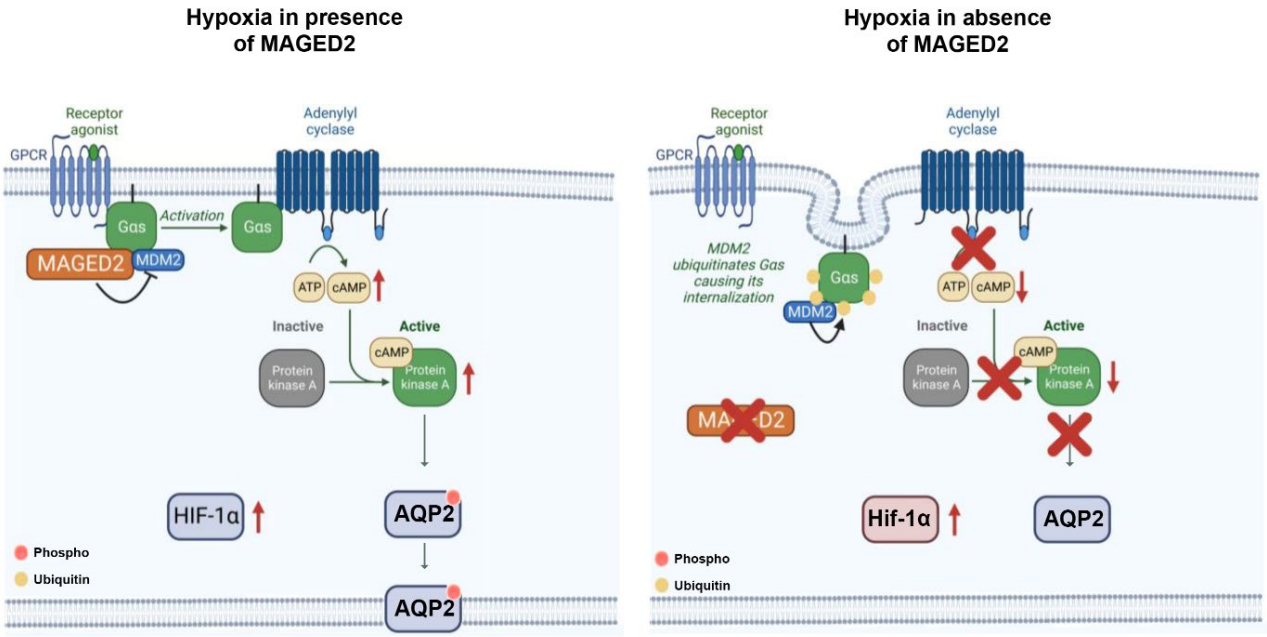

Figure 41: Proposed model for the role of MAGED2 under hypoxic conditions. *Under hypoxia, MAGED2 blocks MDM2-controlled ubiquitination and endocytosis of Gαs, thus, activating adenylate cyclase and boosting production of cAMP which activates PKA. Low cAMP levels cause salt wasting in transient Bartter syndrome due to impaired cAMP-dependent salt reabsorption which probably impairs maturation and correct localization of AQP2 as well as potential other cotransporters. Modified from (Seaayfan, Nasrah, Quell, Kleim, et al., 2022).*

Seaayfan et al. also have demonstrated that MAGED2 is necessary for the proper regulation of *HIF1A* expression in response to hypoxia (Seaayfan, Nasrah, Quell, Kleim, et al., 2022). This finding suggests a mutually reinforcing relationship between these two proteins maybe via altered cAMP signalling processes. While hypoxia leads to increased cAMP levels, increased PKA activation as well as expression, PKA-dependent phosphorylation of HIF1 at Thr63 and Ser692 inhibits its proteasomal degradation (Bullen et al., 2016; Shaikh et al., 2012; Simko et al., 2017). Interestingly, our proteome data shows that also a cluster of proteins is upregulated, which responds to hypoxia (ZFP36L1, TMBIM6, PPARD, BIRC2, FLT1 and PLD2). Of note, Seaayfan et al. also observed an increased abundance of Gαs protein in MAGED2 depleted hypoxic cells, which collectively point to compensatory upregulation of Gas possibly resulting from its impaired function (Seaayfan, Nasrah, Quell, Radi, et al., 2022). The pale skin of affected animals could also point to defective HIF signalling, as it plays an important role in vascularization processes. In the foetus, EPO is primarily produced

in the liver making investigations of *Maged2*$^{R446C/Y}$ liver necessary in further experiments.

3.4.2.3 Downregulated proteins

Proteomic data of the mice show a high number of proteins with differential abundance in *Maged2*$^{R446C/Y}$ mice in comparison to wildtype mice. NCC, a protein suspected to play a significant role in the development of BS5 (Laghmani et al., 2016), was found to be significantly downregulated 3.5-fold in our proteomic data. Defects in this sodium chloride cotransporter lead to the Bartter-like Gitelman syndrome, which is characterized by hypokalemic metabolic alkalosis, hypomagnesemia and low urinary calcium excretion (Gitelman et al., 1966; Knoers & Levtchenko, 2008). In a ROMK-deficient mouse model of antenatal Bartter syndrome II NCC was shown to be compensatorily up-regulated (Cantone et al., 2008). In our former study we have shown that surface and total NCC protein was upregulated in HEK293T cells when co-expressed with MAGED2 (Laghmani et al., 2016). IF stainings from a deceased patient have shown NCC absent from the apical membrane of tubules in comparison to an age-matched control (Laghmani et al., 2016), although this data has to be critically examined as it is derived from just one patient. In the *Maged2*$^{R446C/Y}$ mice the localization of NCC does not seem to differ from wildtype kidneys at P0, although quantification of protein abundance by means of IF pictures is not possible. NCC localization in an earlier stage of disease has to be conducted as suggested in 3.4.1. Also, appropriate segment specific markers for the apical membrane have to be chosen that could uncover even slightest changes of NCC localization from the apical membrane. NCC abundance is controlled by neural precursor cell expressed developmentally down-regulated 4-like (NEDD4-2) induced ubiquitination (Arroyo et al., 2011). NEDD4-2, in turn, is negatively regulated by phosphorylation of serum glucocorticoid 1 (SGK1) (Rozansky et al., 2009). Therefore, a phosphoproteome analysis would be a good follow-up experiment.

The proteome data also shows a slight downregulation of CLC-Ka and BSND, which represent other proteins affected in distinct forms from the Bartter spectrum (Birkenhager et al., 2001; Schlingmann et al., 2004), without reaching significance.

The protein, which is downregulated most significantly is the sulfotransferase

SULT1C2. This protein is a member of the family of sulfotransferases (Sult), which play an important role in the detoxification of various substrates by addition of sulfur groups and, hence, an increase of its water solubility leading to an enhanced clearance via urine (Allali-Hassani et al., 2007; Gamage et al., 2006). Interestingly, this protein was also found to be downregulated in a chemical-induced polycystic kidney disease (PKD) mouse model, which probably leads to abnormal synthesis of extracellular matrix proteins in the tubular basement membrane (Sugimura et al., 2002). The significance of SULT1C2 downregulation for BS5, however, is unclear.

Interestingly, a cluster of proteins located in the brush border of cells is significantly downregulated, which is in line with the weaker PAS staining in kidneys from *Maged2*$^{R446C/Y}$ mice indicating a depauperated brush border. In the kidney, the brush border membrane is the apical membrane of proximal tubule cells. The proximal tubule is the part of the nephron most reabsorptive and responsible for approximately 80% of the fluid and electrolyte recovery like NaCl from the glomerular filtrate (Nakhoul & Batuman, 2011; Walmsley et al., 2010). Also, over 99% of glucose is reabsorbed in this compartment as well as other nutrients and molecules like sulfates, phosphates and proteins (Walmsley et al., 2010). This luminal membrane on the apical side is covered by densely packed microvilli with even height called the brush border which increase the surface of this membrane (Gallardo & Vio, 2022). One of the proteins from the downregulated cluster is Megalin (LRP2). LRP2 is a multiligand, endocytic receptor from the low-density lipoprotein (LDL)-receptor family mainly localized at the apical membrane of renal proximal tubule cells as well as in glomeruli (Christensen & Birn, 2001; Kerjaschki & Farquhar, 1982). It is a transmembranous glycoprotein with a large size of approximately 600 kDa (Raychowdhury et al., 1989). Its main function is the tubular uptake of glomerular-filtered proteins like albumin as well as other low-molecular-weight proteins by receptor-mediated endocytosis (De et al., 2014). According to this, pathologic loss of LRP2 lead to renal diseases like the Donnai-Barrow syndrome or the facio-oculo-renal syndrome which are characterized by albuminuria and low-molecular-weight proteinuria with regards to the kidney phenotype (Kantarci et al., 2007; Pober et al., 2009). In our proteomic data, also albumin is one of the proteins with significantly decreased abundance which could be a hint to an albuminuria in the *Maged2*$^{R446C/Y}$ mice. This has to be validated from plasma and urine concentrations in further experiments. Interestingly, LRP2 is also an interaction partner and, thus, a regulator of sonic hedgehog (SHH), which plays an important role in

embryonic kidney development (McCarthy et al., 2002). With Amnionless (AMN) another protein of this complex is downregulated in the proteome of *Maged2*$^{R446C/Y}$ mouse kidneys. AMN is a type 1 transmembrane protein, which has with cubilin just one ligand, for which it is the anchor in the membrane (Kozyraki & Gofflot, 2007). Cubilin on the other hand forms a Ca^{2+}-dependent complex with LRP2 in order to accomplish endocytotic processes (Nielsen et al., 2016). Dysfunctions of cubilin caused by either mutations in the *cubilin* gene or the *Amn* gene lead to vitamin B12 deficiency as well as proteinuria (Nielsen et al., 2016). Another protein associated with LRP2 is the NHE3 transporter, which is also predominantly found in the proximal tubule, where it acts directly as the mediator of the reabsorption of NaCl and $NaHCO_3$ as well as indirectly as the mediator of the H^+-dependent reabsorption of molecules like citrate, amino acids and oligopeptides (De et al., 2014; Donowitz et al., 2009). Also, passive water reabsorption is accomplished by Na^+ gradients created by NHE3 at the luminal cell membrane and Na^+, K^+-ATPases on the peritubular cell membrane (Du et al., 2004). In a recent study MAGED2 has been shown to interact with NHE3 in HEK293T cells (Ruttkowski, 2021). But more importantly, another protein that interacts with NHE3 is PDZ Domain Containing 1 (PDZK1), which is also significantly downregulated in the kidneys of *Maged2*$^{R446C/Y}$ mice. PDZK1 is member of a gene family with PDZ-domains that interacts with target proteins and are involved in many cellular processes like transport or ion channel signalling (Lee & Zheng, 2010). Together with Na(+)/H(+) Exchange Regulatory Cofactor NHE-RF1 (NHERF1), a protein involved in tubular phosphate reabsorption, it assembles a complex to enable docking of a multitude of signalling molecules and also of PKA, thereby regulating PKA activity in the brush border of proximal tubule cells (Bergsland et al., 2018; Gisler et al., 2003). In a mouse model for inflammatory bowel disease, which results in diarrhoea due to altered sodium metabolism, it has been shown that expression of *NHE3* as well as its localization at the membrane did not change, while its regulators Na(+)/H(+) Exchange Regulatory Cofactor NHE-RF2 (*NHERF2*) and *PDZK1* were downregulated which led to NHE3 dysfunction in the colon (Lenzen et al., 2012). In the proximal tubule, on the other hand, a NHE3 dysfunction due to *PDZK1* knockdown could not be observed, while another chloride transporter *SLC26A6* was downregulated (Thomson et al., 2005). *Pdzk1* knock-down in mice further abolished cAMP-mediated inhibition of NHE3 (Cinar et al., 2007; Yun et al., 1997) indicating a dysregulation of NHE3 activity in *Maged2*$^{R446C/Y}$ mice. Further experiments are needed to analyse the impact of MAGED2 deficiency in

the proximal tubule and the gut.

The kidney and especially the proximal tubule have a high demand of energy and, thus, rely on mitochondrial metabolism, especially as proximal tubular cells are not able to produce ATP anaerobically via glycolysis (Chevalier, 2016). Also, the distal convoluted tubule, which plays an important role in electrolyte reabsorption needs high amounts of energy and is vulnerable to dysfunctional mitochondria (Govers et al., 2021). According to the proteome data there is a downregulation of a cluster of proteins located in the matrix and the inner membrane of mitochondria. Especially, a disturbance of ketone body metabolism can be assumed of the proteomics data. 3-Oxoacid CoA-Transferase 1 (OXCT1) is an enzyme located in the matrix of mitochondria, which is essential for extrahepatic ketone body metabolism, as it catalyzes the transfer of coenzyme A from succinyl-CoA to acetoacetate (Diao et al., 2022). 3-Hydroxybutyrate Dehydrogenase 1 (BDH1) on the other hand is an enzyme located in the inner membrane of mitochondria that catalyzes the reversible transformation of acetoacetate and βOHB, which represent the two major ketone bodies of the fatty acid catabolism (Adami et al., 1993). Both proteins are significantly downregulated in the kidneys of *Maged2*$^{R446C/Y}$ mice. In a mouse model of diabetic kidney disease, a downregulation of these proteins resulted in an accumulation of acetoacetate and an additional decreased amount of βOHB probably contributing to a pro-inflammatory state of the kidney (Diao et al., 2022).

3.5 Final conclusion and outlook

Rare genetic disorders provide an excellent opportunity to gain insight into human physiology and combat illness. BS results from defective tubular transport and leads to excessive urine production and salt loss (Besouw et al., 2019). Given the clinical relevance of fluid and electrolyte homeostasis throughout life, it is important to understand the principle molecular mechanisms exerted by our main organ, the kidney, in greater detail. Investigating *MAGED2* associated kidney disease offers such a rare opportunity to gain knowledge from an orphan disease about the inner workings of the kidney, which otherwise would be difficult to obtain. *MAGED2* associated tubulopathy constitutes the most recently identified BS type, BS5 (OMIM#300971). Although not

rare compared to other BS types accounting for about 10% of all BS cases (Legrand et al., 2018) and probably the most severe form for a particular period of time, BS5 has remained enigmatic for a long time, which has several reasons:

1. Its mode of inheritance is X-linked recessive (XLR) compared to the autosomal recessive (AR) inheritance of all other BS types.
2. Its transient nature characterized by polyhydramnios and perinatal polyuria in contrast to the persistent nature of salt wasting in all other BS types.
3. The molecule MAGED2 itself is associated with XLM and cancer and no obvious connection to kidney.

Since the first report (Laghmani et al., 2016) other groups have confirmed our genetic and clinical findings (Legrand et al., 2018; Ma et al., 2021; X. Wu et al., 2021). *MAGED2* is the first gene of the BS spectrum that does not encode a molecule directly involved in tubular transport and so little is known about the physiological role of MAGED2 in kidney cells.

However, the initial study indicated that impaired maturation and mistargeting of the NKCC2 and NCC cotransporters to the apical membrane may induce the BS5 phenotype (Laghmani et al., 2016).

Based on the interactome data for HEK293T cells, we followed our hypothesis that MAGED2 has a regulatory function in GPCR signalling. In this study we showed that siRNA-induced depletion of *MAGED2* induces numerous changes on the proteomic and the phosphoproteomic level in HEK293T cells, mpkCCD cells and in kidneys of *Maged2*$^{R446C/Y}$ mice. Here, the proteomic data showed a decreased abundance of NCC, slight decreases of CLCNKA and BSND as well as a downregulation of proteins from the proximal tubular brush border. Furthermore, IF stainings of AQP2 indicated an impaired apical localization. All in all, these modifications seem to collectively contribute to the severe prenatal and perinatal phenotype of BS5 in comparison to the other forms of Bartter syndrome, which are caused by mutations in only one cotransporter each. As *MAGED2* depletion led to numerous alterations in phosphorylation signalling in HEK293T and mpkCCD cells, phosphoproteomic analyses are in preparation conducted with the kidneys from the *Maged2*$^{R446C/Y}$ mice, especially relating to Gαs and PKA-dependent signalling. Furthermore, proteomic analyses as well as localization studies should be conducted in further experiments with kidneys of prenatal *Maged2*$^{R446C/Y}$ mice as well as older mice that have survived

the perinatal phase to precisely narrow down the critical period and comprehend the dynamics of aberrant signalling with MAGED2 deficiency. To gain a more detailed view on the transcriptional level, a spatial transcriptomics approach is in preparation with kidney tissue from *Maged2*$^{R446C/Y}$ mice. This technique allows the spatial visualization and quantitative analysis of transcriptomic data in tissue sections on slides covered by reverse transcription primers with positional barcodes (Stahl et al., 2016). Analysis of this spatiotemporal data can give a more detailed insight with regards to specific renal structures. All these experiments could help to understand the mechanism as well as its transient character better.

Former studies had shown that the vasopressin-controlled activity of AC is dependent on the developmental stage with increasing levels of AC from day 2 in rat pups (Rajerison et al., 1976) leading to an increase of cAMP dependent processes like activation of PKA, which, in turn, phosphorylates NKCC2 and NCC leading to their correct membrane trafficking (Rieg et al., 2013). As *Maged2* expression decreases during embryonic development, this process is probably independent of MAGED2 and, thus, could be a compensatory process with a late maturation of NKCC2, NCC and AQP2. This could be associated with the embryonic kidney development under hypoxic conditions. As MAGED2 plays an important role in proper Gαs membranous localization and function under hypoxic conditions (Seaayfan, Nasrah, Quell, Kleim, et al., 2022; Seaayfan, Nasrah, Quell, Radi, et al., 2022), altered cAMP signalling leads to impaired maturation and localization of NKCC2, NCC, AQP2 and potentially other proteins. With increasing oxygenation of the kidney after birth MAGED2 associated processes become less important. Also, the highly increased levels of Gαs that we observed in our mouse model could accelerate cAMP production as soon as the kidney is oxygenated properly and could contribute to the transient character of the disease.

This transient character is the most intriguing aspect that distinguishes BS5 from all other forms of Bartter syndrome. Renal salt and water wasting ended in patients approximately at 30 weeks of gestational age and also hyponatremia, hypokalemia as well as increased renin and aldosterone levels normalized (Laghmani et al., 2016). The follow-up of our patient from the initial study and another patient showed a normal renal development (Laghmani et al., 2016; Ma et al., 2021).

The fact that *MAGED2* expression is crucial for a limited period of time during fetal development could be an advantage for the development of a medical treatment. While many targeted treatments like Lumasiran for Hyperoxaluria type I or Nusinersen for

spinal muscular atrophy have to be repeatedly administered for a lifetime (Bertini et al., 2017; Garrelfs et al., 2021), treatment for BS5 could be limited to a rather short period of time during pregnancy and after birth. X-linked hypohidrotic ectodermal dysplasia (XLHED) is a good example for such a treatment strategy. XLHED is caused by loss-of-function variants of the gene ectodysplasin a (*EDA*) from the tumour necrosis factor (TNF) family resulting in abnormal development of ectodermal structures like missing teeth and sweat glands (Freire-Maia, 1977; Srivastava et al., 1997; Zankl et al., 2001). Abnormal development, especially the inability to sweat, could be permanently rescued in mice by treating pregnant mice with the recombinant ligand EDA1 fused to the FC domain of human IgG1 enabling it to cross from blood to the placenta (Gaide & Schneider, 2003) or by an antibody activating the EDA target receptor EDA receptor (EDAR) (Kowalczyk et al., 2011). In human patients the Fc-EDA fusion protein was administered intraamniotically to affected twins at gestational weeks 26 and 31 as well as to an affected foetus at gestational weak 26 leading to a development without XLHED-related illness (Schneider et al., 2018). Nevertheless, targeted protein replacement treatment of kidney diseases entails some structural problems. The glomerulus actively averts the passing of proteins bigger than 50 kDa and also the slit diaphragm of podocytes is only about 10 nm in size (Rubin & Barry, 2020) while one of the smallest viral vectors is about 25 nm and has a mass over 200 kDa (Rubin et al., 2019). Also, the high diversity of cell types in the kidney (at least 26 different cell types) compared to other organs like the liver (4 cell types) makes a targeted approach difficult (Kmiec, 2001). In further studies we will test if treatment with Forskolin could rescue the depletion of *Maged2* in our mouse model and contribute to proper embryonic development. As impaired Gαs localization to the membrane due to *MAGED2* knockdown in HEK293T cells during hypoxia was shown to be rescued by Forskolin treatment (Seaayfan, Nasrah, Quell, Kleim, et al., 2022), this could be a promising approach. Forskolin is naturally occurring in the roots of *Coleus foskohlii* and increases the production of cellular cAMP by activation of AC (Ammon & Muller, 1985). The usage of forskolin was already widely discussed in the treatment of numerous pathogenic conditions like glaucoma, HIV or cardiac diseases, but it is not widely used in a medical setting (Bodiwala et al., 2009; Caprioli & Sears, 1983; Majeed et al., 2015; Yoneyama et al., 2002). Besides, the safety of forskolin treatment in pregnant women is only poorly documented and studies have shown that forskolin had a negative effect on spontaneous meiotic progression in immature human oocytes and also led to

delayed embryonic development in rats treated with a forskolin containing natural extract (Almeida & Lemonica, 2000; Shu et al., 2008).

In most cases of Bartter Syndrome, the pathomechanism of the disease is well understood. However, *MAGED2* adds a new layer of complexity to the regulation of fluid and electrolyte homeostasis in the development of the kidney. All in all, the studies presented here can serve as a foundation for further research on BS5 particular and fluid homeostasis in general. The mouse model will help us to understand the complex effects of MAGED2 in health and disease in the context of tubulopathies and beyond. Gaining a critical mass of knowledge on the regulation processes executed by MAGED2 could also contribute to the development of new therapeutic strategies for conditions associated with imbalanced AF like oligohydramnios and polyhydramnios or diuretics in later life.

Our studies have already resulted in improved care and management in families with BS5 allowing for timely institution of symptomatic treatment and avoidance of prolonged and unnecessary medication.

4 Material and Methods

4.1 Materials

4.1.1 Reagents used for experiments with nucleic acids

Chemical	Name	Company
Agarose	Agarose Broad Range for electrophoresis	Roth
DNA ladder	GeneRuler DNA 1 kb	Fermentas
DNA ladder	GeneRuler DNA 100 bp	Fermentas
dNTPs	Deoxynucleotides, 10 mM	Thermo Scientific
EDTA	Ethylenediaminetetraacetic acid	Merck
EtOH	Ethanol abs.	Roth
Formamide	HiDi Formamide	Applied Biosystems
Isopropyl alcohol	2-Propanol	Applichem
Loading buffer	DNA gel loading dye 6x	Thermo Scientific
NaOH	Sodium hydroxide	Applichem
Nucleic acid dye	GelRed (10.000x)	Sigma-Aldrich
Primers	Oligonucleotides	IDT/Sigma
Sephadex	Sephadex G-50 Superfine	GE Healthcare
SDS	Sodium dodecylsulfate 10%	AppliChem
TBE	Tris/Borate/EDTA 10x	Invitrogen
TracrRNA	Alt-R® CRISPR-Cas9 tracrRNA	IDT
Tris	Tris(hydroxymethyl)-aminomethan	Roth
Water	HPLC grade	Sigma Aldrich

4.1.2 Solutions used for the analysis of nucleic acids

Genotyping

50x Base solution (50 ml)

Chemical	Amount
5N NaOH	12.5 ml
0.5 M EDTA	1 ml
H_2O	36.5 ml

pH 12

50x Neutralization buffer (50 ml)

Chemical	Amount
Tris-HCl	15.75 g
H_2O	50 ml

pH 5

Gel electrophoresis

1x TBE buffer (1 L)

Chemical	Amount
10x TBE buffer	100 ml
dH2O	900 ml

Agarose gel (1.5%)

Chemical	Amount
Agarose	1.5 g
1x TBE buffer	100 ml
GelRed™	8 µl

4.1.3 Kits

Kit	Use	Company
Big Dye Terminator V1.1 Cycle Sequencing kit	Sanger sequencing	Applied Biosystems
Power SYBR® Green RNA-to-C_T™ 2-Step kit	qPCR	AB Applied Biosystems
QIAquick Gel extraction kit	DNA gel extraction	Qiagen
QIAshredder spin columns	Tissue and cell shredding	Qiagen
QIAGEN Plasmid Mini Kit	Plasmid purification	Qiagen
RevertAid First Strand cDNA synthesis Kit	Reverse transcription	Thermo Scientific
RNeasy Mini Kit	RNA purification	Qiagen

4.1.4 Oligonucleotides

The primers were designed for the desired purpose and ordered from the IDT company (Leuven, Belgium) or from Sigma-Aldrich. They were delivered in a desalted state and were then dissolved in HPLC water to a concentration of 100 pmol/µl as a stock solution. These were diluted to 10 pmol/µl to working dilutions.

4.1.4.1 PCR primers

Primer sequences are indicated in 5’ to 3’ orientation.

Primer pair	Forward	Reverse
***MAGED2*_Exon11_mut_cDNA**	CTGGGGCCTGTGCTCTTACTATGAGACCA	TAGTAAGAGCACAGGCCCCAGAAGAACTC
***Maged2*_genotyping_R446C**	GGCACCATGTAACAAGGAGCAC	CACCCACCAACTTTTCTGAGGC
Mice_sex_determination_SX	GATGATTTGAGTGGAAATGTGAGGTA	CTTATGTTTATAGGCATGCACCATGTA

4.1.4.2 Sequencing primers

Primer sequences are indicated in 5’ to 3’ orientation.

Primer pair	Sequence
***MAGED2*_Seq1**	CACTGAGACCAAAAAGGTCA
***MAGED2*_Seq2**	AGCCTTGCTCTCCCTGAGAT
***MAGED2*_Seq3**	TGGGAACGACTAAGGACT
CMV_fwd	CGCAAATGGGCGGTAGGCGTG
BGH_rev	GGCACCATGTAACAAGGAGCAC

4.1.4.3 qPCR primers

Primer sequences are indicated in 5’ to 3’ orientation.

Primer pair	Forward	Reverse
Maged2	GAGAGGGACTGAGAGGAGCA	CCACTCTCGCTTGTGTCAGA
Actb	AAGAGCTAGGAGCTGCCTGA	TACGGATGTCAACGTCACAC
mHprt1	GCTGACCTGGATTACAT	TTGGGGCTGTACTGCTTAAC
Slc12a1	TGGCGTGGTCATAGTCAGAA	GCCAATCTCTCCTGTTCCAG
Slc12a3	GCTTCTTTGGCATGTTCTCC	TCCAGAAAATGGCCATGAGT
Aqp2	CCTCCATGAGATTACCCC	GGAAGAGCTCCACAGTCACC
Actb	CTGGCTCCTAGCACCATGAA	AGCTCAGTAACAGTCCGCCTA
Avpr2	GTGTCTACCACGTCTGTGCC	CAAGGCCACAGCCACAAAAA
Scnn1b	GCAGGCCACCAACATCTTCT	TAGGCGTGAAGTTCCGATGAC

4.1.4.4 siRNA

Endogenous *MAGED2* expression was knocked down in HEK293T cells with a mix of four MAGED2 siRNAs (Dharmacon):

- GGACGAAGCUGAUAUCGGA
- GCUAAAGACCAGACGAAGA
- AGGCGAUGGAAGCGGAUUU
- GAAAAGGACAGUAGCUCGA

Scrambled siRNA was used as a control (Dharmacon):

- UGGUUUACAUGUCGACUAA

4.1.4.5 Hairpin RNA constructs for *Maged2* knockdown in mpkCCD cells

The hairpin sequences targeting MAGED2 are as follows:

- mMageD2_shERWOOD-no1 (hp1):
  GCTGTTGACAGTGAGCGAAACTGGGACGAAGCTGATATATAGTGAAGCCACAGATGT
  ATATATCAGCTTCGTCCCAGTTGTGCCTACTGCCTCGGA

- mMageD2_shERWOOD-no2 (hp2):
  TGCTGTTGACAGTGAGCGAACCTACCACACAGCTGAGTGATAGTGAAGCCACAGATG
  TATCACTCAGCTGTGTGGTAGGTGTGCCTACTGCCTCGGA

- The control hairpin sequence targets renilla luciferase:

  TGCTGTTGACAGTGAGCGCAGGAATTATAATGCTTATTGCTGTTGACAGTGAGCGCAG
  GAATTATAATGCTTATCTATAGTGAAGCCACAGATGTATAGATAAGCATTATAATTCC
  TATGCCTACTGCCTCGGA

4.1.4.6 CRISPR/Cas9 constructs

The oligonucleotides necessary for the electroporation in mice were ordered from IDT.

Repair template: mMaged2_ssODN_R446C

TAGACTTTGATTCTTTTCTTTAAAGGTACCTGGACTATGCCAGAGTACCCAATAGCAATCCT
CCTGAGTACGAGTTCTTCTGGGGaCTAtGCTCTTACTATGAGACCAGCAAGATGAAAGTTCT
CAA

Repair template: mMaged2_ssODN_Y346

TGGAAGCTGAATTTTATGATTTTATAAGTTTTTCTTCCTATCCATAGGTATTTGGAATCCAA
TTGAAAGAAATTGACAAGAATGAtCACTTGTAgATTCTTCTCAGTACCTTAGAGCCAACTGA
TGC

crRNA:

mMaged2_sgRNA_R446C

TGGTCTCATAGTAAGAGCGT

mMaged2_sgRNA_Y346x:

TACTGAGAAGAATATACAAG

tracrRNA: IDT (1072534)

4.1.5 Enzymes

Enzyme	Product number	Company
Exonuclease I 5,000 U/ml	M0568	NEB
Fast Alkaline phosphatase 1U/µl	EF0651	Fermentas
Multiplex PCR mix	206143	Qiagen
Pfu	EP0501	Fermentas
T4 DNA Ligase 5U/µl	EL0011	Fermentas

4.1.6 Vectors

Plasmid	Use	Company
pcDNA3.1	Expression vector	Invitrogen
PiggyBac PB-CMV-GreenPuro-H1-MCS shRNA vector	shRNA expression vector	Systembio
pCMV hyPBase	Transposase vector	Systembio

4.1.7 Cell culture

4.1.7.1 Reagents for the cell culture

Chemical	Name	Company
Amphotericin	Amphotericin B	Biochrom
dDAVP	Desmopressin	Sigma-Aldrich
Dexamethason		Sigma-Aldrich
DMEM	Dulbecco's Modified Eagle	Gibco
DMEM/Ham-F12	Dulbecco′s Modified Eagle′s M./F-12 HAM	Sigma-Aldrich
DMSO	Dimethylsulfoxide	AppliChem
EGF	Embryonic Growth Factor	Sigma-Aldrich
FCS	Fetal calf serum	Biochrom
Glutamin	L-glutamine solution	Sigma-Aldrich
Insulin		Sigma-Aldrich
Lipofectamine 2000	Transfection reagent	Invitrogen
Opti-MEM	Reduced medium	Life technologies
PBS	Phosphate buffered saline	Gibco
PenStrep	Penicilin & Streptomycin	Gibco
Selenium	Sodium Selenite	Sigma-Aldrich
T3	3,3',5-Triiodo-L- Thyronine	Sigma-Aldrich
Transferrin	apo-Transferrin bovine	Sigma-Aldrich
Trypsin	Trypsin-EDTA solution (1x)	Gibco

4.1.7.2 Cells

Cell-line	Description	Company
HEK293T	Human embryonic kidney 293 cells	Invitrogen
Cos-7	CV-1 in Origin, carrying SV40	Sigma-Aldrich
mpkCCD	Murine principal kidney cortical collecting duct cell line	A gift from Markus Rinschen (University of Aarhus)

4.1.7.3 Culture-medium for HEK293T and Cos-7 cells

Chemical	Amount
Dulbecco's Modified Eagle Medium (1x)	500 ml
FCS	50 ml
PenStrep 100x	5 ml
Amphotericin B (250 µg/ml)	1.4 ml

4.1.7.4 Culture medium for mpkCCD cells

Chemical	Amount
Dulbecco's Modified Eagle's Medium/F-12 HAM	500 ml
Insulin (10 mg/ml)	250 µl
Dexamethason (400 µg/ml)	25 µl
T3 (66,6 µg/ml)	5 µl
EGF (100 µg/ml)	50 µl
Selenium (50 µg/ml)	100 µl
Transferrin (5 mg/ml)	500 µl
FCS	10 ml
Glutamine (200 mM)	5 ml

4.1.8 Bacteria experiments

4.1.8.1 Reagents for bacteria experiments

Reagent	Product Number	Company
Agar-Agar Kobel	1283320	Roth
TOP 10 E.coli	C404010	Fermentas
NaCl	3957.1	Roth
Glycerol	3783.1	Roth
Trypton	8952.2	Roth
Yeast	2363.2	Roth

4.1.8.2 Solutions for bacteria experiments

Freezing medium

Chemical	Amount
Glycerol	800 µl
Bacteria	200 µl

LB medium (1 l)

Chemical	Amount
Trypton	10 g
Yeast extract	5 g
NaCl	5 g
H_2O	1 l

LB-Agar (500 ml)

Chemical	Amount
LB medium	500 ml
Agar	7.5 g

LB medium and agar were autoclaved and stored at 4°C.

4.1.9 Protein experiments

4.1.9.1 Reagents for protein experiments

Chemical	Name	Company
ß-Mercaptoethanol		AppliChem
APS	ammoniumpersulfate	Applichem
ACN	Acetonitrile	ThermoFisher
BSA	Bovine Serum Albumin Fraction V	Roth
CAA	2-Chloroacetamide	ThermoFisher
$CaCl_2$	Calcium chloride	ThermoFisher
Chemiluminescence reagent	Clarity Western ECL Substrate	Bio-Rad
DTT	Dithiothreitol	ThermoFisher
EDTA	Ethylenediaminetetraacetic acid	Merck
Electrophoresis	Tris / Glycine / SDS (10x)	Bio-Rad
Eosin		Roth
EtOH	Ethanol	Roth
FA	Formic acid	ThermoFisher
Formalin	Formalin solution 10%	Sigma Aldrich
Goat serum		Cell Signalling
Hemalum	Mayer´s Hemalum solution	Roth
Haematoxylin		Roth
HEPES	4-(2-hydroxyethyl)-1-piperazineethanesulfonic acid	Applichem
IAA	Indole-3-acetic acid	ThermoFisher
Isopropanol		Applichem
MeOH	Methanol	Roth
Mounting medium	Eukitt	Merck
Mounting medium	ProLong™ Diamond	ThermoFisher
Milk powder	milk powder, blotting grade	AppliChem
NaCl	Sodium Chloride	Roth
NaF	Sodium fluoride	AppliChem
Na_2MoO_4	Sodium molybdate	Applichem
Na_3VO_4	Sodium orthovanadate	AppliChem
NP40	nonyl phenoxypolyethoxylethanol	NEB

OCT	Optimal cutting temperature compound	Tissue-Tek
PA	Periodic acid 1%	Roth
PBS	Phosphate Buffered Saline	Gibco
PMSF	Phenylmethylsulfonylfluorid	AppliChem
PFA	Paraformaldehyde	AppliChem
Polyacrylamide gels	Mini-PROTEAN® TGX Stain-Free™	Bio-Rad
Protease inhibitor	protease inhibitor cocktail	Sigma-Aldrich
Protein ladder	Precision Plus Protein™ Unstained	Bio-Rad
Sample buffer	4x Laemmli Sample Buffer	Bio-Rad
Schiff´s reagent		Roth
SDS	sodium dodecyl sulfate	AppliChem
SP3 beads	solid-phase-enhanced sample-preparation	ThermoFisher
Sub-X	Clearing medium	Leica
TEMED	Tetramethylethylenediamine	AppliChem
Tris	Tris(hydroxymethyl)aminomethane	Roth
Triton X-100	Octoxynol-9	Applichem
Trypsin	MS-Grade	Sigma Aldrich
Tween 20®	Polyoxyethylene 20 Sorbitane mono-Laurate	Roth
Water	HPLC grade	Sigma Aldrich
Xylene	histology grade	Sigma-Aldrich

4.1.9.2Kits

Kit	Use	Product number	Company
BCA Protein Assay Kit	Measuring of protein concentration	23225	Pierce
TGX Stain-Free™ FastCast™ Acrylamide Kit, 10%	Casting of Stain-free gels for Western Blot analysis	#1610183	Bio-Rad

4.1.9.3 Solutions for protein experiments

TGX Stain-Free™ FastCast™ acrylamide resolver solution

Chemical	Amount
Resolver A	3 ml
Resolver B	3 ml
10% APS	30 µl
TEMED	3 µl

TGX Stain-Free™ FastCast™ acrylamide stacker solution

Chemical	Amount
Stacker A	1 ml
Stacker B	1 ml
10% APS	10 µl
TEMED	2 µl

10x TBS buffer (1 L)

Chemical	Amount
Tris	24.2 g
NaCl	87.6 g
dH_2O	1 L
Amphotericin B (250 µg/ml)	1.4 ml

pH 7.4

1x TBS with 0.1% Tween (TBS-T) buffer (1 L)

Chemical	Amount
10x TBS buffer	100 ml
Tween 20	1 ml
dH_2O	1 L

Western Blot blocking buffer (50 ml):

Chemical	Amount
1x TBS with 0.1% Tween	50 ml
Milk powder	2.5 g

Western Blot blocking buffer phospho-proteins (50 ml):

Chemical	Amount
1x TBS with 0.1% Tween	50 ml
BSA	2.5 g

Paraffin section blocking buffer (1 ml):

Chemical	Amount
PBS	1 ml
BSA 1%	0.01 g
Goat serum 3%	30 µl

Protein lysis buffer (10 ml)

Chemical	Amount
Tris	200 µl
NaCl 1 M	1.5 ml
EDTA 10 mM	1 ml
NP-40 (10%)	1 ml
SDS (10%)	250 µl
Protease inhibitor	10 µl
dH_2O	Add to 10 ml

10x Citrate (100 mM) AR (antigen retrieval) buffer (1 l):

Chemical	Amount
Citric acid	0.265 g
Sodium citrate	2.57 g
dH_2O	1 l

pH 6.0

1% Triton X-100 (50 ml)

Chemical	Amount
Triton X-100	0.5 ml
PBS	49.5 ml

Paraformaldehyde solution (50 ml)

Chemical	Amount
PFA	2 g
PBS	50 ml

4.1.9.4 Antibodies

Primary antibodies

Antigen	Number	Company	Dilution	Host
AQP2	AQP-002	Alomone Labs	WB: 1:2,000 IF: 1:200	Rabbit
β-Actin	A2228	Sigma Aldrich	WB: 1:5,000	Mouse
CREB1	sc-377154	Santa Cruz	WB: 1:1,000	Rabbit
FLAG M2 tag	F3165	Sigma-Aldrich	IF: 1:1,000	Mouse
MAGED2		Gift from Olivier de Backer (Université de Namur)	WB: 1:1,000	Rabbit
NCC	SAB5200104	Sigma-Aldrich	IF: 1:200	Rabbit
NKCC2	18970-1-AP	Proteintech	IF: 1:200	Rabbit
pCREB (Ser133)	87G3	Cell Signalling	WB: 1:1,000	Rabbit

p-p44/42 MAPK (Thr202, Tyr204/Thr185,	D13.14.4E	Cell Signalling	WB: 1:1,000	Rabbit
p44/42 MAPK	9102	Cell Signalling	WB: 1:1,000	Rabbit
pAQP2 (Ser256)	1697	Phosphosolutions	WB: 1:1,000	Rabbit
ROMK		A gift from Markus Rinschen (Aarhus Universitet)	IF: 1:200	Rabbit
ZO-1		A gift from Markus Rinschen (Aarhus Universitet)	IF: 1:500	Mouse

Secondary antibodies

Antigen	Number	Company	Dilution	Host
anti-mouse IgG-HRP	Sc-2005	Santa Cruz	WB: 1:5,000	Goat
anti-rabbit IgG-HRP	Sc-2004	Santa Cruz	WB: 1:5,000	Goat
anti-Mouse IgG Alexa Fluor 488 conjugated	A28175	Thermo Fisher	IF: 1:1,000	Goat
anti-rabbit IgG CF™ 568 conjugated	SAB4600084	Sigma-Aldrich	IF: 1:5,000	Goat

4.1.10 Equipment

Equipment	Name	Company
Agarose gel electrophoresis chamber	MGU-402T, MGU-602T C.B.S.	C.B.S. Scientific
Analytical column	Aurora Ultimate 25 cm x 75 µm	IonOpticks
Bacteria incubator	WTC	BINDER
Cell counting chamber	Neubauer chamber	Assistant
Cell incubator	Hera cell 150	Heraeus
Centrifuge	Centrifuge 5415D	Eppendorf
Cover slips	Hemacytometer cover slips	Assistant
Cryostat	CM3050 S	Leica
Freezer (-26°C)	Premium	Liebherr
Heating shaking block	Thermomixer compact	Eppendorf
HPLC columns	Acclaim™ PepMap™ 100 C18	ThermoFisher

Imaging systems	Chemidoc XRS	Bio-Rad
Liquid chromatogryphy	UltiMate3000 RSLC	ThermoFisher
Mass spectrometer	Quadrupole-Orbitrap LC-MS	ThermoFisher
Mass spectrometer	Orbitrap Exploris™ 480	ThermoFisher
Microscope	Axio Imager M2	Carl-Zeiss
Microscope slides	Superfrost™Plus	Sigma Aldrich
Microwave	Micro-chef FM 2915Q	Moulinex
Microtome	RM2	Leica
Paraffin embedding	EG1150 H	Leica
Permeable membrane	0.4 µm pore size, 24 mm	Corning
pH meter	inoLab pH level 1	WTW
Photometer	Biophotometer	Eppendorf
Photometer	Nanodrop ND-1000	Peqlab
Pipettes	Research	Eppendorf
Power supply	EC250-90	Thermo Electro Corporation
SDS gel electrophoresis chamber	Mini-PROTEAN Tetra cell	Bio-Rad
Sequencer	3500 Genetic Analyzer	Applied Biosystems
Shaker	DRS-12	ELMI
Thermocycler	Tetrad2	Bio-Rad
Thermocycler	C1000 Touch Thermal Cycler	Bio-Rad
Tissue culture hood	Hera Safe KS 12	Kendro
Tissue processor	ASP300	Leica
Vortexer	M10	VWR
Western blot membrane		Bio-Rad
Western blot module	Trans-Blot Turbo	Bio-Rad

4.1.11 Computer programs

Program	Company
Finch TV	Geospiza
Graphpad	Prism
Icelogo	Compomics
Illustrator CC	Adobe
Imagelab	Bio-Rad
Lasergene 8 EditSeq	DNASTAR
Mausoleum	Dr. Hanns-Eugen Stöffler
Maxquant	Maxquant

Perseus	Maxquant
PHONEMEs	Saezlab
Photoshop CC	Adobe
RStudio	Posit PBC
SeqBuilder	DNASTAR
SeqMan	DNASTAR
Spectronaut	BIOGNOSYS
Word	Microsoft Office
ZEN 3.3 blue edition	Zeiss

4.1.12 Databases

Database	Web adress
BLAST	http://blast.ncbi.nlm.nih.gov/
ClustalW	http://www.ebi.ac.uk/Tools/clustalw/index.html
ENSEMBLE Genome Browser	http://www.ensembl.org/index.html
ExPASy translate tool	http://web.expasy.org/translate/
GnomAD	https://gnomad.broadinstitute.org/
MutationTaster	http://www.mutationtaster.org/
NCBI	http://www.ncbi.nlm.nih.gov/
PolyPhen-2	http://genetics.bwh.harvard.edu/pph2/
PubMed	http://www.pubmed.gov

4.2 Methods

4.2.1 Nucleic acid methods

4.2.1.1 PCR reactions

The standard PCR reaction was used to amplify exon 11 of *Maged2* from mouse ear-tags for genotyping. A negative control without DNA was included. PCR products were analyzed by agarose gel electrophoresis. The PCR-products were subsequently sequenced by Sanger sequencing.

Standard PCR reaction

Component	Amount
DNA (20 ng/µl)	2 µl
Forward primer (10 pmol/µl)	1 µl
Reverse primer (10 pmol/µl)	1 µl
Qiagen Multiplex PCR reaction mix	5 µl
Add dH_2O to	20 µl

Standard PCR program

Step	Temperature	Duration	Cycles
Initial denaturation	94°C	12 min	1
Denaturation	95°C	30 sec	25 cycles
Annealing	X°C	30 sec	
Elongation	72°C	1 min	
Final elongation	72°C	10 min	1

Activation of the HotStarTaq DNA Polymerase of the Qiagen Multiplex PCR reaction mix is initiated with a 12-minute incubation step at 95°C. In the standard PCR program, the annealing temperature was 58°- 62°C depending on the primer sequence.

4.2.1.2 Sequencing of DNA

To prepare the final sequencing PCR, the nucleic acids were purified from remaining dNTPs and primers by treatment with exonuclease I and Fast Alkaline Phosphatase (FastAP). The reaction took place at 37°C for 15 minutes followed by an inactivation step at 85°C for 15 minutes.

ExoI/FastAP treatment

Component	Amount
Exonuclease I	0.08 µl
FastAP	0.8 µl
PCR template	8 µl
Add dH_2O to	10 µl

The purified DNA fragments were then sequenced by the chain-termination Sanger-method (Sanger et al., 1977).

PCR reaction

Component	Amount
Purified PCR product	0.5 µl
Sequencing primer	0.5 µl
BigDye® V1.1 Reaction Mix	0.5 µl
5x Sequencing Buffer	1.5 µl
Add dH_2O to	10 µl

PCR program

Step	Temperature	Duration	Cycles
Initial denaturation	95°C	30 sec	1
Denaturation	95°C	10 sec	40 cycles
Annealing	55°C	5 sec	
Elongation	60°C	4 min	

Sanger sequencing was carried out on a 3500 Genetic Analyzer (Applied Biosystems). Data analysis was performed using FinchTV and NCBI Blast.

4.2.1.3 Generation of MAGED2^{R446C} cDNA constructs

The site-directed mutagenesis PCR of the wildtype MAGED2 cDNA with overlapping primers bearing the c.1336C>T variant was carried out with the proofreading Pfu polymerase to prevent base errors in amplification. Pfu polymerase is able to prolong DNA strains 200-400 bases per minute.

PCR reaction for mutation of *MAGED2* wildtype cDNA constructs

Component	Amount
DNA (20 ng/µl)	2 µl
Forward primer (10 pmol/µl)	1 µl
Reverse primer (10 pmol/µl)	1 µl
dNTPs (1.25 mM)	8 µl
Pfu polymerase buffer 10x with $MgSO_4$	5 µl
Pfu polymerase	1 µl
Add dH2O to	50 µl

PCR program

Step	Temperature	Duration	Cycles
Initial denaturation	94°C	3 min	1
Denaturation	94°C	30 sec	30 cycles
Annealing	X°C	30 sec	
Elongation	72°C	X min	
Final elongation	72°C	10 min	1

The PCR products were then loaded onto an agarose gel with GelRed to visualize DNA under UV-light. The bands were then cut out and purified with the QIAquick Gel extraction kit from Qiagen according to the manual. The purified DNA fragments were

then transformed into One Shot™ TOP10 chemically competent *E. coli*. For this purpose, 2 µl of the DNA fragments were mixed with 50 µl of the bacteria suspension. The mixture was then incubated on ice for 30 minutes. The mixture was then incubated at 42°C in a water bath for 42 seconds and then for five minutes on ice. Subsequently, 250 µl of LB-medium were added to the mixture and it was incubated for one hour while shaking. The bacteria were then plated on agar plates containing ampicillin and incubated at 37°C overnight. Colonies were picked with yellow pipette tips and given into five ml of LB medium containing ampicillin and incubated at 37°C overnight while shaking. Plasmids were then recovered from overnight cultures with the NucleoBond Mini Kit from Machery-Nagel according to the manual. Genotyping was performed with the standard PCR method with subsequent Sanger sequencing described in 4.2.1.1 and 4.2.1.2. Bacterial cultures bearing the plasmids with the c.1336C>T mutation were then given in 200 ml of LB-medium with ampicillin and incubated at 37°C overnight while shaking. Plasmids were then recovered from overnight cultures with the NucleoBond Xtra Midi kit from Machery-Nagel according to the manual.

4.2.1.4 qPCR analyses

Total RNA was isolated from long-term treated mpkCCD cells and from mice kidneys by using the RNeasy Mini Kit from Qiagen according to the manual. The RNA was then used as template for quantitative PCR (qPCR) analysis with the Power SYBR Green RNA-to-CT 1-Step Kit to analyse changes of the expression. From each sample three technical replicates were analysed. The quantification was performed by using the ΔΔCt method with a normalization of the resulting cycle threshold (Ct) values on the basis of actin mRNA. Fold changes were indicated as changes of mRNA expression levels in relation to the vehicle treated control or between mice kidneys from different embryonical developmental stages.

RT-qPCR program

Step	Temperature	Duration	Cycles
Reverse Transcription	48°C	30 min	1
Termination	95°C	10 min	1
Denaturation	95°C	15 sec	
Annealing and elongation	60°C	4 min	40
Melting	95°C	15 sec	1
curve	60°C	1 min	1
stage	60°C - 95°C in 0.3°C steps	15 sec	1

4.2.1.5 shRNA and generation of stable cell lines

For the generation of a mpkCCD cell-line with stable *Maged2* depletion, short hairpin RNA (shRNA) was utilized. Efficient shRNA sequences were predicted with the shERWOOD algorithm (http://sherwood.cshl.edu:8080/sherwood) (Knott et al., 2014). The DNA encoding a sense-loop-antisense sequence to the gene of interest were amplified by PCR, cloned into a PiggyBac PB-CMV-GreenPuro-H1-MCS shRNA Expression vector (Systembio, Cat. No. PBSI50A-1) and checked by Sanger sequencing. The plasmids were then co-transfected in mpkCCD cells together with the PiggyBac Transposase vector (pCMV hyPbase). The expressed transposase perceives the transposon-specific inverted terminal repeat sequences (ITRs) flanking the transposable sequence in the shRNA expression vector, excises it and integrates it into TTAA chromosomal sites (Zhao et al., 2016). After 48 hours of transfection positive cells were selected with 2 µg/ml puromycin. Under control of the H1 promoter shRNA is then expressed by the endogenous RNA polymerase II and III and silences target gene expression in a RNAi-dependent manner (Moore et al., 2010). Knockdown efficiency was checked by mMageD2 qPCR using mActb and mHprt1 as housekeeping genes as well as Western blot analysis.

4.2.2 Protein methods

4.2.2.1 Immunoblotting

Murine kidney tissue, HEK293T and mpkCCD cells grown on permeable filters were lysed with a buffer containing 0.25% or 4% SDS, respectively. Subsequently, the protein lysates were mechanically shredded by use of Qiagen shredder columns and denaturated by incubation at 96°C for 10 minutes in 4x Laemmli sample buffer from Bio-Rad containing 10% mercaptoethanol. Total protein concentrations were measured with the BCA Protein Assay Kit according to the manual and 20 µg of the protein samples were then separated on a 12% SDS-PAGE gel using the Mini-PROTEAN Tetra cell system from Bio-Rad. Transfer of the proteins from the gel to a nitrocellulose membrane occurred with the Trans-Blot Turbo Transfer system from Bio-Rad. The blots were then blocked with 5% BSA or milk in Tris-buffered saline with Tween-20 (TBST) for one hour at room-temperature. After the blocking the membranes were incubated with the first antibody in blocking buffer at 4°C overnight. After three washing steps with TBST, treatment with the peroxidase-conjugated secondary antibody followed which occurred in TBST for 45 minutes at room-temperature. The peroxidase reaction was induced by using the Clarity Western ECL Substrate and the blots were then developed in the chemidoc XRS from Bio-Rad.
Densitometric quantification was determined with Image Lab from Bio-Rad. Statistical analysis was performed with Excel from Microsoft and Prism 7.03 from GraphPad using a Dunnetts test with Tukeys post-test or t-test as indicated in the figure legends.

4.2.2.2 Proteomic and phosphoproteomic analyses of HEK293T and mpkCCD cells

Sample preparation for proteomics and phosphoproteomics was performed as previously described (Rinschen et al., 2014; Rinschen et al., 2010). HEK293T or mpkCCD cells were lysed in a buffer containing 8 M urea, 50mM ammonium bicarbonate and a protease inhibitor as well as a phosphatase inhibitor cocktail. Proteins were then reduced with 10 mM DTT for 1h at room temperature and alkylated using 40 mM Iodoacetamide for 1h in the dark. Then, urea was diluted to less than 2

M, trypsin was added 1:100 to the mix and proteins were digested for 16 hours on a shaker. After desalting, 800 µg of digested peptides for the phosphoproteome were subjected to phosphopeptide enrichment using IMAC Fe-NTA columns. Eluted peptides were cleaned up with stage tips (Rappsilber et al., 2003). Peptides were then separated using a reverse phase separation with a nano liquid chromatography (nLC). For this purpose, a binary buffer system with buffer A containing 0.1% formic acid (FA) and buffer B containing 80% Acetonitrile (ACN) with 0.1% FA was used. The flow rate was 250 nl/min. The peptide gradient was run for 5 min at 4% buffer B, reaching 6% buffer B at 10 min, followed by a linear gradient to 23% B over 115 min, followed by a linear gradient to 54% buffer B over 7 min, at 138 min switched to 90% B and finished with a column equilibration step of 7 minutes at 5% B. Subsequent analysis was conducted by a Q Exactive plus mass spectrometer. Operation of the machine was performed in positive ion mode. One survey scan (resolution = 70000, m/z 300–1750) was followed by MS2 scans (resolution = 17500, m/z 200–2000). Dynamic exclusion was enabled (20 s). AGC target was 3e6 for MS1 scans, and 5e5 for MS2 scans. (Bartram et al., 2016). One technical run per sample was performed. Overall, 5 replicates were performed for HEK293T cells and 3 replicates for mpkCCD cells.
Raw file annotation was processed with MaxQuant 1.5.1.3 (Cox & Mann, 2008) including the Label Free Quantification (LFQ) algorithm. Subsequent analysis, visualization and normalization was performed using Perseus 1.5.5.3 (Tyanova et al., 2016). Data were log2 transformed and plotted against each other in both cell lines. An analysis was then performed similar to significance in microarrays by Tusher et al. to determine significantly changed proteins (Tusher et al., 2001). Phosphorylation motif analyses of up- or down-regulated phosphopeptides were created using icelogo (Colaert et al., 2009). GO terms were annotated using the Perseus annotation package. The raw data of the study are available as PRIDE/ProteomExchange ID PXD005801, PXD008062 and PXD008059 (Vizcaino et al., 2016; Vizcaino et al., 2014).

4.2.2.3 Phosphorylation network analysis

Based on the effect size data, the differential phosphorylation (dDAVP vs. control) was computed by fitting a linear model for each site for both conditions. The corresponding t- and p-values were obtained by using the empirical Bayes method with R's 'limma'

package v3.34.9 (Ritchie et al., 2015). Phosphorylation network analysis was performed in cooperation with Julio Saez-Rodriguez from the University of Heidelberg with the PHONEMeS tool using the obtained log2 fold-changes (FC) from the *MAGED2* knockdown and control cell lines against a kinase-substrate network obtained from OmniPath (November 2017) (Terfve et al., 2015; Turei et al., 2016). In order to study the downstream phosphorylation signalling of V2R upon stimulation, protein kinase A (PKA) was regarded as the most direct effector kinase (GPCR -> AC -> cAMP -> PKA) and source of the perturbation for the analysis. The effect size of a given phosphorylation site was considered significant if its value was at least 1.5 times higher or lower than the median FC and p-value below 0.2. The resulting networks were plotted using Cytoscape v3.5.1. The scripts for the analysis can be found in the following repository: https://github.com/saezlab/MAGED2_phospho.

4.2.2.4 Proteomic analysis of mouse kidneys

Kidney samples from P0 wildtype or Maged2$^{R446C/Y}$ mice were lysed using 4% SDS, 0.1 M HEPES and 2.5 mM EDTA with beads. Protease and phosphatase inhibitor cocktail (1x, Pierce) had been previously added in the lysis buffer. Samples were then boiled at 95°C for 5 minutes and after centrifugation at 500 g for 5 minutes the supernatant was taken which were quantified via a BCA protein determination assay. Proteins were then reduced using 10 mM DTT at 37°C for 30 minutes and alkylated using 50 mM Iodoacetamide for 30 minutes at room temperature. The reaction was then quenched by addition of final 50 mM DTT for 20 minutes at room temperature. 100 µg were used for further processing, the rest was stored at -20°C. 1 µl of SP3 beads were added per 20 µg of protein and mixed well. Pure HPLC ethanol was then added to achieve a final EtOH concentration of 80% and incubated at room temperature for 18 minutes without shaking. The tubes were then placed in a magnetic rack and the samples were washed twice with 400 µl of 90% EtOH. After the last washing step, the beads were put in the hood for evaporation of remaining liquid. The beads were then resuspended in the digestion buffer (50 mM HEPES pH 7.5, 5 mM $CaCl_2$ and trypsin 1:100). After a short sonification the samples were incubated in a shake incubator at 37°C overnight. The cut peptides were then separated by the beads in the magnetic rack and transferred to a new tube, where they were acidified with 25%

formic acid to achieve a pH < 3 checked with the help of pH strips. The peptides were then purified by C_{18}-DL-StageTips. The C_{18} membrane had to be activated first by adding of 100 µl 100% methanol and centrifugation at 1,000 rpm for 3 minutes. The membrane was then washed twice with 100 µl of H_20 and 0.1% formic acid. After that, the samples were loaded to the columns and washed with 100 µl of H_20 and 0.1% formic acid. The peptides were then eluted with 100 µl of 50% acetonitrile and 0.1% formic acid in a new tube. The eluted samples were then evaporated in the SpeedVac vacuum concentrator at 45°C to dryness for 30 minutes. The dried samples were then resuspended in 30 µl of H_20 and 0.1% formic acid and the concentration was measured with the NanoDrop A_{280} assay.

1 µg of the peptides were then analyzed on an UltiMate3000 RSLC system (Thermo Fisher Scientific) coupled to an Exploris 480 mass spectrometer including the FAIMS pro interface (Thermo Fisher Scientific). A two-column set-up was implemented with a trap column (Acclaim™ PepMap™ 100 C18, 3 µm particle size, 2 cm x 75 µm, ThermoFisher Scientific) at a flowrate of 5 µl/min and an analytical column (Aurora Ultimate 25 cm x 75 µm, IonOpticks) at a flowrate of 400 nl/min using a 120 min gradient with mobile phase A as 0.1% formic acid in LC-MS-grade water and mobile phase B as 0.1% formic acid in LC-MS-grade acetonitrile. The peptide gradient was run for 5 min at 2% B, reaching 8% B at 10 min, followed by a linear gradient to 25% B over 80 min, followed by a linear gradient to 35% B over 10 min, at 101 min switched to 90% B and finished with a column equilibration step from 110 -120 min at 2% B. All MS measurements were performed in data-independent acquisition (DIA) in positive polarity with FAIMS CV voltages of -45 and -60. MS1 spectra were recorded in profile mode at 120 K resolution within a scan range of 380-1500 m/z, with normalized AGC target of 300%, RF lens of 40% and auto maximum injection time. MS2 spectra were recorded at 30K for 400-1000 Da with non-overlapping isolation windows of 15 Da and normalized HCD collision energy of 28%.

MS RAW files were analyzed library-free by Spectronaut v16 using directDIA. Trypsin/P was selected as digestion enzyme allowing for 2 missed cleavages. Cysteine carbamylation was set as fixed modification, methionine oxidation and protein N-terminal acetylation as variable modifications. Data was searched against a Mus musculus database. Peptide and protein identifications were accepted at 1% q value. Further analysis was performed with R in R Studio. Statical analysis was performed with the Limma R package (Ritchie et al., 2015), GO term enrichment analysis and

visualization with ClusterProfiler (T. Wu et al., 2021) and general visualization with the ggplot2 R package (Wickham, 2009).

4.2.2.5 Immunofluorescence stainings of paraffin kidney tissue

First of all, paraffinized kidney sections were deparaffinized with three stations of xylol for 30 seconds and rehydrated with absolute EtOH three times for 30 seconds, with 95% EtOH twice for 30 seconds and with 70% EtOH one time for 30 seconds

Substance	Duration
Xylol	2 x 5 min
100% EtOH	3 x 3 min
95% EtOH	2 x 2 min
70% EtOH	1 x 1 min
PBS	3 x 2.5 min

The slides were then soaked in antigen retrieval (AR) solution and heated in a microwave for 30 minutes by refilling AR solution every couple of minutes due to evaporation. The slides were then cooled on ice for 20 minutes and after that washed with PBS for 5 minutes 2 times. The sections were then marked with a PAP then. Blocking was then performed with 1% BSA and 3% goat serum in PBS. After that, the antibody was diluted in the blocking solution and added to the sections. Incubation was performed at 4°C overnight. After 3 times of washing in PBS the secondary antibody was diluted in PBS and added to the samples. Incubation was performed at room-temperature in the dark for one hour. The samples were again washed 3 times in PBS for 2.5 minutes before they were mounted with ProLong™ Diamond Antifade Mountant with DAPI.

4.2.2.6 Immunofluorescence stainings of cells

First of all, the medium of transiently transfected cells were washed with PBS for three times. The fixation of the cells was then performed with 4% paraformaldehyde in PBS for 20 minutes at room temperature. After the fixation the cells were again washed with PBS for three times. The permeabilization was carried out by 1% Triton X-100 in PBS for 10 minutes at room temperature and was followed by three washing steps with PBS. Unspecific binding was prevented by incubating the cells with 3% milk in PBS for 30 minutes. The primary antibodies against the Flag-tag and calnexin were then added to the blocking solution and cells were incubated at 4°C overnight. The cells were then washed with PBS for three times. The secondary fluorochrome-labelled antibodies were diluted in PBS and an incubation of 1 hour at room temperature in a dark environment followed. The cells were then washed with PBS for three times. The cells were the mounted with ProLong™ Diamond mounting medium.

4.2.2.7 Microscopic analysis

Fluorescence images were acquired with the Zeiss Axio imager M2 fluorescence microscope with an AxioCam MRm camera and an ApoTome system.

4.2.3 Cell culture

4.2.3.1 Maintaining of cells

HEK293T and Cos7 cells were kept in Dulbecco's modified Eagle's medium (DMEM) which contained 10% FCS in an incubator at 37°C with 5% CO_2.
Mouse collecting duct principal (mpkCCD) cells were kept in a 1:1 mixture of DMEM and Ham's F-12 Nutrient Mixture (DMEM-F12) containing 5 µg/ml insulin, 50 nM dexamethasone, 1 nM triiodothyronine, 10 ng/ml epidermal growth factor, 60 nM sodium selenite, 5 µg/ml transferrin and 2% bovine serum in an incubator at 37°C with 5% CO_2 (Bens et al., 1999).
For vasopressin treatment the cells were seeded on permeable filters (Transwell

permeable supports, 0.4 µm pore size, 24 mm diameter, Corning Costar) until grown to confluency and polarization (Figure 42). Vasopressin treatment was performed as previously published (Rinschen et al., 2010; Yu et al., 2009). Long-term treatment was conducted with 1 nm of the V2-specific agonist 1-deamino-8-D-arginine vasopressin (dDAVP) for 72 hours with daily replacement of the medium for induction of aquaporin 2 (AQP2) expression. Short-term treatments included a preceding long-term treatment of with 1 nm dDAVP over a period of 72 hours following a dDAVP deprivation of 6 hours. Subsequently the short-term treatment was performed by incubation with 1 nm dDAVP for 30 minutes in the absence of supplements and growth factors.

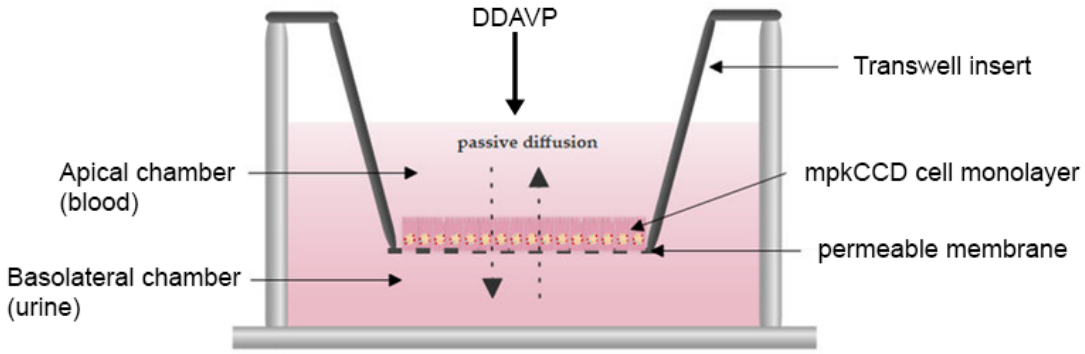

Figure 42: Culture of mpkCCD cells. *Cells were seeded on a permeable membrane. DDAVP treatment was induced by administration in the apical chamber. Modified from (Sanchez et al., 2019).*

4.2.3.2 siRNA transfection

siRNA transfection was carried out with 30 pmol of either siRNA with Lipofectamine 2000 in HEK293T cells according to the manual. The cells were then incubated at 37°C for 48 hours. Harvested cell pellets were then used for Western Blot, proteome and phospho-proteome analyses.

4.2.3.3 Transient expression of MAGED2 constructs

Cos7 cells were transfected with the FuGENE®HD transfection reagent according to the manual. For this purpose, Cos-7 cells were seeded in 6-well-plates for immunofluorescence stainings so that at the day of transfection cells reached a

confluency of approximately 80%. Transfection was performed by using 1 µg of FLAG.MAGED2.Wt and FLAG.MAGED2.R446C cDNA constructs. The cells were then incubated at 37°C under 5% CO_2 for 24 hours.

4.2.3.4 cAMP assay

Direct cAMP concentrations in short-term treated mpkCCD cells were measured with a commercially available ELISA kit (R&D Systems, KGE002B) according to the manufacturer's instructions. In brief, one confluent well of a 6 well transwell plate was diluted 1:10 and lysate (in the lysate buffer provided by the manufacturer) was used as an input for the analysis. The assay was performed exactly as indicated by the manufacturer's instructions. The data were acquired using a PerkinElmer plate reader.

4.2.4 Mouse studies

All animal procedures were performed in accordance with European (EU directive 86/609/EEC), national (TierSchG), and institutional guidelines and were approved by local governmental authorities (LANUV NRW, AZ 84–02.04.2013.A152 and AZ 2019.A460). All experiments were performed in compliance with the ARRIVE guidelines (Kilkenny et al., 2010).

4.2.4.1 Mouse husbandry

The mice were housed according to the standardized specific pathogen-free conditions in the animal facility of the University of Cologne. Mice were kept under a 12 hour light and dark cycle and had free access to food and water.

4.2.4.2 Generation of transgenic mouse lines

The mouse lines were generated in cooperation with Prof. Dr. Bernhard Schermer from the Nephrolab and Prof. Dr. Branko Zevnik from the *in vivo* Research Facility of the

CECAD. Mouse lines were generated for the human *MAGED2* missense mutation R446C and the nonsense mutation Y346X. The background of all animals used in this study was C57BL/6N.
Unfortunately, the generation of a stable mouse line for the Y346X mutation failed so that mouse experiments were conducted only with the R446C mouse line.

4.2.4.3 Electroporation

For both mouse lines crRNA, generic tracrRNA and the ssODN repair templates were ordered from IDT and resuspended in $T_{10}E_{0.1}$ buffer to a concentration of 100 µM.
Electroporation of zygotes was conducted by Dr. Lena Ebert and Dr. Simon Tröder as previously described (Troder et al., 2018). In brief, zygotes collected from the oviducts of superovulated females were washed, transferred to the electroporation mix and electroporated in a BioRad Gene Pulser XCell (30V, 3 ms pulse duration, 2 pulses, 100 ms interval). Embryos were then incubated until the two-cell stage and implanted in pseudo-pregnant foster mice. The F0-generation was then screened for the mutation and hemizygous males used for backcrossing with wildtype female breeder mice.

4.2.4.4 Genotyping of mice

For the genotyping of the transgenic mice ear tags or tail biopsies were used. Tissue was mixed with 75 µl of 1x base solution and incubated at 95°C for 30 minutes. The samples were then cooled down on ice and 75 µl of 1x neutralization buffer were added. The DNA was then used in PCR and Sanger sequencing to determine the genotype.

4.2.4.5 Sample collection

For the qPCR experiments wildtype newborn and embryonic mice were sacrificed by decapitation and pregnant mice were sacrificed by cervical dislocation after removing all embryos under deep narcosis.
For the experiments with the *Maged2*$^{R446C/Y}$ mice, heterozygous females were mated

with male wildtype breeders. At P0 male animals were used for experimental procedures while female pups were used for the further breeding.
Urine was collected from newborn mice, before they were sacrificed by decapitation. The mice were then perfused with PBS, the kidneys were harvested and either directly snap-frozen in liquid nitrogen for the subsequent proteomics experiments or fixed in 10% neutral buffered formalin for 24-48 hours for subsequent paraffin embedding.

4.2.4.6 Urinal electrolyte measurement

Urines of *Maged2*$^{WT/Y}$ and *Maged2*$^{R446C/Y}$ mice were pooled each, 1:1 diluted with distilled water and soaked into a capillary. The urine was then analysed with a ABL800 Flex radiometer.

4.2.4.7 Paraffin embedding of mouse kidneys

Kidney tissue was fixed in 10% neutral buffered formalin for 24-48 hrs before the buffer was changed to 70% EtOH. Tissue paraffin infiltration was carried out in a Leica ASP300 with the following protocol:

Substance	Duration	Temperature
Formalin	15 min	45°C
70% EtOH	30 min	45°C
Isopropanol	3 X 30 min	45°C
Isopropanol	40 min	45°C
Isopropanol	3 X 1h 15 min	45°C
Sub X	15 min	45°C
Paraffin	3 X 2h	65°C

The paraffin infiltrated tissue was then poured in paraffin blocks with the heated paraffin embedding module Leica EG1150 H.
Sectioning of paraffin blocks was performed with the fully automated rotary microtome Leica RM2. The tissue was cut in 4 µm thick sections and transferred to a water bath of 40°C so that the sections could stretch and straighten before they were transferred

on Superfrost™Plus adhesion microscope slides. The sections were then dried at 40°C in an incubator for at least 24 hours.

4.2.4.8 HE stainings of mouse kidneys

For the detection of pathological structures in *Maged2*$^{R446C/Y}$ kidneys, paraffin sections were stained with hematoxylin and eosin (HE). This procedure results in a blue staining of nuclei and a pink staining of proteins, allowing the visualization of anatomical structures (Fischer et al., 2008). Paraffinized kidney sections were deparaffinized and rehydrated as described in 4.2.2.5 to allow staining of the aqueous hematoxylin solution. After a short washing step with tap water, the tissue was stained with hematoxylin twice for 4 minutes each. Unbound hematoxylin was removed by a washing step with water for 30 seconds and a washing step with Hcl-EtOH for 30 seconds. The action of the acid alcohol was then stopped by water rinsing for 5 minutes. The tissue was then stained with eosin for three minutes and dehydrated again with the alcohol series used for hydration in reverse order. The dehydrated sections were then mounted with Eukitt mounting medium and dried for 24 hours under a fume hood.

4.2.4.9 PAS stainings of mouse kidney tissue

For a more detailed view on the kidney structure of *Maged2*$^{R446C/Y}$ mice, paraffin sections were stained with a periodic acid Schiff staining (PAS). This reaction highlights structures that are rich in glycogens like the brush border of proximal tubule cells which are lined by microvilli (Banning, 1959; Yabuki et al., 2001).
Paraffinized kidney section were deparaffinized and rehydrated as described in 4.2.2.5. After a short washing step with water the tissue was hydrolyzed with periodic acid (PA) for 10 minutes. The tissue was then washed with tap water for 10 minutes and with distilled water twice for two minutes. The tissue was then incubated with Schiff's reagent for 15 minutes. After washing steps with warm tap water for 5 minutes and distilled water for one minute, the tissue was counterstained with Mayer's hemalum for 5 minutes followed by rinsing with tap water for 10 minutes. The tissue was then dehydrated again and mounted with Eukitt mounting medium as described in 2.2.4.8.

4.2.5 Statistical analysis

Statistical analyses were performed with Graphpad Prism 9. Graphs from the experiments represent the average by mean and the error bars show the standard deviation. Statistically significant differences between two groups were determined by two-tailed t-tests. Differences between multiple groups were determined by one-way ANOVA followed by Dunnett's multiple comparison test or Tukey's test. Significance is indicated by asterisks meaning ns = not significant, *P<0.05; **P<0.01; ***P<0.001 ****P<0.0001.

5 Appendix

5.1 Tables

5.1.1 Upregulated proteins in hp mpkCCD cells after dDAVP treatment

	Gene name	-Log p-value eV_d_eV_veh	-Log p-value M_d_M_veh	Student's T-test significant
1	Aqp2	1,909441863	3,458138764	+
2	Med14	0,156896345	2,293008292	+
3	Muc4	2,92258948	3,675323509	+
4	Synpo	2,146566211	3,511395156	+
5	Pnpo	0,199416793	2,182382258	+
6	Adh1	0,650945663	2,0675769	+
7	Fcgbp	1,73455412	2,860802872	+
8	Sprr1a	2,421300471	2,415746815	+
9	Tpm1	0,917072151	2,208033596	+

Table 3: Significant differentially expressed proteins in Maged2 depleted mpkCCD cells after long-term vasopressin treatment in comparison to wildtype cells. *Gene names, -log values of the p-values of untreated and treated as well as the significance are listed.*

5.1.2 Proteomic data of upregulated proteins in kidneys of Maged2$^{R446C/Y}$ mice

	GENE name	logFC	P.Value
1	Nabp2	3,42356635	4,2148E-06
2	Gnas	0,81924198	8,1483E-06
3	Myl3	2,46193499	1,04E-05
4	Tsc22d3	2,90137056	1,8184E-05
5	Orc6	0,76952217	2,9693E-05
6	Eif4ebp2	3,19620572	5,2587E-05
7	Clk4	1,2439907	0,00011009
8	Prpf18	0,36570096	0,00012116
9	Cd9	1,00812565	0,0001243
10	Znf385b	1,16857436	0,00023905
11	Rpl35a	0,67414435	0,00023946
12	Cystm1	2,0367528	0,00029568
13	Plk1	0,58913928	0,00031282
14	Col2a1	1,3311156	0,00038326
15	Bet1	0,95725207	0,00039387
16	Man1c1	0,72655723	0,00047833

17	Cald1	0,30451121	0,00064114
18	Tpsb2	1,57486345	0,00064476
19	Sema5a	0,51088988	0,00065195
20	Lrrc15	1,07670509	0,00068354
21	Cyp1b1	1,5423412	0,00070527
22	Ifitm3	1,29959751	0,00076692
23	Zfp36l1	1,25307027	0,00077992
24	Chtf8	0,67366868	0,00085948
25	Dcbld2	0,56205762	0,0008693
26	Tmem42	0,67188117	0,00089701
27	Pacrgl	1,04106311	0,0009584
28	Krt74	2,4959496	0,00096054
29	Dbh	2,46232005	0,0009921
30	Tbc1d31	1,08306564	0,0010003
31	Msantd2	0,45545189	0,00103874
32	Fbxo42	0,38663596	0,00104869
33	Niban1	0,39506409	0,00106391
34	Dbn1	0,4740476	0,00111317
35	Tnnc2	2,93558745	0,00115466
36	Tmbim6	0,38938267	0,00131296
37	Drg1	0,34097982	0,00136319
38	Grb10	0,36086764	0,00140361
39	Ppard	0,9150716	0,00140578
40	Slc38a7	0,99950363	0,0014475
41	Parp2	0,35109027	0,00155378
42	Il23r	0,87848024	0,00158188
43	Pappa2	0,73832686	0,00164628
44	C1qtnf6	0,88056645	0,00166358
45	Mutyh	0,60654475	0,00169468
46	Hmga2	2,75785999	0,0018479
47	Pard6g	0,80255254	0,00186367
48	Reep4	0,45773778	0,00187694
49	Orc1	0,61503989	0,001891
50	Ppp3ca	0,42252433	0,00191857
51	Sptbn5	3,31792671	0,00199777
52	Dixdc1	1,06015465	0,00200157
53	Klhl14	0,28486687	0,00201506
54	MGI:1920462	0,36780761	0,00205437
55	Kiaa0754	0,72853047	0,00208424
56	Scnm1	1,52630179	0,00211701
57	B4galt7	0,51227312	0,00228916
58	Sv2a	1,26257033	0,00239783
59	Cntrob	0,62730242	0,00242715
60	Ddr2	0,64413606	0,00243571
61	Tap2	1,20844329	0,00254854
62	Cecr2	0,87912661	0,00257119
63	Phc3	0,3381243	0,00258978

64	Dctn3	0,44825691	0,00260235
65	Zcchc3	0,37269677	0,0026106
66	Eif1ad	0,92717407	0,00266322
67	Ccn1	0,95921611	0,0026753
68	Fbxo10	0,33033625	0,00273289
69	Manea	0,41646695	0,00276826
70	Ifi44	1,23898071	0,00287516
71	Uros	0,39587002	0,00293719
72	Bsg	0,74793969	0,00299616
73	Zranb3	0,62099241	0,00299952
74	Ndufs7	0,30065646	0,00304395
75	Ankrd27	0,48723576	0,00332161
76	Tmem119	0,62088032	0,00332884
77	Dnajc25	1,45714855	0,00360902
78	Birc2	0,23867452	0,00372357
79	Ccnb1	0,6079876	0,00383803
80	Slc35e1	0,42878639	0,00388334
81	Flt1	0,5179628	0,00395284
82	Bmi1	0,70584913	0,00401806
83	St7	1,94451231	0,00412141
84	Traf1	1,09547623	0,00419342
85	Zfp825	0,97676206	0,00420417
86	Dnah1	0,6590222	0,00423332
87	Dnase1l1	1,95623173	0,00425905
88	Tceal9	1,62014373	0,00439949
89	Tmem231	0,38400532	0,00441465
90	Rasal1	1,61622501	0,00441527
91	Mtmr1	0,35480862	0,00454384
92	Bnip1	0,39735164	0,00458808
93	Rtel1	0,56825709	0,00466606
94	Adarb1	0,3625778	0,00471557
95	Nudt14	0,77291564	0,00471779
96	Rpl7	0,32452217	0,00505081
97	Slc7a6	1,68673973	0,0052117
98	Syngr1	0,90152842	0,00532844
99	Wdr20	1,80426253	0,00533586
100	Atg14	0,36255697	0,00552962
101	Atl1	0,43354117	0,005534
102	Ccnl1	1,09164757	0,00562091
103	Sesn2	0,94948225	0,00568179
104	Gria4	1,01388536	0,00573652
105	Znf516	0,29224382	0,00584967
106	Rab28	0,59480803	0,00605609
107	Pld2	1,01040948	0,00611685
108	Slc16a2	0,7261873	0,00615186
109	Csnk1g2	0,42067305	0,00615649
110	Fbxo2	0,42280427	0,00622013

111	Stk11	0,37385696	0,00625659
112	Spop	0,91890495	0,00626773

Table 4: Significant upregulated proteins in P0 Maged2$^{R446C/Y}$ mice kidney in comparison to wildtype cells. *Gene names, log of the fold change and the p-values are listed.*

5.1.3 Proteomic data of downregulated proteins in kidneys of Maged2$^{R446C/Y}$ mice

	GENE	logFC	P.Value
1	Sult1c2	-0,8841938	1,8782E-05
2	Fabp7	-0,5801116	8,2466E-05
3	Hibadh	-0,4911125	9,4829E-05
4	Cp	-0,6944173	0,00012421
5	Gm2a	-0,647136	0,00014003
6	Ggt1	-0,3904165	0,00014807
7	Naa80	-2,5755011	0,00017246
8	Alb	-0,9509999	0,00017437
9	Bdh1	-0,4334738	0,00018093
10	Ttr	-0,7942864	0,00018854
11	Sord	-0,6298284	0,00019991
12	Kng1	-0,8124683	0,00021137
13	Pdzd2	-1,1209329	0,00021491
14	Dpep1	-0,7756361	0,00022981
15	Gatm	-0,7740099	0,00024392
16	Abat	-0,5507881	0,00026004
17	Maged2	-0,5920998	0,0003545
18	Acmsd	-0,5179706	0,00040461
19	Lrp2	-0,3890455	0,00041685
20	Amn	-0,3694491	0,00041741
21	Aldob	-0,4884674	0,00042473
22	Slc22a19	-0,6316895	0,00042896
23	Fetub	-1,2179254	0,00043791
24	Rbm33	-0,3892641	0,00045025
25	Nccrp1	-1,1111097	0,00045271
26	Ttc7b	-0,3118646	0,00049085
27	Prap1	-1,6157344	0,00054119
28	Gns	-0,3677919	0,0005598
29	Mccc1	-0,3703621	0,00062947
30	Cryab	-0,7530364	0,00066537
31	Gpx1	-0,3307195	0,00072606
32	Ephx2	-0,4159884	0,00074783
33	Coq9	-0,366149	0,00077268

34	Atp1b1	-0,4552182	0,00077526
35	Chil3	-1,1001595	0,00077636
36	Scly	-0,4133914	0,0008341
37	Plg	-0,8527836	0,00090366
38	Alpl	-0,6201981	0,00092925
39	Blvrb	-0,513022	0,00094078
40	Bpnt1	-0,3594805	0,00095458
41	Spp2	-1,1113152	0,00095941
42	Gstz1	-0,3800754	0,00096423
43	Acy3	-0,5889755	0,00098285
44	Papss2	-0,4179897	0,00101569
45	Lyz2	-1,1199435	0,00102384
46	Serpinc1	-0,5503831	0,00107754
47	Lgmn	-0,7964031	0,00109825
48	Ctsz	-0,5221892	0,00115283
49	Tf	-0,6365429	0,00115817
50	Hao2	-0,5804362	0,00121352
51	Gpc4	-0,4195637	0,00121565
52	Glul	-0,7437472	0,0012369
53	Uap1l1	-0,4720862	0,00125304
54	Arsb	-0,5758252	0,00127046
55	Ctsb	-0,5017926	0,00128953
56	Bahcc1	-1,2069286	0,00129853
57	Lyz1	-1,0959303	0,00131726
58	Smpdl3a	-0,4108649	0,00132857
59	Cth	-0,4460751	0,001357
60	Pah	-0,9784229	0,00136127
61	Glud1	-0,3391315	0,0013649
62	Pdzk1	-0,3681183	0,00136966
63	Acsm1	-0,9158044	0,00137785
64	Mme	-0,3918653	0,00140807
65	Ctsa	-0,6233843	0,00142973
66	Hadh	-0,3298885	0,00144012
67	Akr1a1	-0,5011445	0,0014509
68	Tuba4a	-0,3890528	0,0014554
69	Slc12a3	-0,5551845	0,0014843
70	Rilpl2	-1,3887556	0,00152529
71	Triml2	-0,4100447	0,00153819
72	Asah1	-0,3147984	0,00154096
73	Tinag	-0,4264181	0,00157626
74	Veph1	-1,0222691	0,00161624
75	Plbd1	-0,4347788	0,0016813
76	Ly86	-0,9024377	0,00169642
77	Aldh6a1	-0,3743708	0,00180589
78	Cbx3	-0,2777963	0,00183511
79	Ptp4a2	-0,7552925	0,00186448
80	Pklr	-0,5231536	0,00186592

81	Shank2	-0,5560395	0,0019205
82	Oxct1	-0,3052047	0,00193012
83	Aadat	-0,6439654	0,00196249
84	Acox1	-0,5102449	0,0019838
85	Kng2	-0,7508789	0,00200497
86	Cyp2j5	-0,537011	0,00201116
87	F12	-0,8188513	0,00202435
88	Acox2	-0,7256634	0,00214139
89	Ica	-0,5420615	0,00219982
90	Gabpb2	-0,4011471	0,00220647
91	Itga8	-0,3462203	0,00224807
92	Pc	-0,4219425	0,0022683
93	Dcxr	-0,3362248	0,00229274
94	Acp5	-0,9050178	0,00234796
95	Dpp7	-0,4974801	0,00235955
96	Ttc36	-0,531161	0,00239196
97	G6pc	-1,3803322	0,00243127
98	Ace2	-0,5625659	0,00244133
99	Ptgr1	-0,2382604	0,00247875
100	Rufy3	-0,3466574	0,00249973
101	Aldh4a1	-0,400372	0,00250734
102	Msantd4	-0,3349804	0,00251553
103	Idh3g	-0,4118635	0,00253142
104	Gss	-0,482885	0,00253824
105	Naglu	-0,3491833	0,00254061
106	Ighv1-50	-1,0656914	0,00256798
107	Scrn2	-0,3694932	0,00260354
108	Serpina3m	-0,9420065	0,00269538
109	Acsm2	-0,4682941	0,00281237
110	Col15a1	-0,4431107	0,00281925
111	Dlst	-0,2634528	0,00283919
112	Selenbp1	-0,3788116	0,00285591
113	Adhfe1	-0,4568609	0,00289316
114	Cldn2	-0,7713606	0,00289325
115	Gaa	-0,2425437	0,00295566
116	Nhlrc3	-0,3677968	0,00300695
117	Tfrc	-0,4843733	0,00303815
118	Amy1	-1,2226435	0,00308013
119	Mmut	-0,3719537	0,00310051
120	Mecp2	-0,3328462	0,00310922
121	Cst6	-1,6261723	0,00311109
122	Muc16	-1,0378966	0,00312646
123	Dctn5	-0,2641178	0,00319367
124	Fgd4	-0,3517703	0,00327797
125	Gsta4	-0,4246381	0,00327915
126	Fbp1	-0,5258567	0,00330171
127	Lrg1	-1,0973368	0,00340744

128	Agt	-1,4831695	0,00342681
129	Ctss	-0,6790871	0,00347782
130	Gsdmc3	-0,5307857	0,00348831
131	Ambp	-1,1397522	0,00349962
132	Cpb2	-0,5198235	0,00350721
133	Mdh2	-0,2642769	0,00351924
134	Mrps14	-0,3252929	0,00352461
135	Sqor	-0,3583983	0,00362425
136	Ticrr	-2,0045549	0,00369433
137	Hnrnph1	-0,3390765	0,00369439
138	Sult1d1	-0,3701417	0,00370107
139	Serpina3k	-0,9470233	0,00374305
140	Napsa	-0,6792918	0,00375318
141	Ass1	-0,6653775	0,00376382
142	Ptprd	-0,2303484	0,00376788
143	Me1	-0,4442367	0,00379969
144	Cdh16	-0,2960544	0,00385635
145	Fuca1	-0,4349122	0,00386348
146	Hacl1	-0,4730635	0,00391662
147	Slc4a4	-0,4525078	0,00394943
148	Spag7	-0,2435474	0,0039545
149	Acss3	-0,3647956	0,00412968
150	Dmgdh	-0,446698	0,00415618
151	Tmem176b	-0,9424735	0,00416468
152	Tst	-0,4419077	0,00437918
153	Coro7	-0,3178051	0,00441007
154	Rida	-0,3563686	0,00443754
155	Ptpn6	-0,2435845	0,00446363
156	Rpl5	-0,2638771	0,00447249
157	Serpina3n	-0,897636	0,0044931
158	Adamts7	-1,4751485	0,00454037
159	Cdh5	-0,4399973	0,00454545
160	Cox6b1	-0,3557021	0,00458114
161	Gstk1	-0,3540544	0,00458501
162	Cfb	-0,8683323	0,00460041
163	Btd	-0,2814623	0,0046818
164	Slc22a2	-0,5062895	0,00473334
165	Aldh1l1	-0,3918027	0,00476729
166	Slc5a8	-0,4796646	0,00487652
167	C4b	-0,5382045	0,00493244
168	Scpep1	-0,4352951	0,00500981
169	Nmrk1	-0,584629	0,0050112
170	Bpgm	-0,7769228	0,0050326
171	MGI:1918234	-0,4588468	0,00504267
172	Tmem67	-9,4559917	0,00505668
173	Gcdh	-0,3330866	0,00505897
174	Col24a1	-0,5615139	0,00509612

175	Atg3	-0,7595942	0,00518162
176	Akr1b1	-0,3072017	0,00518484
177	Uchl3	-0,2595021	0,0052254
178	Ndufb7	-0,4463242	0,00524995
179	Kynu	-0,3785366	0,00525963
180	Pura	-0,306067	0,00533999
181	Sugct	-0,4550976	0,00542511
182	Fhl2	-0,5698517	0,00554803
183	Rab11fip1	-0,2442294	0,00564071
184	Hscb	-0,486794	0,00570758
185	Rab11fip3	-0,761464	0,00571995
186	Idh1	-0,2487242	0,00588996
187	Plbd2	-0,2538775	0,00593535
188	Xkr4	-1,0628419	0,00598452
189	Arl15	-0,24951	0,00599099
190	Ganc	-0,4080277	0,00600751
191	Ehd1	-0,2520141	0,00606825
192	Iqcj-Schip1	-0,8229248	0,00608901
193	Acat2	-0,3131662	0,00618087
194	Adgrg1	-0,4090218	0,00618716
195	Msra	-0,2906359	0,0062114

Table 5: Significant downregulated proteins in P0 Maged2$^{R446C/Y}$ mice kidney in comparison to wildtype cells. *Gene names, log of the fold change and the p-values are listed.*

5.1.4 GO-enrichment analysis of biological process

5.1.4.1Upregulated clusters

ID	Description	geneID	pvalue	p.adjust
GO:0048639	positive regulation of developmental growth	Sema5a/Dbn1/Ppard/Parp2/Hmga2/Ccnb1/Rasal1	1,2873E-05	0,01527765
GO:0010389	regulation of G2/M transition of mitotic cell cycle	Nabp2/Plk1/Hmga2/Orc1/Ccnb1	2,7692E-05	0,01527765
GO:0044818	mitotic G2/M transition checkpoint	Nabp2/Plk1/Hmga2/Orc1	3,131E-05	0,01527765
GO:1901991	negative regulation of mitotic cell cycle phase transition	Nabp2/Plk1/Zfp36l1/Hmga2/Orc1/Ccnb1	3,1816E-05	0,01527765
GO:0090257	regulation of muscle system process	Myl3/Cald1/Dbn1/Tnnc2/Parp2/Ppp3ca/Flt1	3,4026E-05	0,01527765
GO:1902749	regulation of cell cycle G2/M phase transition	Nabp2/Plk1/Hmga2/Orc1/Ccnb1	4,5729E-05	0,01711023
GO:0010972	negative regulation of G2/M transition of mitotic cell cycle	Nabp2/Plk1/Hmga2/Orc1	6,7858E-05	0,0179377
GO:1902750	negative regulation of cell cycle G2/M phase transition	Nabp2/Plk1/Hmga2/Orc1	7,6875E-05	0,0179377
GO:0048638	regulation of developmental growth	Gnas/Sema5a/Dbn1/Ppard/Parp2/Hmga2/Ccnb1/Rasal1	8,7398E-05	0,0179377
GO:0060547	negative regulation of necrotic cell death	Mutyh/Ddr2/Birc2	9,0897E-05	0,0179377
GO:1901990	regulation of mitotic cell cycle phase transition	Nabp2/Plk1/Zfp36l1/Hmga2/Orc1/Ddr2/Ccnb1	0,00011532	0,0179377
GO:0001666	response to hypoxia	Zfp36l1/Tmbim6/Ppard/Birc2/Flt1/Pld2	0,00011601	0,0179377
GO:0044772	mitotic cell cycle phase transition	Nabp2/Plk1/Zfp36l1/Hmga2/Orc1/Ppp3ca/Ddr2/Ccnb1	0,0001182	0,0179377
GO:0000086	G2/M transition of mitotic cell cycle	Nabp2/Plk1/Hmga2/Orc1/Ccnb1	0,00011985	0,0179377

GO:0007093	mitotic cell cycle checkpoint signaling	Nabp2/Plk1/Hmga2/Orc1/Ccnb1	0,00011985	0,0179377
GO:0045669	positive regulation of osteoblast differentiation	Gnas/Ddr2/Ccn1/Tmem119	0,00014278	0,01887041
GO:0045927	positive regulation of growth	Sema5a/Dbn1/Ppard/Parp2/Hmga2/Ccnb1/Rasal1	0,00014289	0,01887041
GO:0006029	proteoglycan metabolic process	Col2a1/Man1c1/Ppard/B4galt7	0,00015812	0,01929226
GO:0045930	negative regulation of mitotic cell cycle	Nabp2/Plk1/Zfp36l1/Hmga2/Orc1/Ccnb1	0,00016328	0,01929226
GO:0006261	DNA-templated DNA replication	Orc6/Chtf8/Orc1/Zranb3/Rtel1	0,00017804	0,01952088
GO:0010574	regulation of vascular endothelial growth factor production	Cyp1b1/Bsg/Flt1	0,00019256	0,01952088
GO:0044839	cell cycle G2/M phase transition	Nabp2/Plk1/Hmga2/Orc1/Ccnb1	0,00019548	0,01952088
GO:0050767	regulation of neurogenesis	Sema5a/Dbn1/Hmga2/Ppp3ca/Dixdc1/Ankrd27/Flt1/Stk11	0,00020392	0,01952088
GO:0036293	response to decreased oxygen levels	Zfp36l1/Tmbim6/Ppard/Birc2/Flt1/Pld2	0,00021972	0,01952088
GO:0001558	regulation of cell growth	Sema5a/Dcbld2/Dbn1/Ppard/Parp2/Rasal1/Sesn2/Stk11	0,00022278	0,01952088
GO:1901988	negative regulation of cell cycle phase transition	Nabp2/Plk1/Zfp36l1/Hmga2/Orc1/Ccnb1	0,00023987	0,01952088
GO:0071900	regulation of protein serine/threonine kinase activity	Plk1/Hmga2/Ccnb1/Flt1/Ccnl1/Sesn2/Stk11	0,00024618	0,01952088
GO:0001958	endochondral ossification	Gnas/Col2a1/Tmem119	0,00025216	0,01952088
GO:0036075	replacement ossification	Gnas/Col2a1/Tmem119	0,00025216	0,01952088
GO:0010573	vascular endothelial growth factor production	Cyp1b1/Bsg/Flt1	0,00027439	0,02053338
GO:0006937	regulation of muscle contraction	Myl3/Cald1/Dbn1/Tnnc2/Flt1	0,00028654	0,02075078
GO:0022617	extracellular matrix disassembly	Tpsb2/Sema5a/Ddr2	0,00029784	0,02089539
GO:0048814	regulation of dendrite morphogenesis	Dbn1/Ppp3ca/Ankrd27/Stk11	0,00032685	0,02223561
GO:0045926	negative regulation of growth	Gnas/Sema5a/Dcbld2/Ppard/Sesn2/Stk11	0,00034926	0,02306144
GO:0006284	base-excision repair	Parp2/Mutyh/Hmga2	0,00037585	0,02407652
GO:0000075	cell cycle checkpoint signaling	Nabp2/Plk1/Hmga2/Orc1/Ccnb1	0,00038608	0,02407652
GO:0010939	regulation of necrotic cell death	Mutyh/Ddr2/Birc2	0,00040449	0,02454259
GO:0050772	positive regulation of axonogenesis	Sema5a/Dbn1/Dixdc1/Stk11	0,00044738	0,02643093
GO:0042326	negative regulation of phosphorylation	Plk1/Niban1/Grb10/Ddr2/Ccnb1/Adarb1/Atg14	0,00052949	0,02742489
GO:0006304	DNA modification	Gnas/Cyp1b1/Parp2/Bmi1	0,0005371	0,02742489
GO:0014909	smooth muscle cell migration	Cyp1b1/Grb10/Ppard/Ddr2	0,0005371	0,02742489
GO:1901987	regulation of cell cycle phase transition	Nabp2/Plk1/Zfp36l1/Hmga2/Orc1/Ddr2/Ccnb1	0,00053737	0,02742489
GO:0060710	chorio-allantoic fusion	Zfp36l1/Ccn1	0,0005375	0,02742489
GO:0090091	positive regulation of extracellular matrix disassembly	Sema5a/Ddr2	0,0005375	0,02742489
GO:0010948	negative regulation of cell cycle process	Nabp2/Plk1/Zfp36l1/Hmga2/Orc1/Ccnb1	0,00055195	0,02753618
GO:0042593	glucose homeostasis	Dbh/Ppard/Ppp3ca/Sesn2/Stk11/Spop	0,00057226	0,02782988
GO:0033500	carbohydrate homeostasis	Dbh/Ppard/Ppp3ca/Sesn2/Stk11/Spop	0,00058263	0,02782988
GO:0060349	bone morphogenesis	Gnas/Col2a1/Pappa2/Tmem119	0,00061755	0,02888352
GO:0050769	positive regulation of neurogenesis	Sema5a/Dbn1/Dixdc1/Ankrd27/Flt1/Stk11	0,00064796	0,029687
GO:0070482	response to oxygen levels	Zfp36l1/Tmbim6/Ppard/Birc2/Flt1/Pld2	0,00069457	0,0311862
GO:0030308	negative regulation of cell growth	Sema5a/Dcbld2/Ppard/Sesn2/Stk11	0,00077367	0,03405684
GO:0003012	muscle system process	Myl3/Cald1/Dbn1/Tnnc2/Parp2/Ppp3ca/Flt1	0,00080982	0,03496262
GO:0014812	muscle cell migration	Cyp1b1/Grb10/Ppard/Ddr2	0,00085555	0,03574514
GO:0030198	extracellular matrix organization	Col2a1/Tpsb2/Sema5a/Cyp1b1/Ddr2/Ccn1	0,00086422	0,03574514
GO:0043062	extracellular structure organization	Col2a1/Tpsb2/Sema5a/Cyp1b1/Ddr2/Ccn1	0,00087849	0,03574514
GO:0045229	external encapsulating structure organization	Col2a1/Tpsb2/Sema5a/Cyp1b1/Ddr2/Ccn1	0,00089293	0,03574514
GO:0030111	regulation of Wnt signaling pathway	Sema5a/Grb10/Hmga2/Dixdc1/Csnk1g2/Stk11	0,00090756	0,03574514
GO:0090158	endoplasmic reticulum membrane organization	Bnip1/Atl1	0,00107705	0,04168929
GO:0010563	negative regulation of phosphorus metabolic process	Plk1/Niban1/Grb10/Ddr2/Ccnb1/Adarb1/Atg14	0,00115233	0,04311617
GO:0045936	negative regulation of phosphate metabolic process	Plk1/Niban1/Grb10/Ddr2/Ccnb1/Adarb1/Atg14	0,00115233	0,04311617

GO:0030199	collagen fibril organization	Col2a1/Cyp1b1/Ddr2	0,00117847	0,04337162
GO:0010715	regulation of extracellular matrix disassembly	Sema5a/Ddr2	0,00123991	0,0441842
GO:0033690	positive regulation of osteoblast proliferation	Ccn1/Tmem119	0,00123991	0,0441842
GO:0014065	phosphatidylinositol 3-kinase signaling	Zfp36l1/Ppard/Flt1/Pld2	0,00136064	0,04772854
GO:0050773	regulation of dendrite development	Dbn1/Ppp3ca/Ankrd27/Stk11	0,00139783	0,04827877

Table 6: Gene ontology (GO) analysis of significantly upregulated clusters of biological processes.*The ID of the GO term, the description, the gene IDs as well as p-value and adjusted p-value are shown.*

5.1.4.2 Downregulated clusters

ID	Description	geneID	pvalue	p.adjust
GO:1901605	alpha-amino acid metabolic process	Hibadh/Ggt1/Dpep1/Acmsd/Scly/Gstz1/Glul/Cth/Pah/ Glud1/Aldh6a1/Aadat/Ttc36/Aldh4a1/Adhfe1/Mmut/ Mecp2/Ass1/Tst/Kynu	4,48064E-19	1,09686E-15
GO:0006520	cellular amino acid metabolic process	Hibadh/Ggt1/Dpep1/Abat/Acmsd/Scly/Gstz1/Glul/Cth/ Pah/Glud1/Aldh6a1/Aadat/Ttc36/Aldh4a1/Adhfe1/Mmut/ Mecp2/Ass1/Tst/Kynu	2,48866E-17	2,12567E-14
GO:0044282	small molecule catabolic process	Hibadh/Sord/Abat/Acmsd/Aldob/Scly/Bpnt1/Gstz1/Pah/ Glud1/Hadh/Akr1a1/Aldh6a1/Oxct1/Acox1/Acox2/Aldh4a1/ Adhfe1/Hacl1/Aldh1l1/Gcdh/Kynu/Acat2	2,60499E-17	2,12567E-14
GO:0006790	sulfur compound metabolic process	Sult1c2/Ggt1/Dpep1/Gns/Gpx1/Gstz1/Papss2/Cth/Acsm1/ Gss/Acsm2/Mmut/Gsta4/Sqor/Sult1d1/Tst/Gstk1/Btd/Gcdh/ Kynu/Hscb/Idh1	2,32056E-16	1,3048E-13
GO:0016054	organic acid catabolic process	Hibadh/Abat/Acmsd/Scly/Gstz1/Pah/Glud1/Hadh/Akr1a1/ Aldh6a1/Acox1/Acox2/Aldh4a1/Adhfe1/Hacl1/Aldh1l1 /Gcdh/Kynu/Acat2	2,96568E-16	1,3048E-13
GO:0043648	dicarboxylic acid metabolic process	Acmsd/Glul/Glud1/Aadat/Aldh4a1/Idh3g/Dlst/Adhfe1/Mdh2/ Ass1/Me1/Aldh1l1/Kynu/Idh1	3,19805E-16	1,3048E-13
GO:0046395	carboxylic acid catabolic process	Hibadh/Abat/Acmsd/Gstz1/Pah/Glud1/Hadh/Akr1a1/Aldh6a1/ Acox1/Acox2/Aldh4a1/Adhfe1/Hacl1/Aldh1l1/Gcdh/Kynu/Acat2	4,09402E-15	1,43174E-12
GO:0006575	cellular modified amino acid metabolic process	Ggt1/Dpep1/Gatm/Gpx1/Gstz1/Ctsb/Cth/Gss/Gsta4/ Ass1/Dmgdh/Gstk1/Aldh1l1/Idh1	5,42093E-11	1,65881E-08
GO:1901606	alpha-amino acid catabolic process	Hibadh/Acmsd/Scly/Gstz1/Pah/Glud1/Aldh6a1/ Aldh4a1/Adhfe1/Kynu	7,22177E-11	1,96432E-08
GO:0045861	negative regulation of proteolysis	Kng1/Dpep1/Fetub/Cryab/Gpx1/Serpinc1/Ctsz/Ctsb/Kng2/ Ttc36/Serpina3m/Agt/Ambp/Cpb2/Serpina3k/Rpl5/Serpina3n	1,60107E-10	3,91942E-08
GO:0009063	cellular amino acid catabolic process	Hibadh/Abat/Acmsd/Gstz1/Pah/Glud1/Aldh6a1/ Aldh4a1/Adhfe1/Kynu	5,28461E-10	1,17606E-07
GO:0006749	glutathione metabolic process	Ggt1/Dpep1/Gpx1/Gstz1/Cth/Gss/Gsta4/Gstk1/Idh1	2,42955E-09	4,95628E-07
GO:0046394	carboxylic acid biosynthetic process	Ggt1/Gatm/Abat/Acmsd/Glul/Cth/Pah/Acsm1/ Akr1a1/Pklr/Acsm2/Agt/Ass1/Kynu	7,07945E-09	1,29222E-06
GO:0016053	organic acid biosynthetic process	Ggt1/Gatm/Abat/Acmsd/Glul/Cth/Pah/Acsm1/ Akr1a1/Pklr/Acsm2/Agt/Ass1/Kynu	7,39016E-09	1,29222E-06
GO:0010466	negative regulation of peptidase activity	Kng1/Dpep1/Fetub/Cryab/Gpx1/Serpinc1/Ctsb/ Kng2/Serpina3m/Agt/Ambp/Serpina3k/Serpina3n	1,46707E-08	2,39425E-06
GO:0044242	cellular lipid catabolic process	Gm2a/Smpdl3a/Hadh/Asah1/Plbd1/Acox1/Acox2/ Hacl1/Gcdh/Idh1/Plbd2/Acat2	2,30007E-08	3,37817E-06
GO:0016052	carbohydrate catabolic process	Gm2a/Sord/Aldob/Chil3/Pklr/G6pc/Gaa/Fbp1/Slc4a4/Bpgm	2,34595E-08	3,37817E-06
GO:0010951	negative regulation of endopeptidase activity	Kng1/Dpep1/Fetub/Cryab/Gpx1/Serpinc1/Kng2/ Serpina3m/Agt/Serpina3k/Serpina3n	3,45715E-08	4,70172E-06
GO:0006103	2-oxoglutarate metabolic process	Aadat/Idh3g/Dlst/Adhfe1/Idh1	5,69016E-08	7,24641E-06
GO:0010038	response to metal ion	Cp/Sord/Gatm/Abat/Aldob/Lgmn/Glud1/Pklr/Gss/Tfrc/ Mecp2/Fbp1/Ass1	5,92027E-08	7,24641E-06
GO:0006091	generation of precursor metabolites and energy	Aldob/Coq9/Pklr/Oxct1/Acox1/G6pc/Idh3g/Dlst/Gaa/ Fbp1/Mdh2/Slc4a4/Aldh1l1/Bpgm/Idh1	1,42472E-07	1,66082E-05
GO:0009064	glutamine family amino acid metabolic process	Glul/Glud1/Aadat/Aldh4a1/Adhfe1/Mecp2/Ass1	1,5226E-07	1,69424E-05
GO:0052547	regulation of peptidase activity	Kng1/Dpep1/Fetub/Cryab/Gpx1/Serpinc1/Lgmn/Ctsb/ Kng2/Serpina3m/Agt/Ambp/Serpina3k/Serpina3n/ Slc22a2	1,74765E-07	1,8601E-05
GO:0006631	fatty acid metabolic process	Gpx1/Ephx2/Hao2/Acsm1/Hadh/Asah1/Acox1/Cyp2j5/ Acox2/Ptgr1/Acsm2/Agt/Hacl1/Gcdh/Acat2	1,90528E-07	1,94339E-05
GO:0030193	regulation of blood coagulation	Kng1/Abat/Plg/Serpinc1/Kng2/F12/Cpb2	2,34267E-07	2,29395E-05
GO:1900046	regulation of hemostasis	Kng1/Abat/Plg/Serpinc1/Kng2/F12/Cpb2	2,87547E-07	2,70736E-05
GO:0050818	regulation of coagulation	Kng1/Abat/Plg/Serpinc1/Kng2/F12/Cpb2	3,50675E-07	3,17946E-05
GO:0061045	negative regulation of wound healing	Kng1/Abat/Plg/Kng2/F12/Muc16/Cpb2	4,25074E-07	3,71636E-05
GO:0052548	regulation of endopeptidase activity	Kng1/Dpep1/Fetub/Cryab/Gpx1/Serpinc1/Lgmn/	5,43854E-07	4,59088E-05

		Kng2/Serpina3m/Agt/Serpina3k/Serpina3n/ Slc22a2		
GO:0030195	negative regulation of blood coagulation	Kng1/Abat/Plg/Kng2/F12/Cpb2	5,94424E-07	4,8505E-05
GO:1900047	negative regulation of hemostasis	Kng1/Abat/Plg/Kng2/F12/Cpb2	6,73812E-07	5,23037E-05
GO:0051346	negative regulation of hydrolase activity	Kng1/Dpep1/Fetub/Cryab/Gpx1/Serpinc1/Ctsb/Kng2/ Serpina3m/Agt/Ambp/Serpina3k/Serpina3n	6,97074E-07	5,23037E-05
GO:0006536	glutamate metabolic process	Glul/Glud1/Aadat/Aldh4a1/Adhfe1	7,05074E-07	5,23037E-05
GO:0050819	negative regulation of coagulation	Kng1/Abat/Plg/Kng2/F12/Cpb2	7,61677E-07	5,48408E-05
GO:0016042	lipid catabolic process	Gm2a/Smpdl3a/Hadh/Asah1/Plbd1/Acox1/Acox2/ Hacl1/Gcdh/Idh1/Plbd2/Acat2	1,43503E-06	9,88526E-05
GO:0009072	aromatic amino acid family metabolic process	Acmsd/Gstz1/Pah/Ttc36/Kynu	1,45371E-06	9,88526E-05
GO:0050667	homocysteine metabolic process	Dpep1/Cth/Mmut/Tst	1,49955E-06	9,92135E-05
GO:0007596	blood coagulation	Kng1/Abat/Plg/Papss2/Serpinc1/Kng2/F12/Cpb2/Ptpn6	1,66675E-06	0,000107374
GO:0000096	sulfur amino acid metabolic process	Ggt1/Dpep1/Cth/Mmut/Tst	1,71408E-06	0,000107591
GO:0007599	hemostasis	Kng1/Abat/Plg/Papss2/Serpinc1/Kng2/F12/Cpb2/Ptpn6	1,92308E-06	0,000114822
GO:0050817	coagulation	Kng1/Abat/Plg/Papss2/Serpinc1/Kng2/F12/Cpb2/Ptpn6	1,92308E-06	0,000114822
GO:1903035	negative regulation of response to wounding	Kng1/Abat/Plg/Kng2/F12/Muc16/Cpb2	2,06511E-06	0,000120367
GO:0061041	regulation of wound healing	Kng1/Abat/Plg/Serpinc1/Kng2/F12/Muc16/Cpb2	2,26305E-06	0,000128836
GO:0009074	aromatic amino acid family catabolic process	Acmsd/Gstz1/Pah/Kynu	2,69947E-06	0,000146851
GO:0072350	tricarboxylic acid metabolic process	Glud1/Idh3g/Ass1/Idh1	2,69947E-06	0,000146851
GO:0008652	cellular amino acid biosynthetic process	Ggt1/Abat/Glul/Cth/Pah/Ass1	2,76642E-06	0,000147222
GO:0006767	water-soluble vitamin metabolic process	Amn/Alpl/Akr1a1/Btd/Aldh1l1	4,72744E-06	0,000246229
GO:0019395	fatty acid oxidation	Hao2/Hadh/Acox1/Acox2/Hacl1/Gcdh/Acat2	8,13984E-06	0,000415132
GO:0030258	lipid modification	Ephx2/Hao2/Hadh/Acox1/Acox2/Agt/Hacl1/Gcdh/Acat2	1,06578E-05	0,000532454
GO:0034440	lipid oxidation	Hao2/Hadh/Acox1/Acox2/Hacl1/Gcdh/Acat2	1,27528E-05	0,000624377
GO:0072329	monocarboxylic acid catabolic process	Hadh/Akr1a1/Acox1/Acox2/Hacl1/Gcdh/Acat2	1,34572E-05	0,000645947
GO:0016311	dephosphorylation	Ephx2/Alpl/Bpnt1/Ptp4a2/Acp5/G6pc/Fbp1/Ptprd/ Ptpn6/Rpl5/Cdh5	1,48734E-05	0,000699598
GO:0042537	benzene-containing compound metabolic process	Ephx2/Hao2/Aadat/Kynu	1,51465E-05	0,000699598
GO:0006766	vitamin metabolic process	Lrp2/Amn/Alpl/Akr1a1/Btd/Aldh1l1	1,62966E-05	0,000729761
GO:1903034	regulation of response to wounding	Kng1/Abat/Plg/Serpinc1/Kng2/F12/Muc16/Cpb2	1,63958E-05	0,000729761
GO:0042060	wound healing	Kng1/Abat/Gpx1/Plg/Papss2/Serpinc1/Kng2/F12/Muc16/Cpb2/ Ptpn6	2,96052E-05	0,001294169
GO:1901607	alpha-amino acid biosynthetic process	Ggt1/Glul/Cth/Pah/Ass1	3,13441E-05	0,001346147
GO:0009914	hormone transport	Ttr/Abat/Lrp2/Glul/Glud1/Hadh/Oxct1/Cyp2j5/Agt/Rab11fip1/ Rab11fip3	3,42132E-05	0,001444032
GO:0006753	nucleoside phosphate metabolic process	Aldob/Papss2/Smpdl3a/Acsm1/Pklr/Acsm2/Fbp1/Slc4a4/ Nmrk1/Bpgm/Gcdh/Kynu	3,72621E-05	0,001546062
GO:0072521	purine-containing compound metabolic process	Ttr/Aldob/Papss2/Acsm1/Pklr/Acsm2/Fbp1/Slc4a4/ Bpgm/Gcdh/Kynu	4,53125E-05	0,001848749
GO:0009062	fatty acid catabolic process	Hadh/Acox1/Acox2/Hacl1/Gcdh/Acat2	4,64784E-05	0,00186523
GO:0006734	NADH metabolic process	Aldob/Idh3g/Dlst/Mdh2	4,92635E-05	0,001945113
GO:0006000	fructose metabolic process	Sord/Aldob/Fbp1	5,31522E-05	0,002033073
GO:0006534	cysteine metabolic process	Ggt1/Cth/Tst	5,31522E-05	0,002033073
GO:0006099	tricarboxylic acid cycle	Idh3g/Dlst/Mdh2/Idh1	5,57812E-05	0,002100807

Table 7: Gene ontology (GO) analysis of significantly downregulated clusters of biological processes.*The ID of the GO term, the description, the gene IDs as well as p-value and adjusted p-value are shown.*

5.1.5 GO-enrichment analysis of molecular function

5.1.5.1 Upregulated clusters

ID	Description	geneID	pvalue	p.adjust
GO:0140097	catalytic activity, acting on DNA	Chtf8/Mutyh/Hmga2/Cecr2/Zranb3/Dnase1l1/Rtel1	1,4954E-05	0,00508448

Table 8: Gene ontology (GO) analysis of significantly upregulated clusters of molecular function.*The ID of the GO term, the description, the gene IDs as well as p-value and adjusted p-value are shown.*

5.1.5.2 Downregulated clusters

ID	Description	geneID	pvalue	p.adjust
GO:0016614	oxidoreductase activity, acting on CH-OH group of donors	Hibadh/Bdh1/Sord/Hao2/Hadh/Akr1a1/Dcxr/Ptgr1/ Idh3g/Adhfe1/Mdh2/Me1/Idh1	6,8198E-11	2,8302E-08
GO:0016616	oxidoreductase activity, acting on the CH-OH group of donors, NAD or NADP as acceptor	Hibadh/Bdh1/Sord/Hadh/Akr1a1/Dcxr/Ptgr1/ Idh3g/Adhfe1/Mdh2/Me1/Idh1	4,5876E-10	9,5192E-08
GO:0004553	hydrolase activity, hydrolyzing O-glycosyl compounds	Gm2a/Chil3/Lyz2/Lyz1/Naglu/Gaa/Amy1/Fuca1/Ganc	1,4366E-08	1,4905E-06
GO:0008238	exopeptidase activity	Dpep1/Ctsz/Mme/Ctsa/Dpp7/Ace2/Scrn2/Cpb2/Scpep1	1,4366E-08	1,4905E-06
GO:0051287	NAD binding	Hibadh/Sord/Glud1/Hadh/Idh3g/Me1/Idh1	2,0774E-07	1,7242E-05
GO:0019842	vitamin binding	Alb/Abat/Scly/Cth/Aadat/Mmut/Hacl1/Dmgdh/Kynu	2,9639E-07	1,9896E-05
GO:0016798	hydrolase activity, acting on glycosyl bonds	Gm2a/Chil3/Lyz2/Lyz1/Naglu/Gaa/Amy1/Fuca1/Ganc	3,3559E-07	1,9896E-05
GO:0070279	vitamin B6 binding	Alb/Abat/Scly/Cth/Aadat/Kynu	1,2863E-06	6,6725E-05
GO:0004866	endopeptidase inhibitor activity	Kng1/Dpep1/Fetub/Serpinc1/Kng2/ Serpina3m/Agt/Ambp/Serpina3k/Serpina3n	1,7369E-06	8,0091E-05
GO:0030414	peptidase inhibitor activity	Kng1/Dpep1/Fetub/Serpinc1/Kng2/Serpina3m/Agt/ Ambp/Serpina3k/Serpina3n	2,4072E-06	9,99E-05
GO:0015643	toxic substance binding	Alb/Ephx2/Gsta4/Ass1	3,0362E-06	0,0001051
GO:0005504	fatty acid binding	Fabp7/Alb/Acox1/Acox2/Gsta4/Rida	3,2804E-06	0,0001051
GO:0061135	endopeptidase regulator activity	Kng1/Dpep1/Fetub/Serpinc1/Kng2/Serpina3m/Agt/ Ambp/Serpina3k/Serpina3n	3,2922E-06	0,0001051
GO:0031406	carboxylic acid binding	Fabp7/Alb/Glul/Acox1/Acox2/Gss/Gsta4/Dmgdh/Rida	3,6972E-06	0,0001096
GO:0016597	amino acid binding	Scly/Glul/Pah/Glud1/Gss/Ass1	6,7E-06	0,00017937
GO:0004180	carboxypeptidase activity	Ctsz/Ctsa/Ace2/Cpb2/Scpep1	7,0315E-06	0,00017937
GO:0051087	chaperone binding	Cp/Alb/Lrp2/Plg/Dlst/Tfrc/Hscb	7,7801E-06	0,00017937
GO:0072341	modified amino acid binding	Alb/Dpep1/Mme/Gss/Mmut/Gsdmc3/Dmgdh	7,7801E-06	0,00017937
GO:0061134	peptidase regulator activity	Kng1/Dpep1/Fetub/Serpinc1/Kng2/Serpina3m/Agt/ Ambp/Serpina3k/Serpina3n	1,0953E-05	0,00023924
GO:0030170	pyridoxal phosphate binding	Alb/Abat/Cth/Aadat/Kynu	2,3006E-05	0,00047738
GO:0033293	monocarboxylic acid binding	Fabp7/Alb/Acox1/Acox2/Gsta4/Rida	3,4396E-05	0,00067974
GO:0016645	oxidoreductase activity, acting on the CH-NH group of donors	Blvrb/Aldh4a1/Dmgdh/Aldh1l1	4,2558E-05	0,00080279
GO:0016627	oxidoreductase activity, acting on the CH-CH group of donors	Blvrb/Acox1/Acox2/Ptgr1/Gcdh	6,8264E-05	0,00123172
GO:0016791	phosphatase activity	Ephx2/Alpl/Bpnt1/Ptp4a2/Acp5/G6pc/Fbp1/Ptprd/Ptpn6	7,6934E-05	0,00126915
GO:0043177	organic acid binding	Scly/Glul/Pah/Glud1/Gss/Ass1/Dmgdh	7,8538E-05	0,00126915
GO:0000287	magnesium ion binding	Ephx2/Bpnt1/Glul/Pklr/Idh3g/Gss/Hacl1/Idh1	7,9513E-05	0,00126915
GO:0004857	enzyme inhibitor activity	Kng1/Dpep1/Fetub/Serpinc1/Kng2/Serpina3m/Agt/ Ambp/Serpina3k/Rpl5/Serpina3n	8,6246E-05	0,00132563
GO:0016874	ligase activity	Mccc1/Glul/Acsm1/Gss/Acsm2/Ass1/Acss3	9,949E-05	0,00147459
GO:0042578	phosphoric ester hydrolase activity	Ephx2/Alpl/Bpnt1/Smpdl3a/Ptp4a2/Acp5/G6pc/Fbp1/Ptprd/Ptpn6	0,0001303	0,00186462

GO:0016646	oxidoreductase activity, acting on the CH-NH group of donors, NAD or NADP as acceptor	Blvrb/Aldh4a1/Aldh1l1	0,00017515	0,00242295
GO:0016782	transferase activity, transferring sulphur-containing groups	Sult1c2/Oxct1/Sult1d1/Tst/Sugct	0,00018357	0,00245742
GO:0004175	endopeptidase activity	Plg/Lgmn/Ctsz/Ctsb/Mme/F12/Ace2/Ctss/Napsa/Adamts7/Cfb	0,00019834	0,00257224
GO:0015929	hexosaminidase activity	Gm2a/Chil3/Naglu	0,00020917	0,00263051
GO:0004867	serine-type endopeptidase inhibitor activity	Serpinc1/Serpina3m/Agt/Ambp/Serpina3k/Serpina3n	0,00022044	0,00269067
GO:0050660	flavin adenine dinucleotide binding	Acox1/Acox2/Sqor/Dmgdh/Gcdh	0,00025766	0,00305508
GO:0016830	carbon-carbon lyase activity	Acmsd/Aldob/Me1/Hacl1	0,00034866	0,00401927
GO:0016408	C-acyltransferase activity	Acsm1/Acsm2/Acat2	0,00038723	0,00434327
GO:1901681	sulfur compound binding	Naa80/Gns/Serpinc1/Gss/Ambp/Hacl1/Gcdh/Adgrg1	0,00059282	0,00647419
GO:0004602	glutathione peroxidase activity	Gpx1/Gsta4/Gstk1	0,00064131	0,00665358
GO:0016405	CoA-ligase activity	Acsm1/Acsm2/Acss3	0,00064131	0,00665358
GO:0016878	acid-thiol ligase activity	Acsm1/Acsm2/Acss3	0,00088839	0,00899222
GO:0008234	cysteine-type peptidase activity	Lgmn/Ctsz/Ctsb/Scrn2/Ctss/Uchl3	0,00097144	0,00959875
GO:0004364	glutathione transferase activity	Gstz1/Gsta4/Gstk1	0,00108241	0,01044655
GO:0016746	acyltransferase activity	Ggt1/Naa80/Glul/Acsm1/Acsm2/Dlst/Acat2	0,00157448	0,01485019
GO:0004869	cysteine-type endopeptidase inhibitor activity	Kng1/Dpep1/Fetub/Kng2	0,00173529	0,01542287
GO:0016829	lyase activity	Acmsd/Aldob/Scly/Cth/Me1/Hacl1	0,00184318	0,01542287
GO:0003796	lysozyme activity	Lyz2/Lyz1	0,00185104	0,01542287
GO:0015926	glucosidase activity	Gaa/Ganc	0,00185104	0,01542287
GO:0019203	carbohydrate phosphatase activity	G6pc/Fbp1	0,00185104	0,01542287
GO:0016810	hydrolase activity, acting on carbon-nitrogen (but not peptide) bonds	Dpep1/Acy3/Asah1/Rida/Btd	0,00185818	0,01542287
GO:0016634	oxidoreductase activity, acting on the CH-CH group of donors, oxygen as acceptor	Acox1/Acox2	0,00225266	0,0175122
GO:0016209	antioxidant activity	Gpx1/Gsta4/Ambp/Gstk1	0,00227713	0,0175122
GO:0016877	ligase activity, forming carbon-sulfur bonds	Acsm1/Acsm2/Acss3	0,0022787	0,0175122
GO:0071949	FAD binding	Acox1/Acox2/Sqor	0,0022787	0,0175122
GO:0030246	carbohydrate binding	Aldob/Chil3/Gaa/Fbp1/Fuca1/C4b/Ganc	0,00240135	0,01811931
GO:0008236	serine-type peptidase activity	Plg/Ctsa/F12/Dpp7/Cfb/Scpep1	0,00266887	0,01959657
GO:0016846	carbon-sulfur lyase activity	Scly/Cth	0,00269158	0,01959657
GO:0017171	serine hydrolase activity	Plg/Ctsa/F12/Dpp7/Cfb/Scpep1	0,00299775	0,02120047
GO:0008097	5S rRNA binding	Tst/Rpl5	0,0031673	0,02120047
GO:0008484	sulfuric ester hydrolase activity	Gns/Arsb	0,0031673	0,02120047
GO:0015245	fatty acid transmembrane transporter activity	Slc22a19/Slc5a8	0,0031673	0,02120047
GO:0016832	aldehyde-lyase activity	Aldob/Hacl1	0,0031673	0,02120047
GO:0050661	NADP binding	Hibadh/Me1/Idh1	0,00340205	0,02241035
GO:0061783	peptidoglycan muralytic activity	Lyz2/Lyz1	0,00367933	0,02385814
GO:0016747	acyltransferase activity, transferring groups other than amino-acyl groups	Naa80/Glul/Acsm1/Acsm2/Dlst/Acat2	0,00374533	0,02391248
GO:0016879	ligase activity, forming carbon-nitrogen bonds	Glul/Gss/Ass1	0,00383943	0,02414187
GO:0070403	NAD+ binding	Glud1/Hadh	0,00481035	0,02979545
GO:0016853	isomerase activity	Gstz1/Cyp2j5/Mmut/Gsta4/Bpgm	0,00493389	0,03011125
GO:0004197	cysteine-type endopeptidase activity	Lgmn/Ctsz/Ctsb/Ctss	0,00507449	0,03052049
GO:0016667	oxidoreductase activity, acting on a sulfur group of donors	Selenbp1/Sqor/Msra	0,00535074	0,03172227
GO:0004029	aldehyde dehydrogenase (NAD+) activity	Aldh4a1/Aldh1l1	0,00542838	0,03172924
GO:0004601	peroxidase activity	Gpx1/Gsta4/Gstk1	0,00563254	0,03246534
GO:0016620	oxidoreductase activity, acting on the aldehyde or oxo group of donors, NAD or NADP as acceptor	Aldh6a1/Aldh4a1/Aldh1l1	0,00592309	0,03367234

GO:0016805	dipeptidase activity	Dpep1/Scrn2	0,00608078	0,03410165
GO:0004030	aldehyde dehydrogenase [NAD(P)+] activity	Aldh4a1/Aldh1l1	0,00676708	0,03739311
GO:0016684	oxidoreductase activity, acting on peroxide as acceptor	Gpx1/Gsta4/Gstk1	0,0068479	0,03739311
GO:0008235	metalloexopeptidase activity	Dpep1/Ace2/Cpb2	0,00750939	0,04012279
GO:0008237	metallopeptidase activity	Dpep1/Mme/Ace2/Cpb2/Adamts7	0,00754115	0,04012279
GO:0016765	transferase activity, transferring alkyl or aryl (other than methyl) groups	Gstz1/Gsta4/Gstk1	0,00820739	0,04274257
GO:0015645	fatty acid ligase activity	Acsm1/Acsm2	0,00823953	0,04274257
GO:0016903	oxidoreductase activity, acting on the aldehyde or oxo group of donors	Aldh6a1/Aldh4a1/Aldh1l1	0,00971464	0,04977255

Table 9: Gene ontology (GO) analysis of significantly downregulated clusters of molecular function.*The ID of the GO term, the description, the gene IDs as well as p-value and adjusted p-value are shown.*

5.1.6 GO-enrichment analysis of cellular compartment

5.1.6.1 Upregulated clusters

ID	Description	geneID	pvalue	p.adjust
GO:0045177	apical part of cell	Cd9/Ifitm3/Dbh/Pappa2/Pard6g/Sptbn5/Ddr2/Slc16a2	0,0005147	0,04805941
GO:1902554	serine/threonine protein kinase complex	Ccnb1/Ccnl1/Sesn2/Stk11	0,00077494	0,04805941
GO:0030017	sarcomere	Myl3/Tnnc2/Ppp3ca/Rpl7/Stk11	0,00094761	0,04805941
GO:0000137	Golgi cis cisterna	Bet1/Atl1	0,00106225	0,04805941
GO:0000940	outer kinetochore	Plk1/Ccnb1	0,00123626	0,04805941
GO:1902911	protein kinase complex	Ccnb1/Ccnl1/Sesn2/Stk11	0,00132789	0,04805941
GO:0035102	PRC1 complex	Phc3/Bmi1	0,00142296	0,04805941
GO:0030016	myofibril	Myl3/Tnnc2/Ppp3ca/Rpl7/Stk11	0,0015996	0,04805941
GO:0098687	chromosomal region	Nabp2/Plk1/Orc1/Dctn3/Ccnb1/Rtel1	0,00167002	0,04805941

Table 10: Gene ontology (GO) analysis of significantly upregulated clusters of cellular compartment.*The ID of the GO term, the description, the gene IDs as well as p-value and adjusted p-value are shown.*

5.1.6.2 Downregulated clusters

ID	Description	geneID	pvalue	p.adjust
GO:0045177	apical part of cell	Pdzd2/Dpep1/Lrp2/Amn/Atp1b1/Acy3/Lgmn/Ctsb/Pdzk1/Akr1a1/ Slc12a3/Shank2/Itga8/Ace2/Btd/Slc22a2/Slc5a8	1,3259E-08	2,9568E-06
GO:0005759	mitochondrial matrix	Abat/Mccc1/Glud1/Acsm1/Idh3g/Acsm2/Mmut/ Mdh2/Mrps14/Acss3/Dmgdh/Rida/Gstk1	3,79E-08	4,2258E-06
GO:0005743	mitochondrial inner membrane	Bdh1/Gatm/Mccc1/Coq9/Glud1/Hadh/Ambp/Mdh2/Sqor/Tst/ Cox6b1/Gstk1/Gcdh/Ndufb7	1,3611E-06	7,9756E-05
GO:0062023	collagen-containing extracellular matrix	Alb/Kng1/Plg/Serpinc1/Ctsz/Gpc4/Ctsb/Tinag/Kng2/Col15a1/ Ambp/Serpina3k/Col24a1	1,4306E-06	7,9756E-05
GO:0043204	perikaryon	Kng1/Cryab/Glul/Kng2/Itga8/Rufy3/Ass1/Btd	3,1574E-06	0,00011789
GO:0005903	brush border	Lrp2/Amn/Pdzk1/Mme/Shank2/Dcxr/Ace2/Slc5a8	3,8884E-06	0,00011789
GO:0016324	apical plasma membrane	Lrp2/Amn/Atp1b1/Acy3/Ctsb/Pdzk1/Akr1a1/Slc12a3/ Shank2/Ace2/Slc22a2/Slc5a8	4,042E-06	0,00011789
GO:0005777	peroxisome	Ephx2/Hao2/Acox1/Acox2/Hacl1/Rida/Gstk1/Idh1	4,758E-06	0,00011789
GO:0042579	microbody	Ephx2/Hao2/Acox1/Acox2/Hacl1/Rida/Gstk1/Idh1	4,758E-06	0,00011789
GO:0031526	brush border membrane	Lrp2/Amn/Pdzk1/Shank2/Ace2/Slc5a8	1,1365E-05	0,00025343
GO:0005791	rough endoplasmic reticulum	Aldob/Lyz2/Glul/Arsb/Lyz1/F12	2,0978E-05	0,00042528

GO:0098862	cluster of actin-based cell projections	Lrp2/Amn/Pdzk1/Mme/Shank2/Dcxr/Ace2/Slc5a8	4,9543E-05	0,00092067
GO:0043209	myelin sheath	Alb/Cryab/Atp1b1/Glul/Dlst/Mdh2/Ass1/Ehd1	6,6897E-05	0,00114755
GO:0043230	extracellular organelle	Alb/Sord/Alpl/Slc12a3/Naglu/Tfrc	0,00014063	0,00209063
GO:0065010	extracellular membrane-bounded organelle	Alb/Sord/Alpl/Slc12a3/Naglu/Tfrc	0,00014063	0,00209063
GO:0031253	cell projection membrane	Lrp2/Amn/Pdzk1/Shank2/Itga8/Ace2/Slc5a8/Tmem67/Ehd1	0,00019885	0,00277153
GO:0070062	extracellular exosome	Alb/Sord/Slc12a3/Naglu/Tfrc	0,00050813	0,00657677
GO:0005902	microvillus	Amn/Lyz2/Lyz1/Pdzk1/Dcxr	0,00053086	0,00657677
GO:0098858	actin-based cell projection	Amn/Lyz2/Lyz1/Pdzk1/Dcxr/Rufy3/Fgd4	0,00062652	0,00735335
GO:1903561	extracellular vesicle	Alb/Sord/Slc12a3/Naglu/Tfrc	0,00083439	0,00930343
GO:0000137	Golgi cis cisterna	Lyz2/Lyz1	0,00290786	0,03087866
GO:0016323	basolateral plasma membrane	Slc22a19/Atp1b1/Tfrc/Cdh16/Slc4a4/Slc22a2	0,00467068	0,04448752
GO:0055038	recycling endosome membrane	Tfrc/Rab11fip3/Ehd1	0,0047411	0,04448752
GO:0034451	centriolar satellite	Pdzd2/Aldob/Dlst/Rab11fip3	0,00496841	0,04448752
GO:0045239	tricarboxylic acid cycle enzyme complex	Idh3g/Dlst	0,00498739	0,04448752
GO:0060170	ciliary membrane	Shank2/Tmem67/Ehd1	0,00551684	0,04731748

Table 11: Gene ontology (GO) analysis of significantly downregulated clusters of cellular compartment.*The ID of the GO term, the description, the gene IDs as well as p-value and adjusted p-value are shown.*

6 Literature

Abele, H., Starz, S., Hoopmann, M., Yazdi, B., Rall, K., & Kagan, K. O. (2012). Idiopathic polyhydramnios and postnatal abnormalities. *Fetal Diagn Ther*, *32*(4), 251-255. https://doi.org/10.1159/000338659

Adami, P., Duncan, T. M., McIntyre, J. O., Carter, C. E., Fu, C., Melin, M., Latruffe, N., & Fleischer, S. (1993). Monoclonal antibodies for structure-function studies of (R)-3-hydroxybutyrate dehydrogenase, a lipid-dependent membrane-bound enzyme. *Biochem J*, *292 (Pt 3)*(Pt 3), 863-872. https://doi.org/10.1042/bj2920863

Ahn, D., Provasi, D., Duc, N. M., Xu, J., Salas-Estrada, L., Spasic, A., Yun, M. W., Kang, J., Gim, D., Lee, J., Du, Y., Filizola, M., & Chung, K. Y. (2022). Gαs slow conformational transition upon GTP binding and a novel Gαs regulator. *bioRxiv*.

Akinbi, H. T., Narendran, V., Pass, A. K., Markart, P., & Hoath, S. B. (2004). Host defense proteins in vernix caseosa and amniotic fluid. *Am J Obstet Gynecol*, *191*(6), 2090-2096. https://doi.org/10.1016/j.ajog.2004.05.002

Alexander, E. S., Spitz, H. B., & Clark, R. A. (1982). Sonography of polyhydramnios. *AJR Am J Roentgenol*, *138*(2), 343-346. https://doi.org/10.2214/ajr.138.2.343

Allali-Hassani, A., Pan, P. W., Dombrovski, L., Najmanovich, R., Tempel, W., Dong, A., Loppnau, P., Martin, F., Thornton, J., Edwards, A. M., Bochkarev, A., Plotnikov, A. N., Vedadi, M., & Arrowsmith, C. H. (2007). Structural and chemical profiling of the human cytosolic sulfotransferases. *PLoS Biol*, *5*(5), e97. https://doi.org/10.1371/journal.pbio.0050097

Allen, B. L., & Taatjes, D. J. (2015). The Mediator complex: a central integrator of transcription. *Nat Rev Mol Cell Biol*, *16*(3), 155-166. https://doi.org/10.1038/nrm3951

Almeida, F. C., & Lemonica, I. P. (2000). The toxic effects of Coleus barbatus B. on the different periods of pregnancy in rats. *J Ethnopharmacol*, *73*(1-2), 53-60. https://doi.org/10.1016/s0378-8741(00)00275-0

Ammon, H. P., & Muller, A. B. (1985). Forskolin: from an ayurvedic remedy to a modern agent. *Planta Med*, *51*(6), 473-477. https://doi.org/10.1055/s-2007-969566

Arroyo, J. P., Lagnaz, D., Ronzaud, C., Vazquez, N., Ko, B. S., Moddes, L., Ruffieux-Daidie, D., Hausel, P., Koesters, R., Yang, B., Stokes, J. B., Hoover, R. S., Gamba, G., & Staub, O. (2011). Nedd4-2 modulates renal Na+-Cl- cotransporter via the aldosterone-SGK1-Nedd4-2 pathway. *J Am Soc Nephrol*, *22*(9), 1707-1719. https://doi.org/10.1681/ASN.2011020132

Arthuis, C. J., Nizon, M., Komhoff, M., Beck, B. B., Riehmer, V., Bihouee, T., Bruel, A., Benbrik, N., Winer, N., & Isidor, B. (2019). A step towards precision medicine in management of severe transient polyhydramnios: MAGED2 variant. *J Obstet Gynaecol*, *39*(3), 395-397. https://doi.org/10.1080/01443615.2018.1454415

Banning, F. M. (1959). The theory of the PAS method of staining. *Am J Med Technol*, *25*(3), 195-197. https://www.ncbi.nlm.nih.gov/pubmed/13649690

Barker, P. A., & Salehi, A. (2002). The MAGE proteins: emerging roles in cell cycle progression, apoptosis, and neurogenetic disease. *J Neurosci Res*, *67*(6), 705-712. https://doi.org/10.1002/jnr.10160

Bartram, M. P., Habbig, S., Pahmeyer, C., Hohne, M., Weber, L. T., Thiele, H., Altmuller, J., Kottoor, N., Wenzel, A., Krueger, M., Schermer, B., Benzing, T., Rinschen, M. M., & Beck, B. B. (2016). Three-layered proteomic characterization of a novel ACTN4 mutation unravels its pathogenic potential in FSGS. *Hum Mol Genet*, *25*(6), 1152-1164. https://doi.org/10.1093/hmg/ddv638

Bartter, F. C., Pronove, P., Gill, J. R., Jr., & Maccardle, R. C. (1962). Hyperplasia of the juxtaglomerular complex with hyperaldosteronism and hypokalemic alkalosis. A new syndrome. *Am J Med*, *33*, 811-828. https://doi.org/10.1016/0002-9343(62)90214-0

Bartter, F. C., & Schwartz, W. B. (1967). The syndrome of inappropriate secretion of antidiuretic hormone. *The American Journal of Medicine*, *42*(5), 790-806. https://doi.org/https://doi.org/10.1016/0002-9343(67)90096-4

Bassanese, G., Wlodkowski, T., Servais, A., Heidet, L., Roccatello, D., Emma, F., Levtchenko, E., Ariceta, G., Bacchetta, J., Capasso, G., Jankauskiene, A., Miglinas, M., Ferraro, P. M., Montini, G., Oh, J., Decramer, S., Levart, T. K., Wetzels, J., Cornelissen, E., . . . Schaefer, F. (2021). The European Rare Kidney Disease Registry (ERKReg): objectives, design and initial results. *Orphanet Journal of Rare Diseases*, *16*(1), 251. https://doi.org/10.1186/s13023-021-01872-8

Baum, M. A., Ruddy, M. K., Hosselet, C. A., & Harris, H. W. (1998). The perinatal expression of aquaporin-2 and aquaporin-3 in developing kidney. *Pediatr Res*, *43*(6), 783-790. https://doi.org/10.1203/00006450-199806000-00011

Beer, S., Zetterberg, A., Ihrie, R. A., McTaggart, R. A., Yang, Q., Bradon, N., Arvanitis, C., Attardi, L. D., Feng, S., Ruebner, B., Cardiff, R. D., & Felsher, D. W. (2004). Developmental context determines latency of MYC-induced tumorigenesis. *PLoS Biol*, *2*(11), e332. https://doi.org/10.1371/journal.pbio.0020332

Bens, M., Vallet, V., Cluzeaud, F., Pascual-Letallec, L., Kahn, A., Rafestin-Oblin, M. E., Rossier, B. C., & Vandewalle, A. (1999). Corticosteroid-dependent sodium transport in a novel immortalized mouse collecting duct principal cell line. *J Am Soc Nephrol*, *10*(5), 923-934. https://www.ncbi.nlm.nih.gov/pubmed/10232677

Bergsland, K. J., Coe, F. L., Parks, J. H., Asplin, J. R., & Worcester, E. M. (2018). Evidence for a role of PDZ domain-containing proteins to mediate hypophosphatemia in calcium stone formers. *Nephrol Dial Transplant*, *33*(5), 759-770. https://doi.org/10.1093/ndt/gfx284

Bertini, E., Hwu, W. L., Reyna, S. P., Farwell, W., Gheuens, S., Sun, P., Zhong, Z. J., & De Vivo, D. C. (2017). Efficacy and safety of nusinersen in infants with presymptomatic spinal muscular atrophy (SMA): Interim results from the NURTURE study. *European Journal of Paediatric Neurology*, *21*, e14. https://doi.org/10.1016/j.ejpn.2017.04.1218

Bertrand, M., Huijbers, I., Chomez, P., & De Backer, O. (2004). Comparative expression analysis of the MAGED genes during embryogenesis and brain development. *Dev Dyn*, *230*(2), 325-334. https://doi.org/10.1002/dvdy.20026

Besouw, M. T. P., Kleta, R., & Bockenhauer, D. (2019). Bartter and Gitelman syndromes: Questions of class. *Pediatr Nephrol*. https://doi.org/10.1007/s00467-019-04371-y

Birkenhager, R., Otto, E., Schurmann, M. J., Vollmer, M., Ruf, E. M., Maier-Lutz, I., Beekmann, F., Fekete, A., Omran, H., Feldmann, D., Milford, D. V., Jeck, N., Konrad, M., Landau, D., Knoers, N. V., Antignac, C., Sudbrak, R., Kispert, A., & Hildebrandt, F. (2001). Mutation of BSND causes Bartter syndrome with sensorineural deafness and kidney failure. *Nat Genet*, *29*(3), 310-314. https://doi.org/10.1038/ng752

Blaine, J., Chonchol, M., & Levi, M. (2015). Renal control of calcium, phosphate, and magnesium homeostasis. *Clin J Am Soc Nephrol*, *10*(7), 1257-1272. https://doi.org/10.2215/CJN.09750913

Boccaccio, I., Glatt-Deeley, H., Watrin, F., Roeckel, N., Lalande, M., & Muscatelli, F. (1999). The human MAGEL2 gene and its mouse homologue are paternally expressed and mapped to the Prader-Willi region. *Hum Mol Genet*, *8*(13), 2497-2505. https://doi.org/10.1093/hmg/8.13.2497

Bock, J. B., Matern, H. T., Peden, A. A., & Scheller, R. H. (2001). A genomic perspective on membrane compartment organization. *Nature*, *409*(6822), 839-841. https://doi.org/10.1038/35057024

Bodiwala, H. S., Sabde, S., Mitra, D., Bhutani, K. K., & Singh, I. P. (2009). Anti-HIV diterpenes from Coleus forskohlii. *Nat Prod Commun*, *4*(9), 1173-1175. https://www.ncbi.nlm.nih.gov/pubmed/19831022

Boone, M., & Deen, P. M. (2008). Physiology and pathophysiology of the vasopressin-regulated renal water reabsorption. *Pflugers Arch*, *456*(6), 1005-1024. https://doi.org/10.1007/s00424-008-0498-1

Bourque, C. W., Oliet, S. H., & Richard, D. (1994). Osmoreceptors, osmoreception, and osmoregulation. *Front Neuroendocrinol*, *15*(3), 231-274. https://doi.org/10.1006/frne.1994.1010
Brace, R. A., & Wolf, E. J. (1989). Normal amniotic fluid volume changes throughout pregnancy. *Am J Obstet Gynecol*, *161*(2), 382-388. https://doi.org/10.1016/0002-9378(89)90527-9
Brezis, M., & Rosen, S. (1995). Hypoxia of the renal medulla--its implications for disease. *N Engl J Med*, *332*(10), 647-655. https://doi.org/10.1056/NEJM199503093321006
Bullen, J. W., Tchernyshyov, I., Holewinski, R. J., DeVine, L., Wu, F., Venkatraman, V., Kass, D. L., Cole, R. N., Van Eyk, J., & Semenza, G. L. (2016). Protein kinase A-dependent phosphorylation stimulates the transcriptional activity of hypoxia-inducible factor 1. *Sci Signal*, *9*(430), ra56. https://doi.org/10.1126/scisignal.aaf0583
Cantone, A., Yang, X., Yan, Q., Giebisch, G., Hebert, S. C., & Wang, T. (2008). Mouse model of type II Bartter's syndrome. I. Upregulation of thiazide-sensitive Na-Cl cotransport activity. *Am J Physiol Renal Physiol*, *294*(6), F1366-1372. https://doi.org/10.1152/ajprenal.00608.2007
Caprioli, J., & Sears, M. (1983). Forskolin lowers intraocular pressure in rabbits, monkeys, and man. *Lancet*, *1*(8331), 958-960. https://doi.org/10.1016/s0140-6736(83)92084-6
Chaimovitz, C., Levi, J., Better, O. S., Oslander, L., & Benderli, A. (1973). Studies on the site of renal salt loss in a patient with Bartter's syndrome. *Pediatr Res*, *7*(2), 89-94. https://doi.org/10.1203/00006450-197302000-00004
Chassin, C., Bens, M., & Vandewalle, A. (2007). Transimmortalized proximal tubule and collecting duct cell lines derived from the kidneys of transgenic mice. *Cell Biol Toxicol*, *23*(4), 257-266. https://doi.org/10.1007/s10565-006-0169-y
Cheng, C. J., Lo, Y. F., Chen, J. C., Huang, C. L., & Lin, S. H. (2017). Functional severity of CLCNKB mutations correlates with phenotypes in patients with classic Bartter's syndrome. *J Physiol*, *595*(16), 5573-5586. https://doi.org/10.1113/JP274344
Chevalier, R. L. (2016). The proximal tubule is the primary target of injury and progression of kidney disease: role of the glomerulotubular junction. *Am J Physiol Renal Physiol*, *311*(1), F145-161. https://doi.org/10.1152/ajprenal.00164.2016
Choi, S. M., Oh, H., & Park, H. (2008). Microarray analyses of hypoxia-regulated genes in an aryl hydrocarbon receptor nuclear translocator (Arnt)-dependent manner. *FEBS J*, *275*(22), 5618-5634. https://doi.org/10.1111/j.1742-4658.2008.06686.x
Christensen, E. I., & Birn, H. (2001). Megalin and cubilin: synergistic endocytic receptors in renal proximal tubule. *American Journal of Physiology-Renal Physiology*, *280*(4), F562-F573. https://doi.org/10.1152/ajprenal.2001.280.4.F562
Cimprich, K. A., & Cortez, D. (2008). ATR: an essential regulator of genome integrity. *Nat Rev Mol Cell Biol*, *9*(8), 616-627. https://doi.org/10.1038/nrm2450
Cinar, A., Chen, M., Riederer, B., Bachmann, O., Wiemann, M., Manns, M., Kocher, O., & Seidler, U. (2007). NHE3 inhibition by cAMP and Ca2+ is abolished in PDZ-domain protein PDZK1-deficient murine enterocytes. *J Physiol*, *581*(Pt 3), 1235-1246. https://doi.org/10.1113/jphysiol.2007.131722
Colaert, N., Helsens, K., Martens, L., Vandekerckhove, J., & Gevaert, K. (2009). Improved visualization of protein consensus sequences by iceLogo. *Nat Methods*, *6*(11), 786-787. https://doi.org/10.1038/nmeth1109-786
Cox, J., & Mann, M. (2008). MaxQuant enables high peptide identification rates, individualized p.p.b.-range mass accuracies and proteome-wide protein quantification. *Nat Biotechnol*, *26*(12), 1367-1372. https://doi.org/10.1038/nbt.1511
Cunha, T. D. S., & Heilberg, I. P. (2018). Bartter syndrome: causes, diagnosis, and treatment. *Int J Nephrol Renovasc Dis*, *11*, 291-301. https://doi.org/10.2147/IJNRD.S155397
Dabovic, B., Zanaria, E., Bardoni, B., Lisa, A., Bordignon, C., Russo, V., Matessi, C., Traversari, C., & Camerino, G. (1995). A family of rapidly evolving genes from the sex reversal critical region in Xp21. *Mamm Genome*, *6*(9), 571-580. https://doi.org/10.1007/BF00352360

Dashe, J. S., McIntire, D. D., Ramus, R. M., Santos-Ramos, R., & Twickler, D. M. (2002). Hydramnios: anomaly prevalence and sonographic detection. *Obstet Gynecol*, *100*(1), 134-139. https://doi.org/10.1016/s0029-7844(02)02013-6
De Plaen, E., Arden, K., Traversari, C., Gaforio, J. J., Szikora, J. P., De Smet, C., Brasseur, F., van der Bruggen, P., Lethe, B., Lurquin, C., & et al. (1994). Structure, chromosomal localization, and expression of 12 genes of the MAGE family. *Immunogenetics*, *40*(5), 360-369. https://doi.org/10.1007/BF01246677
De, S., Kuwahara, S., & Saito, A. (2014). The endocytic receptor megalin and its associated proteins in proximal tubule epithelial cells. *Membranes (Basel)*, *4*(3), 333-355. https://doi.org/10.3390/membranes4030333
Deen, P. M., Verdijk, M. A., Knoers, N. V., Wieringa, B., Monnens, L. A., van Os, C. H., & van Oost, B. A. (1994). Requirement of human renal water channel aquaporin-2 for vasopressin-dependent concentration of urine. *Science*, *264*(5155), 92-95. https://doi.org/10.1126/science.8140421
Devuyst, O., Knoers, N. V. A. M., Remuzzi, G., & Schaefer, F. (2014). Rare inherited kidney diseases: challenges, opportunities, and perspectives. *The Lancet*, *383*(9931), 1844-1859. https://doi.org/https://doi.org/10.1016/S0140-6736(14)60659-0
Diao, M., Wu, Y., Yang, J., Liu, C., Xu, J., Jin, H., Wang, J., Zhang, J., Gao, F., Jin, C., Tian, H., Xu, J., Ou, Q., Li, Y., Xu, G., & Lu, L. (2022). Identification of Novel Key Molecular Signatures in the Pathogenesis of Experimental Diabetic Kidney Disease. *Front Endocrinol (Lausanne)*, *13*, 843721. https://doi.org/10.3389/fendo.2022.843721
Donowitz, M., Mohan, S., Zhu, C. X., Chen, T. E., Lin, R., Cha, B., Zachos, N. C., Murtazina, R., Sarker, R., & Li, X. (2009). NHE3 regulatory complexes. *J Exp Biol*, *212*(Pt 11), 1638-1646. https://doi.org/10.1242/jeb.028605
Dorsam, R. T., & Gutkind, J. S. (2007). G-protein-coupled receptors and cancer. *Nat Rev Cancer*, *7*(2), 79-94. https://doi.org/10.1038/nrc2069
Doyle, J. M., Gao, J., Wang, J., Yang, M., & Potts, P. R. (2010). MAGE-RING protein complexes comprise a family of E3 ubiquitin ligases. *Mol Cell*, *39*(6), 963-974. https://doi.org/10.1016/j.molcel.2010.08.029
Du, Z., Duan, Y., Yan, Q., Weinstein, A. M., Weinbaum, S., & Wang, T. (2004). Mechanosensory function of microvilli of the kidney proximal tubule. *Proc Natl Acad Sci U S A*, *101*(35), 13068-13073. https://doi.org/10.1073/pnas.0405179101
Duong Van Huyen, J., Bens, M., & Vandewalle, A. (1998). Differential effects of aldosterone and vasopressin on chloride fluxes in transimmortalized mouse cortical collecting duct cells. *J Membr Biol*, *164*(1), 79-90. https://doi.org/10.1007/s002329900395
Dyson, H. J., & Wright, P. E. (2016). Role of Intrinsic Protein Disorder in the Function and Interactions of the Transcriptional Coactivators CREB-binding Protein (CBP) and p300. *J Biol Chem*, *291*(13), 6714-6722. https://doi.org/10.1074/jbc.R115.692020
Ecelbarger, C. A., Kim, G. H., Terris, J., Masilamani, S., Mitchell, C., Reyes, I., Verbalis, J. G., & Knepper, M. A. (2000). Vasopressin-mediated regulation of epithelial sodium channel abundance in rat kidney. *Am J Physiol Renal Physiol*, *279*(1), F46-53. https://doi.org/10.1152/ajprenal.2000.279.1.F46
Ecelbarger, C. A., Terris, J., Frindt, G., Echevarria, M., Marples, D., Nielsen, S., & Knepper, M. A. (1995). Aquaporin-3 water channel localization and regulation in rat kidney. *Am J Physiol*, *269*(5 Pt 2), F663-672. https://doi.org/10.1152/ajprenal.1995.269.5.F663
El-Haddad, M. A., Desai, M., Gayle, D., & Ross, M. G. (2004). In utero development of fetal thirst and appetite: potential for programming. *J Soc Gynecol Investig*, *11*(3), 123-130. https://doi.org/10.1016/j.jsgi.2003.12.001
Estevez, R., Boettger, T., Stein, V., Birkenhager, R., Otto, E., Hildebrandt, F., & Jentsch, T. J. (2001). Barttin is a Cl- channel beta-subunit crucial for renal Cl- reabsorption and inner ear K+ secretion. *Nature*, *414*(6863), 558-561. https://doi.org/10.1038/35107099
Eto, K., Noda, Y., Horikawa, S., Uchida, S., & Sasaki, S. (2010). Phosphorylation of aquaporin-2 regulates its water permeability. *J Biol Chem*, *285*(52), 40777-40784. https://doi.org/10.1074/jbc.M110.151928
Feldman, B. J., Rosenthal, S. M., Vargas, G. A., Fenwick, R. G., Huang, E. A., Matsuda-Abedini, M., Lustig, R. H., Mathias, R. S., Portale, A. A., Miller, W. L., & Gitelman, S.

E. (2005). Nephrogenic syndrome of inappropriate antidiuresis. *N Engl J Med*, *352*(18), 1884-1890. https://doi.org/10.1056/NEJMoa042743
Fischer, A. H., Jacobson, K. A., Rose, J., & Zeller, R. (2008). Hematoxylin and eosin staining of tissue and cell sections. *CSH Protoc*, *2008*, pdb prot4986. https://doi.org/10.1101/pdb.prot4986
Foot, N., Henshall, T., & Kumar, S. (2017). Ubiquitination and the Regulation of Membrane Proteins. *Physiol Rev*, *97*(1), 253-281. https://doi.org/10.1152/physrev.00012.2016
Freire-Maia, N. (1977). Ectodermal dysplasias revisited. *Acta Genet Med Gemellol (Roma)*, *26*(2), 121-131. https://doi.org/10.1017/s0001566000009910
Friedberg, E. C. (2003). DNA damage and repair. *Nature*, *421*(6921), 436-440. https://doi.org/10.1038/nature01408
Furuno, M., Uchida, S., Marumo, F., & Sasaki, S. (1996). Repressive regulation of the aquaporin-2 gene. *Am J Physiol*, *271*(4 Pt 2), F854-860. https://doi.org/10.1152/ajprenal.1996.271.4.F854
Gaide, O., & Schneider, P. (2003). Permanent correction of an inherited ectodermal dysplasia with recombinant EDA. *Nat Med*, *9*(5), 614-618. https://doi.org/10.1038/nm861
Gallardo, P. A., & Vio, C. P. (2022). Functional Anatomy of the Kidney. In *Renal Physiology and Hydrosaline Metabolism* (pp. 7-28). Springer International Publishing. https://doi.org/10.1007/978-3-031-10256-1_2
Gamage, N., Barnett, A., Hempel, N., Duggleby, R. G., Windmill, K. F., Martin, J. L., & McManus, M. E. (2006). Human sulfotransferases and their role in chemical metabolism. *Toxicol Sci*, *90*(1), 5-22. https://doi.org/10.1093/toxsci/kfj061
Gamba, G., Miyanoshita, A., Lombardi, M., Lytton, J., Lee, W. S., Hediger, M. A., & Hebert, S. C. (1994). Molecular cloning, primary structure, and characterization of two members of the mammalian electroneutral sodium-(potassium)-chloride cotransporter family expressed in kidney. *J Biol Chem*, *269*(26), 17713-17722. https://www.ncbi.nlm.nih.gov/pubmed/8021284
Garrelfs, S. F., Frishberg, Y., Hulton, S. A., Koren, M. J., O'Riordan, W. D., Cochat, P., Deschenes, G., Shasha-Lavsky, H., Saland, J. M., Van't Hoff, W. G., Fuster, D. G., Magen, D., Moochhala, S. H., Schalk, G., Simkova, E., Groothoff, J. W., Sas, D. J., Meliambro, K. A., Lu, J., . . . Collaborators, I.-A. (2021). Lumasiran, an RNAi Therapeutic for Primary Hyperoxaluria Type 1. *N Engl J Med*, *384*(13), 1216-1226. https://doi.org/10.1056/NEJMoa2021712
Gasongo, G., Greenbaum, L. A., Niel, O., Kwon, T., Macher, M. A., Maisin, A., Baudouin, V., Dossier, C., Deschenes, G., & Hogan, J. (2019). Effect of nonsteroidal anti-inflammatory drugs in children with Bartter syndrome. *Pediatr Nephrol*, *34*(4), 679-684. https://doi.org/10.1007/s00467-018-4135-8
Gavet, O., & Pines, J. (2010). Activation of cyclin B1-Cdk1 synchronizes events in the nucleus and the cytoplasm at mitosis. *J Cell Biol*, *189*(2), 247-259. https://doi.org/10.1083/jcb.200909144
Ghali, J. K., Hamad, B., Yasothan, U., & Kirkpatrick, P. (2009). Tolvaptan. *Nat Rev Drug Discov*, *8*(8), 611-612. https://doi.org/10.1038/nrd2946
Gilbert, W. M., & Brace, R. A. (1993). Amniotic fluid volume and normal flows to and from the amniotic cavity. *Semin Perinatol*, *17*(3), 150-157. https://www.ncbi.nlm.nih.gov/pubmed/8378799
Gisler, S. M., Madjdpour, C., Bacic, D., Pribanic, S., Taylor, S. S., Biber, J., & Murer, H. (2003). PDZK1: II. an anchoring site for the PKA-binding protein D-AKAP2 in renal proximal tubular cells. *Kidney Int*, *64*(5), 1746-1754. https://doi.org/10.1046/j.1523-1755.2003.00267.x
Gitelman, H. J., Graham, J. B., & Welt, L. G. (1966). A new familial disorder characterized by hypokalemia and hypomagnesemia. *Trans Assoc Am Physicians*, *79*, 221-235. https://www.ncbi.nlm.nih.gov/pubmed/5929460
Gitig, D. M., & Koff, A. (2001). Cdk pathway: cyclin-dependent kinases and cyclin-dependent kinase inhibitors. *Mol Biotechnol*, *19*(2), 179-188. https://doi.org/10.1385/MB:19:2:179

Gjerga, E., Dugourd, A., Tobalina, L., Sousa, A., & Saez-Rodriguez, J. (2021). PHONEMeS: Efficient Modeling of Signaling Networks Derived from Large-Scale Mass Spectrometry Data. *J Proteome Res*, *20*(4), 2138-2144. https://doi.org/10.1021/acs.jproteome.0c00958
Gladziwa, U., Schwarz, R., Gitter, A. H., Bijman, J., Seyberth, H., Beck, F., Ritz, E., & Gross, P. (1995). Chronic hypokalaemia of adults: Gitelman's syndrome is frequent but classical Bartter's syndrome is rare. *Nephrol Dial Transplant*, *10*(9), 1607-1613. https://www.ncbi.nlm.nih.gov/pubmed/8559478
Glickman, M. H., & Ciechanover, A. (2002). The ubiquitin-proteasome proteolytic pathway: destruction for the sake of construction. *Physiol Rev*, *82*(2), 373-428. https://doi.org/10.1152/physrev.00027.2001
Gonzalez, G. A., & Montminy, M. R. (1989). Cyclic AMP stimulates somatostatin gene transcription by phosphorylation of CREB at serine 133. *Cell*, *59*(4), 675-680. https://www.ncbi.nlm.nih.gov/pubmed/2573431
Govers, L. P., Toka, H. R., Hariri, A., Walsh, S. B., & Bockenhauer, D. (2021). Mitochondrial DNA mutations in renal disease: an overview. *Pediatr Nephrol*, *36*(1), 9-17. https://doi.org/10.1007/s00467-019-04404-6
Graham, F. L., Smiley, J., Russell, W. C., & Nairn, R. (1977). Characteristics of a human cell line transformed by DNA from human adenovirus type 5. *J Gen Virol*, *36*(1), 59-74. https://doi.org/10.1099/0022-1317-36-1-59
Graham, J. M., Miller, M. E., Stephan, M. J., & Smith, D. W. (1980). Limb reduction anomalies and early in utero limb compression. *J Pediatr*, *96*(6), 1052-1056. https://doi.org/10.1016/s0022-3476(80)80640-8
Grill, A., Schiessl, I. M., Gess, B., Fremter, K., Hammer, A., & Castrop, H. (2016). Salt-losing nephropathy in mice with a null mutation of the Clcnk2 gene. *Acta Physiol (Oxf)*, *218*(3), 198-211. https://doi.org/10.1111/apha.12755
Gu, P., Deng, W., Lei, M., & Chang, S. (2013). Single strand DNA binding proteins 1 and 2 protect newly replicated telomeres. *Cell Res*, *23*(5), 705-719. https://doi.org/10.1038/cr.2013.31
Gunaratnam, L., & Bonventre, J. V. (2009). HIF in kidney disease and development. *J Am Soc Nephrol*, *20*(9), 1877-1887. https://doi.org/10.1681/ASN.2008070804
Haase, V. H. (2006). Hypoxia-inducible factors in the kidney. *Am J Physiol Renal Physiol*, *291*(2), F271-281. https://doi.org/10.1152/ajprenal.00071.2006
Haglund, K., & Dikic, I. (2012). The role of ubiquitylation in receptor endocytosis and endosomal sorting. *J Cell Sci*, *125*(Pt 2), 265-275. https://doi.org/10.1242/jcs.091280
Hamza, A., Herr, D., Solomayer, E. F., & Meyberg-Solomayer, G. (2013). Polyhydramnios: Causes, Diagnosis and Therapy. *Geburtshilfe Frauenheilkd*, *73*(12), 1241-1246. https://doi.org/10.1055/s-0033-1360163
Hannemann, A., Christie, J. K., & Flatman, P. W. (2009). Functional expression of the Na-K-2Cl cotransporter NKCC2 in mammalian cells fails to confirm the dominant-negative effect of the AF splice variant. *J Biol Chem*, *284*(51), 35348-35358. https://doi.org/10.1074/jbc.M109.060004
Hashimoto, R., Kanda, M., Takami, H., Shimizu, D., Oya, H., Hibino, S., Okamura, Y., Yamada, S., Fujii, T., Nakayama, G., Sugimoto, H., Koike, M., Nomoto, S., Fujiwara, M., & Kodera, Y. (2015). Aberrant expression of melanoma-associated antigen-D2 serves as a prognostic indicator of hepatocellular carcinoma outcome following curative hepatectomy. *Oncol Lett*, *9*(3), 1201-1206. https://doi.org/10.3892/ol.2014.2823
Hasler, U., Mordasini, D., Bens, M., Bianchi, M., Cluzeaud, F., Rousselot, M., Vandewalle, A., Feraille, E., & Martin, P. Y. (2002). Long term regulation of aquaporin-2 expression in vasopressin-responsive renal collecting duct principal cells. *J Biol Chem*, *277*(12), 10379-10386. https://doi.org/10.1074/jbc.M111880200
Hayashi, M., Sasaki, S., Tsuganezawa, H., Monkawa, T., Kitajima, W., Konishi, K., Fushimi, K., Marumo, F., & Saruta, T. (1996). Role of vasopressin V2 receptor in acute regulation of aquaporin-2. *Kidney Blood Press Res*, *19*(1), 32-37. https://doi.org/10.1159/000174043

Hebert, S. C. (1998). Roles of Na-K-2Cl and Na-Cl cotransporters and ROMK potassium channels in urinary concentrating mechanism. *Am J Physiol*, *275*(3), F325-327. https://doi.org/10.1152/ajprenal.1998.275.3.F325
Hennings, J. C., Andrini, O., Picard, N., Paulais, M., Huebner, A. K., Cayuqueo, I. K., Bignon, Y., Keck, M., Corniere, N., Bohm, D., Jentsch, T. J., Chambrey, R., Teulon, J., Hubner, C. A., & Eladari, D. (2017). The ClC-K2 Chloride Channel Is Critical for Salt Handling in the Distal Nephron. *J Am Soc Nephrol*, *28*(1), 209-217. https://doi.org/10.1681/ASN.2016010085
Hill, L. M., Breckle, R., Thomas, M. L., & Fries, J. K. (1987). Polyhydramnios: ultrasonically detected prevalence and neonatal outcome. *Obstet Gynecol*, *69*(1), 21-25. https://www.ncbi.nlm.nih.gov/pubmed/3540761
Ho, K., Nichols, C. G., Lederer, W. J., Lytton, J., Vassilev, P. M., Kanazirska, M. V., & Hebert, S. C. (1993). Cloning and expression of an inwardly rectifying ATP-regulated potassium channel. *Nature*, *362*(6415), 31-38. https://doi.org/10.1038/362031a0
Hobbins, J. C., Grannum, P. A., Berkowitz, R. L., Silverman, R., & Mahoney, M. J. (1979). Ultrasound in the diagnosis of congenital anomalies. *Am J Obstet Gynecol*, *134*(3), 331-345. https://doi.org/10.1016/s0002-9378(16)33043-5
Hozawa, S., Holtzman, E. J., & Ausiello, D. A. (1996). cAMP motifs regulating transcription in the aquaporin 2 gene. *Am J Physiol*, *270*(6 Pt 1), C1695-1702. https://doi.org/10.1152/ajpcell.1996.270.6.C1695
Huang, J., Gong, Z., Ghosal, G., & Chen, J. (2009). SOSS complexes participate in the maintenance of genomic stability. *Mol Cell*, *35*(3), 384-393. https://doi.org/10.1016/j.molcel.2009.06.011
Huilgol, D., Venkataramani, P., Nandi, S., & Bhattacharjee, S. (2019). Transcription Factors That Govern Development and Disease: An Achilles Heel in Cancer. *Genes (Basel)*, *10*(10). https://doi.org/10.3390/genes10100794
Huttlin, E. L., Bruckner, R. J., Paulo, J. A., Cannon, J. R., Ting, L., Baltier, K., Colby, G., Gebreab, F., Gygi, M. P., Parzen, H., Szpyt, J., Tam, S., Zarraga, G., Pontano-Vaites, L., Swarup, S., White, A. E., Schweppe, D. K., Rad, R., Erickson, B. K., . . . Harper, J. W. (2017). Architecture of the human interactome defines protein communities and disease networks. *Nature*, *545*(7655), 505-509. https://doi.org/10.1038/nature22366
Hwang, D. S., & Bordoni, B. (2021). Polyhydramnios. In *StatPearls*. https://www.ncbi.nlm.nih.gov/pubmed/32965811
Ikeda, H., & Kakeya, H. (2021). Targeting hypoxia-inducible factor 1 (HIF-1) signaling with natural products toward cancer chemotherapy. *J Antibiot (Tokyo)*, *74*(10), 687-695. https://doi.org/10.1038/s41429-021-00451-0
Insoft, R. M., & Todres, I. D. (2009). CHAPTER 2 - Growth and Development. In C. J. Coté, J. Lerman, & I. D. Todres (Eds.), *A Practice of Anesthesia for Infants and Children (Fourth Edition)* (pp. 7-24). W.B. Saunders. https://doi.org/https://doi.org/10.1016/B978-141603134-5.50006-8
Ito, M., Okano, H. J., Darnell, R. B., & Roeder, R. G. (2002). The TRAP100 component of the TRAP/Mediator complex is essential in broad transcriptional events and development. *EMBO J*, *21*(13), 3464-3475. https://doi.org/10.1093/emboj/cdf348
Ji, W., Foo, J. N., O'Roak, B. J., Zhao, H., Larson, M. G., Simon, D. B., Newton-Cheh, C., State, M. W., Levy, D., & Lifton, R. P. (2008). Rare independent mutations in renal salt handling genes contribute to blood pressure variation. *Nat Genet*, *40*(5), 592-599. https://doi.org/10.1038/ng.118
Jia, B., Zhao, X., Wang, Y., Wang, J., Wang, Y., & Yang, Y. (2019). Prognostic roles of MAGE family members in breast cancer based on KM-Plotter Data. *Oncol Lett*, *18*(4), 3501-3516. https://doi.org/10.3892/ol.2019.10722
Kanda, M., Nomoto, S., Oya, H., Takami, H., Shimizu, D., Hibino, S., Hashimoto, R., Kobayashi, D., Tanaka, C., Yamada, S., Fujii, T., Nakayama, G., Sugimoto, H., Koike, M., Fujiwara, M., & Kodera, Y. (2016). The Expression of Melanoma-Associated Antigen D2 Both in Surgically Resected and Serum Samples Serves as Clinically Relevant Biomarker of Gastric Cancer Progression. *Ann Surg Oncol*, *23 Suppl 2*, S214-221. https://doi.org/10.1245/s10434-015-4457-8

Kantarci, S., Al-Gazali, L., Hill, R. S., Donnai, D., Black, G. C., Bieth, E., Chassaing, N., Lacombe, D., Devriendt, K., Teebi, A., Loscertales, M., Robson, C., Liu, T., MacLaughlin, D. T., Noonan, K. M., Russell, M. K., Walsh, C. A., Donahoe, P. K., & Pober, B. R. (2007). Mutations in LRP2, which encodes the multiligand receptor megalin, cause Donnai-Barrow and facio-oculo-acoustico-renal syndromes. *Nat Genet*, *39*(8), 957-959. https://doi.org/10.1038/ng2063

Katsura, T., Gustafson, C. E., Ausiello, D. A., & Brown, D. (1997). Protein kinase A phosphorylation is involved in regulated exocytosis of aquaporin-2 in transfected LLC-PK1 cells. *Am J Physiol*, *272*(6 Pt 2), F817-822. https://www.ncbi.nlm.nih.gov/pubmed/9227644

Katz, A. I., & Epstein, F. H. (1967). The role of sodium-potassium-activated adenosine triphosphatase in the reabsorption of sodium by the kidney. *J Clin Invest*, *46*(12), 1999-2011. https://doi.org/10.1172/JCI105689

Kemter, E., Rathkolb, B., Becker, L., Bolle, I., Busch, D. H., Dalke, C., Elvert, R., Favor, J., Graw, J., Hans, W., Ivandic, B., Kalaydjiev, S., Klopstock, T., Racz, I., Rozman, J., Schrewe, A., Schulz, H., Zimmer, A., Fuchs, H., . . . Aigner, B. (2014). Standardized, systemic phenotypic analysis of Slc12a1I299F mutant mice. *J Biomed Sci*, *21*(1), 68. https://doi.org/10.1186/s12929-014-0068-0

Kerjaschki, D., & Farquhar, M. G. (1982). The pathogenic antigen of Heymann nephritis is a membrane glycoprotein of the renal proximal tubule brush border. *Proc Natl Acad Sci U S A*, *79*(18), 5557-5561. https://doi.org/10.1073/pnas.79.18.5557

Kieferle, S., Fong, P., Bens, M., Vandewalle, A., & Jentsch, T. J. (1994). Two highly homologous members of the ClC chloride channel family in both rat and human kidney. *Proc Natl Acad Sci U S A*, *91*(15), 6943-6947. https://doi.org/10.1073/pnas.91.15.6943

Kilkenny, C., Browne, W. J., Cuthill, I. C., Emerson, M., & Altman, D. G. (2010). Improving bioscience research reporting: the ARRIVE guidelines for reporting animal research. *PLoS Biol*, *8*(6), e1000412. https://doi.org/10.1371/journal.pbio.1000412

Klaassen, I., & Kemper, M. J. (2010). Oligohydramnion. *Monatsschrift Kinderheilkunde*, *158*(12), 1224-1230. https://doi.org/10.1007/s00112-010-2247-8

Kleta, R., & Bockenhauer, D. (2006). Bartter syndromes and other salt-losing tubulopathies. *Nephron Physiol*, *104*(2), p73-80. https://doi.org/10.1159/000094001

Kleta, R., & Bockenhauer, D. (2018). Salt-Losing Tubulopathies in Children: What's New, What's Controversial? *J Am Soc Nephrol*, *29*(3), 727-739. https://doi.org/10.1681/ASN.2017060600

Kmiec, Z. (2001). Cooperation of liver cells in health and disease. *Adv Anat Embryol Cell Biol*, *161*, III-XIII, 1-151. https://doi.org/10.1007/978-3-642-56553-3

Knoers, N. V. (2006). Gitelman syndrome. *Adv Chronic Kidney Dis*, *13*(2), 148-154. https://doi.org/10.1053/j.ackd.2006.01.014

Knoers, N. V., & Levtchenko, E. N. (2008). Gitelman syndrome. *Orphanet J Rare Dis*, *3*, 22. https://doi.org/10.1186/1750-1172-3-22

Knott, S. R. V., Maceli, A., Erard, N., Chang, K., Marran, K., Zhou, X., Gordon, A., Demerdash, O. E., Wagenblast, E., Kim, S., Fellmann, C., & Hannon, G. J. (2014). A computational algorithm to predict shRNA potency. *Mol Cell*, *56*(6), 796-807. https://doi.org/10.1016/j.molcel.2014.10.025

Kompatscher, A., de Baaij, J. H. F., Aboudehen, K., Farahani, S., van Son, L. H. J., Milatz, S., Himmerkus, N., Veenstra, G. C., Bindels, R. J. M., & Hoenderop, J. G. J. (2018). Transcription factor HNF1beta regulates expression of the calcium-sensing receptor in the thick ascending limb of the kidney. *Am J Physiol Renal Physiol*, *315*(1), F27-F35. https://doi.org/10.1152/ajprenal.00601.2017

Konrad, M., Nijenhuis, T., Ariceta, G., Bertholet-Thomas, A., Calo, L. A., Capasso, G., Emma, F., Schlingmann, K. P., Singh, M., Trepiccione, F., Walsh, S. B., Whitton, K., Vargas-Poussou, R., & Bockenhauer, D. (2021). Diagnosis and management of Bartter syndrome: executive summary of the consensus and recommendations from the European Rare Kidney Disease Reference Network Working Group for Tubular Disorders. *Kidney Int*, *99*(2), 324-335. https://doi.org/10.1016/j.kint.2020.10.035

Kortenoeven, M. L., Trimpert, C., van den Brand, M., Li, Y., Wetzels, J. F., & Deen, P. M. (2012). In mpkCCD cells, long-term regulation of aquaporin-2 by vasopressin occurs independent of protein kinase A and CREB but may involve Epac. *Am J Physiol Renal Physiol*, *302*(11), F1395-1401. https://doi.org/10.1152/ajprenal.00376.2011
Kowalczyk, C., Dunkel, N., Willen, L., Casal, M. L., Mauldin, E. A., Gaide, O., Tardivel, A., Badic, G., Etter, A. L., Favre, M., Jefferson, D. M., Headon, D. J., Demotz, S., & Schneider, P. (2011). Molecular and therapeutic characterization of anti-ectodysplasin A receptor (EDAR) agonist monoclonal antibodies. *J Biol Chem*, *286*(35), 30769-30779. https://doi.org/10.1074/jbc.M111.267997
Kozyraki, R., & Gofflot, F. (2007). Multiligand endocytosis and congenital defects: roles of cubilin, megalin and amnionless. *Curr Pharm Des*, *13*(29), 3038-3046. https://doi.org/10.2174/138161207782110507
Krupnick, J. G., & Benovic, J. L. (1998). The role of receptor kinases and arrestins in G protein-coupled receptor regulation. *Annu Rev Pharmacol Toxicol*, *38*, 289-319. https://doi.org/10.1146/annurev.pharmtox.38.1.289
Kuo, K. T., Yang, C. W., & Yu, M. J. (2018). Dexamethasone enhances vasopressin-induced aquaporin-2 gene expression in the mpkCCD cells. *Am J Physiol Renal Physiol*, *314*(2), F219-F229. https://doi.org/10.1152/ajprenal.00218.2017
Laghmani, K., Beck, B. B., Yang, S. S., Seaayfan, E., Wenzel, A., Reusch, B., Vitzthum, H., Priem, D., Demaretz, S., Bergmann, K., Duin, L. K., Gobel, H., Mache, C., Thiele, H., Bartram, M. P., Dombret, C., Altmuller, J., Nurnberg, P., Benzing, T., . . . Komhoff, M. (2016). Polyhydramnios, Transient Antenatal Bartter's Syndrome, and MAGED2 Mutations. *N Engl J Med*, *374*(19), 1853-1863. https://doi.org/10.1056/NEJMoa1507629
Lallar, M., Anam Ul, H., & Nandal, R. (2015). Perinatal Outcome in Idiopathic Polyhydramnios. *J Obstet Gynaecol India*, *65*(5), 310-314. https://doi.org/10.1007/s13224-014-0625-1
Langnaese, K., Kloos, D. U., Wehnert, M., Seidel, B., & Wieacker, P. (2001). Expression pattern and further characterization of human MAGED2 and identification of rodent orthologues. *Cytogenet Cell Genet*, *94*(3-4), 233-240. https://doi.org/10.1159/000048822
Lee, A. K., & Potts, P. R. (2017). A Comprehensive Guide to the MAGE Family of Ubiquitin Ligases. *J Mol Biol*, *429*(8), 1114-1142. https://doi.org/10.1016/j.jmb.2017.03.005
Lee, H.-J., & Zheng, J. J. (2010). PDZ domains and their binding partners: structure, specificity, and modification. *Cell Communication and Signaling*, *8*(1), 8. https://doi.org/10.1186/1478-811X-8-8
Lee, J. W., Chou, C. L., & Knepper, M. A. (2015). Deep Sequencing in Microdissected Renal Tubules Identifies Nephron Segment-Specific Transcriptomes. *J Am Soc Nephrol*, *26*(11), 2669-2677. https://doi.org/10.1681/ASN.2014111067
Legrand, A., Treard, C., Roncelin, I., Dreux, S., Bertholet-Thomas, A., Broux, F., Bruno, D., Decramer, S., Deschenes, G., Djeddi, D., Guigonis, V., Jay, N., Khalifeh, T., Llanas, B., Morin, D., Morin, G., Nobili, F., Pietrement, C., Ryckewaert, A., . . . Vargas-Poussou, R. (2018). Prevalence of Novel MAGED2 Mutations in Antenatal Bartter Syndrome. *Clin J Am Soc Nephrol*, *13*(2), 242-250. https://doi.org/10.2215/cjn.05670517
Lenzen, H., Lunnemann, M., Bleich, A., Manns, M. P., Seidler, U., & Jorns, A. (2012). Downregulation of the NHE3-binding PDZ-adaptor protein PDZK1 expression during cytokine-induced inflammation in interleukin-10-deficient mice. *PLoS One*, *7*(7), e40657. https://doi.org/10.1371/journal.pone.0040657
Lethagen, S. (1994). Desmopressin (DDAVP) and hemostasis. *Ann Hematol*, *69*(4), 173-180. https://doi.org/10.1007/BF02215950
Li, R., Gong, J., Xiao, C., Zhu, S., Hu, Z., Liang, J., Li, X., Yan, X., Zhang, X., Li, D., Liu, W., Chong, Y., & Jie, Y. (2020). A comprehensive analysis of the MAGE family as prognostic and diagnostic markers for hepatocellular carcinoma. *Genomics*, *112*(6), 5101-5114. https://doi.org/10.1016/j.ygeno.2020.09.026

Limbutara, K., Kelleher, A., Yang, C. R., Raghuram, V., & Knepper, M. A. (2019). Phosphorylation Changes in Response to Kinase Inhibitor H89 in PKA-Null Cells. *Sci Rep*, *9*(1), 2814. https://doi.org/10.1038/s41598-019-39116-2
Liu, A., Yu, X., & Liu, S. (2013). Pluripotency transcription factors and cancer stem cells: small genes make a big difference. *Chin J Cancer*, *32*(9), 483-487. https://doi.org/10.5732/cjc.012.10282
Liu, X., Zhou, T., Kuriyama, R., & Erikson, R. L. (2004). Molecular interactions of Polo-like-kinase 1 with the mitotic kinesin-like protein CHO1/MKLP-1. *J Cell Sci*, *117*(Pt 15), 3233-3246. https://doi.org/10.1242/jcs.01173
Lucas, S., Brasseur, F., & Boon, T. (1999). A new MAGE gene with ubiquitous expression does not code for known MAGE antigens recognized by T cells. *Cancer Res*, *59*(16), 4100-4103. https://www.ncbi.nlm.nih.gov/pubmed/10463614
Lucas, S., De Plaen, E., & Boon, T. (2000). MAGE-B5, MAGE-B6, MAGE-C2, and MAGE-C3: four new members of the MAGE family with tumor-specific expression. *Int J Cancer*, *87*(1), 55-60. https://www.ncbi.nlm.nih.gov/pubmed/10861452
Lucas, S., De Smet, C., Arden, K. C., Viars, C. S., Lethe, B., Lurquin, C., & Boon, T. (1998). Identification of a new MAGE gene with tumor-specific expression by representational difference analysis. *Cancer Res*, *58*(4), 743-752. https://www.ncbi.nlm.nih.gov/pubmed/9485030
Lurquin, C., De Smet, C., Brasseur, F., Muscatelli, F., Martelange, V., De Plaen, E., Brasseur, R., Monaco, A. P., & Boon, T. (1997). Two members of the human MAGEB gene family located in Xp21.3 are expressed in tumors of various histological origins. *Genomics*, *46*(3), 397-408. https://doi.org/10.1006/geno.1997.5052
Ma, M., Zhang, M., Zhou, Y., Yao, F., Wei, M., Li, Z., & Qiu, Z. (2021). A novel MAGED2 variant in a Chinese preterm newborn with transient antenatal Bartter's syndrome with 4 years follow-up. *BMC Nephrol*, *22*(1), 408. https://doi.org/10.1186/s12882-021-02553-1
Magann, E. F., Chauhan, S. P., Doherty, D. A., Lutgendorf, M. A., Magann, M. I., & Morrison, J. C. (2007). A review of idiopathic hydramnios and pregnancy outcomes. *Obstet Gynecol Surv*, *62*(12), 795-802. https://doi.org/10.1097/01.ogx.0000290349.58707.e0
Majeed, M., Nagabhushanam, K., Natarajan, S., Vaidyanathan, P., Karri, S. K., & Jose, J. A. (2015). Efficacy and safety of 1% forskolin eye drops in open angle glaucoma - An open label study. *Saudi J Ophthalmol*, *29*(3), 197-200. https://doi.org/10.1016/j.sjopt.2015.02.003
Manning, F. A., Hill, L. M., & Platt, L. D. (1981). Qualitative amniotic fluid volume determination by ultrasound: antepartum detection of intrauterine growth retardation. *Am J Obstet Gynecol*, *139*(3), 254-258. https://doi.org/10.1016/0002-9378(81)90004-1
Mansoor, S. E., Dewitt, M. A., & Farrens, D. L. (2010). Distance mapping in proteins using fluorescence spectroscopy: the tryptophan-induced quenching (TrIQ) method. *Biochemistry*, *49*(45), 9722-9731. https://doi.org/10.1021/bi100907m
Manzo, G. (1989). Phylogenesis--ontogenesis--oncogenesis. *Med Hypotheses*, *30*(4), 245-257. https://doi.org/10.1016/0306-9877(89)90033-9
Manzo, G. (2019). Similarities Between Embryo Development and Cancer Process Suggest New Strategies for Research and Therapy of Tumors: A New Point of View. *Front Cell Dev Biol*, *7*, 20. https://doi.org/10.3389/fcell.2019.00020
Masilamani, S., Kim, G. H., Mitchell, C., Wade, J. B., & Knepper, M. A. (1999). Aldosterone-mediated regulation of ENaC alpha, beta, and gamma subunit proteins in rat kidney. *J Clin Invest*, *104*(7), R19-23. https://doi.org/10.1172/JCI7840
Matsumura, Y., Uchida, S., Kondo, Y., Miyazaki, H., Ko, S. B., Hayama, A., Morimoto, T., Liu, W., Arisawa, M., Sasaki, S., & Marumo, F. (1999). Overt nephrogenic diabetes insipidus in mice lacking the CLC-K1 chloride channel. *Nat Genet*, *21*(1), 95-98. https://doi.org/10.1038/5036
Matsumura, Y., Uchida, S., Rai, T., Sasaki, S., & Marumo, F. (1997). Transcriptional regulation of aquaporin-2 water channel gene by cAMP. *J Am Soc Nephrol*, *8*(6), 861-867. https://doi.org/10.1681/ASN.V86861

Matsuoka, S., Ballif, B. A., Smogorzewska, A., McDonald, E. R., 3rd, Hurov, K. E., Luo, J., Bakalarski, C. E., Zhao, Z., Solimini, N., Lerenthal, Y., Shiloh, Y., Gygi, S. P., & Elledge, S. J. (2007). ATM and ATR substrate analysis reveals extensive protein networks responsive to DNA damage. *Science*, *316*(5828), 1160-1166. https://doi.org/10.1126/science.1140321

Matsuoka, S., Rotman, G., Ogawa, A., Shiloh, Y., Tamai, K., & Elledge, S. J. (2000). Ataxia telangiectasia-mutated phosphorylates Chk2 in vivo and in vitro. *Proc Natl Acad Sci U S A*, *97*(19), 10389-10394. https://doi.org/10.1073/pnas.190030497

Maxwell, P. H., Wiesener, M. S., Chang, G. W., Clifford, S. C., Vaux, E. C., Cockman, M. E., Wykoff, C. C., Pugh, C. W., Maher, E. R., & Ratcliffe, P. J. (1999). The tumour suppressor protein VHL targets hypoxia-inducible factors for oxygen-dependent proteolysis. *Nature*, *399*(6733), 271-275. https://doi.org/10.1038/20459

McCarthy, R. A., Barth, J. L., Chintalapudi, M. R., Knaak, C., & Argraves, W. S. (2002). Megalin Functions as an Endocytic Sonic Hedgehog Receptor*. *Journal of Biological Chemistry*, *277*(28), 25660-25667. https://doi.org/https://doi.org/10.1074/jbc.M201933200

McKusick, V. A. (2007). Mendelian Inheritance in Man and its online version, OMIM. *Am J Hum Genet*, *80*(4), 588-604. https://doi.org/10.1086/514346

Meyer, M., Berrios, M., & Lo, C. (2018). Transient Antenatal Bartter's Syndrome: A Case Report. *Front Pediatr*, *6*, 51. https://doi.org/10.3389/fped.2018.00051

Miller, M. E., Graham, J. M., Jr., Higginbottom, M. C., & Smith, D. W. (1981). Compression-related defects from early amnion rupture: evidence for mechanical teratogenesis. *J Pediatr*, *98*(2), 292-297. https://doi.org/10.1016/s0022-3476(81)80664-6

Milligan, G., & Kostenis, E. (2006). Heterotrimeric G-proteins: a short history. *Br J Pharmacol*, *147 Suppl 1*(Suppl 1), S46-55. https://doi.org/10.1038/sj.bjp.0706405

Moeller, H. B., Rittig, S., & Fenton, R. A. (2013). Nephrogenic diabetes insipidus: essential insights into the molecular background and potential therapies for treatment. *Endocr Rev*, *34*(2), 278-301. https://doi.org/10.1210/er.2012-1044

Moh, W., Graham, J. M., Jr., Wadhawan, I., & Sanchez-Lara, P. A. (2012). Extrinsic factors influencing fetal deformations and intrauterine growth restriction. *J Pregnancy*, *2012*, 750485. https://doi.org/10.1155/2012/750485

Montminy, M. R., & Bilezikjian, L. M. (1987). Binding of a nuclear protein to the cyclic-AMP response element of the somatostatin gene. *Nature*, *328*(6126), 175-178. https://doi.org/10.1038/328175a0

Moore, C. B., Guthrie, E. H., Huang, M. T., & Taxman, D. J. (2010). Short hairpin RNA (shRNA): design, delivery, and assessment of gene knockdown. *Methods Mol Biol*, *629*, 141-158. https://doi.org/10.1007/978-1-60761-657-3_10

Moore, T. R., & Cayle, J. E. (1990). The amniotic fluid index in normal human pregnancy. *Am J Obstet Gynecol*, *162*(5), 1168-1173. https://doi.org/10.1016/0002-9378(90)90009-v

Muscatelli, F., Walker, A. P., De Plaen, E., Stafford, A. N., & Monaco, A. P. (1995). Isolation and characterization of a MAGE gene family in the Xp21.3 region. *Proc Natl Acad Sci U S A*, *92*(11), 4987-4991. https://doi.org/10.1073/pnas.92.11.4987

Nakhoul, N., & Batuman, V. (2011). Role of proximal tubules in the pathogenesis of kidney disease. *Contrib Nephrol*, *169*, 37-50. https://doi.org/10.1159/000313944

Nedvetsky, P. I., Stefan, E., Frische, S., Santamaria, K., Wiesner, B., Valenti, G., Hammer, J. A., 3rd, Nielsen, S., Goldenring, J. R., Rosenthal, W., & Klussmann, E. (2007). A Role of myosin Vb and Rab11-FIP2 in the aquaporin-2 shuttle. *Traffic*, *8*(2), 110-123. https://doi.org/10.1111/j.1600-0854.2006.00508.x

Newman, J. A., Cooper, C. D., Roos, A. K., Aitkenhead, H., Oppermann, U. C., Cho, H. J., Osman, R., & Gileadi, O. (2016). Structures of Two Melanoma-Associated Antigens Suggest Allosteric Regulation of Effector Binding. *PLoS One*, *11*(2), e0148762. https://doi.org/10.1371/journal.pone.0148762

Nguengang Wakap, S., Lambert, D. M., Olry, A., Rodwell, C., Gueydan, C., Lanneau, V., Murphy, D., Le Cam, Y., & Rath, A. (2020). Estimating cumulative point prevalence of rare diseases: analysis of the Orphanet database. *European Journal of Human Genetics*, *28*(2), 165-173. https://doi.org/10.1038/s41431-019-0508-0

Nichols, J., Zevnik, B., Anastassiadis, K., Niwa, H., Klewe-Nebenius, D., Chambers, I., Scholer, H., & Smith, A. (1998). Formation of pluripotent stem cells in the mammalian embryo depends on the POU transcription factor Oct4. *Cell*, *95*(3), 379-391. https://doi.org/10.1016/s0092-8674(00)81769-9
Nielsen, R., Christensen, E. I., & Birn, H. (2016). Megalin and cubilin in proximal tubule protein reabsorption: from experimental models to human disease. *Kidney Int*, *89*(1), 58-67. https://doi.org/10.1016/j.kint.2015.11.007
Nielsen, S., Chou, C. L., Marples, D., Christensen, E. I., Kishore, B. K., & Knepper, M. A. (1995). Vasopressin increases water permeability of kidney collecting duct by inducing translocation of aquaporin-CD water channels to plasma membrane. *Proc Natl Acad Sci U S A*, *92*(4), 1013-1017. https://doi.org/10.1073/pnas.92.4.1013
Nijenhuis, T., Vallon, V., van der Kemp, A. W., Loffing, J., Hoenderop, J. G., & Bindels, R. J. (2005). Enhanced passive Ca2+ reabsorption and reduced Mg2+ channel abundance explains thiazide-induced hypocalciuria and hypomagnesemia. *J Clin Invest*, *115*(6), 1651-1658. https://doi.org/10.1172/JCI24134
Ning, L., Suleiman, H. Y., & Miner, J. H. (2020). Synaptopodin Is Dispensable for Normal Podocyte Homeostasis but Is Protective in the Context of Acute Podocyte Injury. *J Am Soc Nephrol*, *31*(12), 2815-2832. https://doi.org/10.1681/ASN.2020050572
Ohlsson, A., Sieck, U., Cumming, W., Akhtar, M., & Serenius, F. (1984). A variant of Bartter's syndrome. Bartter's syndrome associated with hydramnios, prematurity, hypercalciuria and nephrocalcinosis. *Acta Paediatr Scand*, *73*(6), 868-874. https://doi.org/10.1111/j.1651-2227.1984.tb17793.x
Oksche, A., & Rosenthal, W. (1998). The molecular basis of nephrogenic diabetes insipidus. *J Mol Med (Berl)*, *76*(5), 326-337. https://doi.org/10.1007/s001090050224
Ostergard, D. R. (1970). The physiology and clinical importance of amniotic fluid. A review. *Obstet Gynecol Surv*, *25*(4), 297-319. https://doi.org/10.1097/00006254-197004000-00001
Paek, J., Kalocsay, M., Staus, D. P., Wingler, L., Pascolutti, R., Paulo, J. A., Gygi, S. P., & Kruse, A. C. (2017). Multidimensional Tracking of GPCR Signaling via Peroxidase-Catalyzed Proximity Labeling. *Cell*, *169*(2), 338-349 e311. https://doi.org/10.1016/j.cell.2017.03.028
Papageorgio, C., Brachmann, R., Zeng, J., Culverhouse, R., Zhang, W., & McLeod, H. (2007). MAGED2: a novel p53-dissociator. *Int J Oncol*, *31*(5), 1205-1211.
Paquet, N., Adams, M. N., Leong, V., Ashton, N. W., Touma, C., Gamsjaeger, R., Cubeddu, L., Beard, S., Burgess, J. T., Bolderson, E., O'Byrne, K. J., & Richard, D. J. (2015). hSSB1 (NABP2/ OBFC2B) is required for the repair of 8-oxo-guanine by the hOGG1-mediated base excision repair pathway. *Nucleic Acids Res*, *43*(18), 8817-8829. https://doi.org/10.1093/nar/gkv790
Peipert, J. F., & Donnenfeld, A. E. (1991). Oligohydramnios: a review. *Obstet Gynecol Surv*, *46*(6), 325-339. https://doi.org/10.1097/00006254-199106000-00002
Peti-Peterdi, J. (2015). Newly stemming functions of macula densa-derived prostanoids. *Hypertension*, *65*(5), 987-988. https://doi.org/10.1161/HYPERTENSIONAHA.115.04739
Phelan, J. P., Ahn, M. O., Smith, C. V., Rutherford, S. E., & Anderson, E. (1987). Amniotic fluid index measurements during pregnancy. *J Reprod Med*, *32*(8), 601-604. https://www.ncbi.nlm.nih.gov/pubmed/3309290
Pirlot, C., Thiry, M., Trussart, C., Di Valentin, E., Piette, J., & Habraken, Y. (2016). Melanoma antigen-D2: A nucleolar protein undergoing delocalization during cell cycle and after cellular stress. *Biochim Biophys Acta*, *1863*(4), 581-595. https://doi.org/10.1016/j.bbamcr.2015.12.010
Pober, B. R., Longoni, M., & Noonan, K. M. (2009). A review of Donnai-Barrow and facio-oculo-acoustico-renal (DB/FOAR) syndrome: clinical features and differential diagnosis. *Birth Defects Res A Clin Mol Teratol*, *85*(1), 76-81. https://doi.org/10.1002/bdra.20534
Potter, E. L. (1946). Bilateral renal agenesis. *J Pediatr*, *29*, 68-76. https://doi.org/10.1016/s0022-3476(46)80241-5

Preininger, A. M., Meiler, J., & Hamm, H. E. (2013). Conformational flexibility and structural dynamics in GPCR-mediated G protein activation: a perspective. *J Mol Biol*, *425*(13), 2288-2298. https://doi.org/10.1016/j.jmb.2013.04.011

Pri-Paz, S., Khalek, N., Fuchs, K. M., & Simpson, L. L. (2012). Maximal amniotic fluid index as a prognostic factor in pregnancies complicated by polyhydramnios. *Ultrasound Obstet Gynecol*, *39*(6), 648-653. https://doi.org/10.1002/uog.10093

Rajerison, R. M., Butlen, D., & Jard, S. (1976). Ontogenic development of antidiuretic hormone receptors in rat kidney: comparison of hormonal binding and adenylate cyclase activation. *Mol Cell Endocrinol*, *4*(4), 271-285. https://doi.org/10.1016/0303-7207(76)90061-7

Rappsilber, J., Ishihama, Y., & Mann, M. (2003). Stop and go extraction tips for matrix-assisted laser desorption/ionization, nanoelectrospray, and LC/MS sample pretreatment in proteomics. *Anal Chem*, *75*(3), 663-670. https://www.ncbi.nlm.nih.gov/pubmed/12585499

Raychowdhury, R., Niles, J. L., McCluskey, R. T., & Smith, J. A. (1989). Autoimmune target in Heymann nephritis is a glycoprotein with homology to the LDL receptor. *Science*, *244*(4909), 1163-1165. https://doi.org/10.1126/science.2786251

Regulation (EC) N°141/2000 of the European Parliament and of the Council of 16 December 1999 on orphan medicinal products, (2000). http://eurlex.europa.eu/LexUriServ/LexUriServ.do?uri=OJ:L:2000:018:0001:0005:EN:PDF

Reinalter, S., Devlieger, H., & Proesmans, W. (1998). Neonatal Bartter syndrome: spontaneous resolution of all signs and symptoms. *Pediatr Nephrol*, *12*(3), 186-188. https://doi.org/10.1007/s004670050433

Reinhardt, H. C., & Yaffe, M. B. (2009). Kinases that control the cell cycle in response to DNA damage: Chk1, Chk2, and MK2. *Curr Opin Cell Biol*, *21*(2), 245-255. https://doi.org/10.1016/j.ceb.2009.01.018

Reusch, B., Bartram, M. P., Dafinger, C., Palacio-Escat, N., Wenzel, A., Fenton, R. A., Saez-Rodriguez, J., Schermer, B., Benzing, T., Altmuller, J., Beck, B. B., & Rinschen, M. M. (2021). MAGED2 controls vasopressin-induced aquaporin-2 expression in collecting duct cells. *J Proteomics*, 104424. https://doi.org/10.1016/j.jprot.2021.104424

Rezvani, H. R., Ali, N., Nissen, L. J., Harfouche, G., de Verneuil, H., Taieb, A., & Mazurier, F. (2011). HIF-1alpha in epidermis: oxygen sensing, cutaneous angiogenesis, cancer, and non-cancer disorders. *J Invest Dermatol*, *131*(9), 1793-1805. https://doi.org/10.1038/jid.2011.141

Richard, D. J., Bolderson, E., Cubeddu, L., Wadsworth, R. I., Savage, K., Sharma, G. G., Nicolette, M. L., Tsvetanov, S., McIlwraith, M. J., Pandita, R. K., Takeda, S., Hay, R. T., Gautier, J., West, S. C., Paull, T. T., Pandita, T. K., White, M. F., & Khanna, K. K. (2008). Single-stranded DNA-binding protein hSSB1 is critical for genomic stability. *Nature*, *453*(7195), 677-681. https://doi.org/10.1038/nature06883

Richter, W. F., Nayak, S., Iwasa, J., & Taatjes, D. J. (2022). The Mediator complex as a master regulator of transcription by RNA polymerase II. *Nat Rev Mol Cell Biol*, *23*(11), 732-749. https://doi.org/10.1038/s41580-022-00498-3

Rieg, T., Tang, T., Uchida, S., Hammond, H. K., Fenton, R. A., & Vallon, V. (2013). Adenylyl cyclase 6 enhances NKCC2 expression and mediates vasopressin-induced phosphorylation of NKCC2 and NCC. *Am J Pathol*, *182*(1), 96-106. https://doi.org/10.1016/j.ajpath.2012.09.014

Rinschen, M. M., Wu, X., Konig, T., Pisitkun, T., Hagmann, H., Pahmeyer, C., Lamkemeyer, T., Kohli, P., Schnell, N., Schermer, B., Dryer, S., Brooks, B. R., Beltrao, P., Krueger, M., Brinkkoetter, P. T., & Benzing, T. (2014). Phosphoproteomic analysis reveals regulatory mechanisms at the kidney filtration barrier. *J Am Soc Nephrol*, *25*(7), 1509-1522. https://doi.org/10.1681/ASN.2013070760

Rinschen, M. M., Yu, M. J., Wang, G., Boja, E. S., Hoffert, J. D., Pisitkun, T., & Knepper, M. A. (2010). Quantitative phosphoproteomic analysis reveals vasopressin V2-receptor-dependent signaling pathways in renal collecting duct cells. *Proc Natl Acad Sci U S A*, *107*(8), 3882-3887. https://doi.org/10.1073/pnas.0910646107

Ritchie, M. E., Phipson, B., Wu, D., Hu, Y., Law, C. W., Shi, W., & Smyth, G. K. (2015). limma powers differential expression analyses for RNA-sequencing and microarray studies. *Nucleic Acids Res*, *43*(7), e47. https://doi.org/10.1093/nar/gkv007
Ritter, S. L., & Hall, R. A. (2009). Fine-tuning of GPCR activity by receptor-interacting proteins. *Nat Rev Mol Cell Biol*, *10*(12), 819-830. https://doi.org/10.1038/nrm2803
Robinson, P. J., Trnka, M. J., Pellarin, R., Greenberg, C. H., Bushnell, D. A., Davis, R., Burlingame, A. L., Sali, A., & Kornberg, R. D. (2015). Molecular architecture of the yeast Mediator complex. *Elife*, *4*. https://doi.org/10.7554/eLife.08719
Rodriguez-Soriano, J., Vallo, A., Perez de Nanclares, G., Bilbao, J. R., & Castano, L. (2005). A founder mutation in the CLCNKB gene causes Bartter syndrome type III in Spain. *Pediatr Nephrol*, *20*(7), 891-896. https://doi.org/10.1007/s00467-005-1867-z
Rogner, U. C., Wilke, K., Steck, E., Korn, B., & Poustka, A. (1995). The melanoma antigen gene (MAGE) family is clustered in the chromosomal band Xq28. *Genomics*, *29*(3), 725-731. https://doi.org/10.1006/geno.1995.9945
Rosenthal, W., Seibold, A., Antaramian, A., Lonergan, M., Arthus, M. F., Hendy, G. N., Birnbaumer, M., & Bichet, D. G. (1992). Molecular identification of the gene responsible for congenital nephrogenic diabetes insipidus. *Nature*, *359*(6392), 233-235. https://doi.org/10.1038/359233a0
Roy, N., & Hebrok, M. (2015). Regulation of Cellular Identity in Cancer. *Dev Cell*, *35*(6), 674-684. https://doi.org/10.1016/j.devcel.2015.12.001
Rozansky, D. J., Cornwall, T., Subramanya, A. R., Rogers, S., Yang, Y. F., David, L. L., Zhu, X., Yang, C. L., & Ellison, D. H. (2009). Aldosterone mediates activation of the thiazide-sensitive Na-Cl cotransporter through an SGK1 and WNK4 signaling pathway. *J Clin Invest*, *119*(9), 2601-2612. https://doi.org/10.1172/JCI38323
Rubin, J. D., & Barry, M. A. (2020). Improving Molecular Therapy in the Kidney. *Mol Diagn Ther*, *24*(4), 375-396. https://doi.org/10.1007/s40291-020-00467-6
Rubin, J. D., Nguyen, T. V., Allen, K. L., Ayasoufi, K., & Barry, M. A. (2019). Comparison of Gene Delivery to the Kidney by Adenovirus, Adeno-Associated Virus, and Lentiviral Vectors After Intravenous and Direct Kidney Injections. *Hum Gene Ther*, *30*(12), 1559-1571. https://doi.org/10.1089/hum.2019.127
Ruttkowski, L. L. (2021). *Der Einfluss von MAGED2 auf NHE3 in humanen embryonalen Nierenzellen (HEK293)*. Philipps-Universität Marburg. https://doi.org/10.17192/z2021.0270
Ryan, H. E., Lo, J., & Johnson, R. S. (1998). HIF-1 alpha is required for solid tumor formation and embryonic vascularization. *EMBO J*, *17*(11), 3005-3015. https://doi.org/10.1093/emboj/17.11.3005
Sanchez, A. B., Calpena, A. C., Mallandrich, M., & Clares, B. (2019). Validation of an Ex Vivo Permeation Method for the Intestinal Permeability of Different BCS Drugs and Its Correlation with Caco-2 In Vitro Experiments. *Pharmaceutics*, *11*(12). https://doi.org/10.3390/pharmaceutics11120638
Sandoval, P. C., Claxton, J. S., Lee, J. W., Saeed, F., Hoffert, J. D., & Knepper, M. A. (2016). Systems-level analysis reveals selective regulation of Aqp2 gene expression by vasopressin. *Sci Rep*, *6*, 34863. https://doi.org/10.1038/srep34863
Schaaf, C. P., Gonzalez-Garay, M. L., Xia, F., Potocki, L., Gripp, K. W., Zhang, B., Peters, B. A., McElwain, M. A., Drmanac, R., Beaudet, A. L., Caskey, C. T., & Yang, Y. (2013). Truncating mutations of MAGEL2 cause Prader-Willi phenotypes and autism. *Nat Genet*, *45*(11), 1405-1408. https://doi.org/10.1038/ng.2776
Schenk, L. K., Bolger, S. J., Luginbuhl, K., Gonzales, P. A., Rinschen, M. M., Yu, M. J., Hoffert, J. D., Pisitkun, T., & Knepper, M. A. (2012). Quantitative proteomics identifies vasopressin-responsive nuclear proteins in collecting duct cells. *J Am Soc Nephrol*, *23*(6), 1008-1018. https://doi.org/10.1681/ASN.2011070738
Schepkens, H., Stubbe, J., Hoeben, H., Vanholder, R., & Lameire, N. (2001). Severe hyponatraemia and hypouricaemia in Gitelman's syndrome. *Nephrol Dial Transplant*, *16*(11), 2250-2252. https://doi.org/10.1093/ndt/16.11.2250
Schlingmann, K. P., Konrad, M., Jeck, N., Waldegger, P., Reinalter, S. C., Holder, M., Seyberth, H. W., & Waldegger, S. (2004). Salt wasting and deafness resulting from

mutations in two chloride channels. *N Engl J Med*, *350*(13), 1314-1319. https://doi.org/10.1056/NEJMoa032843
Schneider, H., Faschingbauer, F., Schuepbach-Mallepell, S., Korber, I., Wohlfart, S., Dick, A., Wahlbuhl, M., Kowalczyk-Quintas, C., Vigolo, M., Kirby, N., Tannert, C., Rompel, O., Rascher, W., Beckmann, M. W., & Schneider, P. (2018). Prenatal Correction of X-Linked Hypohidrotic Ectodermal Dysplasia. *N Engl J Med*, *378*(17), 1604-1610. https://doi.org/10.1056/NEJMoa1714322
Seaayfan, E., Nasrah, S., Quell, L., Kleim, M., Weber, S., Meyer, H., Laghmani, K., & Komhoff, M. (2022). MAGED2 Is Required under Hypoxia for cAMP Signaling by Inhibiting MDM2-Dependent Endocytosis of G-Alpha-S. *Cells*, *11*(16). https://doi.org/10.3390/cells11162546
Seaayfan, E., Nasrah, S., Quell, L., Radi, A., Kleim, M., Schermuly, R. T., Weber, S., Laghmani, K., & Komhoff, M. (2022). Reciprocal Regulation of MAGED2 and HIF-1alpha Augments Their Expression under Hypoxia: Role of cAMP and PKA Type II. *Cells*, *11*(21). https://doi.org/10.3390/cells11213424
Seyberth, H. W., Rascher, W., Schweer, H., Kuhl, P. G., Mehls, O., & Scharer, K. (1985). Congenital hypokalemia with hypercalciuria in preterm infants: a hyperprostaglandinuric tubular syndrome different from Bartter syndrome. *J Pediatr*, *107*(5), 694-701. https://doi.org/10.1016/s0022-3476(85)80395-4
Seyberth, H. W., & Schlingmann, K. P. (2011). Bartter- and Gitelman-like syndromes: salt-losing tubulopathies with loop or DCT defects. *Pediatr Nephrol*, *26*(10), 1789-1802. https://doi.org/10.1007/s00467-011-1871-4
Seys, E., Andrini, O., Keck, M., Mansour-Hendili, L., Courand, P. Y., Simian, C., Deschenes, G., Kwon, T., Bertholet-Thomas, A., Bobrie, G., Borde, J. S., Bourdat-Michel, G., Decramer, S., Cailliez, M., Krug, P., Cozette, P., Delbet, J. D., Dubourg, L., Chaveau, D., . . . Vargas-Poussou, R. (2017). Clinical and Genetic Spectrum of Bartter Syndrome Type 3. *J Am Soc Nephrol*, *28*(8), 2540-2552. https://doi.org/10.1681/ASN.2016101057
Shaikh, D., Zhou, Q., Chen, T., Ibe, J. C., Raj, J. U., & Zhou, G. (2012). cAMP-dependent protein kinase is essential for hypoxia-mediated epithelial-mesenchymal transition, migration, and invasion in lung cancer cells. *Cell Signal*, *24*(12), 2396-2406. https://doi.org/10.1016/j.cellsig.2012.08.007
Shayman, J. A. (2006). Thinking about rare kidney diseases. *J Am Soc Nephrol*, *17*(1), 15-16. https://doi.org/10.1681/ASN.2005101143
Shen, Y., Zhang, Y., Du, J., Jiang, B., Shan, T., Li, H., Bao, H., & Si, Y. (2021). CXCR5 down-regulation alleviates cognitive dysfunction in a mouse model of sepsis-associated encephalopathy: potential role of microglial autophagy and the p38MAPK/NF-kappaB/STAT3 signaling pathway. *J Neuroinflammation*, *18*(1), 246. https://doi.org/10.1186/s12974-021-02300-1
Shu, Y. M., Zeng, H. T., Ren, Z., Zhuang, G. L., Liang, X. Y., Shen, H. W., Yao, S. Z., Ke, P. Q., & Wang, N. N. (2008). Effects of cilostamide and forskolin on the meiotic resumption and embryonic development of immature human oocytes. *Hum Reprod*, *23*(3), 504-513. https://doi.org/10.1093/humrep/dem344
Sigmon, D. F., Eovaldi, B. J., & Cohen, H. L. (2022). Duodenal Atresia And Stenosis. In *StatPearls*. https://www.ncbi.nlm.nih.gov/pubmed/29261981
Simko, V., Iuliano, F., Sevcikova, A., Labudova, M., Barathova, M., Radvak, P., Pastorekova, S., Pastorek, J., & Csaderova, L. (2017). Hypoxia induces cancer-associated cAMP/PKA signalling through HIF-mediated transcriptional control of adenylyl cyclases VI and VII. *Sci Rep*, *7*(1), 10121. https://doi.org/10.1038/s41598-017-09549-8
Simon, D. B., Bindra, R. S., Mansfield, T. A., Nelson-Williams, C., Mendonca, E., Stone, R., Schurman, S., Nayir, A., Alpay, H., Bakkaloglu, A., Rodriguez-Soriano, J., Morales, J. M., Sanjad, S. A., Taylor, C. M., Pilz, D., Brem, A., Trachtman, H., Griswold, W., Richard, G. A., . . . Lifton, R. P. (1997). Mutations in the chloride channel gene, CLCNKB, cause Bartter's syndrome type III. *Nat Genet*, *17*(2), 171-178. https://doi.org/10.1038/ng1097-171

Simon, D. B., Karet, F. E., Hamdan, J. M., DiPietro, A., Sanjad, S. A., & Lifton, R. P. (1996). Bartter's syndrome, hypokalaemic alkalosis with hypercalciuria, is caused by mutations in the Na-K-2Cl cotransporter NKCC2. *Nat Genet*, *13*(2), 183-188. https://doi.org/10.1038/ng0696-183

Simon, D. B., Karet, F. E., Rodriguez-Soriano, J., Hamdan, J. H., DiPietro, A., Trachtman, H., Sanjad, S. A., & Lifton, R. P. (1996). Genetic heterogeneity of Bartter's syndrome revealed by mutations in the K+ channel, ROMK. *Nat Genet*, *14*(2), 152-156. https://doi.org/10.1038/ng1096-152

Simon, M. C., & Keith, B. (2008). The role of oxygen availability in embryonic development and stem cell function. *Nat Rev Mol Cell Biol*, *9*(4), 285-296. https://doi.org/10.1038/nrm2354

Soliman, N. A. (2012). Orphan Kidney Diseases. *Nephron Clinical Practice*, *120*(4), c194-c199. https://doi.org/10.1159/000339785

Soutourina, J. (2018). Transcription regulation by the Mediator complex. *Nat Rev Mol Cell Biol*, *19*(4), 262-274. https://doi.org/10.1038/nrm.2017.115

Soutourina, J., Wydau, S., Ambroise, Y., Boschiero, C., & Werner, M. (2011). Direct interaction of RNA polymerase II and mediator required for transcription in vivo. *Science*, *331*(6023), 1451-1454. https://doi.org/10.1126/science.1200188

Srivastava, A. K., Pispa, J., Hartung, A. J., Du, Y., Ezer, S., Jenks, T., Shimada, T., Pekkanen, M., Mikkola, M. L., Ko, M. S., Thesleff, I., Kere, J., & Schlessinger, D. (1997). The Tabby phenotype is caused by mutation in a mouse homologue of the EDA gene that reveals novel mouse and human exons and encodes a protein (ectodysplasin-A) with collagenous domains. *Proc Natl Acad Sci U S A*, *94*(24), 13069-13074. https://doi.org/10.1073/pnas.94.24.13069

Stahl, P. L., Salmen, F., Vickovic, S., Lundmark, A., Navarro, J. F., Magnusson, J., Giacomello, S., Asp, M., Westholm, J. O., Huss, M., Mollbrink, A., Linnarsson, S., Codeluppi, S., Borg, A., Ponten, F., Costea, P. I., Sahlen, P., Mulder, J., Bergmann, O., . . . Frisen, J. (2016). Visualization and analysis of gene expression in tissue sections by spatial transcriptomics. *Science*, *353*(6294), 78-82. https://doi.org/10.1126/science.aaf2403

Starremans, P. G., Kersten, F. F., Knoers, N. V., van den Heuvel, L. P., & Bindels, R. J. (2003). Mutations in the human Na-K-2Cl cotransporter (NKCC2) identified in Bartter syndrome type I consistently result in nonfunctional transporters. *J Am Soc Nephrol*, *14*(6), 1419-1426. https://doi.org/10.1097/01.asn.0000064948.39199.a0

Steffen, D. J., Tiriac, H., Valera, J. L. C., Amornphimoltham, P., Kim, W., Taylor, S., Hunter, T., Tamayo, P., & Gutkind, J. S. (2020). Gαs (GNAS) suppression of the p53 genomic-stability checkpoint unleashes RAS-driven oncogenesis. *The FASEB Journal*, *34*(S1), 1-1. https://doi.org/https://doi.org/10.1096/fasebj.2020.34.s1.04604

Stevens, J. L., Cantin, G. T., Wang, G., Shevchenko, A., Shevchenko, A., & Berk, A. J. (2002). Transcription control by E1A and MAP kinase pathway via Sur2 mediator subunit. *Science*, *296*(5568), 755-758. https://doi.org/10.1126/science.1068943

Stevenson, M., Pagnamenta, A. T., Mack, H. G., Savige, J., Giacopuzzi, E., Lines, K. E., Taylor, J. C., & Thakker, R. V. (2022). The Bartter-Gitelman Spectrum: 50-Year Follow-up With Revision of Diagnosis After Whole-Genome Sequencing. *J Endocr Soc*, *6*(7), bvac079. https://doi.org/10.1210/jendso/bvac079

Sugimura, K., Tanaka, T., Tanaka, Y., Takano, H., Kanagawa, K., Sakamoto, N., Ikemoto, S., Kawashima, H., & Nakatani, T. (2002). Decreased sulfotransferase SULT1C2 gene expression in DPT-induced polycystic kidney. *Kidney Int*, *62*(3), 757-762. https://doi.org/10.1046/j.1523-1755.2002.00512.x

Takahashi, N., Chernavvsky, D. R., Gomez, R. A., Igarashi, P., Gitelman, H. J., & Smithies, O. (2000). Uncompensated polyuria in a mouse model of Bartter's syndrome. *Proc Natl Acad Sci U S A*, *97*(10), 5434-5439. https://doi.org/10.1073/pnas.090091297

Takata, K., Matsuzaki, T., Tajika, Y., Ablimit, A., & Hasegawa, T. (2008). Localization and trafficking of aquaporin 2 in the kidney. *Histochem Cell Biol*, *130*(2), 197-209. https://doi.org/10.1007/s00418-008-0457-0

Tamura, K., Stecher, G., & Kumar, S. (2021). MEGA11: Molecular Evolutionary Genetics Analysis Version 11. *Mol Biol Evol*, *38*(7), 3022-3027. https://doi.org/10.1093/molbev/msab120

Tarpey, P. S., Smith, R., Pleasance, E., Whibley, A., Edkins, S., Hardy, C., O'Meara, S., Latimer, C., Dicks, E., Menzies, A., Stephens, P., Blow, M., Greenman, C., Xue, Y., Tyler-Smith, C., Thompson, D., Gray, K., Andrews, J., Barthorpe, S., . . . Stratton, M. R. (2009). A systematic, large-scale resequencing screen of X-chromosome coding exons in mental retardation. *Nat Genet*, *41*(5), 535-543. https://doi.org/10.1038/ng.367

Terfve, C. D., Wilkes, E. H., Casado, P., Cutillas, P. R., & Saez-Rodriguez, J. (2015). Large-scale models of signal propagation in human cells derived from discovery phosphoproteomic data. *Nat Commun*, *6*, 8033. https://doi.org/10.1038/ncomms9033

Terris, J., Ecelbarger, C. A., Marples, D., Knepper, M. A., & Nielsen, S. (1995). Distribution of aquaporin-4 water channel expression within rat kidney. *Am J Physiol*, *269*(6 Pt 2), F775-785. https://doi.org/10.1152/ajprenal.1995.269.6.F775

Thakur, C., Qiu, Y., Zhang, Q., Carruthers, N. J., Yu, M., Bi, Z., Fu, Y., Wadgaonkar, P., Almutairy, B., Seno, A., Stemmer, P. M., & Chen, F. (2022). Deletion of mdig enhances H3K36me3 and metastatic potential of the triple negative breast cancer cells. *iScience*, *25*(10), 105057. https://doi.org/10.1016/j.isci.2022.105057

Thomsen, A. R. B., Plouffe, B., Cahill, T. J., 3rd, Shukla, A. K., Tarrasch, J. T., Dosey, A. M., Kahsai, A. W., Strachan, R. T., Pani, B., Mahoney, J. P., Huang, L., Breton, B., Heydenreich, F. M., Sunahara, R. K., Skiniotis, G., Bouvier, M., & Lefkowitz, R. J. (2016). GPCR-G Protein-beta-Arrestin Super-Complex Mediates Sustained G Protein Signaling. *Cell*, *166*(4), 907-919. https://doi.org/10.1016/j.cell.2016.07.004

Thomson, R. B., Wang, T., Thomson, B. R., Tarrats, L., Girardi, A., Mentone, S., Soleimani, M., Kocher, O., & Aronson, P. S. (2005). Role of PDZK1 in membrane expression of renal brush border ion exchangers. *Proc Natl Acad Sci U S A*, *102*(37), 13331-13336. https://doi.org/10.1073/pnas.0506578102

Troder, S. E., Ebert, L. K., Butt, L., Assenmacher, S., Schermer, B., & Zevnik, B. (2018). An optimized electroporation approach for efficient CRISPR/Cas9 genome editing in murine zygotes. *PLoS One*, *13*(5), e0196891. https://doi.org/10.1371/journal.pone.0196891

Trussart, C., Pirlot, C., Di Valentin, E., Piette, J., & Habraken, Y. (2018). Melanoma antigen-D2 controls cell cycle progression and modulates the DNA damage response. *Biochem Pharmacol*, *153*, 217-229. https://doi.org/10.1016/j.bcp.2018.01.035

Tseng, H. Y., Chen, L. H., Ye, Y., Tay, K. H., Jiang, C. C., Guo, S. T., Jin, L., Hersey, P., & Zhang, X. D. (2012). The melanoma-associated antigen MAGE-D2 suppresses TRAIL receptor 2 and protects against TRAIL-induced apoptosis in human melanoma cells. *Carcinogenesis*, *33*(10), 1871-1881. https://doi.org/10.1093/carcin/bgs236

Tsujii, M., Kawano, S., Tsuji, S., Sawaoka, H., Hori, M., & DuBois, R. N. (1998). Cyclooxygenase regulates angiogenesis induced by colon cancer cells. *Cell*, *93*(5), 705-716. https://doi.org/10.1016/s0092-8674(00)81433-6

Tudor, M., Murray, P. J., Onufryk, C., Jaenisch, R., & Young, R. A. (1999). Ubiquitous expression and embryonic requirement for RNA polymerase II coactivator subunit Srb7 in mice. *Genes Dev*, *13*(18), 2365-2368. https://doi.org/10.1101/gad.13.18.2365

Turan, S., & Bastepe, M. (2015). GNAS Spectrum of Disorders. *Curr Osteoporos Rep*, *13*(3), 146-158. https://doi.org/10.1007/s11914-015-0268-x

Turei, D., Korcsmaros, T., & Saez-Rodriguez, J. (2016). OmniPath: guidelines and gateway for literature-curated signaling pathway resources. *Nat Methods*, *13*(12), 966-967. https://doi.org/10.1038/nmeth.4077

Tusher, V. G., Tibshirani, R., & Chu, G. (2001). Significance analysis of microarrays applied to the ionizing radiation response. *Proc Natl Acad Sci U S A*, *98*(9), 5116-5121. https://doi.org/10.1073/pnas.091062498

Tyanova, S., Temu, T., Sinitcyn, P., Carlson, A., Hein, M. Y., Geiger, T., Mann, M., & Cox, J. (2016). The Perseus computational platform for comprehensive analysis of (prote)omics data. *Nat Methods*, *13*(9), 731-740. https://doi.org/10.1038/nmeth.3901

Underwood, M. A., Gilbert, W. M., & Sherman, M. P. (2005). Amniotic fluid: not just fetal urine anymore. *J Perinatol*, *25*(5), 341-348. https://doi.org/10.1038/sj.jp.7211290
Unwin, R. J., & Capasso, G. (2006). Bartter's and Gitelman's syndromes: their relationship to the actions of loop and thiazide diuretics. *Curr Opin Pharmacol*, *6*(2), 208-213. https://doi.org/10.1016/j.coph.2006.01.002
van der Bruggen, P., Traversari, C., Chomez, P., Lurquin, C., De Plaen, E., Van den Eynde, B., Knuth, A., & Boon, T. (1991). A gene encoding an antigen recognized by cytolytic T lymphocytes on a human melanoma. *Science*, *254*(5038), 1643-1647. https://doi.org/10.1126/science.1840703
Varghese, A., Tenbroek, E. M., Coles, J., Jr., & Sigg, D. C. (2006). Endogenous channels in HEK cells and potential roles in HCN ionic current measurements. *Prog Biophys Mol Biol*, *90*(1-3), 26-37. https://doi.org/10.1016/j.pbiomolbio.2005.05.002
Vergine, G., Fabbri, E., Pedini, A., Tedeschi, S., & Borsa, N. (2018). Bartter Syndrome Type 1 Presenting as Nephrogenic Diabetes Insipidus. *Case Rep Pediatr*, *2018*, 9175271. https://doi.org/10.1155/2018/9175271
Verma, S., Chanchlani, R., Siu, V. M., & Filler, G. (2020). Transient hyponatremia of prematurity caused by mild Bartter syndrome type II: a case report. *BMC Pediatr*, *20*(1), 311. https://doi.org/10.1186/s12887-020-02214-6
Vizcaino, J. A., Csordas, A., del-Toro, N., Dianes, J. A., Griss, J., Lavidas, I., Mayer, G., Perez-Riverol, Y., Reisinger, F., Ternent, T., Xu, Q. W., Wang, R., & Hermjakob, H. (2016). 2016 update of the PRIDE database and its related tools. *Nucleic Acids Res*, *44*(D1), D447-456. https://doi.org/10.1093/nar/gkv1145
Vizcaino, J. A., Deutsch, E. W., Wang, R., Csordas, A., Reisinger, F., Rios, D., Dianes, J. A., Sun, Z., Farrah, T., Bandeira, N., Binz, P. A., Xenarios, I., Eisenacher, M., Mayer, G., Gatto, L., Campos, A., Chalkley, R. J., Kraus, H. J., Albar, J. P., . . . Hermjakob, H. (2014). ProteomeXchange provides globally coordinated proteomics data submission and dissemination. *Nat Biotechnol*, *32*(3), 223-226. https://doi.org/10.1038/nbt.2839
Wallace, M. A. (1998). Anatomy and physiology of the kidney. *AORN J*, *68*(5), 800, 803-816, 819-820; quiz 821-804. https://doi.org/10.1016/s0001-2092(06)62377-6
Walmsley, S. J., Broeckling, C., Hess, A., Prenni, J., & Curthoys, N. P. (2010). Proteomic analysis of brush-border membrane vesicles isolated from purified proximal convoluted tubules. *Am J Physiol Renal Physiol*, *298*(6), F1323-1331. https://doi.org/10.1152/ajprenal.00711.2009
Wang, H., Wang, Y., Yang, J., Zhao, Q., Tang, N., Chen, C., Li, H., Cheng, C., Xie, M., Yang, Y., & Xie, Z. (2021). Tissue- and stage-specific landscape of the mouse translatome. *Nucleic Acids Res*, *49*(11), 6165-6180. https://doi.org/10.1093/nar/gkab482
Weber, E. M., Hultgren, J., Algers, B., & Olsson, I. A. (2016). Do Laboratory Mouse Females that Lose Their Litters Behave Differently around Parturition? *PLoS One*, *11*(8), e0161238. https://doi.org/10.1371/journal.pone.0161238
Weinberg, L. E., Dinsmoor, M. J., & Silver, R. K. (2010). Severe hydramnios and preterm delivery in association with transient maternal diabetes insipidus. *Obstet Gynecol*, *116 Suppl 2*, 547-549. https://doi.org/10.1097/AOG.0b013e3181e6c683
Westerling, T., Kuuluvainen, E., & Makela, T. P. (2007). Cdk8 is essential for preimplantation mouse development. *Mol Cell Biol*, *27*(17), 6177-6182. https://doi.org/10.1128/MCB.01302-06
Wickham, H. (2009). *ggplot2 : Elegant Graphics for Data Analysis*. Springer. https://doi.org/10.1007/978-0-387-98141-3
Wold, M. S. (1997). Replication protein A: a heterotrimeric, single-stranded DNA-binding protein required for eukaryotic DNA metabolism. *Annu Rev Biochem*, *66*, 61-92. https://doi.org/10.1146/annurev.biochem.66.1.61
Wong, J. S., Meliambro, K., Ray, J., & Campbell, K. N. (2016). Hippo signaling in the kidney: the good and the bad. *Am J Physiol Renal Physiol*, *311*(2), F241-248. https://doi.org/10.1152/ajprenal.00500.2015
Wu, T., Hu, E., Xu, S., Chen, M., Guo, P., Dai, Z., Feng, T., Zhou, L., Tang, W., Zhan, L., Fu, X., Liu, S., Bo, X., & Yu, G. (2021). clusterProfiler 4.0: A universal enrichment tool for

interpreting omics data. *Innovation (Camb)*, *2*(3), 100141. https://doi.org/10.1016/j.xinn.2021.100141
Wu, X., Huang, L., Luo, C., Liu, Y., & Niu, J. (2021). A Case Report and Literature Review of a Novel Mutation in the MAGED2 Gene of a Patient With Severe Transient Polyhydramnios. *Front Pediatr*, *9*, 778814. https://doi.org/10.3389/fped.2021.778814
Xiao, K., Sun, J., Kim, J., Rajagopal, S., Zhai, B., Villen, J., Haas, W., Kovacs, J. J., Shukla, A. K., Hara, M. R., Hernandez, M., Lachmann, A., Zhao, S., Lin, Y., Cheng, Y., Mizuno, K., Ma'ayan, A., Gygi, S. P., & Lefkowitz, R. J. (2010). Global phosphorylation analysis of beta-arrestin-mediated signaling downstream of a seven transmembrane receptor (7TMR). *Proc Natl Acad Sci U S A*, *107*(34), 15299-15304. https://doi.org/10.1073/pnas.1008461107
Xu, S., Wu, Y., Chen, Q., Cao, J., Hu, K., Tang, J., Sang, Y., Lai, F., Wang, L., Zhang, R., Li, S. P., Zeng, Y. X., Yin, Y., & Kang, T. (2013). hSSB1 regulates both the stability and the transcriptional activity of p53. *Cell Res*, *23*(3), 423-435. https://doi.org/10.1038/cr.2012.162
Yabuki, A., Suzuki, S., Matsumot, M., Kurohmaru, M., Hayashi, Y., & Nishinakagawa, H. (2001). Staining pattern of the brush border and detection of cytoplasmic granules in the uriniferous tubules of female DBA/2Cr mouse kidney: comparison among various fixations and stains. *J Vet Med Sci*, *63*(12), 1339-1342. https://doi.org/10.1292/jvms.63.1339
Yamamoto, J., Miyake, K., Han, Q., Tan, Y., Inubushi, S., Sugisawa, N., Higuchi, T., Tashiro, Y., Nishino, H., Homma, Y., Matsuyama, R., Chawla, S. P., Bouvet, M., Singh, S. R., Endo, I., & Hoffman, R. M. (2020). Oral recombinant methioninase increases TRAIL receptor-2 expression to regress pancreatic cancer in combination with agonist tigatuzumab in an orthotopic mouse model. *Cancer Lett*, *492*, 174-184. https://doi.org/10.1016/j.canlet.2020.07.034
Yang, K., Huo, X., Zhang, Y., Zhang, M., Gao, Y., Wu, D., Lou, G., Qi, N., Zhang, B., & Wang, D. (2019). [Genetic analysis of a pedigree affected with Bartter's syndrome]. *Zhonghua Yi Xue Yi Chuan Xue Za Zhi*, *36*(7), 701-703. https://doi.org/10.3760/cma.j.issn.1003-9406.2019.07.011
Yoneyama, M., Sugiyama, A., Satoh, Y., Takahara, A., Nakamura, Y., & Hashimoto, K. (2002). Cardiovascular and adenylate cyclase stimulating effects of colforsin daropate, a water-soluble forskolin derivative, compared with those of isoproterenol, dopamine and dobutamine. *Circ J*, *66*(12), 1150-1154. https://doi.org/10.1253/circj.66.1150
Yu, M. J., Miller, R. L., Uawithya, P., Rinschen, M. M., Khositseth, S., Braucht, D. W., Chou, C. L., Pisitkun, T., Nelson, R. D., & Knepper, M. A. (2009). Systems-level analysis of cell-specific AQP2 gene expression in renal collecting duct. *Proc Natl Acad Sci U S A*, *106*(7), 2441-2446. https://doi.org/10.1073/pnas.0813002106
Yun, C. H., Oh, S., Zizak, M., Steplock, D., Tsao, S., Tse, C. M., Weinman, E. J., & Donowitz, M. (1997). cAMP-mediated inhibition of the epithelial brush border Na+/H+ exchanger, NHE3, requires an associated regulatory protein. *Proc Natl Acad Sci U S A*, *94*(7), 3010-3015. https://doi.org/10.1073/pnas.94.7.3010
Zankl, A., Addor, M. C., Cousin, P., Gaide, A. C., Gudinchet, F., & Schorderet, D. F. (2001). Fatal outcome in a female monozygotic twin with X-linked hypohydrotic ectodermal dysplasia (XLHED) due to a de novo t(X;9) translocation with probable disruption of the EDA gene. *Eur J Pediatr*, *160*(5), 296-299. https://doi.org/10.1007/s004310100738
Zaoral, M., Kolc, J., & Šorm, F. (1967). Amino acids and peptides. LXXI. Synthesis of 1-deamino-8-D-γ-aminobutyrine-vasopressin, 1-deamino-8-D-lysine-vasopressin, and 1-deamino-8-D-arginine-vasopressin. *Collection of Czechoslovak Chemical Communications*, *32*(3), 1250-1257. https://doi.org/doi:10.1135/cccc19671250
Zhai, R., Snyder, J., Montgomery, S., & Sato, P. Y. (2022). Double life: How GRK2 and β-arrestin signaling participate in diseases. *Cellular Signalling*, *94*, 110333. https://doi.org/https://doi.org/10.1016/j.cellsig.2022.110333

Zhang, X., Odom, D. T., Koo, S. H., Conkright, M. D., Canettieri, G., Best, J., Chen, H., Jenner, R., Herbolsheimer, E., Jacobsen, E., Kadam, S., Ecker, J. R., Emerson, B., Hogenesch, J. B., Unterman, T., Young, R. A., & Montminy, M. (2005). Genome-wide analysis of cAMP-response element binding protein occupancy, phosphorylation, and target gene activation in human tissues. *Proc Natl Acad Sci U S A*, *102*(12), 4459-4464. https://doi.org/10.1073/pnas.0501076102

Zhao, H., & Piwnica-Worms, H. (2001). ATR-mediated checkpoint pathways regulate phosphorylation and activation of human Chk1. *Mol Cell Biol*, *21*(13), 4129-4139. https://doi.org/10.1128/MCB.21.13.4129-4139.2001

Zhao, S., Jiang, E., Chen, S., Gu, Y., Shangguan, A. J., Lv, T., Luo, L., & Yu, Z. (2016). PiggyBac transposon vectors: the tools of the human gene encoding. *Transl Lung Cancer Res*, *5*(1), 120-125. https://doi.org/10.3978/j.issn.2218-6751.2016.01.05

Zheng, N., & Shabek, N. (2017). Ubiquitin Ligases: Structure, Function, and Regulation. *Annual Review of Biochemistry*, *86*(1), 129-157. https://doi.org/10.1146/annurev-biochem-060815-014922

7 Publications

2023:

Steffen A, **Reusch B**, Gruteser N, Mainz D, Roncarati R, Baumann A, Stradal TEB, Knebel-Mörsdorf D. Baculovirus Actin Rearrangement-Inducing Factor 1 Can Remodel the Mammalian Actin Cytoskeleton. Microbiol Spectr. 2023. https://doi.org/10.1128/spectrum.05189-22. Preproof.

Odenthal J, Dittrich S, Ludwig V, Merz T, Reitmeier K, **Reusch B**, Höhne M, Cosgun ZC, Hohenadel M, Putnik J, Göbel H, Rinschen MM, Altmüller J, Koehler S, Schermer B, Benzing T, Beck BB, Brinkkötter PT, Habbig S, Bartram MP. Modeling of ACTN4-based podocytopathy using Drosophila nephrocytes. Kidney Int Rep. 2023 Feb: 8(2);317-329. https://doi.org/10.1016/j.ekir.2022.10.024

2022:

Schurek H, -J, Maisel P, Helmchen U, **Reusch B**, Pekrun A: Triosephosphate-Isomerase Deficiency: Epiphenomenon or Cause of Loin Pain Haematuria Syndrome? Case Rep Nephrol Dial 2022:226-233. doi: 10.1159/000527330

Erger F, Aryal R, **Reusch B**, Matsumoto Y, Meyer R, Zeng J, Knopp C, Noel M, Wenzel A, Kohl S, Tschernoster N, Rappl G, Schröder-Braunstein J, Seibert F, Thiele H, Häusler M, Weber L, Büttner-Herold M, Elbracht M, Cummings S, Altmüller J, Habbig S, Cummings R, Beck B. Germline C1GALT1C1 Mutation Causes a Multisystemic Chaperonopathy with Global Deficiency of Core 1-derived O-Glycosylation. doi:10.21203/rs.3.rs-1716400/v1. PPR:PPR515567.

Reusch B, Bartram MP, Dafinger C, Palacio-Escat N, Wenzel A, Fenton RA, Saez-Rodriguez J, Schermer B, Benzing T, Altmüller J, Beck BB, Rinschen MM. MAGED2 controls vasopressin-induced aquaporin-2 expression in collecting duct cells. J Proteomics. 2022 Feb 10;252:104424. doi: 10.1016/j.jprot.2021.104424.

2021:

Fabretti F, Tschernoster N, Erger F, Hedergott A, Buescher AK, Dafinger C, **Reusch B**, Köntges VK, Kohl S, Bartram MP, Weber LT, Thiele H, Altmueller J, Schermer B, Beck BB, Habbig S. Expanding the Spectrum of FAT1 Nephropathies by Novel Mutations That Affect Hippo Signaling. Kidney Int Rep. 2021 Jan 29;6(5):1368-1378. doi: 10.1016/j.ekir.2021.01.023.

2018:

Belostotsky R, Lyakhovetsky R, Sherman MY, Shkedy F, Tzvi-Behr S, Bar R, Hoppe B, **Reusch B**, Beck BB, Frishberg Y. Translation inhibition corrects aberrant localization of mutant alanine-glyoxylate aminotransferase: possible therapeutic approach for hyperoxaluria. J Mol Med (Berl). 2018 Jul;96(7):621-630. doi: 10.1007/s00109-018-1651-8.

2016:

Laghmani K, Beck BB, Yang SS, Seaayfan E, Wenzel A, **Reusch B**, Vitzthum H, Priem D, Demaretz S, Bergmann K, Duin LK, Göbel H, Mache C, Thiele H, Bartram MP, Dombret C, Altmüller J, Nürnberg P, Benzing T, Levtchenko E, Seyberth HW, Klaus G, Yigit G, Lin SH, Timmer A, de Koning TJ, Scherjon SA, Schlingmann KP, Bertrand MJ, Rinschen MM, de Backer O, Konrad M, Kömhoff M. Polyhydramnios, Transient Antenatal Bartter's Syndrome, and MAGED2 Mutations. N Engl J Med. 2016 May 12;374(19):1853-63. doi: 10.1056/NEJMoa1507629.

8 Acknowledgements

First of all, I would like to thank my supervisor PD Dr. Bodo Beck for giving me the possibility to perform studies in his group on this project that is very close to my heart. Thank you very much for your ideas and for giving me the possibilities to learn new techniques.

I also want to thank Prof. Dr. Brunhilde Wirth, the director of the institute for human genetics, for giving me the opportunity to be a part of this institute and for giving me great advice and support to finish this work.

Moreover, I want to thank Prof. Siegfried Roth and Prof. Niels Gehring for being part of my thesis committee.

I also want to thank all members of the Institute of Human Genetics. Special thanks here go to Dr. Andrea Wenzel for great support and discussions! I also want to thank the diagnostic lab which created a welcoming atmosphere right from the beginning and who were always there when I had questions and problems! Thanks here go to Saskia Seland, Serjoscha Blick, Katharina Nohl, Laura Wilden and Jenny Reiter. A special thank also goes to Dr. Uwe Becker, the good soul of the institute, for always fast support and lending an ear in all situations.

Thanks also go to Prof. Dr. Bernhard Schermer, Dr. Claudia Dafinger, Dr. Simon Tröde and Dr. Lena Ebert from the CECAD for the generation of our mouse model and the further cooperation. Thanks especially go to Claudia for the PBS perfusing of the animals, for the great help with the preparation of the mice and for answering all my questions regarding mouse work. A big thank you also goes to the animal care takers and especially to Christopher Knabe, Mira Storms, Mandy Götsche and Julia Mönkediek from the amber barrier!

A big thanks goes to our cooperation partners Dr. Malte Bartram and Prof. Dr. Markus Rinschen who helped me during the whole project being an inexhaustible source for good ideas. Special thanks here go to Markus, who gave me the possibility to perform the proteomics experiments of our mouse kidneys myself at the University of Aarhus in Denmark. Special thanks here also go to Dr. Fatih Demir and Dr. Anja Billing who supervised me during my time in Aarhus.

Many thanks also go to Dr. Eduardo Salido for giving me the possibility to learn advanced techniques of mouse preparation and staining at the university hospital of

La Laguna on Tenerife in Spain.
Thanks also go to Dr. Heike Göbel from the pathologic institute of the University Hospital of Cologne for providing us age-matched fetal kidney control tissue and to Melanie Nelles from the CMMC Tissue Embedding & Histology facility for the help with the paraffin sectioning.

My greatest thank goes to my family for the great support during my whole life and for always believing in me and for always being there fo me! Thank you to my parents Beate and Gerald, my sister Kerstin, my niece Elisa and Francesco.
My deepest gratitude goes to Marcel. You were always there for me and the biggest emotional support I could ever wish for!

9 Erklärung zur Dissertation

Ich versichere, dass ich die von mir vorgelegte Dissertation selbständig angefertigt, die benutzten Quellen und Hilfsmittel vollständig angegeben und die Stellen der Arbeit − einschließlich Tabellen, Karten und Abbildungen −, die anderen Werken im Wortlaut oder dem Sinn nach entnommen sind, in jedem Einzelfall als Entlehnung kenntlich gemacht habe; dass diese Dissertation noch keiner anderen Fakultät oder Universität zur Prüfung vorgelegen hat; dass sie − abgesehen von unten angegebenen Teilpublikationen − noch nicht veröffentlicht worden ist, sowie, dass ich eine solche Veröffentlichung vor Abschluss des Promotionsverfahrens nicht vornehmen werde. Die Bestimmungen der Promotionsordnung sind mir bekannt. Die von mir vorgelegte Dissertation ist von PD Dr. Bodo Beck (direkter Betreuer) und Prof. Dr. Brunhilde Wirth offizielle Betreuerin) betreut worden.

Teilpublikationen:

Reusch B, Bartram MP, Dafinger C, Palacio-Escat N, Wenzel A, Fenton RA, Saez-Rodriguez J, Schermer B, Benzing T, Altmüller J, Beck BB, Rinschen MM. MAGED2 controls vasopressin-induced aquaporin-2 expression in collecting duct cells. J Proteomics. 2022 Feb 10;252:104424. doi: 10.1016/j.jprot.2021.104424. Epub 2021 Nov 12. PMID: 34775100.

…… ……..

Datum Unterschrift